PLATE KINEMATIC MODELS

SAPIENZA
UNIVERSITÀ DI ROMA

Università degli Studi di Roma "La Sapienza"
Dottorato di Ricerca in Scienze della Terra
XIX Ciclo

PLATE KINEMATIC MODELS

Tesi di Dottorato
Settore Scientifico Disciplinare GEO/03

Membri della Commissione di Dottorato

Prof. Mattia Crespi .....
DITS – Area di Geodesia e Geomatica,
Università degli Studi di Roma "La Sapienza", Roma, Italy

Prof. Claudio Faccenna .....
Dipartimento di Scienze Geologiche,
Università degli Studi "Roma Tre", Roma, Italy

Prof. Susanna Zerbini .....
Dipartimento di Fisica – Sezione di Geofisica,
Università degli Studi di Bologna, Bologna, Italy

Cordinatore	*Docente Guida*	*Candidato*
Prof. Raffaello Trigila	*Prof. Carlo Doglioni*	*Marco Cuffaro*

....

Dipartimento di Scienze della Terra,
Università degli Studi di Roma "La Sapienza", Roma, Italy

Sessione di Dottorato 27 Marzo 2007
Anno Accademico 2005/2006

UNIVERSITY OF ROME "LA SAPIENZA"

PLATE KINEMATIC MODELS

A DISSERTATION FOR THE DEGREE OF
DOCTOR OF PHILOSOPHY

FIELD IN GEODYNAMICS AND GEOPHYSICS

BY
MARCO CUFFARO

ROME, ITALY
FEBRUARY 2007

[...] διόπερ ῥᾷστον ἁπάντων ἐστὶν
αὐτὸν ἐξαπαντῆσαι· ὃ γὰρ || βούλεται,
τοῦθ' ἕκαστος καὶ οἴεται [...]

"Nothing is easier than self–deceit.
For what each man wishes,
that he also believes to be true."

Demosthenes

"If the idea is not absurd at first,
then there is no hope for it."

Albert Einstein

"The intensity of the conviction that a hypothesis is true
has no bearing on whether it is true or not.
The importance of the strength of our conviction is only
to provide a proportionally strong incentive to find out
if the hypothesis will stand up to critical examination."

Sir Peter Medawar

Ph.D. Thesis
PLATE KINEMATIC MODELS

With the advising of
Prof. Carlo Doglioni

The research described in this thesis was carried out at
Department of Earth Sciences
University of Rome "La Sapienza"
P.le A. Moro 5
00185 Rome, Italy

For further information
marco.cuffaro@uniroma1.it
http://tetide.geo.uniroma1.it/dst/Cuffaro

Contents

Abstract

Plate motions with respect to the mantle represent the most direct evidence to infer the causes of plate tectonic processes. The research described in this dissertation contributes to the knowledge of global scale plate kinematics in absolute reference frames, incorporating both geological–geophysical, and space geodesy data. Geophysical observations and geological signatures of subduction and rift zones independently show a global polarity of current plate motions, suggesting a "westward" displacement of the whole lithosphere relative to the underlying mantle. We basically modeled this tectonic pattern in an analytic way, first testing predictions of previous plate kinematic models in absolute reference systems, and then defining a new hotspot framework with variable depths of the source, in which to obtain new plate angular velocities. Moreover, lines of geological evidence suggest that lithospheric plates could experience further and contemporaneous rotations, while they move on the Earth's surface. We have introduced the concept of the sub–rotations and their analytic description, studying the motion of the North America plate over most of the Cenozoic Era, and its current movement in the mean–lithosphere framework. Furthermore, using updated plate boundaries for the present, we have computed new geometrical factors for plates, useful for kinematic calculations and to obtain the net–rotation of the lithosphere and the plate velocities in the mean-lithosphere reference frame. We tested different plate configurations, with the "classic" 15 plates, and with 20, and 52 plates, depending on the addition of middle plates and microplates into the model respectively. The results show that it is possible to define a reference frame based on geodynamic rules, in which the "westward" polarization of plate motions is a real and quantified phenomenon. Finally, a comparison between horizontal and vertical plate motions allows a brief and alternative dynamic speculation on the causes of plate tectonics. All these research lines are supported by the definition of equations of motion, using spherical trigonometry, and by estimates of uncertainties of global plate kinematics, i.e. error ellipses and rotation–rate errors of angular velocities.

Acknowledgments

I would like to thank all the people who have made this research possible, with useful help, discussions, suggestions and comments.

First of all, it is a pleasure for me to thank Carlo Doglioni, a friend before than an advisor, who had the insanity to trust in my spare abilities in geodynamics, and for the bravery he proved involving me in his research activities, when we met six years ago. I thank him for observing the development of this project with discretion, without any imposition, for his enthusiasm and curiosity, discussing aspects of plate tectonics (also during adventurous one–day–skiing holidays, or in the middle of a rise on top of a mountain), and for his patience, giving suggestions and correcting my mistakes. I would like to extend my appreciation to him for financially supporting my participation at conferences, and at Northwestern University in 2005, to improve my knowledge in plate kinematic models, and plate motion computations.

I also wish to thank that institution and Donna M. Jurdy for their hospitality: in particular, from her I have learned most of the techniques presented in the dissertation, and how to solve practical problems about plate motions. The Chapter 6 is the result of this constructive collaboration, and I appreciated that she gave me the possibility to use some of her programs, such as the "`line`" one, useful to compute plate geometrical factors.

I am very grateful to Eugenio Carminati for the huge availability in talking about research topics, methods and approaches, and for introducing me into the magic world of the Generic Mapping Tools of *Wessel and Smith* [1995], which most of the figures of the thesis were made with. Federica Lenci, Sabina Bigi and Davide Scrocca are warmly thanked for the useful discussions about geodynamics, pure research, politics and science fiction, especially during the daily lunch break.

My gratitude is all for Federica Antonucci, because she has proved a huge tolerance, staying close to me during these years, and for the reason that she substantially con-

tributed to the realization of this study, with necessary comments and critical reviews of theoretical computations. I offer my thanks to my “acquired brother” Federico Iacobini, who has basically followed all the advances of this research project, patiently listening and giving useful suggestions.

Critical reading by Michele Caputo and Alessandro Caporali, was extremely necessary to improve the validity of this dissertation. Moreover, I would like to thank all the other people who directly or indirectly red some chapters (or pieces of them) of the thesis, and who inspired me with help, comments and tips about the topics treated in this study. In alphabetic order, many of them are: Donald F. Argus, Enrico Bonatti, Mattia Crespi, Gillian R. Foulger, Francesca Giannone, Alice E. Gripp, Michael Stefanick, Seth Stein, Joann Stock and Federica Riguzzi. Also I thank Peter Bird for sharing his plate boundary data in digital form, from his PB2002 model [*Bird*, 2003].

The realization of this project was also possible for the presence of my relatives and friends, who have created a positive and inspiring atmosphere around me.

My parents are thanked for support, love and understanding, especially in this last year. I apologize for the anxiety I caused to them, and to the fact I have not gone to visit them for months, focusing the attention only on the dissertation project.

All my friends have been important, supporting and contributing in distracting me all the times I overacted with work. Many special of them are: Chiara Fiori, Marco Brandano and their little *Giacomino*, for their brilliant and sincere friendship; Simona Mazziotti Tagliani, Silvia Simei and Elisa Melis, for their reliable generosity and overall cheerfulness; all the habitual users of the graduate student office, who have generally made these years less tiring. Finally, I would like to extend many thanks to all the people who have stayed close to me in February 2006.

In conclusion, I wish to make just a short comment about the third quotation: I found it in *Stein and Wysession* [2003], and also in the class material of *Tectonophysics*, offered by Seth Stein at Northwestern University in Spring 2005, and for the beauty, the intensity, and the truth of the words, I decided to insert it in this dissertation, hoping to always follow the meaning of those lines.

Preface

One of the aspects of plate tectonics is plate kinematics. Plate motions correspond to the first evidence of geodynamic processes and provide the basics to study and understand the evolution of the planet and the Earth's surface.

The global kinematics is basically separated in relative and absolute plate motions, studying the motions of plates with respect to the others, and relative to mantle respectively. The aims of these two sides of the same subject are focused on different topics of geodynamics and solid Earth geophysics. Relative motions regard the movements of plates along a common boundary and they are useful to describe how plates move, and to verify the mechanisms of mountain building, earthquakes, and volcanic eruptions, whereas absolute motions correspond to the displacements with respect to the underlying mantle, and offer a global point of view to understand the reasons and the causes of plate tectonic processes.

The main difficulty in describing plate kinematics is the choice of the reference system. This problem is solved doing relative analysis, because one of the two plates is stated fixed and plate displacements can be directly observed and computed by data coming from geology, geophysics and space geodesy. In contrast, there is not a direct way to measure absolute motions, and they need to be indirectly inferred, using results of relative plate kinematic models.

Since the beginning of studies of plate kinematics, two absolute reference systems have been defined, the hotspots and the mean–lithosphere, both constrained by different geophysical and conventional assumptions, but they do not arrive at similar results, on a large scale presenting different plate movements. Because absolute plate motions describe how the entire lithosphere moves relative to the mantle, and are most important in understanding why plates move and what forces are involved, one of the basic questions of plate kinematics is: which is the more appropriate reference frame for plate tectonics? And more, is it possible to define an alternative framework based on a complete set of

geodynamic ties?

All the geoscientists agree on the fact that plate kinematics, the plate motions themselves, is the most direct evidence to discover what drives the lithosphere, and, in accordance with the results obtained in the two different reference frames, principally believe that the plates i) randomly move on the Earth's surface, ii) they actively drive themselves by subduction of cooling lithosphere, and iii) they are passively carried by mantle convection.

On the contrary, geological and geophysical signatures of subduction and rift zones independently show a global trend, suggesting a complete "westward" rotation of the lithosphere and a relative "eastward" motion of the mantle. Plates move along a sort of undulate mainstream, and this westward drift of the lithosphere implies that plates have a general sense of motion and that they are not randomly moving, but following preferential trajectories, which undulate and are not exactly E–W oriented.

Global shear-wave splitting directions are quite consistent with such undulate flow, only deviating at subduction zones, which should represent obstacles to the relative mantle motion. In fact, along this flow, west-directed subduction zones are steeper than those that are E– or NE–directed; orogens associated with the E–directed subductions are characterized by lower structural and topographic elevations with backarc basins, while W–directed subduction zones show higher structural and morphological elevation and no backarc basins. The global scale asymmetry of tectonic features and the westward drift of the lithosphere could support a rotational component for the origin of plate tectonics. Moreover, according to the hypothesis of this global tectonic mainstream, and on the basis of additional geological evidence, the plates can be affected by further and contemporaneous rotations while they move on the Earth's surface, entailing a composed displacement and a different plate dynamics.

In this dissertation, we present the results of a research project about global scale plate kinematics. We have studied basic plate kinematic techniques and we have investigated absolute plate motions and their associated reference frames, to demonstrate the existence of a global polarity for the whole lithosphere. In fact, if the hypothesis of tectonic mainstream for plate displacements can be shown and proved by geology, there is not a reference system in which the westward drift is a well-quantified phenomenon, and there are not Euler poles and angular velocities, with their uncertainties, constraining absolute plate motions toward the west on undulate trajectories.

The main purpose of this thesis is to find a reference frame, based on geodynamic rules, in which the global tectonic pattern could be represented, and where to study all

the contemporaneous rotations that some plates could experience.

This dissertation is organized in eight chapters and two appendices, showing step by step the findings, the used methods and the discussions about the implications of the obtained results. We have started with a brief introduction in the Chapter 1, about plate tectonics, plate kinematics, basic reference frames, and the global tectonic pattern, whereas in the Chapter 2, we basically constrained absolute reference frames to the existence of the global mainstream itself, testing previous plate kinematic models and estimating correlations between predicted azimuths of velocity vectors and main trajectories for plate motions.

Due to the presence of the constrains, we decided to define another absolute reference frame, based on the hotspots, without any assumption about the tectonic pattern, changing the depths of the hotspot source, as suggested by growing geological evidence. In the Chapter 3, we tested plate motions relative to the deep and shallow hotspots, incorporating geological and geophysical data, whereas in the Chapter 4 we used similar methods, incorporating space geodesy data.

In the Chapter 5, the concepts and the theoretical methods of the sub–rotations were introduced. There were also presented the lines of geological evidence, entailing these composed rotations and two applications to plate motions in the conventional absolute reference frames, i.e. the hotspots and the mean–lithosphere.

The Chapter 6 is the result of a constructive cooperation with Prof. Donna M. Jurdy, at Northwestern University. We have investigated absolute motions of the microplates, obtaining angular velocities relative to the hotspots, and studying plate characteristics grouping by size.

The Chapter 7 and the Chapter 8 are strictly correlated, because a comparison between horizontal and vertical plate motions is made in the first, and, on the base of these results, a dynamic speculation is presented in the later.

Finally, in the Appendix A, the methods to obtain equations of motion for simple and composed plate displacements are proposed, by making use of spherical trigonometry, whereas in the Appendix B, methods to obtain plate motion uncertainties are presented.

Some of these chapters were utilized for the production of the related papers: the Chapter 3 [*Cuffaro and Doglioni*, 2007], the second application in the Chapter 5 [*Cuffaro et al.*, 2004], the Chapter 6 [*Cuffaro and Jurdy*, 2006], the Chapter 7 and a small part of the Chapter 8 [*Cuffaro et al.*, 2006]. The external reviews of these research topics were extremely useful to improve the validity of the results.

Chapter 1

Introduction

In 1915 Alfred Wegener published a theory, proposing that continents had slowly moved about [*Wegener*, 1915, 1924]. This theory of continental drift accounted for the complementarity of the shapes of the coastlines on opposite sides of oceans, and for the palaeontological, zoological and botanical evidence. It was accepted by few geologists, as for example *Du Troit* [1937], but it was not well received by the most of members of the scientific community. Most of the geophysicists, in fact, pointed out that it was physically impossible to move the continents through the solid rock of the ocean floor.

In the 50s, after some oceanographic expeditions to investigate the oceans, works on magnetism of oceanic and continental rocks indicated that in the past, the continents must have moved relative to each other. Moreover, the discovery of the midocean ridges produced again a discussion among geophysicists about the continental drift, and *Hess* [1962] presented one of the most important publication of the solid Earth sciences, proposing the process of the sea–floor spreading, that it had been involved in the continental drift. As the continents moved apart, new sea–floor material rose from the mantle along the midocean ridges to fill the vacancy.

In the following years, the theory of plate tectonics was developed, successfully taking into account physical and geological observations. This theory has become the unifying factor in the study of geology and geophysics.

1.1 Basic concepts of plate tectonics

Plate tectonics is a model in which the outer shell of the Earth, the lithosphere, is divided into a number of thin and rigid plates that are in motion relative to the underlying mantle,

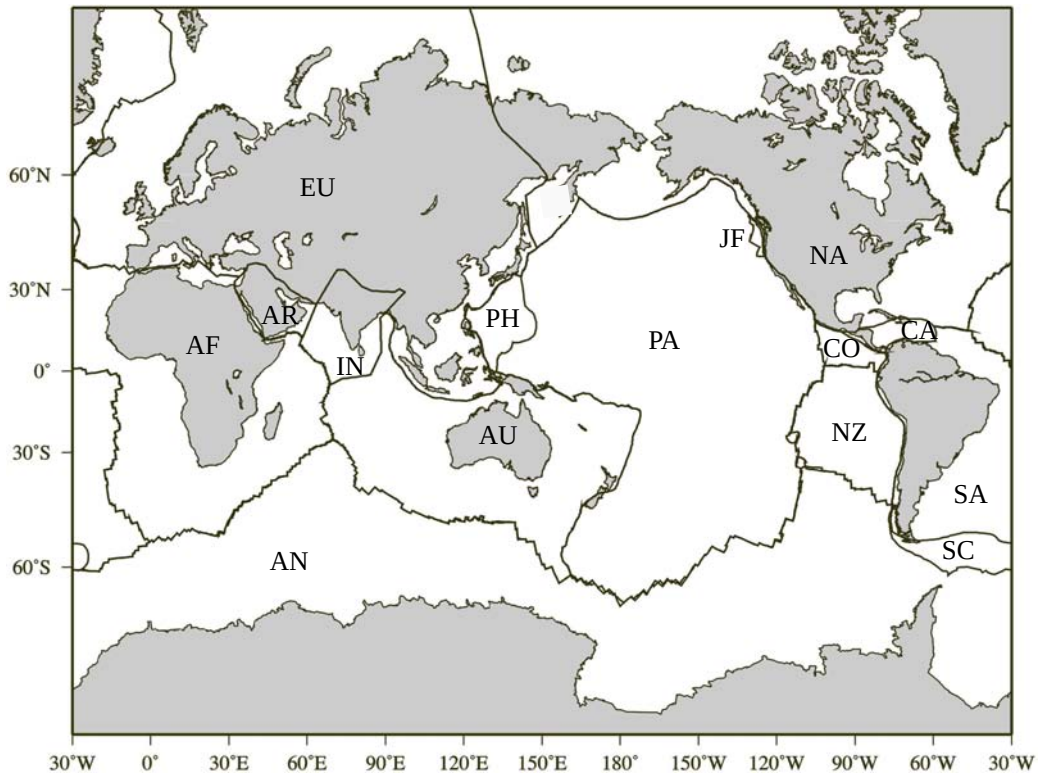

Figure 1.1: Lithospheric plates. Africa (AF), Antarctica (AN), Arabia (AR), Australia (AU), Caribbean (CA), Cocos (CO), Eurasia (EU), India (IN), Juan De Fuca (JF), North America (NA), Nazca (NZ), Pacific (PA), Philippine (PH), South America (SA), Scotia (SC).

and in relative motion with respect to one another. The relative velocities of the plates are of the order of tens of millimeters per year, and a large fraction of earthquakes, volcanic eruptions, and mountain building occur at plate boundaries. Most of the deformations which result from plate motions, as stretching, folding or shearing, take place at the edge of plates and deformation inside the boundary is negligible. The distribution of the plates on the Earth's surface is illustrated in Figure 1.1.

There are seven large plates as the Africa (AF), the Antarctica (AN), the Australia (AU), the Eurasia (EU), the North America (NA), the Pacific (PA), the South America (SA), of which the largest is the Pacific, and numerous smaller plates such as Nazca (NZ) and Cocos (CO) for a total of 15 plates (Figure 1.1).

The boundaries of plates are generally of three types i) divergent, ii) convergent, and iii) conservative (Figure 1.2).

Along divergent margins, also called accreting or constructive, plates are moving

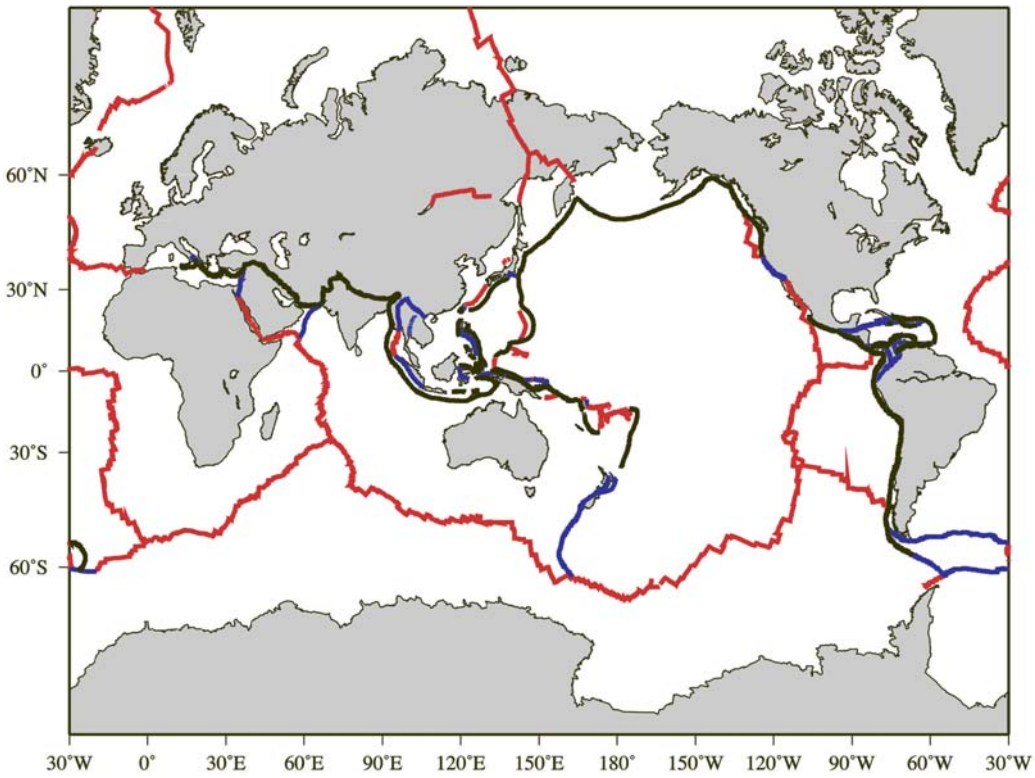

Figure 1.2: Different types of plate boundaries, divergent (red), convergent (black) and conservative (blue).

away from each other. At these kind of boundaries new material derived from the mantle is added to the lithosphere. The divergent plate margin is represented by the midocean ridge system.

Along convergent boundaries, also called consuming or destructive, plates are approaching each other. These margins are represented by oceanic trenchs, island arcs and systems of subduction zones, where one of the colliding plates descends into the mantle and is destroyed. Example of convergent boundaries are the Japan and the Himalaya.

Finally, along conservative margins, the lithosphere is neither created nor destroyed and plates move laterally relative to each other. These plate boundaries are represented by transform faults of which the San Andreas fault in California is an example.

The theory of plate tectonics is based on several assumption that state that the generation of new plate material occurs by sea–floor spreading and the new lithosphere is generated along the active midocean ridges. The new oceanic lithosphere, once created, forms part of a rigid plate. This plate may or may not include continental material. More-

over, the Earth's surface remains constant and relative motion of plate is taken up only along boundaries.

Although the plates are made up of both oceanic an continental material, usually only the oceanic part of any plate is created or destroyed.

1.2 Plate kinematics

Plate kinematics can be described in both relative and absolute reference frames, using the Euler's theorem of the fixed point, that states:

Theorem 1 *The most general displacement of a rigid body with a fixed point is equivalent to a rotation about an axis through that fixed point.*

Considering a plate as a rigid body, and choosing the Earth's center as a fixed point, the theorem can be restated as:

Theorem 2 *Every displacement on the Earth's surface can be regarded as a rotation about a rotation axis passing through the center of the Earth.*

This theorem was firstly applied by *Bullard et al.* [1965] in a publication describing the fitting of the coastlines of the South America and the Africa. The rotation axis cuts the Earth's surface in two points called the rotation poles (or the Euler poles). Every plate displacement is characterized by a rotation about an Euler pole with an angular velocity $\vec{\omega}$. The vector $\vec{\omega}$ lies on the rotation axis and the sign convention used is that rotation is positive if it is right–handed, viewed from the axis itself. Thus a rotation pole is positive and the other is negative (anti–pole).

Every plate point moves with a linear velocity $\vec{v}$, and its absolute value is defined as following:

$$v = \omega \mathrm{R} \sin \phi \tag{1.1}$$

where v is the linear velocity, ω is the angular velocity rate, R is the Earth's radius, and ϕ is the angular distance between the Euler pole and a single plate point.

The factor of $\sin \phi$ implies that, for example, along a boundary the linear velocity v change with the positions from a minimum velocity $v = 0$, when $\phi = 0, \pi$, to a maximum value $v = \omega$R, when $\phi = \frac{\pi}{2}$ from the rotation pole.

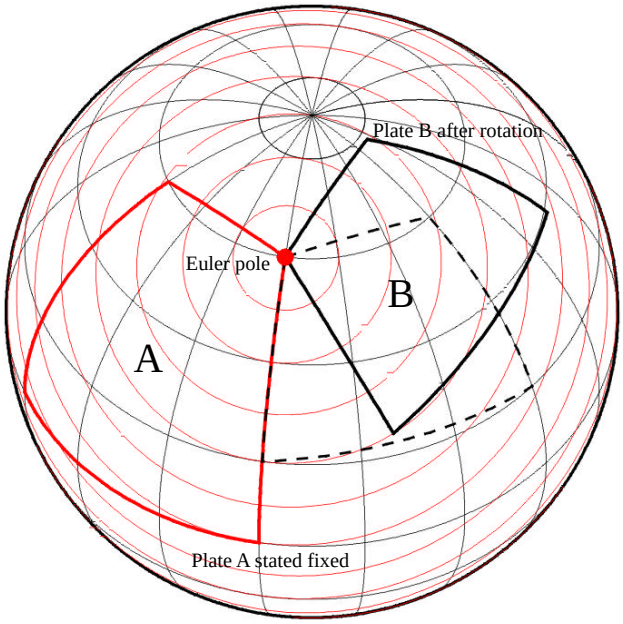

Figure 1.3: Relative plate motions. The plate A is stated fixed whereas the plate B rotates around the Euler pole. Red circles represent the trajectories of motion.

1.3 Reference frames of plate kinematics

Present–day relative plate motions are rotations about instantaneous rotation poles, with instantaneous angular velocities between pairs of plates sharing a margin (or not). "Instantaneous" refers to a geological instant, that is a value averaged over period of time ranging from few years to millions of years, depending of the method used.

Absolute plate motions describe how the entire lithosphere moves relative to the mantle, and are most important in understanding why plates move. They are also a good reference for comparisons with results of plate dynamic models. There is not a direct way to measure absolute motions, and they need to be indirectly inferred, using results of relative plate kinematic models.

1.3.1 Relative plate motions

Relative plate motions are useful to describe how plates sharing a boundary, move along the boundary itself. As represented in Figure 1.3, a plate B moves with respect to a plate A stated fixed making a rotation about the Euler pole. All the points of the plate B move on circles of the Euler pole.

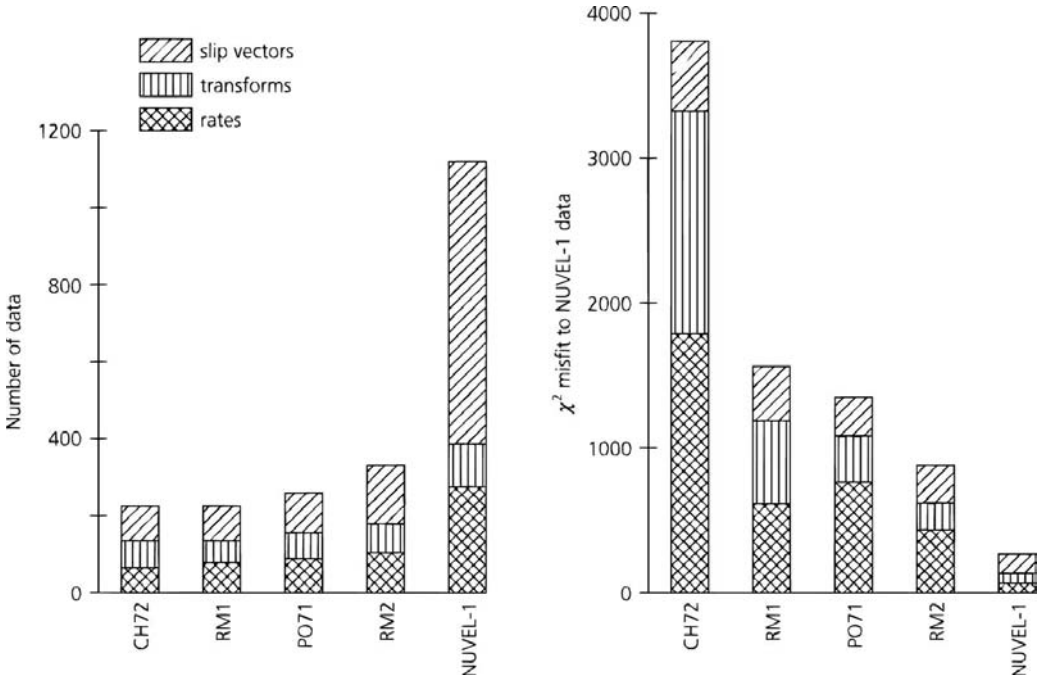

Figure 1.4: Evolution of successive global plate motion models. As the amount of data increases (left), the misfit is reduced (right). Figure from *Stein and Wysession* [2003].

In the past years, many authors have proposed present–day relative plate kinematic models as the CH72 [*Chase*, 1972], the RM1 [*Minster et al.*, 1974], the PO71 [*Chase*, 1978], the RM2 [*Minster and Jordan*, 1978], the NUVEL–1 [*DeMets et al.*, 1990] and the NUVEL1A [*DeMets et al.*, 1994].

Relative plate motions can be directly observed from geological and geophysical data, and can be computed from magnetic anomalies [e.g. *Vine and Matthews*, 1963; *Vine*, 1966; *Pitman and Heirtzler*, 1966; *Raff*, 1968; *Bergh and Norton*, 1976; *Barker and Lawver*, 1988], that give information about rates of plate kinematics, transform faults [e.g. *Norton*, 1976; *Gallo et al.*, 1986; *Searle*, 1986; *Lawver and Dick*, 1983], and seismology (slip vectors or fault plane solution) [e.g. *Chapman and Solomon*, 1976; *Perez and Jacob*, 1980; *Choy and Dewey*, 1988; *DeMets et al.*, 1990], that give information about the azimuth of motions.

Since 1972, when the first plate kinematic model was made, the amount of available data has increased, and data have become better, due to the advances in seismology, sea floor imaging, and marine magnetic measurements. The misfit of the data has also been reduced, also both to the higher quality of data and to improvements in the models, such

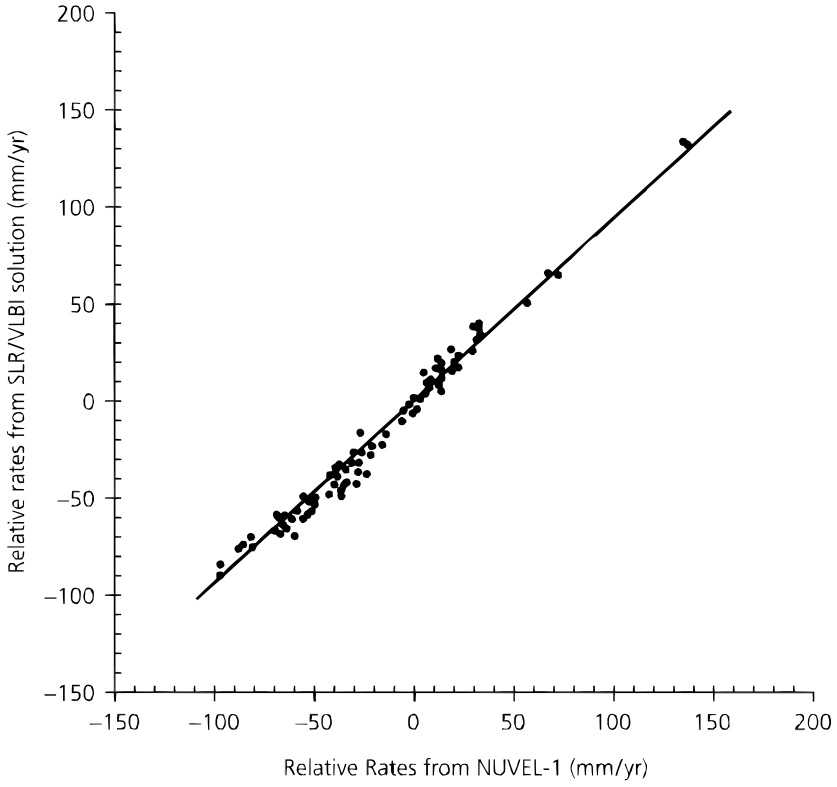

Figure 1.5: Comparison of rates computed by space geodesy and predicted rates by the NUVEL–1 [*DeMets et al.*, 1990]. The slope of the line is 0,94, and indicates good correlation between different techniques of evaluating relative plate motions. Figure from *Robbins et al.* [1993].

as treating the India and the Australia as separate plates (Figure 1.4).

Recently, relative plate motions can be computed also from space geodesy techniques [*Gordon and Stein*, 1992], as satellite laser ranging (SRL) [*Smith et al.*, 1990; *Robbins et al.*, 1993; *Cazenave et al.*, 1993; *Sengoku*, 1998], very long baseline interferometry (VLBI) [*Clark et al.*, 1987; *Argus and Gordon*, 1990; *Robaudo and Harrison*, 1993; *Ryan et al.*, 1993; *Sato*, 1993], Doppler Orbitography and Radiopositioning Integrated by Satellite (DORIS) [*Cazenave et al.*, 1992; *Soudarin and Cazenave*, 1993, 1995; *Cretaux et al.*, 1998] and global position system (GPS) [*Dixon et al.*, 1991; *Dixon*, 1993; *Argus and Heflin*, 1995; *Larson et al.*, 1997; *Dixon and Mao*, 1997; *Prawirodirdjo and Bock*, 2004].

Space geodesy can measure both the rate and the azimuth of motion between sites, and can thus be used to compute relative plate motions. One of the most important results

of space geodesy is that plate motions have remained generally steady over the past few million years. This is shown by the striking agreement between motions measured over few years by space geodesy and the predictions of global plate motion models that average the past three million years (Figure 1.5). Most studies suggest that the great majority of plate velocities estimated from space geodesy are consistent with the NUVEL-1A model within 95% confidence. However, uncertainties in the geodetic estimates have been large enough that important differences may have been missed. The true uncertainty of space geodetic data has also been difficult to quantify. Therefore it has been difficult to address an important tectonophysical problem, namely, the extent to which individual plate velocities may change over the last few million years and to what extent such changes, if they occur, can be understood in terms of simple plate–driving forces.

Space geodesy data and new analytical techniques now permit a significant refinement of our description of present–day plate motions. A very large geodetic data set is now publicly available through the efforts of many individuals, institutions, and geodetic agencies, permitting more accurate and more comprehensive geodetic plate motion models.

Relative plate motions better describe *how* plates move along a common boundary, but they are not so useful to understand *why* they move, because their motion relative to the mantle is not accounted for. To investigate the dynamics of the lithosphere from plate kinematics, plate motions have to be referred with respect to the mantle, where all the lithosphere moves as a whole.

1.3.2 Absolute plate motions

Absolute plate motions represent motions of plates relative to the mesosphere. To describe displacements of the lithosphere, two different absolute frameworks are often used: the hotspots and the mean–lithosphere.

The hotspots

The hotspot framework is based on the assumption that the hotspots are fixed relative to the mesosphere and to each other [*Morgan*, 1971, 1972; *Wilson*, 1973], and the orientation and the age progressions along their surface traces reflect the motion of the overlying lithospheric plate relative to the hotspots.

In fact, when a plate passes on a hotspot, a seamount volcanic chain is formed, such as the well–documented, monotonic, nearly linear age progression along the Hawaiian

Island seamount chain [*Dalrymple et al.*, 1980], and then it is possible to compute the rate and the azimuth of the plate displacement.

Hotspot traces staying within plates directly give information of the overlying plate motion with respect to the mesosphere, whereas the motion of the other plates, without any track, must be tied in the framework with a circuit of seafloor spreading data relating plates separated by a ridge [*Jurdy*, 1990].

The most recent plate kinematic models relative to the hotspots are the HS2–NUVEL1 [*Gripp and Gordon*, 1990] and the HS3–NUVEL1A [*Gripp and Gordon*, 2002] that respectively incorporate the relative plate motion model NUVEL–1 [*DeMets et al.*, 1990] and the NUVEL1A [*DeMets et al.*, 1994].

Although unresolved questions about hotspots remain, such as the number, and the source depth [*Norton*, 2000; *Foulger et al.*, 2005], nonetheless the hotspot reference frame remains a convenient – and easy to visualize – framework in which to study plate kinematics and dynamics.

The mean–lithosphere

This alternative reference frame is based on the fact that no net torque can be exerted by the lithosphere on the asthenosphere [*Solomon and Sleep*, 1974]. This approach does not yield a unique solution for absolute motions, because the nature and lateral variation of the coupling between the lithosphere and the asthenosphere are unknown.

Most of the basic studies of plate motions in the no–net–torque framework [e.g. *Solomon et al.*, 1977; *Jurdy*, 1978; *Davis and Solomon*, 1981; *Jurdy and Gordon*, 1984], have widely applied the simplest no–net–rotation (NNR) condition in which the coupling between the lithosphere and asthenosphere is assumed to have no lateral variation. This "uniform drag" no–net–torque reference frame is equivalent to a reference frame simply defined from plate kinematics, a no–net–rotation reference frame, i.e. a framework that yields a value of zero for the following integral:

$$\int_S \mathbf{v} \times \mathbf{r} \, \mathrm{d}S \tag{1.2}$$

where $\mathbf{v}$ is the surface velocity of a plate relative to the mesosphere, $\mathbf{r}$ is a position vector, S is the whole surface, and $\mathrm{d}S$ is the area element. The no–net–rotation frame is also defined as the "mean–lithosphere", because the global vector average of $\mathbf{v} \times \mathbf{r}$ is zero in this framework.

The no–net–rotation is a simple framework in which to obtain results and it is often used. A plate kinematic model with respect to the NNR–framework, incorporating the NUVEL–1, is the NNR –NUVEL1 [*Argus and Gordon*, 1991], whereas there are many other models that incorporate relative motions from GPS measurements [*Kreemer and Holt*, 2001; *Sella et al.*, 2002; *Drewes and Meisel*, 2003; *Kreemer and Holt*, 2003].

Both the absolute reference frames are referred to the mesosphere, and any difference between the mean–lithosphere and the hotspots is interpreted as a net–rotation of the lithosphere with respect to the mesosphere [*Forsyth and Uyeda*, 1975].

The net–rotation of the lithosphere concept [*Solomon and Sleep*, 1974; *Lliboutry*, 1974] also describes the NNR framework rotation with respect to the hotspot frame [*Argus and Gordon*, 1991].

To compute the net–rotation angular velocity ω_{nr}, it is firstly useful to define the symmetric tensor I_p [*Gordon and Jurdy*, 1986; *Jurdy*, 1990] describing plate geometry for a single plate p on a unit sphere:

$$\mathrm{I}_p = \int_S \begin{bmatrix} 1-x^2 & -xy & -xz \\ -xy & 1-y^2 & -yz \\ -xz & -yz & 1-z^2 \end{bmatrix} \mathrm{d}S \tag{1.3}$$

where x,y,z are the Cartesian co-ordinates of a plate p, S is the plate surface and $\mathrm{d}S$ is the area element. The x-, y-, and z-directions are defined from the center of the Earth to (0°N, 0°E), (0°N, 90°E), and (90°N, 0°E) respectively. The elements of the tensor I_p are called the geometrical factors of the single plate p [*Jurdy*, 1974, 1990].

In Table 1.1, are reported the plate geometrical factors proposed by *Argus and Gordon* [1991], using the computation technique of *Jurdy* [1974]. Recently, many other different techniques have been proposed to obtain plate geometrical factors [*Schettino*, 1999a,b; *Jin and Zhu*, 2004], that provided results not so different of those of the Table 1.1. Thus, the net–rotation angular velocity ω_{nr} can be computed with a matrix equation [*Jurdy*, 1974, 1990]:

$$\omega_{nr} = \frac{3}{8\pi} \sum_{p=1}^{P} \mathrm{I}_p \omega_p \tag{1.4}$$

where P is the the total number of plates, I_p are the geometrical factors for the plate p, and ω_p are the angular velocities of plates, computed in the hotspot reference frame.

As an example, in their paper, *Argus and Gordon* [1991] show that the resulting

Table 1.1: Plate geometrical factors from *Argus and Gordon* [1991]. Plate identifiers are those of the Figure 1.1 and LS corresponds to the whole lithosphere.

PLATE	Area	I_{xx}	I_{yy}	I_{zz}	I_{xy}	I_{xz}	I_{yz}
AF	1.9124	0.6567	1.5366	1.6315	-0.2501	0.0553	0.1088
AN	1.4756	1.3638	1.2102	0.3772	-0.0466	0.0636	0.0715
AR	0.1252	0.0777	0.0690	0.1037	-0.0501	-0.0308	-0.0326
AU	1.2056	0.8349	0.6325	0.9438	0.2193	-0.2252	0.2902
CA	0.0916	0.0844	0.0125	0.0863	0.0207	-0.0054	0.0198
CO	0.0761	0.0747	0.0037	0.0738	-0.0064	0.0014	0.0112
EU	1.6729	1.3958	1.0749	0.8751	0.0961	-0.1620	-0.4086
IN	0.2976	0.2776	0.0424	0.2752	-0.0582	-0.0140	-0.0595
JF	0.0070	0.0057	0.0048	0.0035	-0.0017	0.0021	0.0028
NA	1.4231	1.2717	0.9996	0.5749	0.0730	0.0241	0.3751
NZ	0.4061	0.3941	0.0710	0.3471	-0.0134	-0.0036	-0.1164
PA	2.6536	1.1958	2.0171	2.0943	-0.3986	0.0719	-0.0556
PH	0.1416	0.0799	0.0780	0.1253	0.0613	0.0293	-0.0292
SA	1.0780	0.6647	0.6254	0.8659	0.3546	0.1935	-0.1773
LS	12.5664	8.3775	8.3777	8.3776	-0.0001	0.0002	0.0002

Units are in steradians

present net–rotation of the lithosphere relative to the mesosphere is described by a right–handed rotation about an Euler pole located at 49.20 °S, 64.90 °E with a rate of 0.33 $^{\circ}\mathrm{Myr}^{-1}$. To obtain this result, they used plate velocities of the HS2–NUVEL1 [*Gripp and Gordon*, 1990] and the geometrical factors of the Table 1.1.

1.4 The westward drift of the lithosphere

Since the intuition of *Wegener* [1915], there have been a number of papers describing a westward drift of the lithosphere relative to the mantle [*Le Pichon*, 1968].

Tidal or Earth's rotation effects were invoked to explain this polarization [*Bostrom*, 1971; *Knopoff and Leeds*, 1972; *Moore*, 1973], but *Jordan* [1974] and *Jeffreys* [1975] denied any effect of the moon on the lithosphere, and the model was abandoned.

Nevertheless there is a general agreement on the existence of the westward drift which

is proven by independent data sets such as the hotspot reference frame [*Ricard et al.*, 1991; *O'Connell et al.*, 1991; *Gordon*, 1995; *Gripp and Gordon*, 2002], space geodesy [*Heflin et al.*, 2004] and asymmetries of subduction and rift zones [*Doglioni et al.*, 1999, 2003]. However the westward drift has not been fully understood, and its implications are far to be applied. In spite of the observed westward drift, plate kinematics and space geodesy frames of measurement of plate velocities are still anchored to no–net–rotation models [*Argus and Gordon*, 1991; *Heflin et al.*, 2004].

The classic evidence of the drift was also obtained, measuring plate motions relative to Antarctica [*Le Pichon*, 1968; *Knopoff and Leeds*, 1972]. *Argus and Gordon* [1991] and *Gripp and Gordon* [2002] computed an average net–rotation of the lithosphere to the "west" using the hotspot reference frame.

There still are doubts about i) what is generating the westward drift, and ii) whether it affects the entire lithosphere or it is rather only a mean value, with most of the lithosphere moving "west", but part of it still moving in the opposite direction relative to the mantle. According to this last opinion, only some plates would move westward, and since one of them is the Pacific plate, which is the largest and the fastest moving WNW-ward, the sum of all vectors would maintain a residual westward component, without a complete polarization. *Ricard et al.* [1991] proposed that the westward drift is only a mean value due to the lower asthenospheric viscosity at the base of the Pacific plate, but recently, *Scoppola et al.* [2006] proposed an alternative interpretation of the drift as rather a global effect induced by the combination of both tidal and convection torques excited by Earth's rotation.

1.5 An alternative kinematic model

Generally, the geologists and geophysicists consider that lithospheric plates randomly move [e.g., *O'Connell et al.*, 1991; *Gripp and Gordon*, 2002]. On the contrary, geological and geophysical signatures of subduction and rift zones show a global pattern, suggesting an "eastward" motion of the mantle relative to the lithosphere, and viceversa, regardless the choice of the reference frame [*Doglioni*, 1990, 1991].

Plates are moving along a sort of mainstream depicting a sinusoid [*Doglioni*, 1990, 1993] (Figure 1.6). To visualize this global pattern, we can consider the first order tectonic structures along the boundaries of six large plates of Earth (Pacific, Nazca, South America, Africa, Arabia-India, and Eurasia), reported in Figure 1.7: the East Pacific Rise (1), the Mid Atlantic ridge (2), and the Red Sea – Indian ridge (3), for extensional mar-

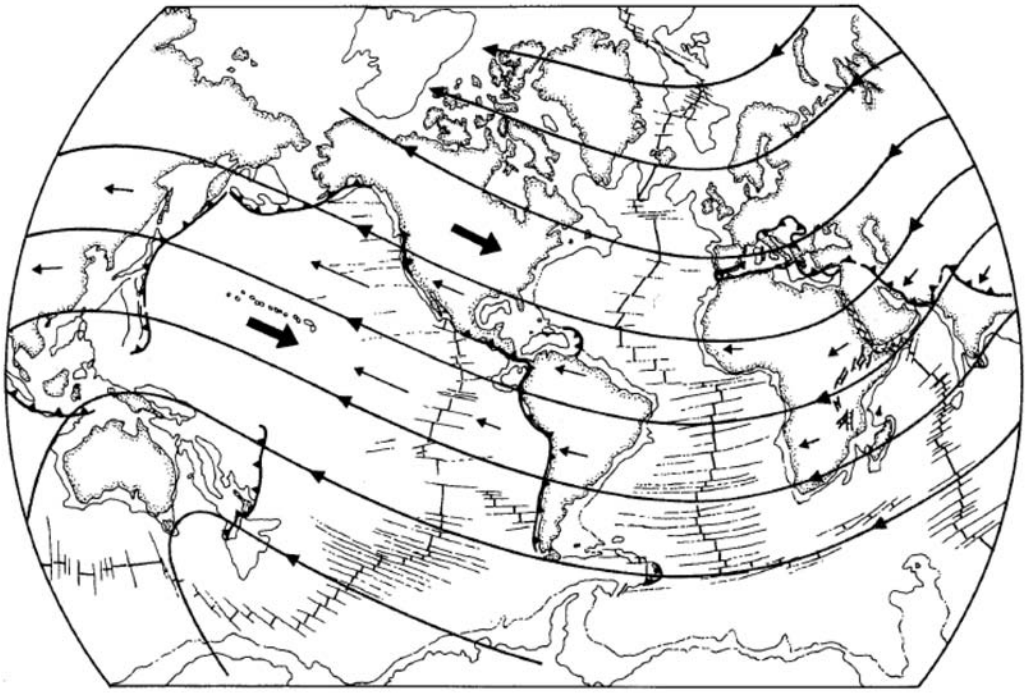

Figure 1.6: Connecting the directions of plate motions, that we can infer from large–scale rift zones or convergent belts from the past 40 Myr, we observe a coherent sinusoidal global flow field along which plates appear to move at different relative velocities in the geographic coordinate system. Thin and big arrows respectively represent the motion of plates relative to the mantle and viceversa. Figure form *Doglioni* [1990].

gins, and the western Pacific subduction zones (4), the western northern and southern Americas Cordilleras (5), and the Alpine-Himalayas system (6) for convergent margins.

In the extensional tectonic settings, we assume that transform faults are parallel to the relative plate motions, whereas in convergent settings, the relative plate motions are constrained by the dominant trend of folds and thrusts, where no significant transpressive tectonics occurs.

Analyzing the relative motions across these tectonic structures crossing the whole lithosphere, it appears that all the lithospheric plates do not move randomly, but follow a global mainstream, with a sinusoidal shape (Figure 1.8). Also in a Pacific–fixed reference frame [*DeMets et al.*, 1994], trajectories of plate motions may be described by the global polarization of movements, except for the North America (NA), that rotates about an internal Euler pole (Figure 1.9). The tectonic mainstream [*Doglioni*, 1990, 1993] can be

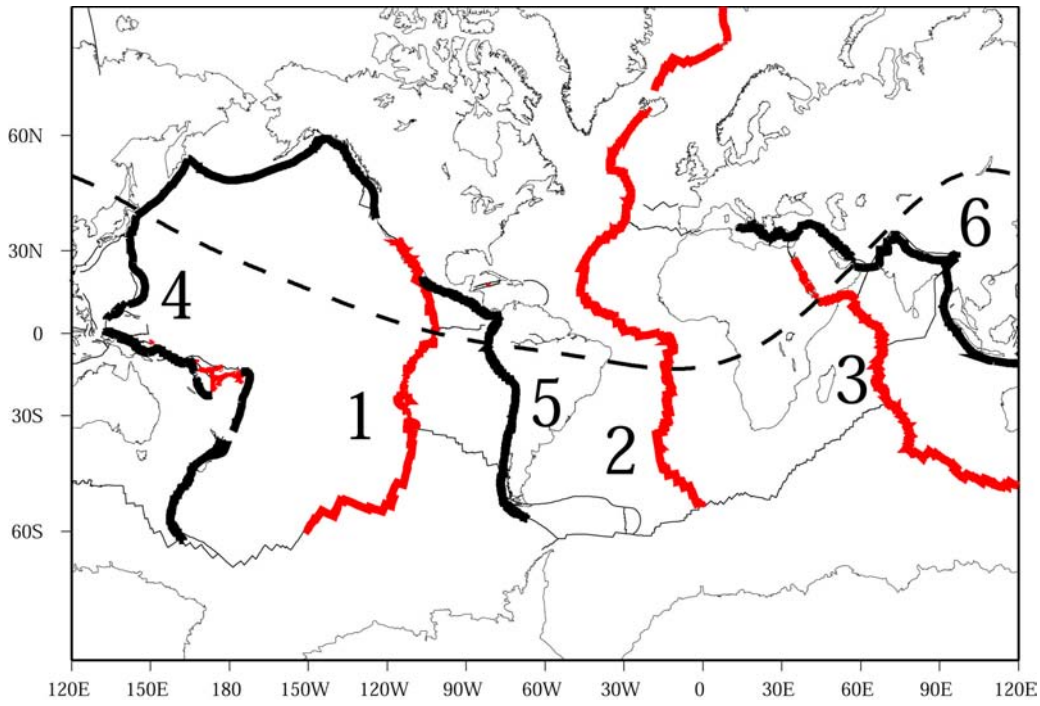

Figure 1.7: Construction of a *main tectonic sinusoid* or *tectonic equator* (black dash line), starting from the Pacific motion direction and linking all the other relative motions in a global circuit using first order tectonic features such as the East Pacific Rise (1), the Atlantic rift (2), the Red Sea, the Indian Ocean rift (3) for the rift zones, and the west Pacific subduction (4), the Andean subduction (5), and the Zagros-Himalayas subduction (6) for convergent margins.

presented here as an imaginary line named the *main tectonic sinusoid*, or *tectonic equator* [*Riguzzi et al.*, 2006] with a great undulation from east Africa to the western Pacific.

The westward drift is then polarizing the tectonic mainstream, i.e., plates move, although at different velocities, toward the ”west” with respect to the underlying mantle (Figure 1.10). The tectonic mainstream may be described as a series of flow lines representing the main plate motion trajectories (Figure 1.6). The main tectonic sinusoid is the line roughly in the middle of the flow where the velocity toward the ”west” is maximum within the plates crossed by the sinusoid [*Riguzzi et al.*, 2006].

The existence of the global tectonic pattern [*Doglioni*, 1990, 1993] can be supported by a geodynamic evidence, such as the directions of the subduction zones, that principally follow the flow lines of the Figure 1.6, and the angle asymmetry of their related slabs (Figure 1.11), that can be worldwide verified. In fact, along this flow, west-directed

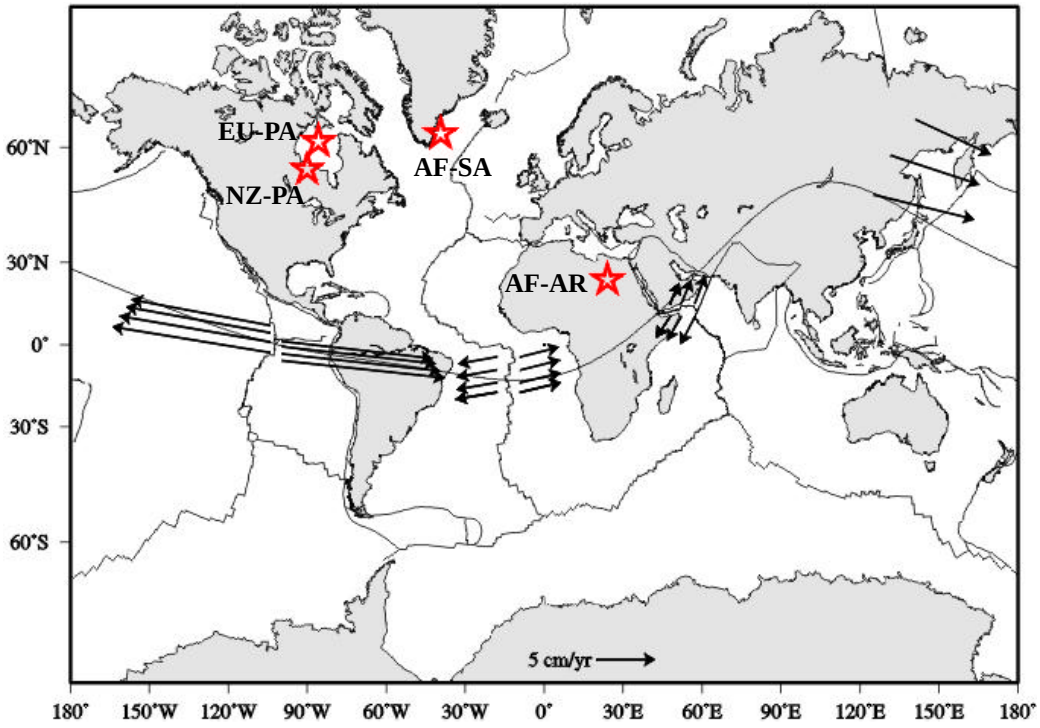

Figure 1.8: Relative plate motions of pairs of plates sharing a boundary show good agreement with the shape of the tectonic equator (black line). Red stars represent relative rotation poles. Data are from the NUVEL–1 plate kinematic model [*DeMets et al.*, 1990].

subduction zones are steeper than those E– or NE–directed, and the associated orogens are respectively characterized by lower structural and topographic elevation, backarc basin, and in the other side by higher structural and morphological elevation and no backarc basin [*Doglioni et al.*, 1999] (Figure 1.11). The asymmetry is striking when comparing western and eastern Pacific subduction zones, and it has usually been interpreted as related to the age of the downgoing oceanic lithosphere. In fact, it is usually considered older, cooler and denser in the western side. However these differences persist elsewhere, regardless the age and composition of the downgoing lithosphere, e.g., in the Mediterranean Apennines and Carpathians Vs Alps and Dinarides, or in the Banda and Sandwich arcs, where even continental or zero-age oceanic lithosphere is almost vertical along west-directed subduction zones. Rift zones are also asymmetric, being the “eastern” side more elevated of about 100-300 m worldwide [*Doglioni et al.*, 2003]. The “westward” drift of the lithosphere implies that plates have a general sense of motion and that they are not moving randomly. If we accept this postulate, plates are moving along this trend at

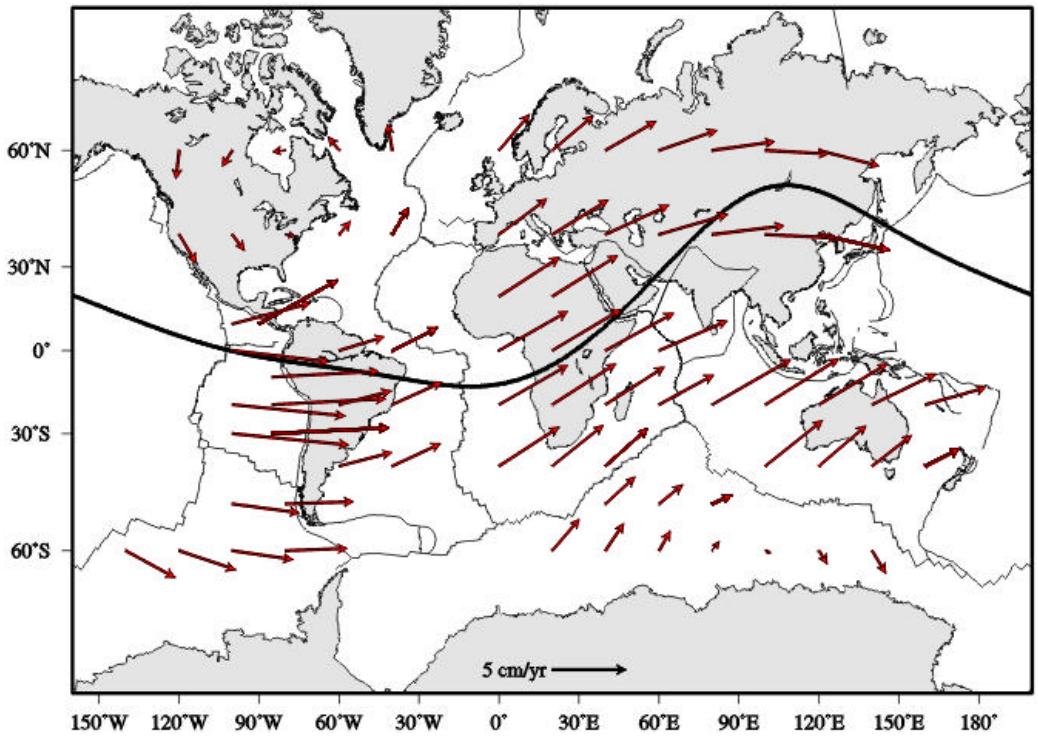

Figure 1.9: Global plate motions in a Pacific–fixed reference frame may describe the shape of the tectonic equator (black line) except for the NA plate, that rotates around an Euler internal pole. Data from the NUVEL–1 plate kinematic model [*DeMets et al.*, 1990].

different velocities toward the "west" relative to the mantle along the flow lines of Figure 1.6, which undulate and are not E–W parallel.

In this view, plates would be more or less detached with respect to the mantle, as a function of the decoupling at their base. The degree of decoupling would be mainly controlled by the thickness and viscosity of the asthenosphere. Lateral variations in decoupling could control the variable velocity of the overlying lithosphere (Figure 1.10). When a plate moves faster toward west with respect to an adjacent plate to the east, the resulting plate margin is extensional; when a plate moves faster to the west with respect to the adjacent plate to the west, their common margin will be of the convergent type (Figure 1.10). The global scale asymmetry of tectonic features and the westward drift of the lithosphere supports a rotational component for the origin of plate tectonics [*Scoppola et al.*, 2006]. The westward drift can be a combined effect of three processes: i) tidal torques act on the lithosphere generating a westerly directed torque decelerating Earth's

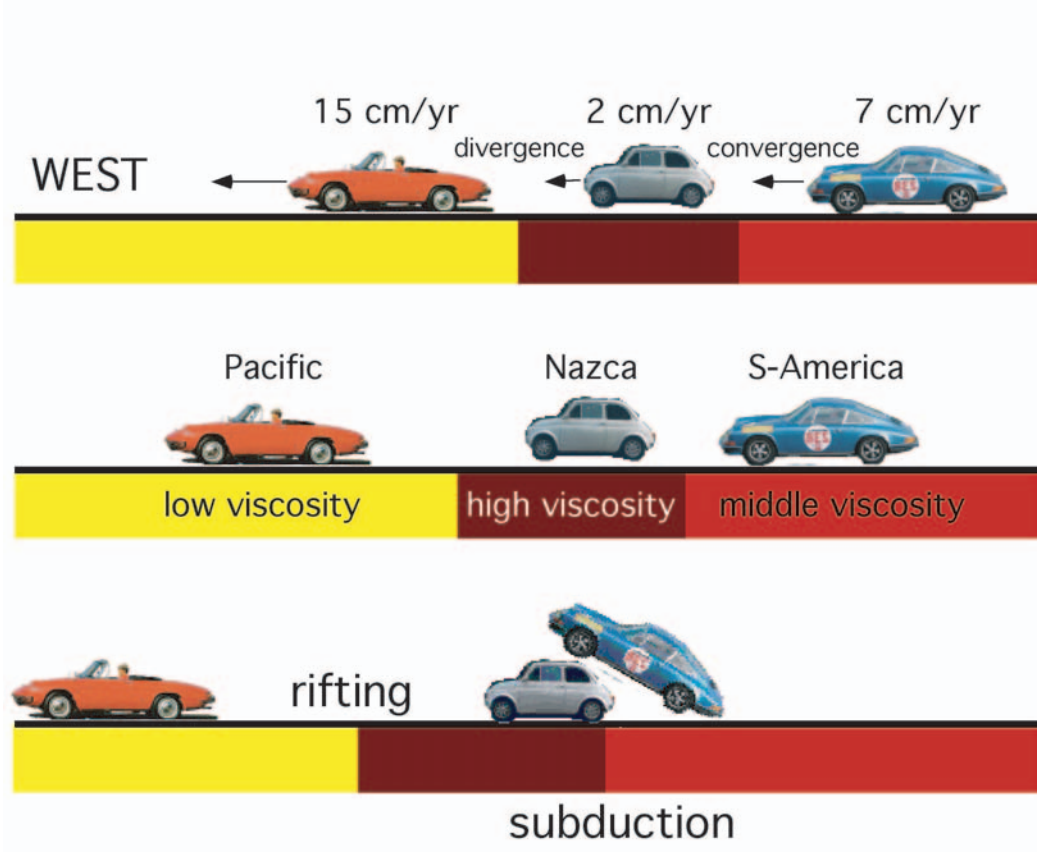

Figure 1.10: Cartoon illustrating that plates (cars) move along a common trail (e.g. the lines of Figure 1.6) but with different velocities toward the west, as indicated by the ”westward” drift of the lithosphere relative to the mantle. The differential velocities control the tectonic environment and result from different viscosities in the decoupling surface, i.e., the asthenosphere. There is extension when the western plate moves westward faster with respect to the plate to the east, while convergence occurs when the plate to the east moves westward faster with respect to the plate to the west. When the car in the middle is “subducted”, the tectonic regime switches to extension because the car to the west moves faster [after *Doglioni*, 1993].

spin; ii) the downwelling of the denser material toward the bottom of the mantle and in the core slightly decreases the moment of inertia and speeding up Earth’s rotation, only partly counterbalancing the tidal drag; iii) thin (3–30 km) layers of very low viscosity hydrate channels should occur in the asthenosphere.

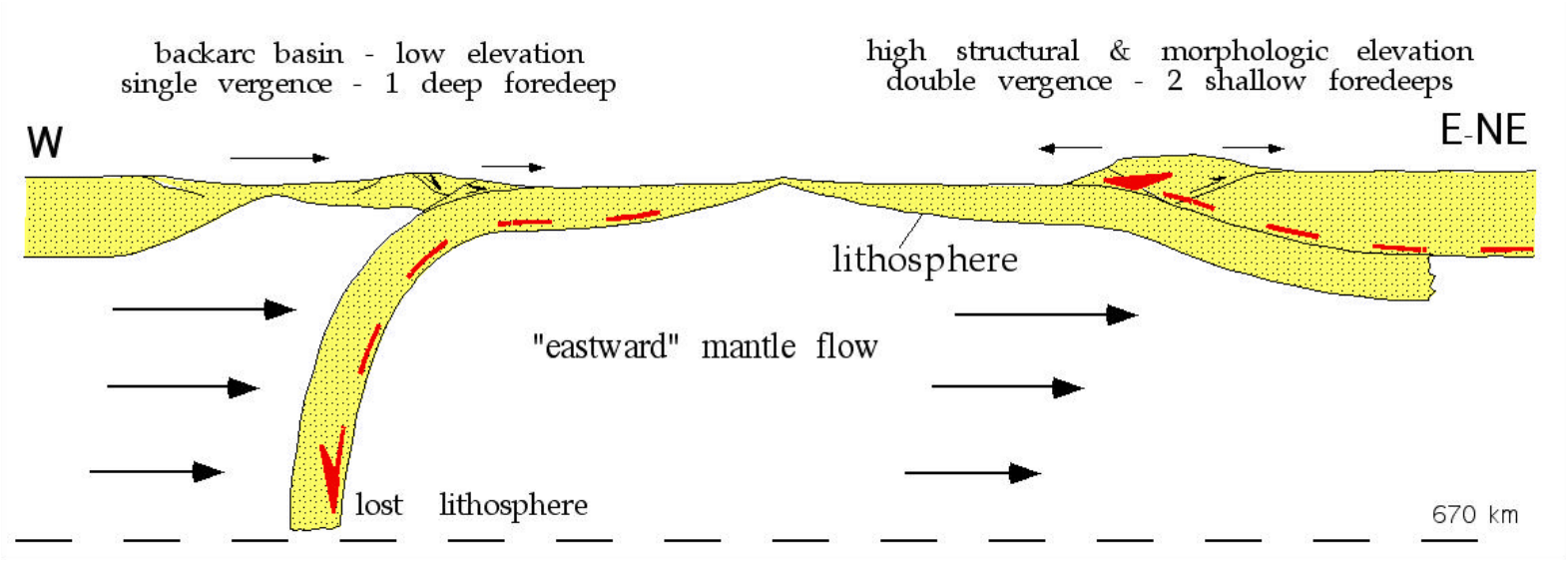

Figure 1.11: West–directed subduction zones are steeper than those E– or NE–directed, and the associated orogens are respectively characterized by lower structural an topographic elevation, backarc basin, and in the other side by higher structural and morphological elevation and no backarc basin. This asymmetry would be explained by the relative motion between the whole lithosphere (toward the west) and the underlying mantle (toward the east) [*Doglioni et al.*, 1999].

Chapter 2

Kinematics on the tectonic equator

The motion of the lithosphere with respect to the underlying mantle seems to be directed along a global mainstream and all the lithospheric plates, over the Earth's surface, follow global flow lines, that mainly represent trajectories of the motion. Lines of geological evidence suggest that one of these flow lines is strongly characterized as the tectonic equator, that is not a common geographical great circle, but is generally WNW-ESE, with a large SW-NE trending undulation from east Africa to the western Pacific.

Some plate kinematic models describe plate motions in absolute reference frames (e.g. the mean–lithosphere or NNR), but the global tectonic pattern is not well recognized and emphasized. Space geodesy data may support the existence of the flow lines and it is largely possible to individuate the tectonic equator direction.

In this chapter, we investigate the correlation of plate velocities by making use of the predictions of many plate kinematic models in the NNR framework and the main trajectory for plate motions (i.e. the tectonic equator), comparing the angle distribution of the velocity vectors with the shape of the tectonic equator, making statistical estimates of the correlation coefficient R. We analyzed four of the most important absolute kinematic models of plate tectonics, one deriving from geological and geophysical data, such as the NNR-NUVEL1A [*Argus and Gordon*, 1991], and the other three deriving from space geodesy data, such as the REVEL [*Sella et al.*, 2002], the APKIM [*Drewes and Meisel*, 2003], and the GSRM1 [*Kreemer and Holt*, 2003] and we found that the tectonic equator is on a large scale confirmed. Moreover, choosing a priori the existence of the global tectonic pattern, we obtained that, adding by vector summation, different values of the westward net rotation, the correlation coefficient becomes higher as far as, for an indicative westward velocity value, the correlation tends to the maximum.

2.1 Introduction

A difficult task in geodynamics is the definition of an absolute reference frame useful for the representation of plate motions, due to a number of kinematic uncertainties (e.g., lateral variations of the coupling between the lithosphere and the asthenosphere, or the depths of the hotspots). The most updated information on present plate motions is based on space geodesy data [*Heflin et al.*, 2004], where the rate of motions are essentially estimated from GPS continuous observations (Figure 2.1) in a no-net-rotation frame (NNR) [*Solomon and Sleep*, 1974], as assumed by the International Terrestrial Reference Frame (ITRF2000) [*Altamimi et al.*, 2002, 2003].

The NNR condition is currently applied by aligning the TRF (Terrestrial Reference Frame) [*Altamimi et al.*, 2002] to the NNR–NUVEL1A model [*Argus and Gordon*, 1991] to try to guarantee its co-rotation with the Earth surface. These data largely confirm the NNR–NUVEL1 data set, the NUVEL–1 in a no–net–rotation frame, based on past ocean floor magnetic anomalies and focal mechanisms [*DeMets et al.*, 1990; *Argus and Gordon*, 1991; *DeMets et al.*, 1994], with a good match between past and present day plate motions [*Stein*, 1993]; therefore, it is assumed that present analysis is a good indicator of the main Cenozoic and Neozoic plate movements.

Since the NNR hypothesis is an arbitrary choice introduced in order to fix the rank deficiency proper of the positions estimation problem based on space geodesy observations, this information is able to describe only for relative plate motions [*Dermanis*, 2001, 2002], whereas any absolute motion relative to the mantle is not accounted for.

On the other hand, under the hypothesis of the global tectonic pattern (see section 1.5) the absolute plate motions described in the NNR framework, as space geodesy data [*Heflin et al.*, 2004] largely confirm the existence of the global pattern, (Figure 2.1), especially in the Pacific and along the undulation.

Here, we try to estimate how strong could be the correlation between NNR plate kinematic models and the shape of the global tectonic pattern.

2.2 Methods

2.2.1 Analytic representation of the tectonic equator

Under the hypothesis of a global tectonic pattern, the tectonic equator represents the main trajectory for plate motions. This particular curve, build following the direction of the six major tectonic features over the Earth's surface, as the three mid-ocean ridge (e.g. Pacific,

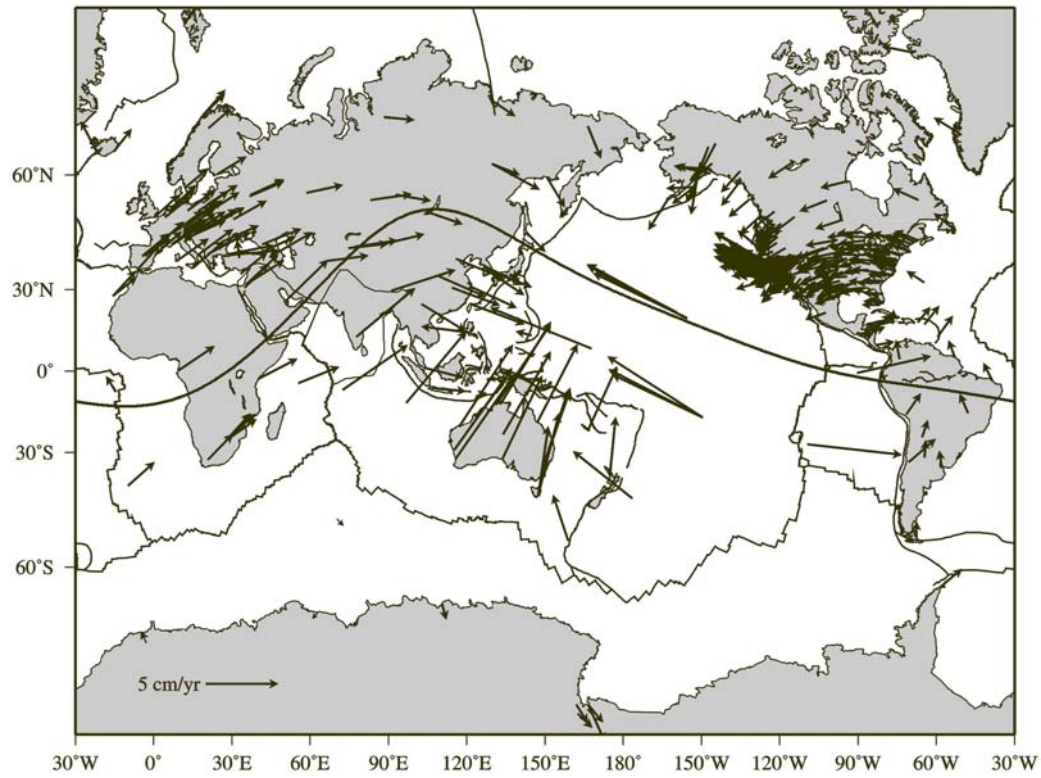

Figure 2.1: Space geodesy data [*Heflin et al.*, 2004] vs the tectonic equator. The data largely confirm the existence of the global pattern especially in the Pacific region and, on large scale, along the undulation of 15000 km from east Africa to the western Pacific. It is possible to note how near the Australian and Pacific boundary, velocity vectors confirm the flow lines that have a quite instantaneous inversion (see also Figure 1.6).

Atlantic and Indian ridge) and the three principal trenches (e.g. the west Pacific the South America and the himalayan trench), passes through six lithospheric plate, starting from the Pacific and closing the circuit in Eurasia (see section 1.5).

Riguzzi et al. [2006] presented an analytic representation of the tectonic equator, useful to describe plate motions with respect to the mantle. Following these methods, a 3^{rd} order trigonometric polynomial in geographic co–ordinates (θ, λ), being the latitude and the longitude in radians respectively, can be used to describe the shape of the tectonic equator:

$$f(\lambda) \cong \frac{a_0}{2} + \sum_{i=1}^{3} \Big(a_i \cos(i\lambda) + b_i \sin(i\lambda) \Big) \tag{2.1}$$

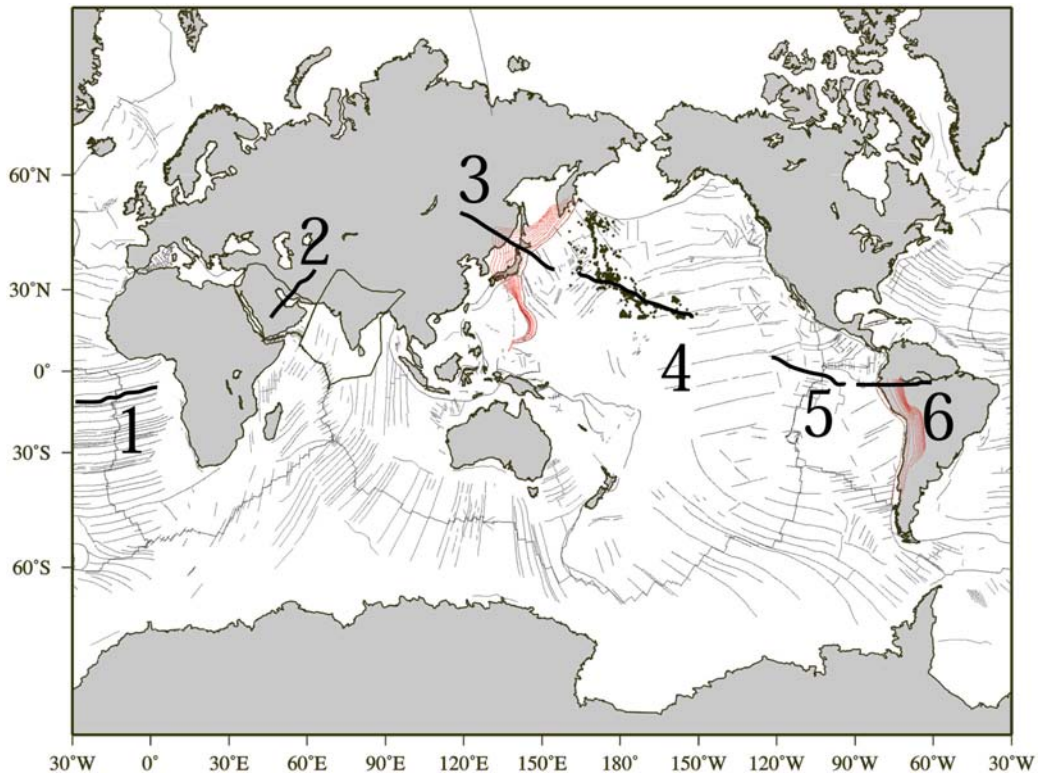

Figure 2.2: Map of the main tectonic features selected to introduce azimuthal constraints into the main tectonic sinusoid estimation 1 = MAR, Mid Atlantic Ridge; 2 = RSEAR, Red Sea and East Africa Rift; 3 = JS, Japan Subduction; 4 = HH, Hawaiian sea–mount chain; 5 = EPR, East Pacific Rise; 6 = AS Andean Subduction, . See Table 2.1

where the seven approximated parameters are reported in Table 2.1.

The shape of the tectonic equator defined by the equation (2.1) (Figure 2.4a), is constrained to some geological conditions: the direction of the tectonic line must be equal to the mean azimuth of the direction of motion across the largest tectonic features [*Searle*, 1986; *Gordon*, 1995]. This implies to equate the first derivative of the analytical expression of the tectonic mainstream to the tangent of the mean azimuth.

For this purpose, *Riguzzi et al.* [2006] selected the directions of some principal tectonic structures (Table 2.1 and Figure 2.2), used for the analytical representation of the global tectonic pattern: the Mid Atlantic Ridge (MAR), the Red Sea and East Africa Rift (RSEAR), the Japan Subduction (JS), the Hawaiian sea–mount chain (HH), the East Pacific Rise (EPR) and the Andean Subduction (AS). The parameters of the tectonic equator

Table 2.1: Azimuth of the tectonic structures chosen for the definition of the tectonic equator and parameters of the tectonic equator function.

Number	Identifier	Definition	Position[a]		Azimuth[b]
			°N	°E	
1	MAR	Mid Atlantic Ridge	-15.012	344.978	80
2	RSEAR	Red Sea and East Africa Rift	30.023	59.989	36
3	JS	Japan Subduction	44.977	147.995	301
4	HH	Hawaiian Sea–mount chain	19.996	205.004	293
5	EPR	East Pacific Rise	0.000	260.008	279
6	AS	Andean Subduction	0.000	27.020	90

Approximated parameters of the Tectonic Equator Function

a_0	a_1	a_2	a_3	b_1	b_2	b_3
0.54417	-0.34078	-0.13687	-0.01431	0.40611	-0.0558	-0.04333

[a] Position is calculated as a mean value.

[b] In degrees clockwise from north.

function of defined by *Riguzzi et al.* [2006] (equation 2.1) are estimated according to the least squares principle, in an iterative fashion, due to the non–linearity of the their equation system, starting from their approximated values. The final precision of the tectonic equator, or main tectonic sinusoid, after the least squares estimation is $\sigma = 0.2$ rad, which corresponds to about 1000 km of uncertainty along the N–S direction.

2.2.2 Theory of angle comparison

Most of the absolute plate kinematic models describe the motion of the lithosphere relative to the mean–lithosphere frame (NNR) and the motion directions of all the plates seem to confirm the existence of the tectonic equator (Figure 2.1). Here, we want to investigate if there is a correlation between the velocity vector distribution of plate kinematic models

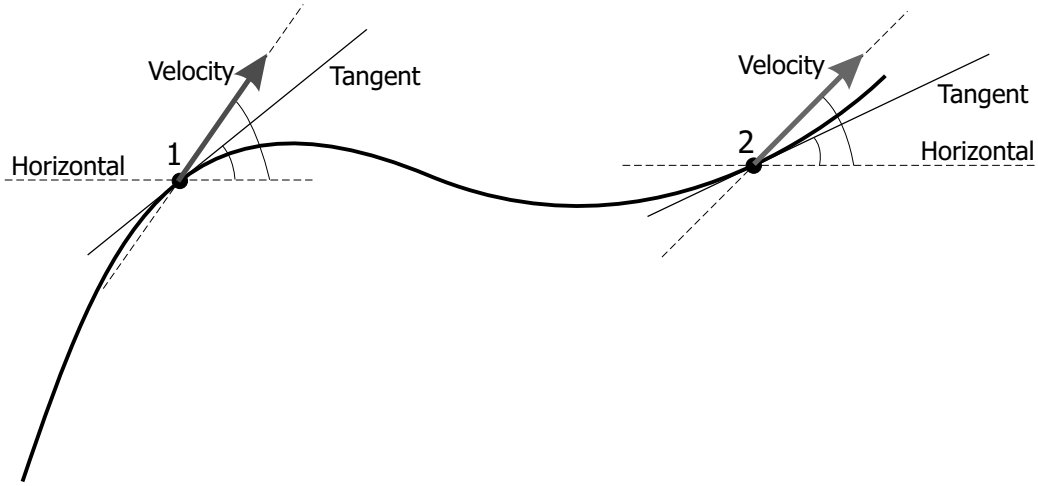

Figure 2.3: Generic scheme to demonstrate the existence of a global tectonic pattern. A velocity vector always lies on a tangent of the trajectory; after selecting a curve that is not the main trajectory for plate motion, on the two generic points, a plate kinematic model is applied. The angles β_i, $i = 1, 2$, referred to the horizontal, indicate the motion direction of vector velocities and they have to be compared with the angle α_i, $i = 1, 2$, that represent the angle of the tangents at the curve. If the $\beta_i - \alpha_i$ angles are close to zero, the plate kinematic model imply the curve is the trajectory for plate motion.

in the NNR–framework and the shape of tectonic equator, since the velocity vectors of the points of a plate imply trajectories for that plate motion.

In general, a velocity vector of a plate point lies on a tangent, computed in that point, of the plate trajectory, and it forms an angle with the horizontal that characterizes the motion direction. To reach the aim that there are some pieces of kinematic evidence for the existence of the tectonic equator, it is necessary to select some points of the $f(\lambda)$ (Equation 2.1) and then to apply a kinematic model. The angle of the velocity vector in a point has to be compared with the angle of the tangent at the tectonic equator in that point itself. In Figure 2.3 is represented a scheme where two velocity vectors are applied in two generic points of a curve that is not the trajectory implied by the vectors themselves. To calculate how the angle β_i, $i = 1, 2$ (referred to the horizontal) of velocity vectors, obtained with a plate kinematic model, differ from the tangents of the curve, the values of the angles α_i, $i = 1, 2$ are requested. Once the $\beta_i - \alpha_i$ angles are close to or exactly zero, this implies the curve is approximatively or exactly the trajectory for plate motion described by that plate kinematic model.

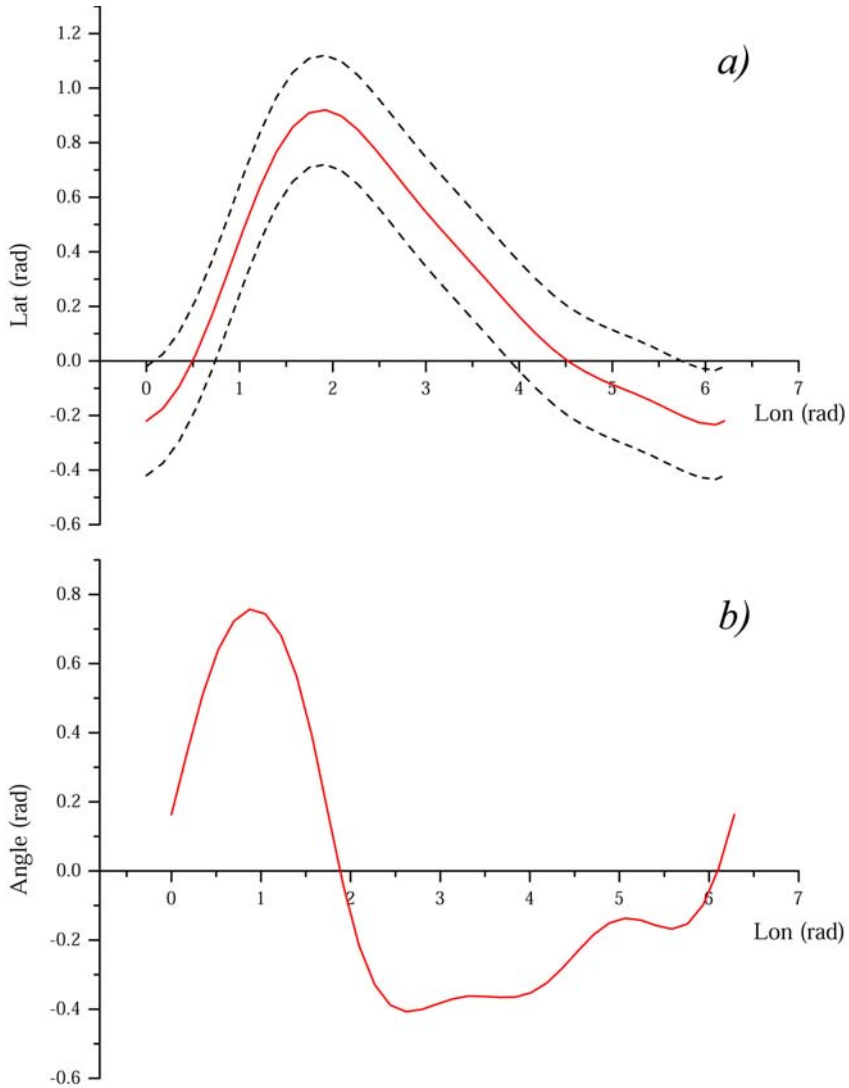

Figure 2.4: (a) Tectonic equator function with 1–σ confident limit. (b) Distribution of angles of the tangents of the tectonic equator. This curve (called the *angle distribution*) is a six free-parameter function and it is used to estimate correlation between the global tectonic pattern and plate kinematic models.

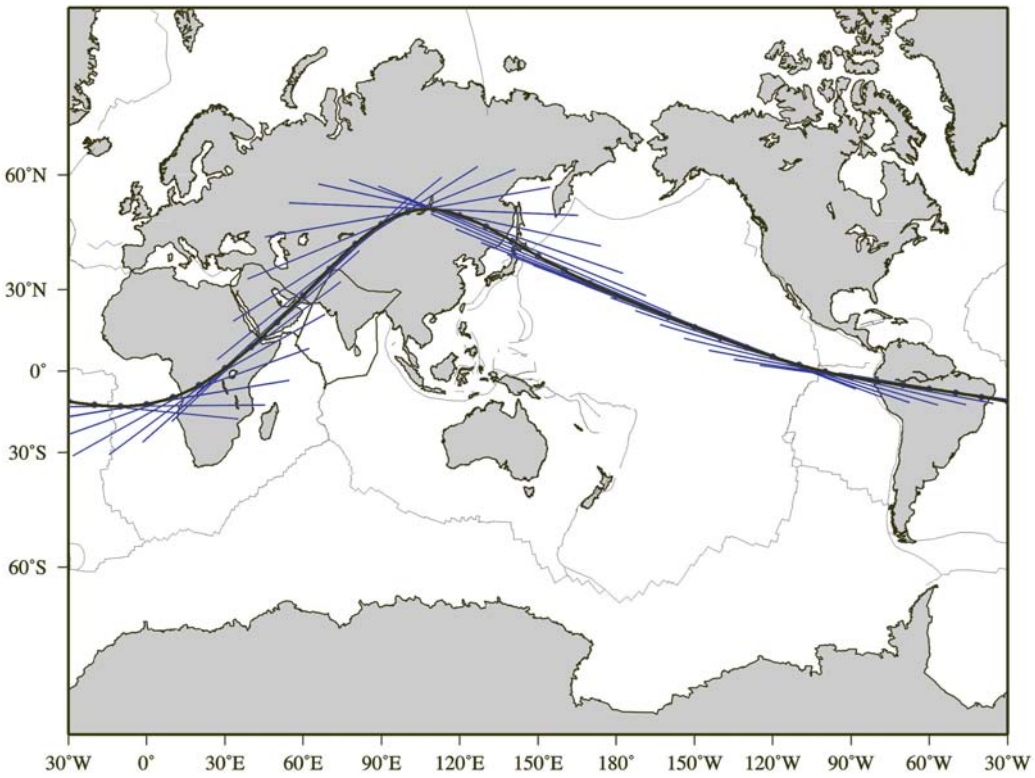

Figure 2.5: Tangents of the the tectonic equator at selected 36 points.

In the case of the global tectonic pattern, the generic curve of the Figure 2.3 becomes the tectonic equator that is the pretty well described in an analytic way by the $f(\lambda)$ (Figure 2.4a).

To obtain the angles α_i of the tangents at the tectonic equator, the first step consists in making the first derivative of the $f(\lambda)$ (Equation 2.1) as following:

$$g(\lambda) = \frac{\mathrm{d}}{\mathrm{d}\lambda} f(\lambda) \tag{2.2}$$

where the $g(\lambda)$ represents the values of the angular coefficients of the tangents of the tectonic equator relative to the horizontal.

To obtain the angle distribution α_i, we use the following

$$h(\lambda) = \tan^{-1} g(\lambda) \tag{2.3}$$

where the $h(\lambda)$ represents the values of the angle α_i of the tangents relative to the horizontal and it is reported in Figure 2.4b.

To study the correlation between the angle α_i and the angles of the velocity vectors of the plate kinematic models, we need to know the values of the β_i angles that we compute as following:

$$\beta = \tan^{-1}\left(\frac{V^{(\theta)}}{V^{(\lambda)}}\right) \tag{2.4}$$

where $V^{(\theta)}$ and $V^{(\lambda)}$ are the transversal and the longitudinal component of the velocity vector computed in a point respectively (see Appendix A).

The verification of the existence of the tectonic pattern consists in the application of some absolute plate kinematic models on the selected points of the tectonic equator that passes on six lithospheric plates. The Equations 2.3 and 2.4, formulated on the base of the arctangent function in the interval $[0, \frac{\pi}{2}]$, allow to compare the angles of the velocity vectors with the angle distribution (Figure 2.4b) of the tangents of the tectonic equator. The best fit would result if vector angle values lied on the angle distribution.

To estimate this correlation, we use a statistical fit based on the angle distribution, with six free parameters and statistical estimates are only about the correlation coefficient R that indicates if two data distributions differ or not. The correlation is mainly based on the orientation of the tectonic equator relative to the horizontal and not on the motion direction. In this case it is sufficient that velocity vectors indicate a good agreement with the tectonic equator tangent angles.

2.3 Correlation estimates in the NNR–framework

We selected 36 points of the tectonic equator, one every ten degrees. At those points we compute the tangents at the trajectory and then we applied different plate kinematic model to estimate the correlation. The tectonic equator passes through six lithospheric plates, the Africa, the Arabia, the Eurasia, the Pacific, the Nazca and the South America.

We analyzed four of the most important absolute kinematic models of plate tectonics, one deriving from geological and geophysical data, the NNR-NUVEL1A [*Argus and Gordon*, 1991], and the other three deriving from space geodesy data, the REVEL [*Sella et al.*, 2002], the APKIM [*Drewes and Meisel*, 2003], and the GSRM1 [*Kreemer and Holt*, 2003], choosing the kinematic parameters of the six plates crossed by the tectonic equator (Table 2.2 and Table 2.3).

Table 2.2: Euler poles and angular velocities of the six plates where tectonic equator passes through. Data are about the plate kinematic models analyzed, the NNR-NUVEL1A [*Argus and Gordon*, 1991; *DeMets et al.*, 1994], and the REVEL [*Sella et al.*, 2002].

	NNR–NUVEL1A			REVEL		
PLATE	Euler Pole		ω	Euler Pole		ω
	°N	°E	$^\circ$ Myr^{-1}	°N	°E	$^\circ$ Myr^{-1}
AFRICA	50.569	-73.978	0.290	52.250	-80.180	0.253
ARABIA	45.233	-4.464	0.546	51.470	2.890	0.327
EURASIA	50.631	-112.275	0.234	58.270	-102.210	0.257
PACIFIC	-63.045	107.325	0.641	-64.210	112.740	0.655
NAZCA	47.408	-100.130	0.743	44.450	-99.490	0.647
SOUTH AMERICA	-25.325	-124.43	0.116	-25.830	-135.380	0.106

Table 2.3: Euler poles and angular velocities of the six plates where tectonic equator passes through. Data are about the plate kinematic models analyzed, the APKIM [*Drewes and Meisel*, 2003], and GSRM1 [*Kreemer and Holt*, 2003]

	APKIM			GSRM–1		
PLATE	Euler Pole		ω	Euler Pole		ω
	°N	°E	$^\circ$ Myr^{-1}	°N	°E	$^\circ$ Myr^{-1}
AFRICA	51.610	-98.480	0.290	52.600	-72.300	0.294
ARABIA	29.380	-82.420	0.414	50.600	-2.700	0.550
EURASIA	56.530	-98.480	0.272	56.400	-97.400	0.279
PACIFIC	-64.300	105.52	0.658	-64.900	105.500	0.650
NAZCA	46.210	-99.930	0.652	44.400	-98.400	0.651
SOUTH AMERICA	-10.740	-120.370	0.109	-14.500	-119.500	0.114

Table 2.4: Comparison among parameters of angle distribution of the tangents of the tectonic equator for 36 selected points and angles of velocity vectors of different NNR plate motion models.

	Free Parameters					
Model	P1	P2	P3	P4	P5	P6
Angle Distribution	0.34073	0.40602	0.27375	-0.11153	0.04289	-0.13005
NNR–NUVEL1A	0.54580	0.56350	0.83416	0.30733	0.57585	0.17631
REVEL	0.55549	0.46210	0.71315	0.24831	0.47884	0.19767
APKIM	0.78128	0.52267	0.98954	0.30327	0.62181	0.26648
GSRM1	0.68174	0.47441	0.86887	0.25852	0.54873	0.22892

The angle distribution (Equation 2.3 and Figure 2.4b) can be used as the statistical estimator to make correlation estimates between plate kinematic models and the tectonic equator. By definition, the function $h(\lambda)$ (Equation 2.3) has six parameters P_i, $i = 1 \ldots 6$. This estimator can be utilized in a six-free-parameter non–linear fit applied on angles of velocity vectors of plate motions. Estimated parameters of the angle distribution are reported in Table 2.4.

Applying the statistical fit to the vector angles of the selected plate kinematic model in the NNR–framework, corresponds to make a comparison between the parameters P_i of the angle distribution and the estimated parameters of the vector angles of those plate motion models. This comparison is quantified by making use of the correlation coefficient R. The parameters of angle distribution of the Table 2.4 result in a correlation coefficient $R = 1$. Any difference of angles computed after applying plate kinematic models, gives a lower value of R.

The plate kinematic models analyzed are very similar and do not differ too much, except for small values of plate angular velocities and co-ordinates of Euler poles (Table 2.2 and Table 2.3). This implies that correlation results are very similar. Correlation estimates are reported in Table 2.5.

Results (Figures 2.6, 2.7, 2.8, 2.9) show that the velocity vectors both deriving from geological and geophysical data and from space geodesy, may describe a pattern.

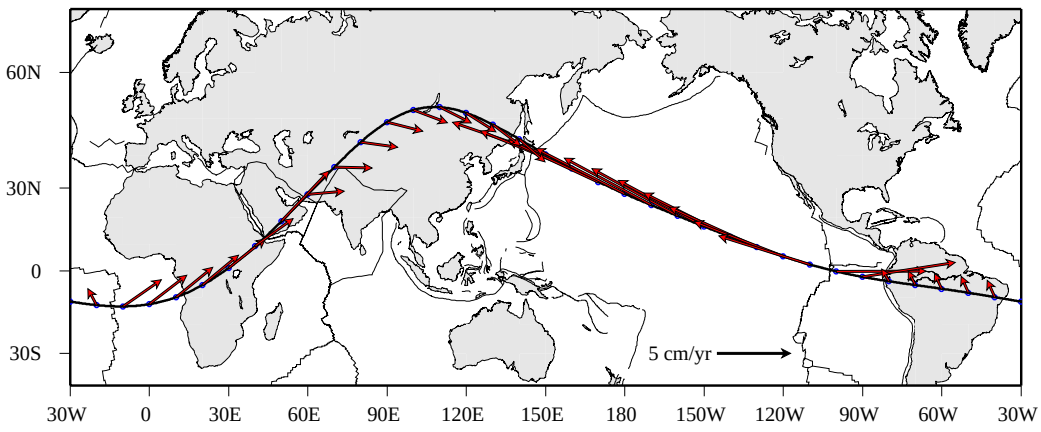

(a)

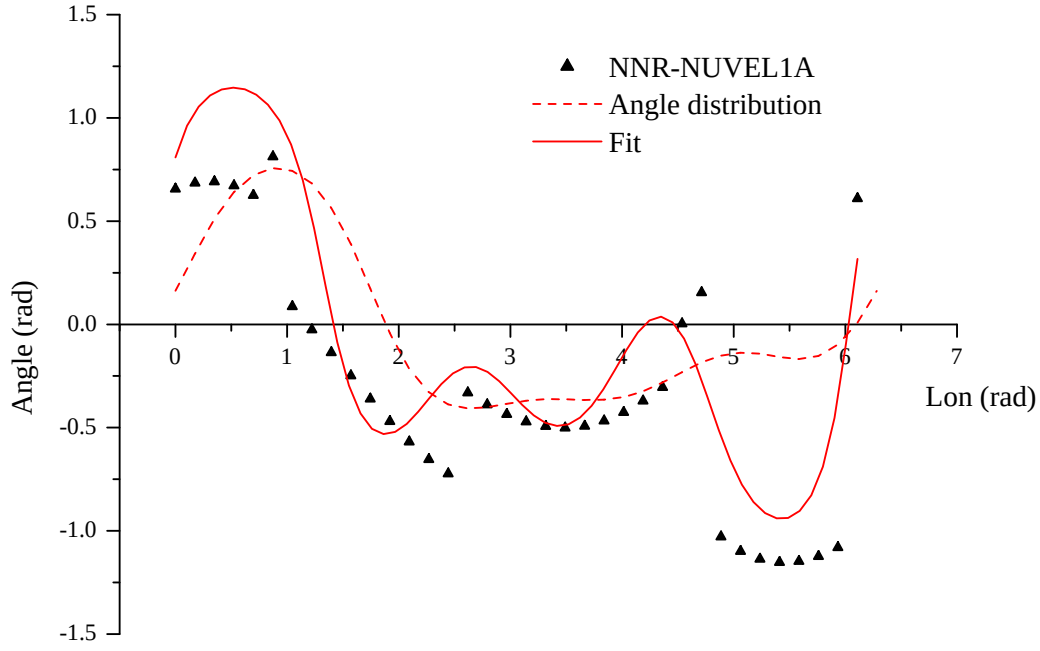

(b)

Figure 2.6: (a) The NNR–NUVEL1A plate kinematic model [*Argus and Gordon*, 1991] applied at the 36 selected points on six lithospheric plate crossed by the tectonic equator. (b) Statistical comparison between angles of the tangents of the tectonic equator and the angles of the velocity vectors of the NNR–NUVEWL1A. Correlation estimates give $R = 0.82647$.

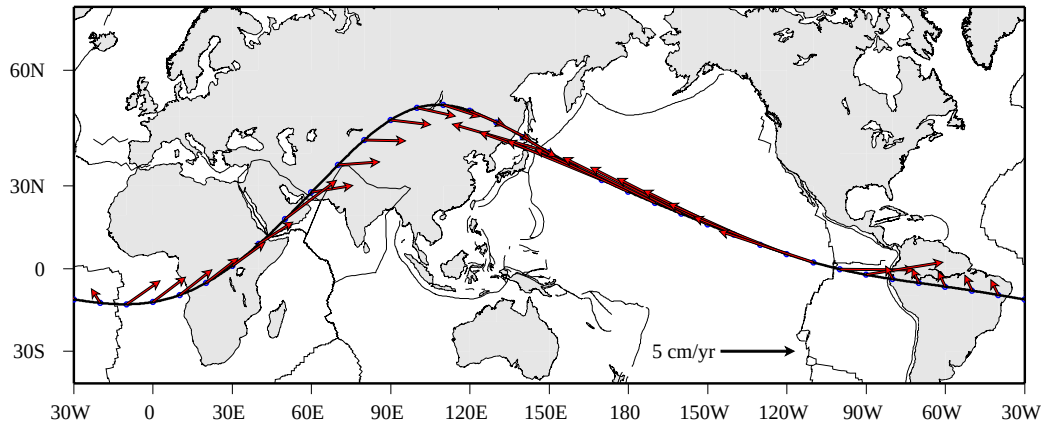

(a)

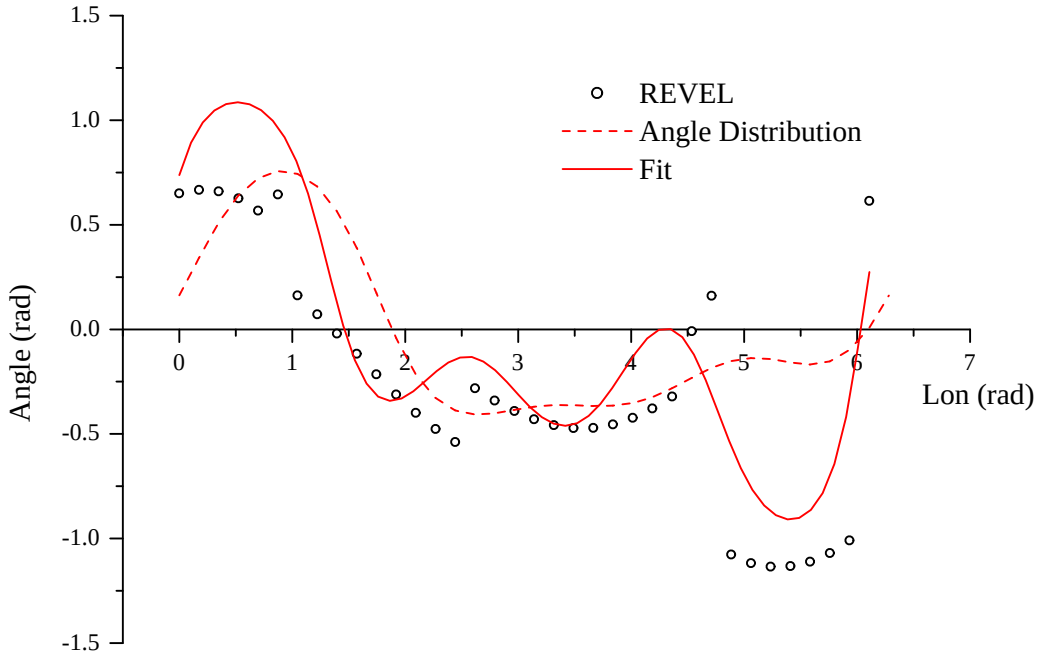

(b)

Figure 2.7: (a) The REVEL plate kinematic model [*Sella et al.*, 2002] applied at the 36 selected points on six lithospheric plate crossed by the tectonic equator. (b) Statistical comparison between angles of the tangents of the tectonic equator and the angles of the velocity vectors of the REVEL. Correlation estimates give $R = 0.82860$.

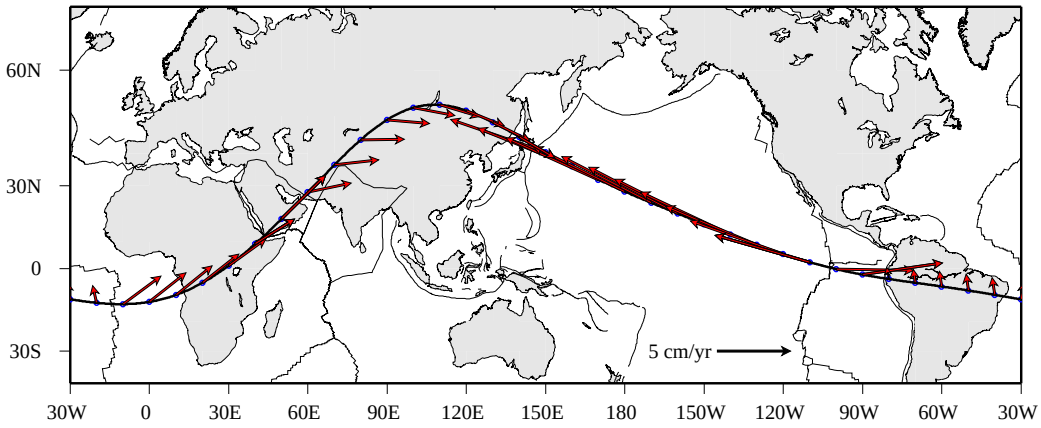

(a)

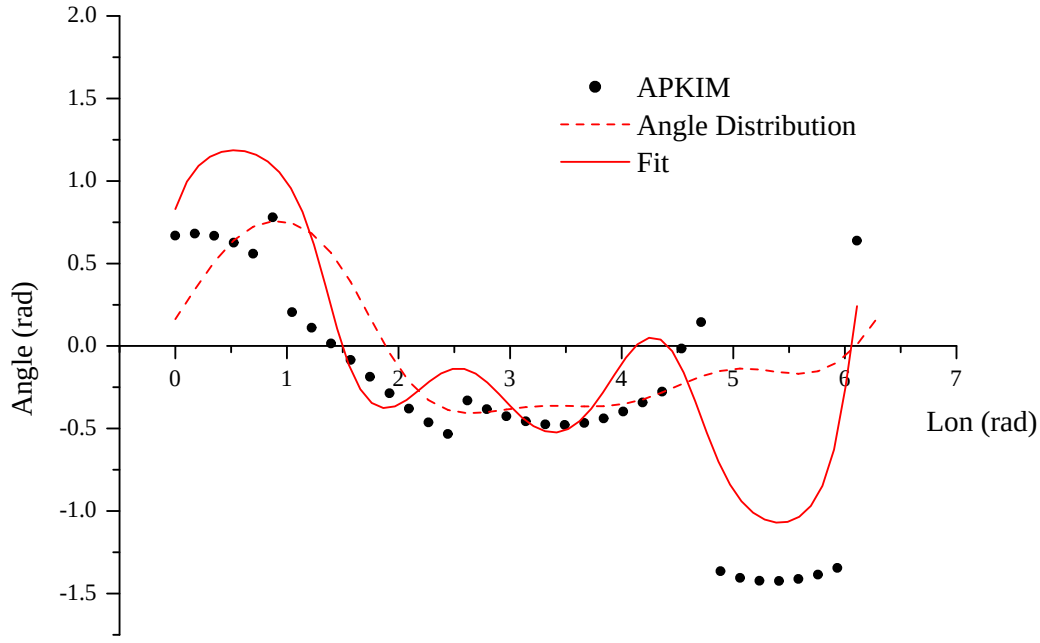

(b)

Figure 2.8: (a) The APKIM plate kinematic model [*Drewes and Meisel*, 2003] applied at the 36 selected points on six lithospheric plate crossed by the tectonic equator. (b) Statistical comparison between angles of the tangents of the tectonic equator and the angles of the velocity vectors of the APKIM. Correlation estimates give $R = 0.82062$.

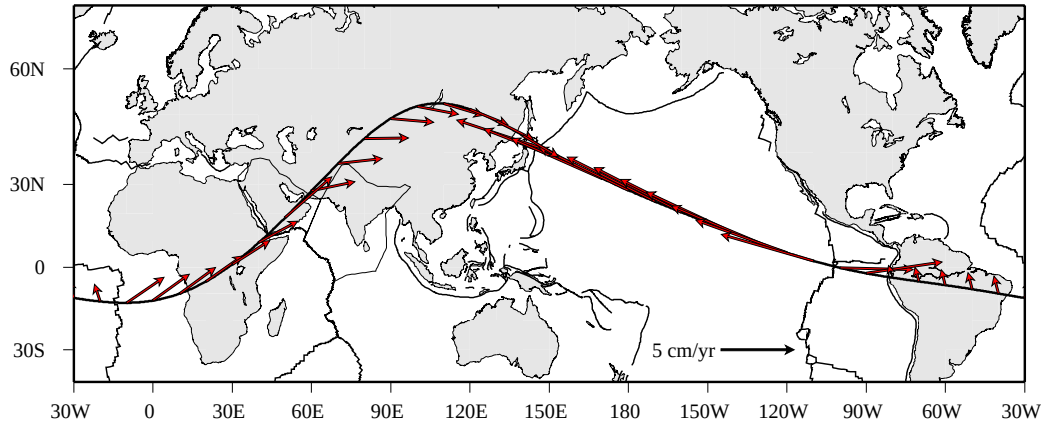

(a)

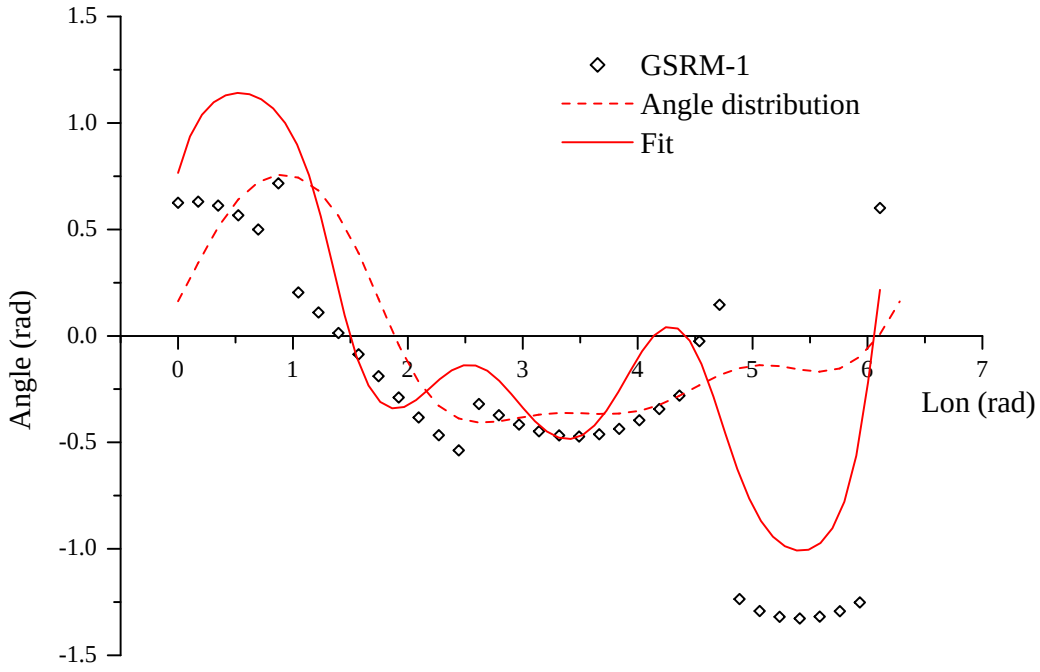

(b)

Figure 2.9: (a) The GSRM–1 plate kinematic model [*Kreemer and Holt*, 2003] applied at the 36 selected points on six lithospheric plate crossed by the tectonic equator. (b) Statistical comparison between angles of the tangents of the tectonic equator and the angles of the velocity vectors of the GSRM–1. Correlation estimates give $R = 0.80844$.

Table 2.5: Correlation between angle distribution and plate kinematic models, by making use of the coefficient of determination R^2 and correlation coefficient R.

Model	Reference	R^2	R
NNR–NUVEL1A	[*Argus and Gordon*, 1991]	0.68305	0.82647
REVEL	[*Sella et al.*, 2002]	0.68658	0.82860
APKIM	[*Drewes and Meisel*, 2003]	0.67342	0.82062
GSRM1	[*Kreemer and Holt*, 2003]	0.65358	0.80844

A global tectonic pattern, here represented by the shape of the tectonic equator, is well described by NNR plate kinematic models especially in the Pacific, the Arabia and the East Africa. The great undulation passing through the Baikal Rift is approximately described by the clockwise rotation of the Eurasia. In the Nazca plate the analyzed velocities show differences of angles, whereas in the South America plate there is a complete misfit with the S–N direction of the velocity vectors versus the E–W direction of the tectonic equator.

It is useful to remember again that, at this stage, the comparison is not made with the directions of plate motions, but with the azimuths of their trajectories, that would be aligned to the shape of the tectonic equator to reach the maximum of the correlation.

Moreover, to be consistent with the NNR-NUVEL1A [*Argus and Gordon*, 1991], the Somalia plate presented in the REVEL [*Sella et al.*, 2002], the APKIM [*Drewes and Meisel*, 2003] and GSRM–1 [*Kreemer and Holt*, 2003] was here treated as a part of the Africa plate, after testing not evident differences of the angle directions computed with the motion parameters of the Somalia plate, with respect to the the angles obtained with the Africa motion parameters.

This first analysis gives that there is best agreement for the REVEL model with $R = 0.82860$, then follow the NNR–NUVL1A with $R = 0.82647$ and the APKIM with $R = 0.82062$, that have very similar values. The GSRM–1 show instead a lower agreement with the tectonic equator with a correlation coefficient $R = 0.80844$.

2.4 Correlation estimates in a particular hotspot frame

The plate kinematic models analyzed in the previous section describe plate motion in the NNR–framework. Methods proposed, for example, by *Jurdy* [1990] and *Argus and*

Table 2.6: Computed net–rotation angular velocities after testing two different Pacific plate motions (*option 1* from *Gripp and Gordon* [2002] and *option 2* from *Wessel and Kroenke* [1997]). Geometrical factors used come from *Argus and Gordon* [1991], whereas relative plate motions are related to the NUVEL1A [*DeMets et al.*, 1990, 1994]

	Pacific Euler Vector			Computed Net–Rotation	
	$^{\circ}$N	$^{\circ}$E	$^{\circ}$ Myr^{-1}	$^{\circ}$ Myr^{-1}	mm yr^{-1}
option 1	-61.467	90.326	1.0613	0.4359	48.473
option 2	-25.000	153.000	1.2000	0.9066	100.810

Gordon [1991] are useful to change the reference frame passing from the NNR to the hotspot frame by making use of the net–rotation angular velocity.

Here, we defined a particular hotspot frame based on the assumption of the existence of the tectonic equator and there we made correlation estimates, as in the previous section. This means that we added the net-rotation velocity to the plate kinematic model on the tectonic equator, assuming that on this line it reaches the maximum value. We tested two options of net–rotation, one proposed by *Gripp and Gordon* [2002] and the other newly computed (Table 2.6). Using Equation 1.4 and geometrical factor proposed by *Argus and Gordon* [1991] (Table 1.1) we find a net–rotation velocity using a Pacific plate velocity proposed by *Wessel and Kroenke* [1997]. In fact, using the Table 15 of *Gripp and Gordon* [2002] that compares other estimates of the Pacific angular velocity relative to the hotspots, we chose the rate proposed by *Wessel and Kroenke* [1997], because it gives a completely different net–rotation angular velocity (Table 2.6). With these two options, two net–rotation velocities are found, one of 0.4359 $^{\circ}$ Myr^{-1} (*option 1*) with a maximum linear velocity of 48.473 mm yr^{-1}, and the other of 0.9066 $^{\circ}$ Myr^{-1} (*option 2*), that gives a linear velocity of 100.810 mm yr^{-1}.

Riguzzi et al. [2006] defined the tectonic equator as the line where the surface velocity toward the ”west” is maximum within the plates crossed by the pattern. This allows to apply the maximum value of the net–rotation linear velocities of the two options on the tangents of the tectonic equator (Figures 2.10a and 2.10b). They are added, by vector summation, to the models in the NNR–framework (except the GSRM–1, because shows less correlation with the tectonic mainstream) to study the correlation estimates in this particular hotspot frame. Results are in Figures 2.11, 2.12, 2.13, 2.14, 2.15, and 2.16.

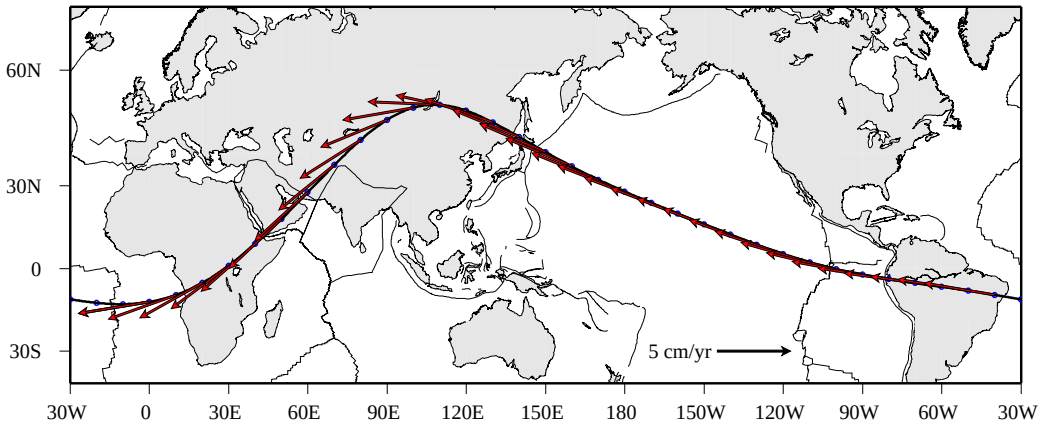

(a)

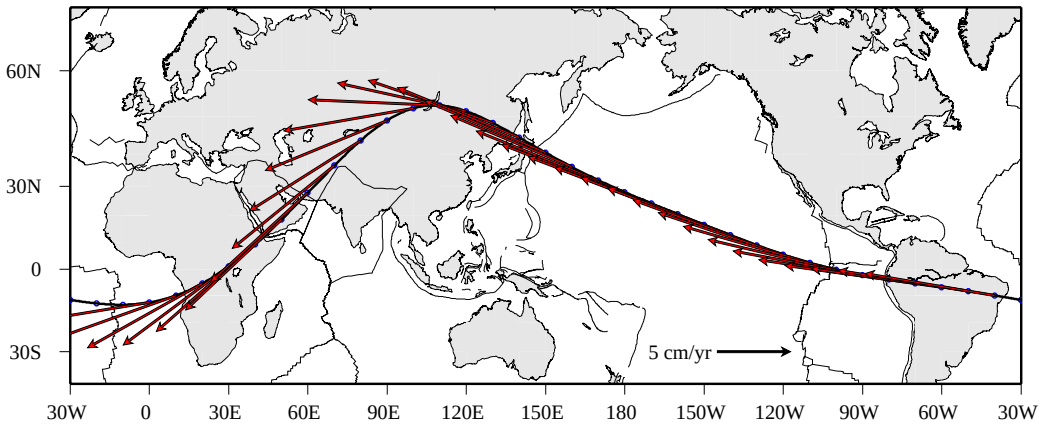

(b)

Figure 2.10: (a) Net–rotation velocities from *Gripp and Gordon* [2002] (option 1) applied on the tangents of the tectonic equator (see also Figure 2.5). The length of the vectors corresponds to a velocity of 48.473 mm yr^{-1}. (b) Net–rotation velocities from *Wessel and Kroenke* [1997] (option 1) applied on the tangents of the tectonic equator. The length of the vectors corresponds to a velocity of 100.810 mm yr^{-1}.

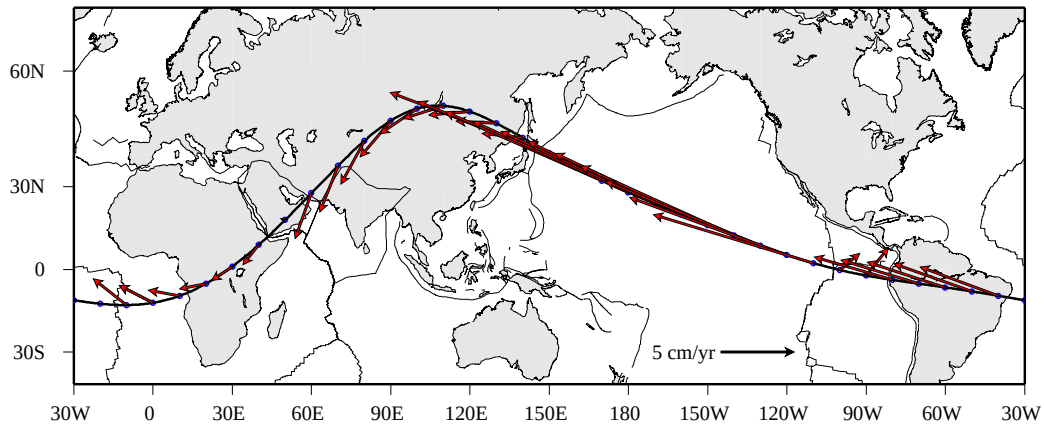

(a)

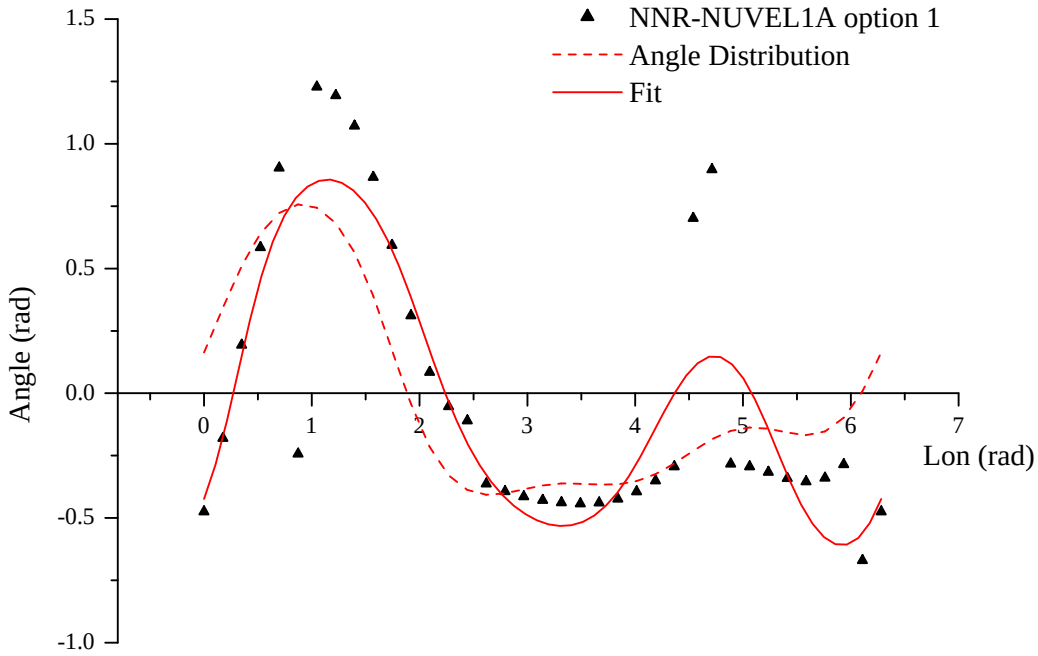

(b)

Figure 2.11: (a) The NNR–NUVEL1A plate kinematic model [*Argus and Gordon*, 1991] applied at the 36 selected points on six lithospheric plate crossed by the tectonic equator plus net–rotation velocity of the option 1. (b) Statistical comparison between angles of the tangents of the tectonic equator and the angles of the velocity vectors of the NNR–NUVEL1A, option 1. Correlation estimates give $R = 0.85127$.

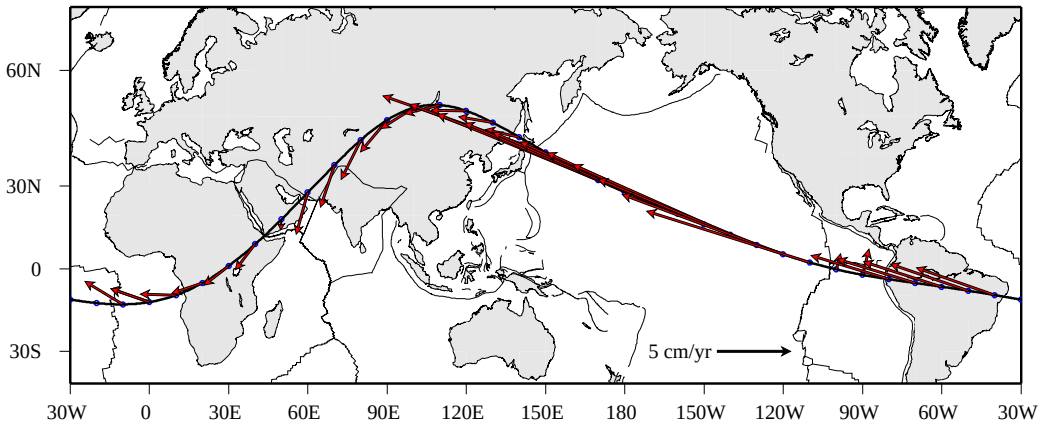

(a)

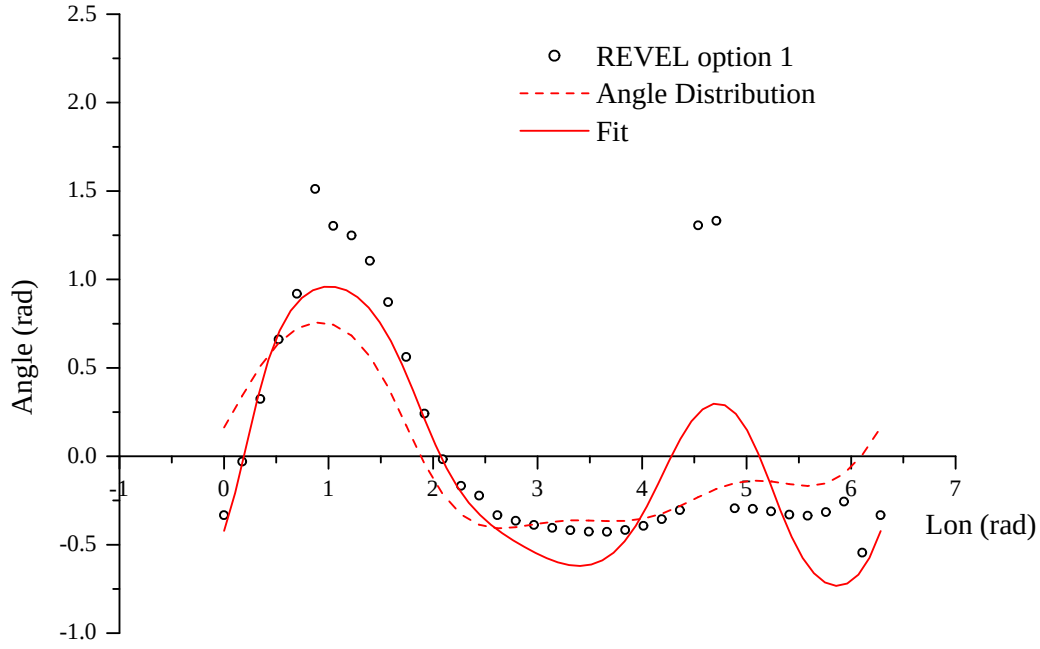

(b)

Figure 2.12: (a) The REVEL plate kinematic model [*Sella et al.*, 2002] applied at the 36 selected points on six lithospheric plate crossed by the tectonic equator plus net–rotation velocity of the option 1. (b) Statistical comparison between angles of the tangents of the tectonic equator and the angles of the velocity vectors of the REVEL, option 1. Correlation estimates give $R = 0.85101$.

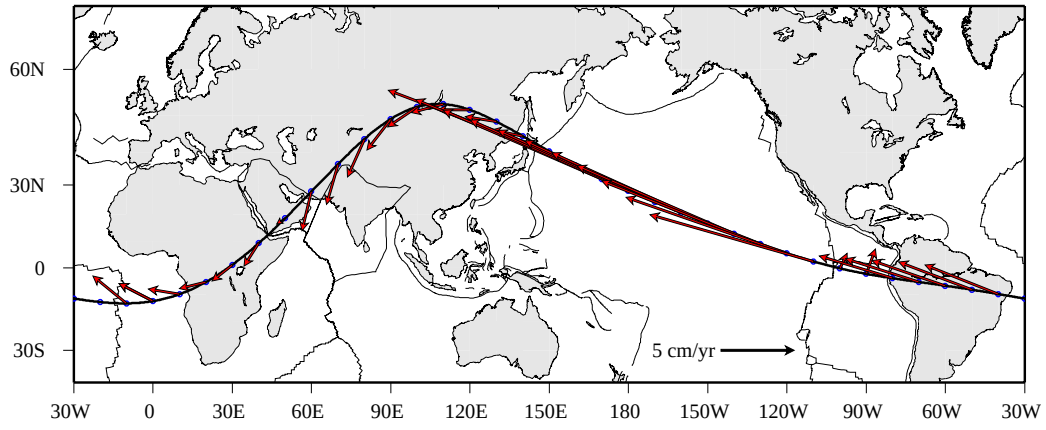

(a)

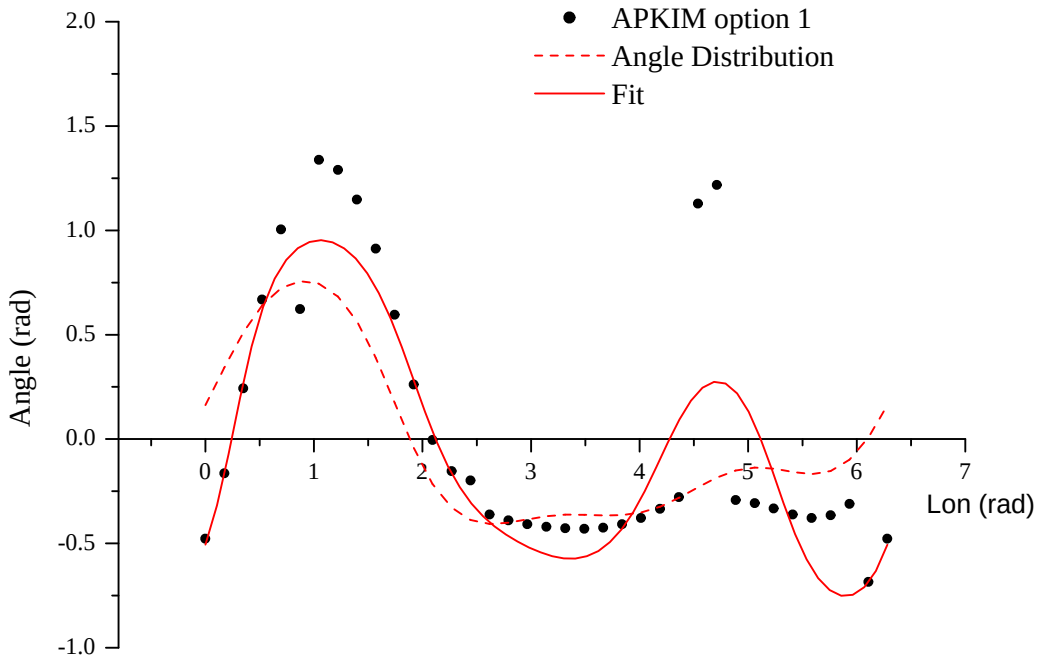

(b)

Figure 2.13: (a) The APKIM plate kinematic model [*Drewes and Meisel*, 2003] applied at the 36 selected points on six lithospheric plate crossed by the tectonic equator plus net–rotation velocity of the option 1. (b) Statistical comparison between angles of the tangents of the tectonic equator and the angles of the velocity vectors of the APKIM, option 1. Correlation estimates give $R = 0.87308$.

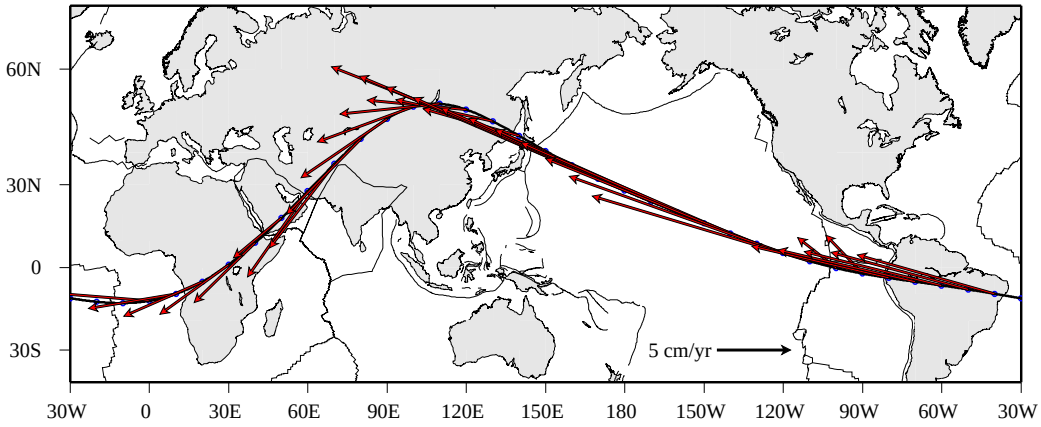

(a)

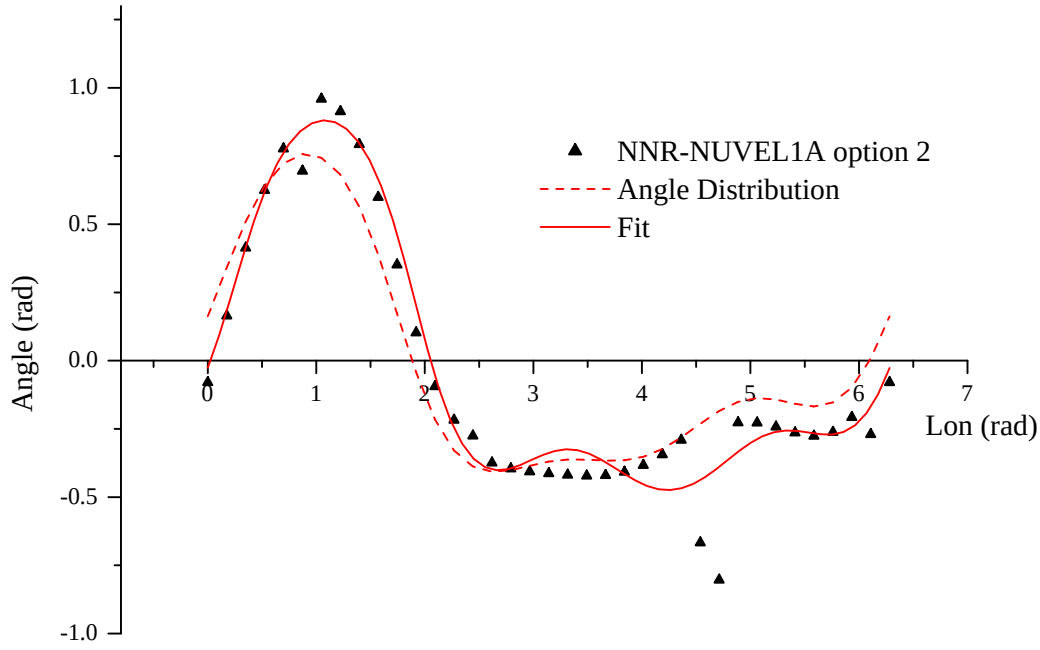

(b)

Figure 2.14: (a) The NNR–NUVEL1A plate kinematic model [*Argus and Gordon*, 1991] applied at the 36 selected points on six lithospheric plate crossed by the tectonic equator plus net–rotation velocity of the option 2. (b) Statistical comparison between angles of the tangents of the tectonic equator and the angles of the velocity vectors of the NNR–NUVEL1A, option 2. Correlation estimates give $R = 0.97383$.

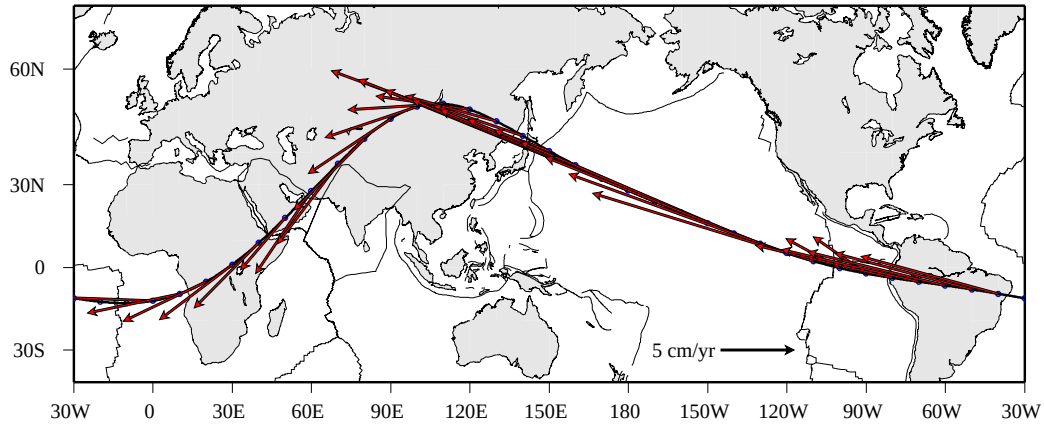

(a)

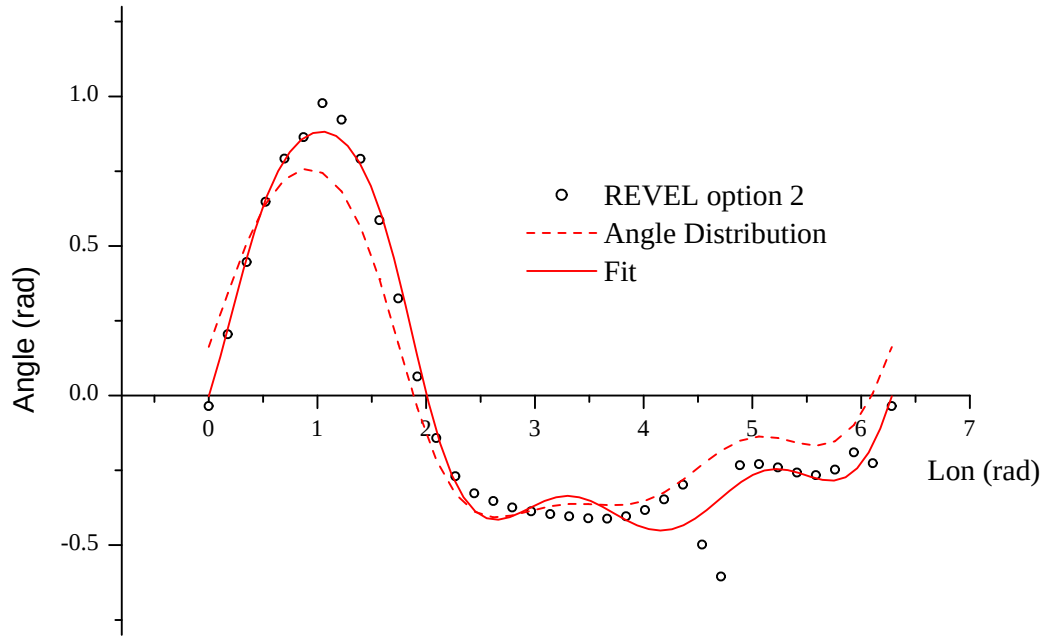

(b)

Figure 2.15: (a) The REVEL plate kinematic model [*Sella et al.*, 2002] applied at the 36 selected points on six lithospheric plate crossed by the tectonic equator plus net–rotation velocity of the option 2. (b) Statistical comparison between angles of the tangents of the tectonic equator and the angles of the velocity vectors of the REVEL, option 2. Correlation estimates give $R = 0.98857$.

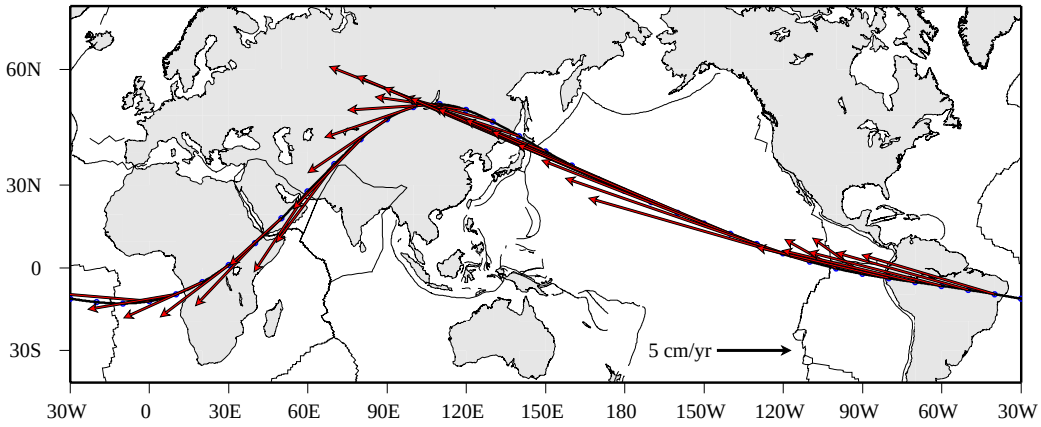

(a)

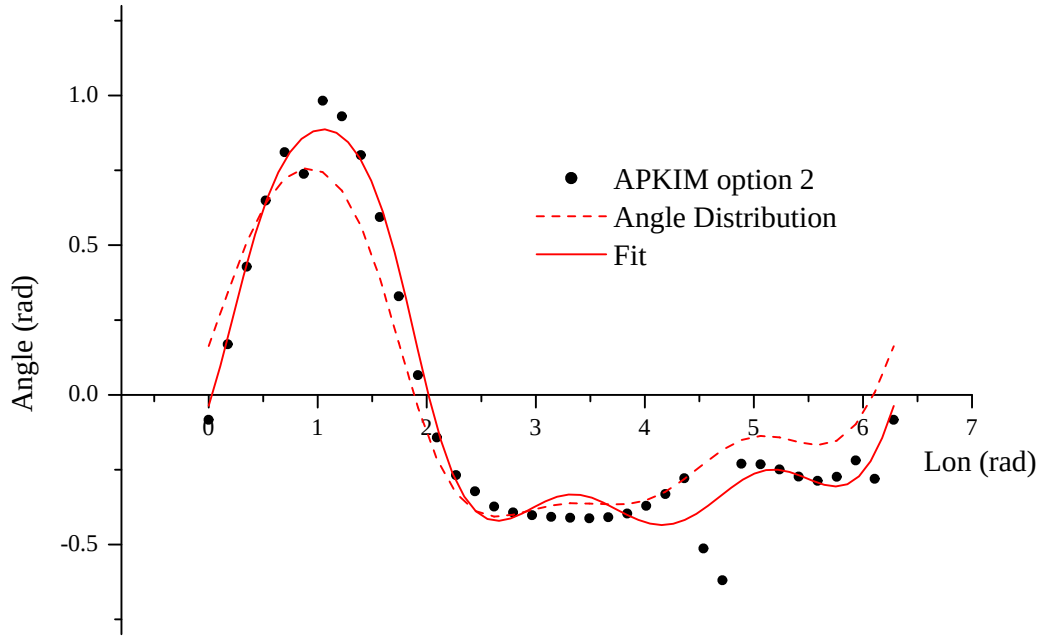

(b)

Figure 2.16: (a) The APKIM plate kinematic model [*Drewes and Meisel*, 2003] applied at the 36 selected points on six lithospheric plate crossed by the tectonic equator plus net–rotation velocity of the option 2. (b) Statistical comparison between angles of the tangents of the tectonic equator and the angles of the velocity vectors of the APKIM, option 2. Correlation estimates give $R = 0.98516$.

Table 2.7: Comparison among parameters of angle distribution of the tangents of the tectonic equator for 36 selected points and angles of velocity vectors of different NNR plate motion models, testing two different options of net–rotation velocities

	Free Parameters					
Model	P1	P2	P3	P4	P5	P6
Angle Distribution	0.34073	0.40602	0.27375	-0.11153	0.04289	-0.13005
$option1$	*Net–rotation from Gripp and Gordon [2002]*					
NNR–NUVEL1A	0.46057	0.19933	0.28012	-0.51084	0.09940	-0.13982
REVEL	0.48611	0.30524	0.43549	-0.55841	0.23578	-0.19590
APKIM	0.49433	0.23666	0.41928	-0.58536	0.19204	-0.20491
$option2$	*Net–rotation from Wessel and Kroenke [1997]*					
NNR–NUVEL1A	0.55822	0.36008	0.29478	-0.18837	-0.03967	-0.19780
REVEL	0.52851	0.38053	0.31791	-0.18098	-0.00901	-0.20175
APKIM	0.53099	0.36571	0.32554	-0.19943	-0.01410	-0.20310

Parameter estimates, following the two different options, are reported in Table 2.7. Testing the *option 1* (Table 2.8 option 1) results that there is a good agreement, with vector angles and tectonic equator, again in the Pacific, Arabia and East Africa. Less differences result in the South America and Eurasia, with respect to the previous section, whereas a great misfit is evident in the Nazca plate. Except for the S–N direction of the velocity vectors in the Nazca plate, all the points of the six lithospheric plates move toward the west with different relative rates.

The shape of the tectonic equator is not completely implied as a main trajectory, but correlation estimates are higher than those estimated in the NNR–framework (Table 2.8 option 1). The highest correlation is obtained with the APKIM plate kinematic model [*Drewes and Meisel*, 2003] where the correlation coefficient $R = 0.87308$. Then, the NRR–NUVEL1A [*Argus and Gordon*, 1991] and the REVEL [*Sella et al.*, 2002] present a very similar correlation with $R = 0.85127$ and $R = 0.85101$ respectively.

Table 2.8: Correlation between angle distribution and plate kinematic models, by making use of the coefficient of determination R^2 and correlation coefficient R, for two options of net–rotation velocity.

Model	Reference	R^2	R
$option1$	*Net–rotation from Gripp and Gordon [2002]*		
NNR–NUVEL1A	[*Argus and Gordon*, 1991]	0.72466	0.85127
REVEL	[*Sella et al.*, 2002]	0.72421	0.85101
APKIM	[*Drewes and Meisel*, 2003]	0.76226	0.87308
$option2$	*Net–rotation from Wessel and Kroenke [1997]*		
NNR–NUVEL1A	[*Argus and Gordon*, 1991]	0.94835	0.97383
REVEL	[*Sella et al.*, 2002]	0.97728	0.98857
APKIM	[*Drewes and Meisel*, 2003]	0.97055	0.98516

The *option 2*, instead, gives the best tested correlation (Table 2.8 option 2). Parameter estimates give a similar result with the estimated parameters of the angle distribution (Table 2.7). Testing the *option 2* gives a best fit between the angles of the velocity vectors and the angle distribution.

The agreement is well verified in the Pacific, the Arabia, the Africa, the South America, and on the great undulation in Eurasia. Only in the Nazca plate there is an higher misfit with the NW–ward motion of the plate points. All the plates move toward the west, well describing the shape of the tectonic equator.

The correlation rises over the 90% (Table 2.8), and the fit tends to the shape of the angle distribution, especially for the REVEL plate kinematic model [*Sella et al.*, 2002] with a correlation coefficient $R = 0.98857$. Then, the APKIM [*Drewes and Meisel*, 2003] and the NNR–NUVEL1A [*Argus and Gordon*, 1991] models show an estimated $R = 0.98516$ and $R = 0.98516$.

In Figure 2.17 is reported a summary of comparison among estimated parameters P_i of the angle distribution and the those of velocity vectors in the NNR–framework for the plate kinematic models analyzed in the previous section. It is easy to visualize that adding the two different net–rotation velocities of the option 1 and 2, the estimated parameters tend of those of the angle distribution with the maximum of the correlation.

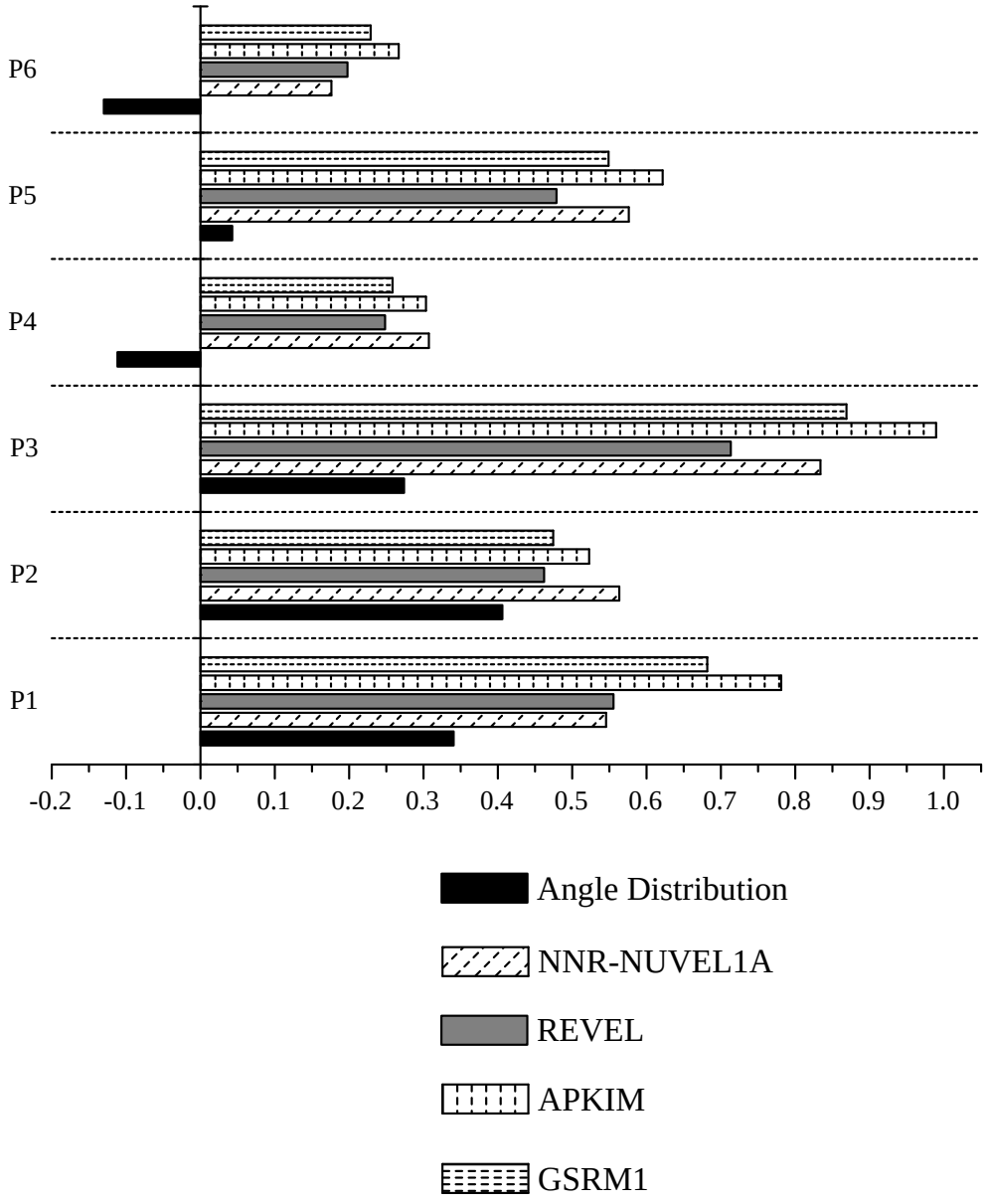

Figure 2.17: Comparison among parameters of angle distribution of the tangents of the tectonic equator for 36 selected points and angles of velocity vectors of different NNR plate motion models. Comparison is also made testing two different options of net–rotation velocities (option 1 and option 2).

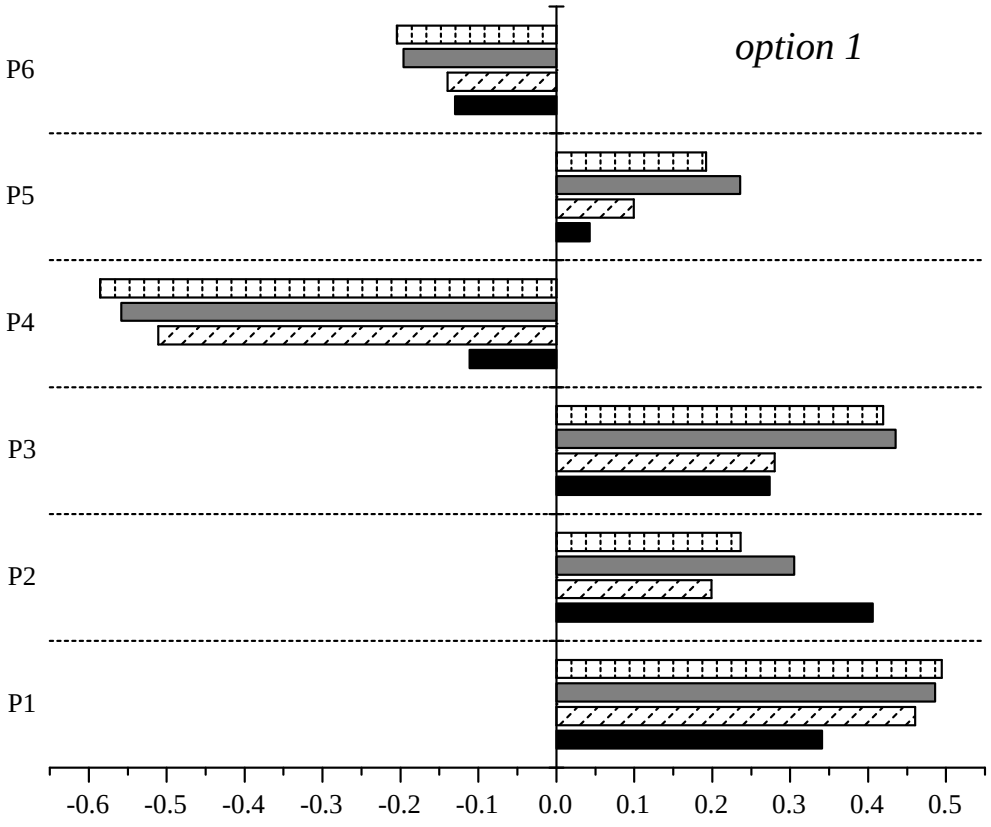

Figure 2.17: (continued)

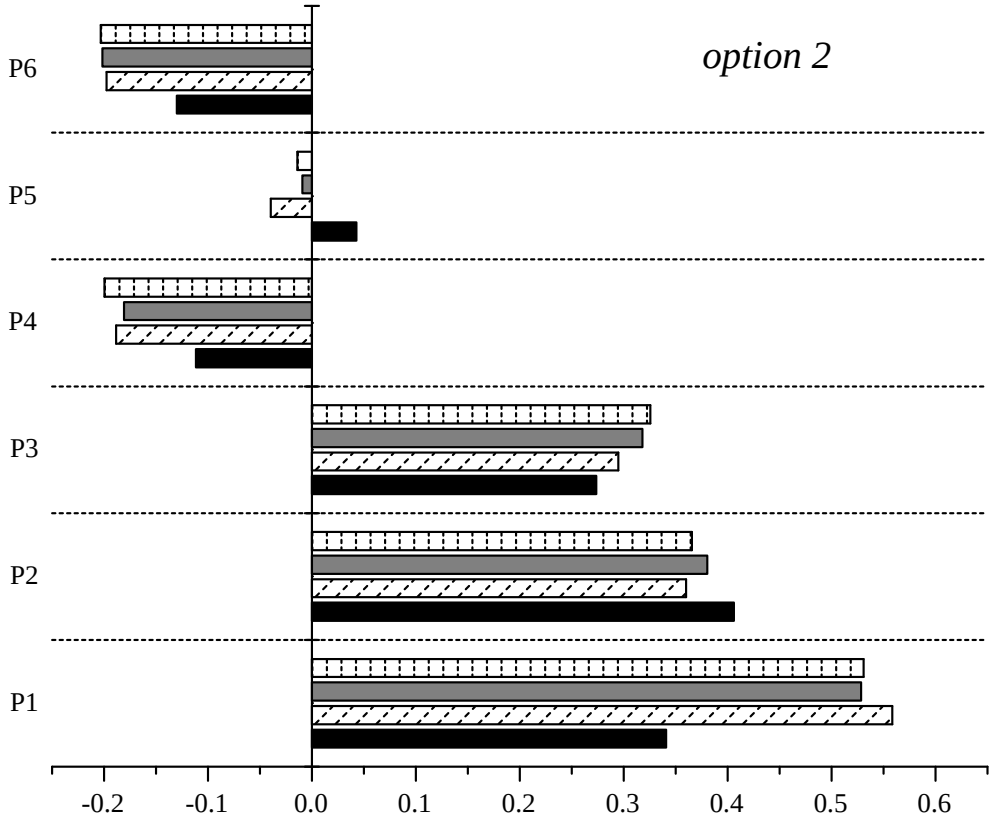

Figure 2.17: (continued)

2.5 Discussion

In this chapter, considering a priori the existence of the tectonic equator, we showed that in the NNR–framework, plate kinematic models deriving from geophysical and geological data and from space geodesy, well define the main trajectory of the global tectonic pattern.

The agreement of plate motions on the main trajectory in that frame reaches the 80%, also if not all the plates move toward the west (e.g Africa, Eurasia, Nazaca, South America). At this first stage, the comparison made only on the shape of the mainstram, could suggest that, in any case, the global plate motions are on a well–defined direction.

On the contrary, passing to the particular hotspot reference frame, defined in the previous section, and testing two hypotheses of net–rotation velocity, the correlation between motion direction and tectonic mainstream rises to the 85% for the option 1 (Table 2.8, page 44) and to a maximum of the 98% for the option 2 (Table 2.8, page 44). Morever, under this last condition, all the plates have a westward conponent, and the westward drift relative to mantle becomes a real and quantified phenomenon and not a simple averaged value.

We well know that this analysis is strongly tied to the existence and the shape of the tectonic equator. Any change in the approximated parameters of the tectonic equator function, would result in different correlation coefficients. Furthermore, most of the geophysicists believe that the NNR-framework is not useful to describe the absolute plate motion of the lithosphere relative to the mantle, and this reason could invalidate results. Moreover, the choice to apply the net–rotation velocity on the tangents of the tectonic equator is a further stronger passage, that contributes to align results and to obtain higher correlations.

Though the previous comments may support critical reviews about the behavior of the results, the aim reached in this chapter consists in utilizing a first and approximated shape of the global tectonic pattern, defined in an analytic form, for plate kinematic comparisons. Using a new version of the tectonic mainstream, proposed by *Crespi et al.* [2007] the results may change reaching better correlations. The use of the analytic form of the tectonic equator is a first step to quantify the idea of the global tectonic pattern and the westward drift of the lithosphere. At this stage, it is strongly constrained, but it gives good results.

Then, in the next chapters, we will try to obtain evidence of a tectonic mainstream and westward drift from kinematic analysis, using different methods, not tied to the mainstream itself.

Chapter 3

Global kinematics relative to the deep and shallow hotspots

Plume traces at the Earth's surface have likely variegate origins such as wet spots, simple rifts and shear heating. Since plate boundaries move relative to each other and relative to the mantle, plumes located on, or close to them cannot be considered reliable for a reference frame. Using only relatively fixed intraplate Pacific hotspots, plate motions in two different absolute hotspot reference frames, one fed from below the asthenosphere, and one fed by the asthenosphere itself, provide different kinematic results. Plates move faster relative to the mantle, if the source of hotspots is located in the middle–upper asthenosphere, because hotspot tracks would not record the entire decoupling occurring in the low velocity zone. The shallow intra–asthenospheric origin of hotspots would raise the Pacific deep–fed velocity from a value of 10 $\mathrm{cm\,yr^{-1}}$ to a faster hypothetic velocity of about 20 $\mathrm{cm\,yr^{-1}}$. In this setting, the net–rotation of the lithosphere relative to the mesosphere would increase from a value of 0.4359 $^{\circ}\,\mathrm{Myr^{-1}}$ (deep–fed hotspots) to 1.4901 $^{\circ}\,\mathrm{Myr^{-1}}$ (shallow–fed hotspots). In this configuration all plates move westward and plate rotation poles are largely located in a restricted area at a mean latitude of 58°S.

3.1 Introduction

Absolute plate motions represent movements of plates relative to the mesosphere. When plate motions are measured in the "classic" hotspot reference frame, the lithosphere shows a net "westward" rotation [*Bostrom*, 1971; *O'Connell et al.*, 1991; *Ricard et al.*, 1991; *Gripp and Gordon*, 2002; *Crespi et al.*, 2007]. This so-called W-ward drift has been so

far considered only as an average motion of the lithosphere due to the larger weight of the Pacific plate in the global plate motion computation. But the W-ward drift persists also when plate motions are computed relative to Antarctica [*Le Pichon*, 1968; *Knopoff and Leeds*, 1972]. Moreover, and more important, it is confirmed by independent geological and geophysical asymmetries along subduction zones and rifts [*Doglioni*, 1990, 1993], showing a global tuning and not just an average asymmetry.

In order to check whether the W–ward drift is only an average casual component or is rather a globally persistent signature, we analyze the different kinematics, resulting from different hotspot reference frames. The hotspot tracks have been used for computing the motion of plates relative to the mantle. For this purpose it is fundamental to know whether hotspots are i) fixed relative to the mantle, ii) if they are fixed relative to each other, and iii) from what depth they are fed. Looking at maps of hotspots [e.g., *Anderson and Schramm*, 2005], plumes occur both in intraplate settings, or close or along plate boundaries. Hotspot reference frames have been used and misused possibly because the volcanic tracks have been considered monogenic and with similar source depth. A number of models have been produced to quantify the relative motion among hotspots and their reliability to generate a reference frame.

Hotspots have been used often uncritically, regardless their real nature. Rejuvenating volcanic tracks at the Earth's surface may be a result of intraplate plumes (e.g. Hawaii), retrogradation of a subducting slab, migration of a back–arc spreading, along strike propagation of a rift (e.g. East Africa), or propagation of transform faults with a transtensive component (Chagos?). All those volcanic trails may have different depths of the mantle source and they should be differentiated (Figure 3.1). Plate boundaries are by definition moving relative to each other and relative to the mantle [e.g., *Garfunkel et al.*, 1986; *Doglioni et al.*, 2003]. Therefore, any hotspot located along plate boundaries cannot be used for the reference frame. For example, *Norton* [2000] grouped hotspots into three main families that have very little internal relative motion (Pacific, Indo–Atlantic and Iceland). In fact, he concluded that a global hotspot reference frame is inadequate because Pacific hotspots move relative to Indo-Atlantic hotspots and Iceland. Since Indo-Atlantic and Iceland hotspots are located along ridges, they do not satisfy the required fixity. In his analysis, Pacific plate hotspots are reasonably fixed relative to each other during the last 80 Myr, and they are located in intraplate settings. Therefore, they are unrelated to plate margin processes and do not move with any margin. The screening of volcanic tracks to be used for the hotspot reference frame provides a very limited number of hot-lines and only the Pacific ones satisfy the requirements.

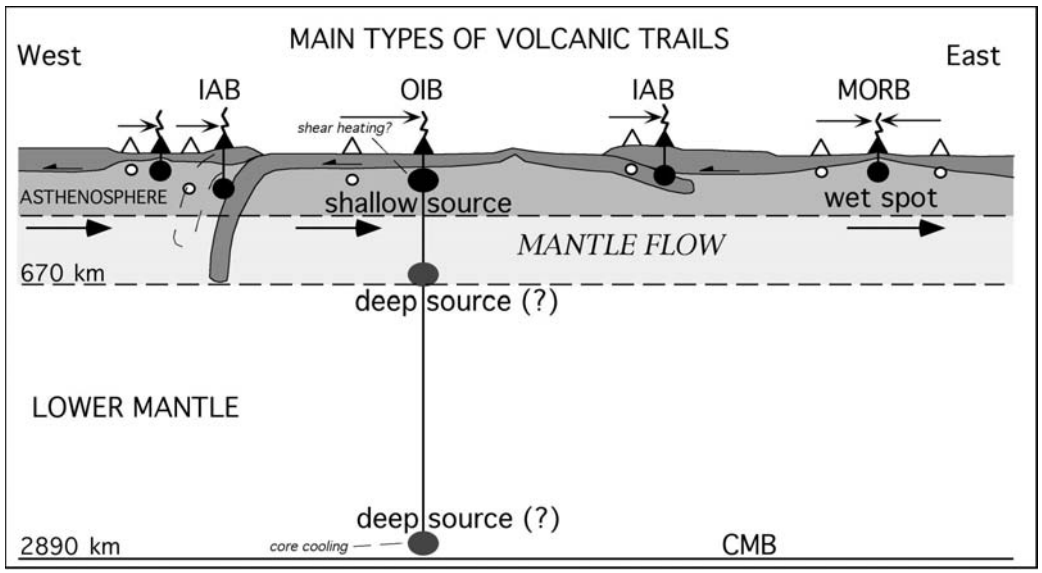

Figure 3.1: The main volcanic chains at the Earth's surface may have different origins and depths. The thin arrows indicate the direction of migration of volcanism with time. Filled triangles represent the youngest volcanic products. Volcanic trails originating on ridges may be wetspots [in sensu, *Bonatti*, 1990] and fed from a fluid–rich asthenosphere. The hotspots located on plate boundaries are not fixed by definition, since both ridges and trenches move relative to one another and with respect to the mantle. Pacific hotspots, regardless their source depth, are located within the plate and are virtually the only ones that can be considered reliable for a hotspot reference frame [after *Doglioni*, 1993].

Hotspots may have short ($<$15Myr) or long ($>$50Myr) time gap between their emplacement and the age of the oceanic crust on which they reside. A shorter time frame suggests a closer relation with the formation of the oceanic crust, particularly when i) the location is steadily close to the ridge and ii) two ridges form in both sides of the rifts [*Doglioni et al.*, 2005]. Therefore ridge–related plumes should move with a speed close to the absolute velocity of the plate boundary. Although moving relative to each other, hotspots have always a speed slower than plate motions and have been considered useful for a reference frame [e.g., *Wang and Wang*, 2001]. However, the velocity of the plate boundaries tends to be slower than the velocity of the relative plate motion among pairs of plates. For example the Mid Atlantic Ridge moves west at rates comparable to the relative motion between the Pacific and the Atlantic hotspots, but this intra–hotspot motion could be related to the absolute motion of the Mid Atlantic Ridge. Moreover, assuming a deep source of the hotspots, a number of models have been computed to infer the

deep mantle circulation [e.g. *Steinberger and O'Connell*, 1998; *Steinberger*, 2000]. These models argue that volcanic tracks move opposite to plate motions. However, this may be regarded again as a problem of reference. For example, in the no–net–rotation reference frame Africa moves "east", opposite with respect to Ascencion and Tristan da Cuna, but in HS3–NUVEL1A [*Gripp and Gordon*, 2002] Africa moves in the same direction, to the "west", although at different velocity. Therefore the assumption that the hotspots move always opposite to plate motions is misleading, if not wrong. In most of the models so far published on mantle circulation and hotspot reference frames, two main issues are disregarded: i) plumes have different origin and different kinematic weight for the reference frames and ii) in case plumes are shallow asthenospheric features, this determines a different kinematic scenario with respect to the deep mantle circulation pattern.

Growing evidence suggests that hotspots are mostly shallow features [*Bonatti*, 1990; *Smith and Lewis*, 1999; *Anderson*, 2000; *Foulger*, 2002; *Foulger et al.*, 2005]. For example Atlantic hotspots might be interpreted more as wetspots rather than hot lines, as suggested by *Bonatti* [1990]. An asthenospheric source richer in fluids lowering the melting point can account for the overproduction of magma. Propagating rifts are shallow phenomena, which are not fixed to any deep mantle layer. The only hotspots that should be relevant to the reference frame are those located within plate. For a compelling petrological, geophysical and kinematic analysis on the shallow origin of plumes *Foulger et al.* [2005] could be a useful support. In that book a number of data support the shallow source of hotspots (such as upper mantle, asthenosphere and base lithosphere). Several theoretical models have been proposed to explain the different settings, such as rift zones, fluids in the asthenosphere, shear heating at the lithosphere–asthenosphere decoupling zone, lateral mantle compositional variations etc., all models which could be valid, but applied to different cases. Therefore, we disagree in using acritically all so–called hotspots because their different origin can lead to a lower degree of accuracy in the reconstruction of the lithosphere–mantle relative motion

In this chapter we present two different hotspot frameworks, one deep–fed and the other shallow–fed, using Pacific intraplate volcanic tracks. Since geometrically two fixed points are enough for constructing a kinematic reference frame, we used only Pacific intraplate hotspots which are significantly fixed relative to each other [*Gripp and Gordon*, 2002]. Computing absolute plate motions in these two frames. we followed methods used by *Gripp and Gordon* [2002], obtaining the HS3–NUVEL1A results in case of deep source and new angular velocities in case of shallow source. Unlike *Wang and Wang* [2001] and *Wang and Liu* [2006], we find a much faster net–rotation of the lithosphere.

3.2 Decoupling in the asthenosphere

The origin of intraplate Pacific magmatism is rather obscure, and the depth of its source and the mechanism of melting are still under discussion [*Foulger et al.*, 2005]. Since the Pacific is the fastest plate, the shear heating along the basal decollement has been interpreted as a potential mechanism for generating localized hotspot tracks (Figure 3.2a). Areas with viscosity higher than normal in the asthenospheric decollement should generate larger shear heating.

Kennedy et al. [2002] have shown how mantle xenoliths recorded a shear possibly located at the lithosphere-asthenosphere interface. This supports the notion of a flow in the upper mantle and some decoupling at the base of the lithosphere as indicated by seismic anisotropy [*Russo and Silver*, 1996; *Doglioni et al.*, 1999; *Bokelmann and Silver*, 2000]. The fastest plate on Earth in the hotspot reference frame (i.e., the Pacific) is the one affected by the most widespread intraplate magmatism.

It is noteworthy that the fastest Pacific plate overlies the asthenosphere with the mean lowest viscosity [5×10^{17} Pa s, *Pollitz et al.*, 1998], and possibly the most undepleted mantle, therefore prone to melt. Because of the melting characteristics of peridotite with minor carbon plus hydrogen (lherzolite–(C+H+O) system), the asthenosphere is already partly molten [e.g., *Schubert et al.*, 2001] and it is at a temperature of about 1430°C [e.g., *Green and Falloon*, 1998; *Green et al.*, 2001]. The rise of temperature of only few tens of degrees will increase the degree of melting which, in a deforming material, will migrate toward the surface. We postulate that locally, the viscosity of the asthenosphere can also increase (e.g., 10^{19} Pa s) due to refractory geochemical anisotropies, or decrease due to locally higher water activity. Shear stress could be irregularly distributed in such inhomogeneous materials, and consequently higher shear heating [*Shaw*, 1973] may be locally developed to generate punctiform magmatism.

3.3 Plate motions relative to the deep and shallow hotspots

Most of the used hotspots are neither fixed, nor they represent a fixed reference frame because they are located on plate margins such as moving ridges (Galapagos, Easter Island, Iceland, Ascension, etc.), transform faults (Reunion), above subduction zones, or continental rifts (Afar), being features in motion relative to each other and relative to the mantle. On the contrary, Pacific hotspots are reasonably fixed relative to each other and their volcanic tracks can be used for the hotspot reference frame.

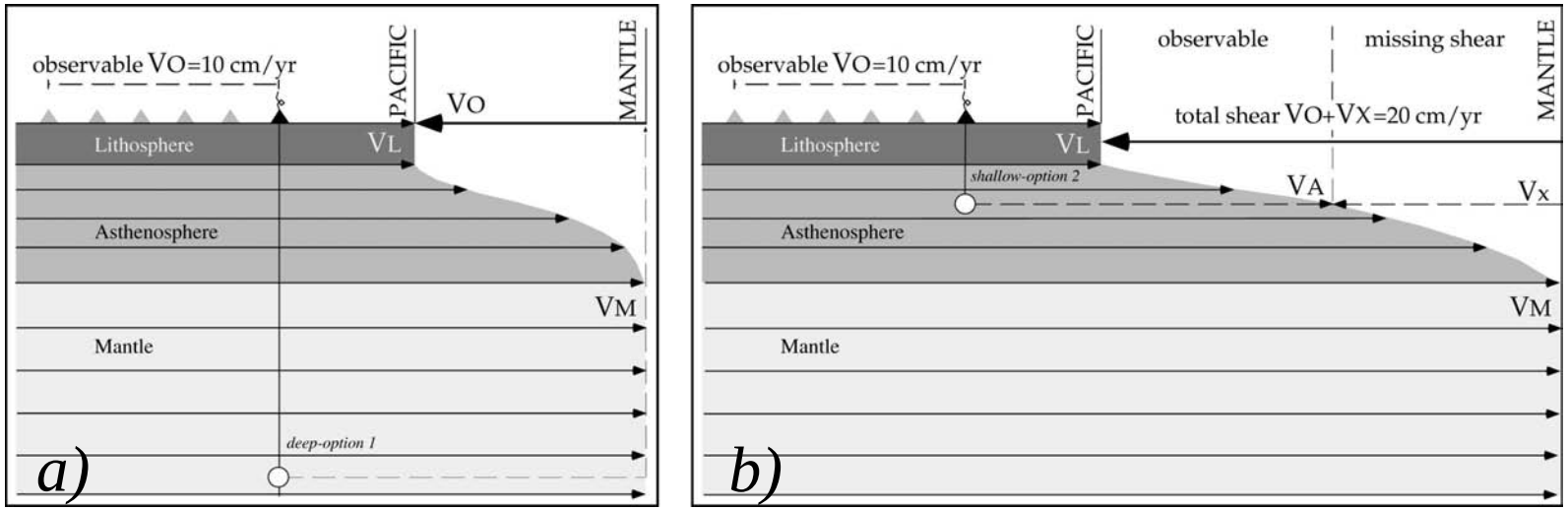

Figure 3.2: The Hawaiian volcanic track indicates that there is decoupling between the magma source and the lithosphere, which is moving relatively toward the WNW. a) If the source is below the asthenosphere (e.g., in the sub-asthenospheric mantle, the track records the entire shear between lithosphere and mantle. b) In the case of an asthenospheric source for the Hawaiian hotspot, the volcanic track does not record the entire shear between the lithosphere and sub–asthenospheric mantle, since part of it operates below the source (deep missing shear). Moreover the larger decoupling implies larger shear heating, which could be responsible for the scattered, punctiform Pacific intraplate magmatism [after *Doglioni et al.*, 2005].

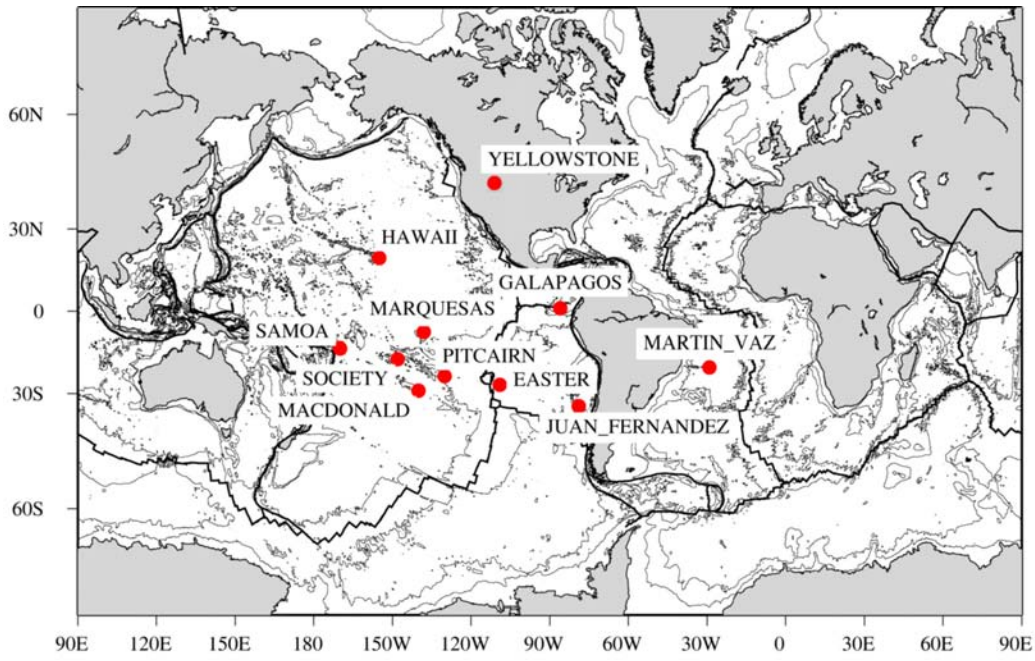

Figure 3.3: The eleven hotspots used to obtain the HS3–NUVEL1A plate kinematic model [*Gripp and Gordon*, 2002]. Segment trends and two propagation rates (those of Hawaii and Society) of volcanic tracks were estimated, then, incorporating the NUVEL–1A relative plate motion model [*DeMets et al.*, 1990, 1994], the absolute plate velocities were computed.

The WNW-motion of the Pacific plate relative to the underlying mantle is inferred from the Hawaiian and the other major intraplate hotspot tracks (Marquesas, Society, Pitcairn, Samoan, Macdonald), which show an average velocity of about 103–118 mm yr^{-1}, and also move along the same trend (290°–300°, WNW).

Under the hypothesis of deep–fed hotspots, after assuming that shear is distributed throughout the asthenospheric channel [*Gung et al.*, 2003] (Figure 3.2a), and providing that the linear velocity $\vec{V}_L$ of the Pacific lithosphere toward ESE (110°-120°) is slower than that of the underlying sub–asthenospheric mantle $\vec{V}_M$ ($\vec{V}_M > \vec{V}_L$), the relative velocity $\vec{V}_O$ corresponding to the WNW delay of the lithosphere is:

$$\vec{V}_O = \vec{V}_L - \vec{V}_M \tag{3.1}$$

For the case of the Hawaii, the observed linear velocity is $V_O = 103$ mm yr^{-1}, corresponding to the propagation rate of the Hawaiian volcanic track (Figure 3.2a).

The HS3–NUVEL1A [*Gripp and Gordon*, 2002] absolute plate motion model is based on the deep–fed hotspot hypothesis. *Gripp and Gordon* [2002] computed absolute plate motions, estimating first eleven segment trends and two propagation rates of volcanic tracks (Figure 3.3), and then incorporating the NUVEL–1A relative plate motion model [*DeMets et al.*, 1990, 1994].

Volcanic propagation rates used by *Gripp and Gordon* [2002] are those of Hawaii and Society, both on the Pacific plate, and they give a Pacific angular velocity of 1.0613 $^{\circ}$Myr^{-1} about a pole located at 61.467 $^{\circ}$S, 90.326 $^{\circ}$E. Adding this Pacific plate angular velocity to the relative model NUVEL-1A [*DeMets et al.*, 1990, 1994] gives the present–day velocities in the deep hotspot reference frame (Table 3.1 and Figure 3.4). Using these methods, absolute plate angular velocities with respect to the deep hotspot framework are obtained utilizing only rates of the Pacific intraplate hotspots [*Gripp and Gordon*, 2002].

In case the location of the Hawaiian melting spot is in the middle of the asthenosphere (Figure 3.2b) instead of the lower mantle (Figure 3.2a), this would imply that the shear recorded by the volcanic track at the surface is only the one occurring from the asthenospheric source and the top of the asthenosphere, i.e. only half of the total displacement, if the source is located in the middle of the asthenosphere. Under this condition, the velocity recorded at the surface is:

$$\vec{V_O} = \vec{V_L} - \vec{V_A} \tag{3.2}$$

with

$$\vec{V_A} = \vec{V_M} + \vec{V_X} \tag{3.3}$$

where $V_O = 103$ mm yr^{-1} is still the observed propagation rate of the volcanic track (for example the Hawaii), $\vec{V_A}$ is the velocity recorded at the shallow source of the hotspot, and $\vec{V_X}$ is the not–recored velocity, due to the missing shear.

Substituting the equation (3.3) in the equation (3.2), we have:

$$\vec{V_O} = \vec{V_L} - \vec{V_M} - \vec{V_X} \tag{3.4}$$

and

Table 3.1: Global plate motions with respect to the deep and shallow hotspot reference frame. Data are presented with three significant digits for the Euler poles, and four for the angular velocities, as reported by *Gripp and Gordon* [2002].

		Deep Source[a]			Shallow Source		
PLATE		Euler Pole		ω	Euler Pole		ω
		°N	°E	° Myr^{-1}	°N	°E	° Myr^{-1}
AF	Africa	-43.386	21.136	0.1987	-61.750	76.734	1.2134
AN	Antarctica	-47.339	74.514	0.2024	-59.378	86.979	1.2564
AR	Arabia	2.951	23.175	0.5083	-46.993	56.726	1.2393
AU	Australia	-0.091	44.482	0.7467	-38.865	62.780	1.4878
CA	Caribbean	-73.212	25.925	0.2827	-65.541	82.593	1.3216
CO	Cocos	13.171	-116.997	1.1621	-42.844	-135.856	0.9818
EU	Eurasia	-61.901	73.474	0.2047	-62.352	87.511	1.2647
IN	India	3.069	26.467	0.5211	-46.051	57.930	1.2563
JF	Juan de Fuca	-39.211	61.633	1.0122	-51.452	72.836	2.0104
NA	N. America	-74.705	13.400	0.3835	-67.520	79.790	1.4094
NZ	Nazca	35.879	-90.913	0.3231	-71.733	91.649	0.7824
PA	Pacific	-61.467	90.326	1.0613	-61.467	90.326	2.1226
PH	Philippine	-53.880	-16.668	1.1543	-68.889	25.661	1.9989
SA	S. America	-70.583	80.401	0.4358	-64.176	88.125	1.4925
SC	Scotia	-76.912	52.228	0.4451	-66.654	84.271	1.4877
LS	Lithosphere	-55.908	69.930	0.4359	-60.244	83.662	1.4901

[a]Data from HS3-NUVEL1A [*Gripp and Gordon*, 2002]

$$\vec{V}_O + \vec{V}_X = \vec{V}_L - \vec{V}_M \tag{3.5}$$

The observed velocity $V_O = 103$ mm yr^{-1} of the Hawaii is the velocity of total displacement, if the magmatic source is located in the deep mantle, whereas it represents

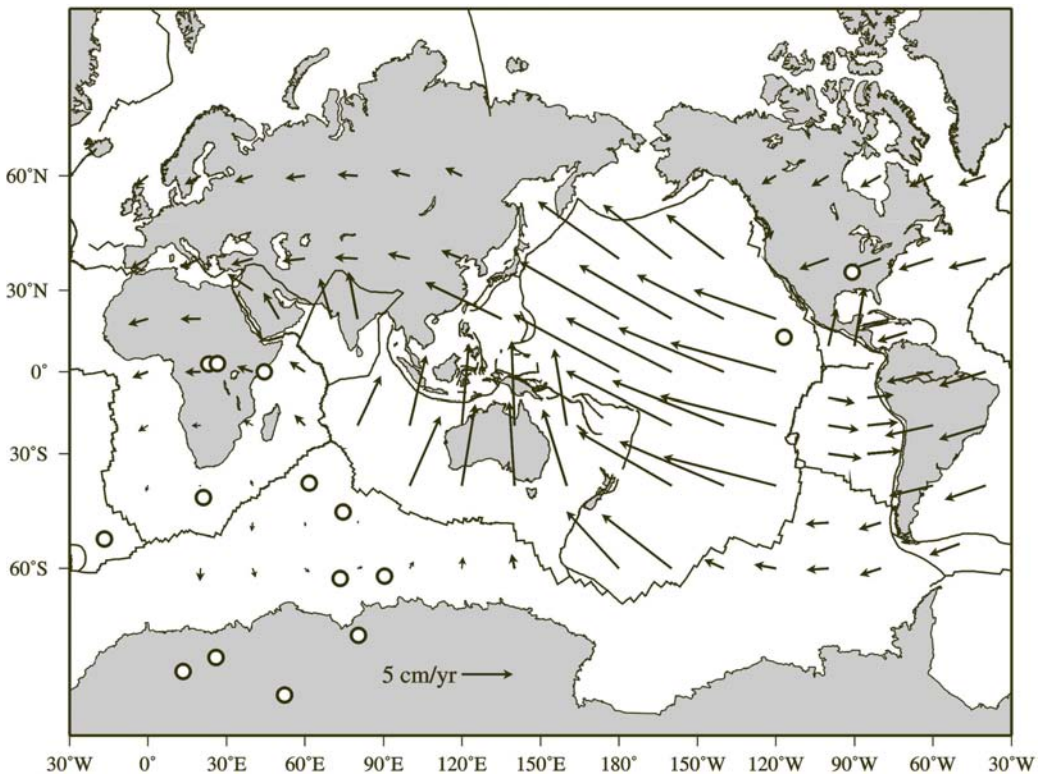

Figure 3.4: Current velocities with respect to the deep hotspot reference frame. Data from HS3-NUVEL1A [*Gripp and Gordon*, 2002]. Open circles are the rotation poles.

only the half of the whole shear, if the source is located in the middle of the asthenosphere. In this last case, to refer plate motions again with respect to the mesosphere, the velocity $\vec{V}_X$ has to be added to the observed velocity $\vec{V}_O$ (Figure 3.2b), as it is shown in the equation (3.5).

If the source of the Pacific hotspots is located in the middle of the asthenosphere, half of the lithosphere-sub-asthenospheric mantle relative motion is unrecorded, which means that, for example, the total relative displacement of the Hawaii would amount about $V_O + V_X = 200$ mm yr^{-1} (Figure 3.2b).

Under the hypothesis of a shallow source for the Pacific hotspots, located in the middle of the asthenosphere, and referring to the HS3–NUVEL1A methods [*Gripp and Gordon*, 2002], the Pacific plate rotation would occur about a pole located at 61.467 °S, 90.326 °E, but with a rate of 2.1226 °Myr^{-1}.

Adding this rotation to the NUVEL–1A relative plate motion model [*DeMets et al.*,

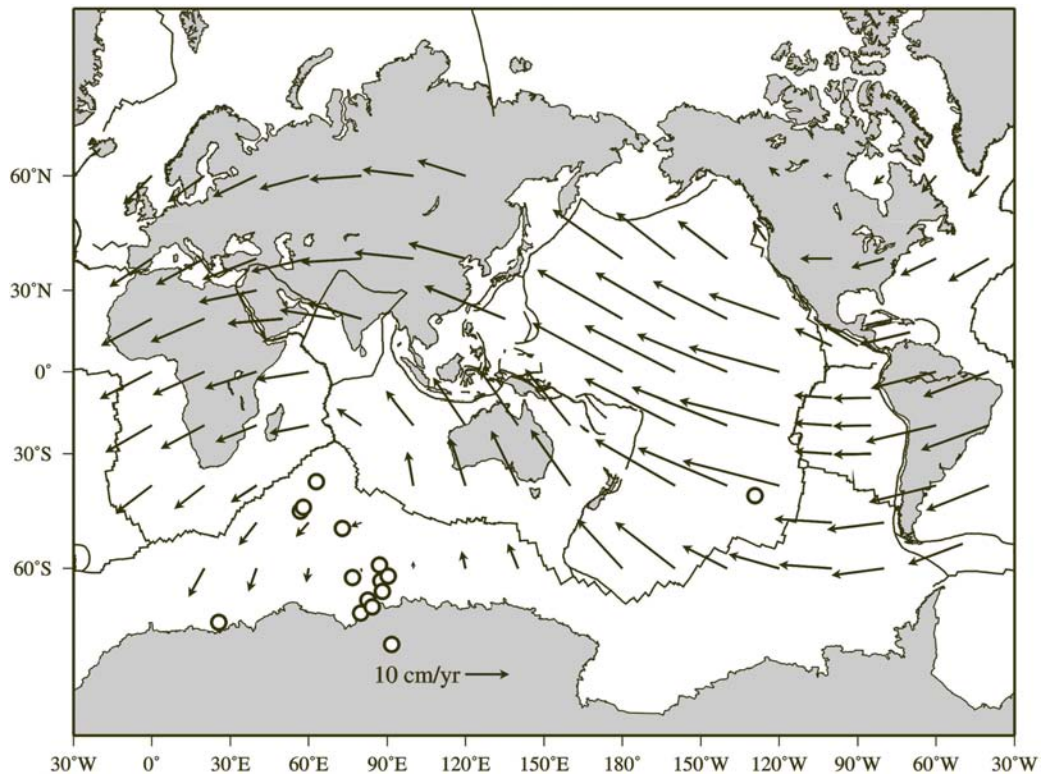

Figure 3.5: Present–day plate velocities in the shallow hotspot reference frame, incorporating the NUVEL–1A relative plate motions model [*DeMets et al.*, 1990, 1994]. Note that in this frame all plates have a westward component. Open circles are the rotation poles.

1990, 1994] results in absolute plate motions with respect to the shallow hotspot reference frame (Table 3.1 and Figure 3.5).

Moreover, referring to the plate geometrical factors proposed by *Argus and Gordon* [1991], and using methods described by *Gordon and Jurdy* [1986] and *Jurdy* [1990], we computed net–rotation of the lithosphere relative to the mesosphere, that, under the shallow hotspot hypothesis, amounts about 1.4901 $^{\circ}\,\mathrm{Myr}^{-1}$ (Table 3.1), and it is higher than the one computed by *Gripp and Gordon* [2002] (0.4359 $^{\circ}\,\mathrm{Myr}^{-1}$, deep hotspot condition, Table 3.1).

This faster velocity of the Pacific plate has these basic consequences, i) it expands the westward drift of the lithosphere to all plates (Figure 3.5), ii) the westward drift is more than twice with respect to the deep hotspot reference frame, and iii) it raises the shear heating released within the asthenosphere.

3.4 Shallow Hawaii plume

There is evidence that the propagation rate of Pacific ”hotspots” or seamount tracks has varied with time, even with jumps back and forth and oblique propagation relative to the ”absolute” plate motions, casting doubts on both the notion of absolute plate motions computed in the hotspot reference frame, and the nature of the magmatism itself [deep plumes, or rather shallow plumes generated by cracks or boudins of the lithosphere, *Winterer and Sandwell*, 1987; *Sandwell et al.*, 1995; *Lynch*, 1999; *Natland and Winterer*, 2003], filled by a mantle with compositional heterogeneity and no demonstrable thermal anomaly in hotspot magmatism relative to normal mid-oceanic ridges.

Janney et al. [2000] described a velocity of the Pukapuka volcanic ridge (interpreted as either an hotspot track or a leaky fracture zone), located in eastern Central Pacific, between 5 and 12 Myr of about 200–300 mm yr^{-1}. They also inferred a shallow mantle source for the Pacific hotspots, based on their geochemical characteristics.

Relative plate motions can presently be estimated with great accuracy by space geodesy data [e.g., *Robbins et al.*, 1993; *Heflin et al.*, 2004], refining the earlier NUVEL-1A plate motions model [*DeMets et al.*, 1990, 1994].

The East Pacific Rise (EPR), separating the Pacific and the Nazca plates, opens at rates of 128 mm yr^{-1} just to the south of the equator [e.g., *Heflin et al.*, 2004]. At the same latitude the shortening along the Andean subduction, where the Nazca plate subducts underneath South America, has been computed to about 68 mm yr^{-1}. When inserted in a reference frame, where the Hawaiian hotspot is considered fixed and positioned in the sub-asthenospheric mantle, these relative motions imply that the Nazca plate is moving eastward relative to the sub-asthenospheric mantle at about 25 mm yr^{-1} [see Figure 7, option 1 of *Doglioni et al.*, 2005]. If we assume that the source of the Pacific intraplate hotspots is rather in the middle asthenosphere and there is half of the lithosphere–sub–asthenospheric mantle relative motion missing in the Hawaiian track (Figure 3.2b), the movement could rise to 200 mm yr^{-1}, as also suggested by some segments of the Pukapuka volcanic ridge [*Janney et al.*, 2000]. Note that in this configuration Nazca would rather move west relative to the mantle of 72 mm yr^{-1} [see Figure 7, option 2 of *Doglioni et al.*, 2005] and therefore all three plates would move “westward” relative to the sub-asthenospheric mantle.

This last case agrees with the E-W-trending shear-wave splitting anisotropies beneath the Nazca plate and turning to N-S when encroaching the Andean slab, suggesting an E-ward mantle flow relative to the overlying plate [*Russo and Silver*, 1994]. This flow could

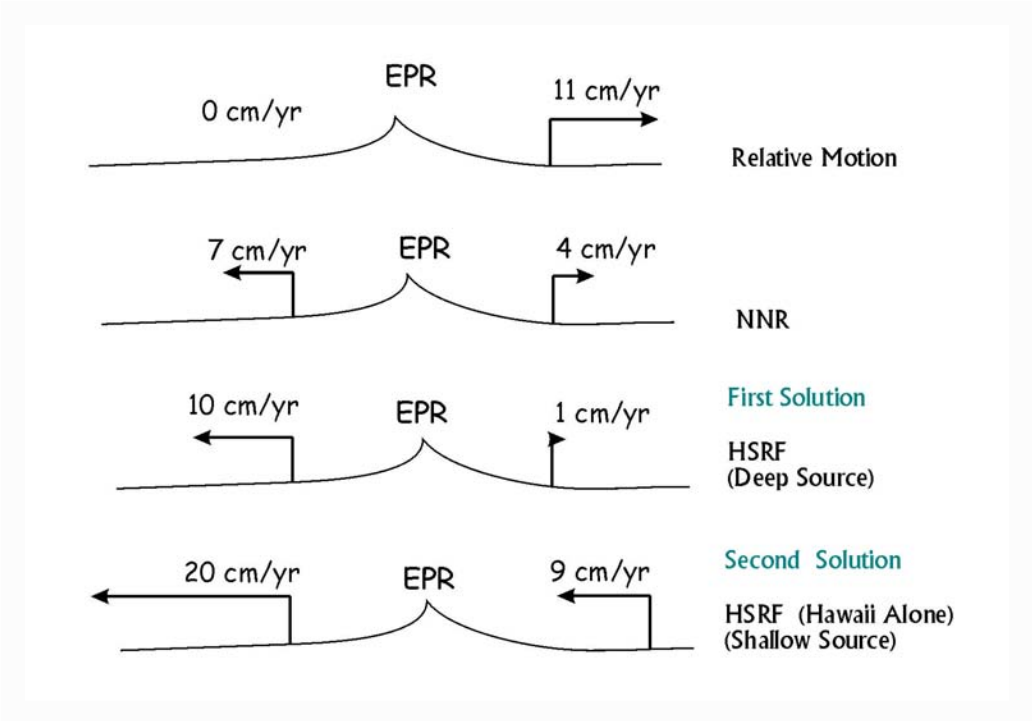

Figure 3.6: Pacific plate motion and situation across the East Pacific Rise (EPR). From the top to the bottom: Pacific plate fixed (relative plate motion); classical NNR solution; hotspot deep source (first solution); hotspot shallow source (second solution) [after *Riguzzi et al.*, 2006]

also explain the low dip of the Andean slab, which both suggest a relative eastward mantle flow. Similar eastward mantle flow was proposed for the North America plate [*Silver and Holt*, 2002]. The low dip of the Andean slab has alternatively been attributed to the young age of the subducting lithosphere. However the oceanic age has been proved not to be sufficient to explain the asymmetry between "westerly"–directed (steep and deep) vs. "easterly"–directed (low dip and shallow) subduction zones [*Cruciani et al.*, 2005]. In fact the geographically related asymmetry persists even where the same lithosphere (regardless oceanic or continental) subducts in both sides, such as in the Mediterranean orogens [*Doglioni et al.*, 1999].

Another consequence to have a shallower source of the Hawaiian magmatism is to increase the westward motion of the Pacific plate to a velocity faster than the spreading rate of the EPR [see Figure 7, option 2 of *Doglioni et al.*, 2005]. The shallow, intra-asthenospheric origin of the Pacific hotspots provides a kinematic frame in which all mid oceanic ridges move westward. As a consequence, the ridge migrates continuously over

a fertile mantle. The rift generates melting and the increase of viscosity of the residual mantle, providing a mechanism for maintaining slower the plate to the east.

To summarize the concepts presented above, in Figure 3.6 different kinematic cases along the East Pacific Rise are presented. Assuming for sake of simplicity that the relative motion is of about 11 cm yr^{-1}, all the velocities of plates are presented in the different reference frames. In case of shallow hotspots, the two plate move toward the west.

The deep and shallow hotspot interpretations generate two hotspot reference frames. In case of deep mantle source of the hotspots, there still are few plates moving eastward relative to the mantle (Figure 3.4), whereas in the shallow one, all plates, although at different velocities, have a westward component (Figure 3.5).

3.5 Discussion

We have computed absolute plate motions in two different hotspot reference frames, one deep–fed and the other shallow–fed, using only Pacific intraplate volcanic propagation rates. In the first case, we exactly obtained the HS3–NUVEL1A results [*Gripp and Gordon*, 2002], whereas, in the second case, we obtained new faster plate motions with respect to the mesosphere. Moreover in the deep hotspot frame, rotation poles are largely scattered and most of the plates move toward the west except for Nazca, Cocos, Juan de Fuca. On the contrary, relative to the shallow hotspot framework, all plates have a westward direction and rotation poles are mostly located in a restricted area at mean latitude and longitude of 58°S and 90°E respectively.

Furthermore, we computed net–rotation of the lithosphere (faster in case of a shallow–sourced hotspot), useful to compute plate motions in the mean–lithosphere reference frame (NNR) [*Jurdy*, 1990]. The mean-lithosphere is also the framework for space geodesy applications to plate tectonics [*Heflin et al.*, 2004]. Most of the geodetic plate kinematic models are referred to the NNR–frame [*Sella et al.*, 2002; *Drewes and Meisel*, 2003]. The International Terrestrial Reference Frame (ITRF2000) [*Altamimi et al.*, 2002] is the framework where site velocities are estimated. The ITRF2000 angular velocity is defined using the mean–lithosphere. As suggested by *Argus and Gross* [2004], it would be better to estimate site positions and velocities relative to the hotspots, continuing firstly to estimate velocity in the ITRF2000 and the adding the net–rotation angular velocity.

The results obtained in this chapter represent an advance with respect to those obtained in the Chapter 2. We have demonstrated that, assuming a shallower source of the hotspots, all the plates move toward the west, and the westward drift of the lithosphere

is not only one of the mean values [e.g., *O'Connell et al.*, 1991; *Gripp and Gordon*, 2002], but may be a real and quantified aspect of global geodynamics. Moreover, all the plates, moving westward, would follow trajectories that are very similar to the flow lines described in *Doglioni* [1990] (Figure 1.6).

The shallow hotspot reference frame makes the idea of the global tectonic pattern, stronger and well quantified. With respect to the methods used in the Chapter 2, these new results are not tied to existence of the pattern itself, but come out after testing a different geodynamic hypothesis about the depth of the hotspots that is becoming common among the geoscientists [*Foulger et al.*, 2005]. This implies that the shallow hotspot reference frame could be a good framework where to cross results coming from plate dynamic models.

Chapter 4

Hotspots and space geodesy

In this chapter, we obtained absolute plate motions relative to the hotspots, incorporating the REVEL plate kinematic model [*Sella et al.*, 2002], using methods presented in the Chapter 3 and testing both the deep and shallow hypothesis for the source of the Pacific intraplate hotspots. We computed two new different net–rotation angular velocities and we present plate kinematics relative to the hotspots for a total of 20 plates, using 17 relative plate motions deriving from space geodesy, whereas we used three plate motion parameters from the NUVEL1A [*DeMets et al.*, 1994]. To do this, we modified plate boundary data in digital form presented by *Bird* [2003], including the microplates lying at the interface of large plates, into the large plate themselves.

As in the Chapter 3, the shallow hotspot reference frame incorporating space geodesy data makes evident the global tectonic pattern and the westward drift of the lithosphere.

4.1 Introduction

The first goal of plate kinematics concerns to investigate relative plate motions. Global inverse solutions on boundaries provide Euler poles and angular velocities, which are useful to understand how a plate moves with respect to one another. This kind of information can be the standard reference to study mechanisms of accumulating stress, release of energy during an earthquake, or to make earthquake predictions.

On the other hand, relative plate motions fail in discovering the reasons and causes of plate tectonics. To answer to these questions, plate kinematics has to be referred to absolute reference frames, where a complete view of motions relative to the mantle is necessary to understand the dynamics involved in the tectonic processes.

There is still a debate among geophysicists about the goodness of the two absolute reference frames, e.g. the hotspots and the mean–lithosphere (see also Section 1.3.2, page 8), useful to describe plate motions relative to the mesosphere.

A conclusion has still to be reached, but in the past few years there has been a complete separation between absolute plate motions deriving from different techniques (e.g. geophysical data and space geodesy). In fact, the hotspot framework is the reference system in which relative plate motions coming from geophysical and geological data are generally incorporated [e.g. *Gripp and Gordon*, 1990, 2002]. On the other hand, the NNR reference frame is the system in which motions between two plates deriving from space geodesy data are always recalibrated [e.g. *Sella et al.*, 2002; *Drewes and Meisel*, 2003; *Kreemer and Holt*, 2003].

In their paper, *Argus and Gross* [2004] discuss the validity of the hotspot reference frame with respect to the mean–lithosphere (NNR). They conclude that, for a better knowledge of absolute plate kinematic processes, the new space geodesy techniques applied to geodynamics should be utilized in the hotspot framework. The NNR–frame is a simple reference system in which to obtain results coming from space geodesy. For this reason, they propose to firstly estimate site positions and velocities relative to mean–lithosphere and then to make a passage of reference into the hotspots, by making use of the net–rotation of the lithosphere (see Section 1.3).

We believe that the more appropriate reference frame describing plate motions relative to the mesosphere is the hotspot system, because is based on more geophysical assumptions and better indicates the decoupling in the asthenosphere between the lithosphere and the mesosphere.

In this chapter, we obtained absolute plate motions in the hotspot reference frame incorporating relative motions deriving from space geodesy data, using the REVEL plate kinematic model [*Sella et al.*, 2002]. We also computed different net–rotation angular velocities, testing the deep and shallow hypothesis for the source of hotspots.

Because *Sella et al.* [2002] used a much more extensive space geodetic dataset to construct their model for recent plate velocities, and a robust statistical approach to estimate the uncertainties of the motion rates, this choice guarantees an accurate evaluations of relative motions. It also ensures that the calculated relative motions are not affected by local stress release along plate margins, because motion of plates and crustal blocks are evaluated choosing sites located $>$100 km from significant plate boundary zone–related seismicity.

Since in the REVEL model, motions of new plates are proposed, we had to modify

plate boundary data to obtain the correct net–rotation angular velocities. To do this we used the PB2002 model [*Bird*, 2003] and its plate boundary data proposed in digital form.

4.2 Plate boundary data

Plate kinematic models generally give Euler vectors of plates, but there are no standard references on plate boundaries worldwide. Authors of global inverse solutions for Euler poles of large plates [e.g. *Chase*, 1972, 1978; *Minster et al.*, 1974; *Minster and Jordan*, 1978; *DeMets et al.*, 1990, 1994] provided boundaries of the largest plates in the form of small-scale maps, and lists of locations of discrete plate-boundary data used in the inversion. In those models, the ideal number of plates is generally around 15 (see Figure 1.1).

Bird [2003] presented his PB2002 model and proposed new plate boundary data in digital form of 14 large plates and 38 microplates for a total of 52 plates. He classified "plates" those part of the lithosphere presenting clear geological boundaries, whereas he called "orogens" the complex zones of the Earth, as the Alpine-Himalayan mountain belt, in which is difficult to define plate margins (Figure 4.1)

Sella et al. [2002], in their REVEL plate kinematic model, presented plate motions of seven additional plates, the Amuria (AM), the Anatolia (AT), the Okhotsk (OK), the South Cina (CS), the Sierra Nevada (SR), the Somalia (SO) and the Sunda (SU).

We modified the digital data of the PB2002 model [*Bird*, 2003] to obtain 20 lithospheric plates (Figure 4.2) that cover the whole surface of the lithosphere, treating the microplates of the PB2002 model [*Bird*, 2003] which lie at the interfaces of large plates as deformation zones and including them into the large plates themselves. We also included the South China (CS) and the Sierra (SR) of the REVEL model [*Sella et al.*, 2002] in the Eurasia plate (EU) and in the North America plate (NA) respectively.

In fact,of the Sierra Nevada plate (SR) of *Dixon et al.* [2000] and *Sella et al.* [2002] is also treated by *Bird* [2003] as a "orogen" (Figure 4.1), and this makes stronger the idea that it is very difficult to find evidence of its plate boundaries, and probably it is better to interpret different velocities of that region as a consequence of its nature of deformation zone of the North America plate. The South China plate (CS) instead,, also defined Yangtze Plate (YA) by *Bird* [2003], is an aseismic region in southwestern China [*Giardini et al.*, 1999], which seems to be unaffected by the Hymalaian continental collision. The only distinct boundary of the South China (CS) is in the east, where it collides with the Philippine plate (PH), whereas the other boundaries corresponds to the "orogens" of the

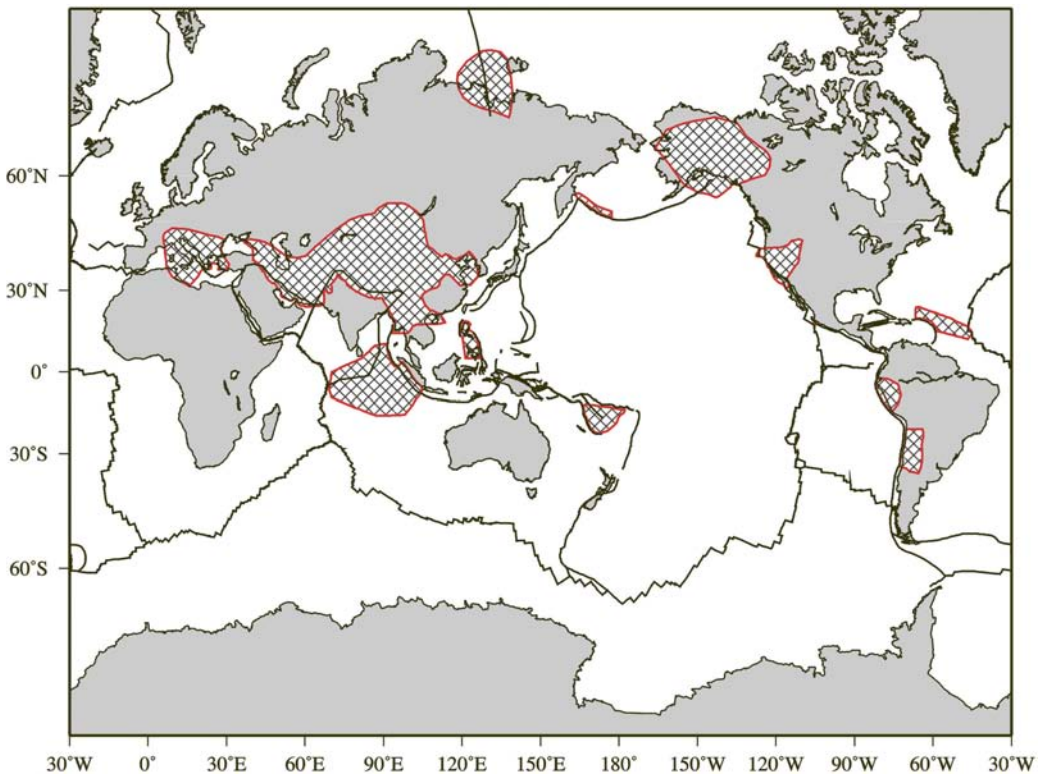

Figure 4.1: Deformation zones (cross–hatched areas) represent complex zones of the Earth in which is difficult to define plate boundaries, as the Alpine-Himalayan mountain belt, and they were classified as “orogens”, while present large plates show a clear geolgical evidence [after *Bird*, 2003].

Hymalian system (Figure 4.1). Moreover, GPS geodesy [*Heki et al.*, 1999] has shown that the region contains three stations whose velocity is consistent with the hypothesis that they belong to a rigid plate: WUHN (Wuhan), SHAO (Shanghai), and Taipei. Their common motion is different from that of Eurasia by about 13 mm yr^{-1} to the ESE, well in excess of measurement errors. We believe that, as in the previous case, these differences of velocities can be the consequence of local deformations and the South China (CS) can be consider as a deformation zone. For those reasons, we included it in Eurasia plate (EU).

Then, of the seven additional plates studied by *Sella et al.* [2002], we decided to save only five of them, the Amuria (AM), the Anatolia (AT), the Okhotsk (OK), the Somalia (SO) and the Sunda (SU).

In early 15–plate models of the Earth such as RM2 [*Minster and Jordan*, 1978],

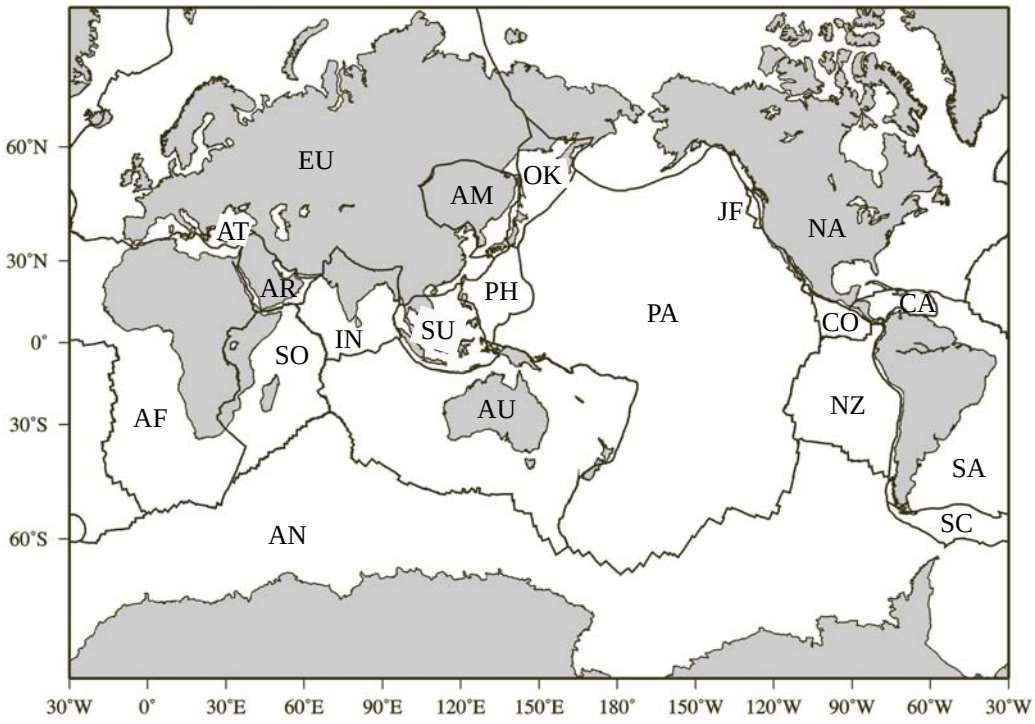

Figure 4.2: Lithospheric plates and additional plates. Amuria (AM), Africa (AF), Antarctica (AN), Arabia (AR), Antatolia (AT), Australia (AU), Caribbean (CA), Cocos (CO), Eurasia (EU), India (IN), Juan De Fuca (JF), North America (NA), Nazca (NZ), Okhotsk (OK), Pacific (PA), Philippine (PH), South America (SA), Scotia (SC), Somalia (SO), Sunda (SU). Plate boundary data are from the modified PB2002 model [*Bird*, 2003].

NUVEL–1 and NUVEL1A [*DeMets et al.*, 1990, 1994], the North America plate (NA) was considered to extend across the Bering Sea and include the Kamchatka Peninsula, the Sea of Okhotsk, and northern Honshu [*Chapman and Solomon*, 1976]. *Savostin et al.* [1982, 1983] used the name "Okhotsk plate" (OK) for the region lying south of a chain of small sedimentary basins in the Cherskii Mountains, which they interpreted as active grabens in an extensional OK-NA boundary. *Cook et al.* [1986] studied a chain of earthquakes in this region, and found focal mechanisms along the proposed OK–NA boundary to be sinistral-transpressive, rejecting the previous interpretation that the small sedimentary basins are active grabens. *Seno et al.* [1996] studied those regions and found an Euler vector for OK–EU relative plate motion using space geodesy.

The name "Amur microplate" (AM) was also proposed by *Savostin et al.* [1982, 1983] for the parts of eastern Mongolia, north China, and southeastern Russia which lie south-

east of the Lake Baikal extensional province and they proposed that this block moved southeast with respect to Eurasia (EU). *Miyazaki et al.* [1996] combined GPS velocities from Japan and Korea with seismic slip vectors from Baikal and the Stanovoy Mountains to confirm that this motion occurs at several millimeters per year. *Wei and Seno* [1998] performed a six–plate analysis (PA, NA, EU, OK, PS, AM) of earthquake slip vectors and NUVEL–1 data, including an Amur plate (AM) distinct from EU, and still concluded that OK is distinct from NA. Additional GPS geodetic results of *Takahashi et al.* [1999] were interpreted as confirming the *Miyazaki et al.* [1996] model for AM-EU motion, but the most recent geodetic study on Amur plate (AM) motion is *Heki et al.* [1999]. Using 15 GPS stations, they find that AM separates from EU at 9–10 mm yr^{-1}, and compute its Euler pole. Their direction of relative velocity at Baikal is nearly E–W.

The Sunda plate (SU) includes most of southeast Asia, the South China Sea, the Malay Peninsula, most of Sumatra, Java, Borneo, and the intervening shallow seas [*Rangin et al.*, 1999] and in early 15–plate models of the Earth, this region was considered part of the Eurasia plate (EU). *Genrich et al.* [1996] used GPS to define a "Sunda shelf block" (SU) which was indistinguishable from a rigid body, but they lacked the network breadth to precisely fix its rotation with respect to Eurasia. The GEODYSSEA geodetic campaigns of 1994 and 1996 resulted in a solution with a SU–EU rotation pole [*Chamot-Rooke and Le Pichon*, 1999; *Rangin et al.*, 1999].

The East Africa rift appears to be a slowly spreading plate boundary, based on topography, seismicity, and volcanism. *McKenzie et al.* [1970] were the first to use the name "Somalian plate" (SO) and computed net AF–SO separation since 20 Ma to be up to 65 km in the NW–SE direction. Global plate kinematic model presented in the next years [*Minster and Jordan*, 1978; *DeMets et al.*, 1990, 1994] considered this possible boundary and rejected it because the inferred motion was unreasonable. Later, *Chu and Gordon* [1999] studied again this boundary and found that SO and AF motions are distinct with high confidence, finding a relative pole of rotation which implies separation at 6 mm yr^{-1} at the north end of the AF–SO boundary.

Finally, the recognition of discrete plates between Africa (AF) and Eurasia (EU) started with the study of *McKenzie* [1972], who combined historical and instrumental seismicity, focal mechanisms, geology, and topography to propose that Anatolia plate (AT) is extruded westward to escape the collision of Arabia (AR) with Eurasia (EU). He also proposed a separate Aegean block which travels southwestward with respect to Eurasia (EU), diverging from the Anatolia plate and overriding the Africa plate at the Aegean Trench. *Jackson* [1992] and *Westaway* [1994] supported and developed the model by

Table 4.1: Plate geometrical factors modified after *Bird* [2003]. Plate identifiers are those of the Figure 4.2 and LS corresponds to the whole lithosphere.

PLATE	Area	I_{xx}	I_{yy}	I_{zz}	I_{xy}	I_{xz}	I_{yz}
AF	1.4407	0.3726	1.3012	1.2075	-0.0513	-0.0054	0.0442
AM	0.1306	0.1082	0.0895	0.0636	0.0287	0.0363	-0.0513
AN	1.4344	1.3284	1.1762	0.3642	-0.0508	0.0528	0.0806
AR	0.1208	0.0742	0.0668	0.1006	-0.0488	-0.0296	-0.031
AT	0.0221	0.0118	0.0186	0.0138	-0.0059	-0.0092	-0.0053
AU	1.2174	0.8177	0.6635	0.9536	0.2178	-0.2334	0.2904
CA	0.0798	0.0726	0.0123	0.0747	0.0190	-0.0054	0.0181
CO	0.0751	0.0737	0.0035	0.0729	-0.0062	0.0013	0.0109
EU	1.2587	1.0572	0.9189	0.5411	-0.0159	-0.2016	-0.3324
IN	0.3191	0.2990	0.0428	0.2964	-0.0562	-0.0130	-0.0624
JF	0.0064	0.0052	0.0044	0.0031	-0.0015	0.0019	0.0025
NA	1.3657	1.2286	0.9416	0.5612	0.0662	-0.0036	0.3963
NZ	0.4032	0.3911	0.0706	0.3447	-0.0145	-0.0040	-0.1159
OK	0.0748	0.0534	0.0664	0.0298	0.0130	0.0303	-0.0179
PA	2.6194	1.1956	1.9833	2.0599	-0.4045	0.0811	-0.0586
PH	0.1450	0.0820	0.0789	0.1291	0.0629	0.0292	-0.0294
SA	1.0749	0.6660	0.6154	0.8684	0.3521	0.1928	-0.1745
SC	0.0464	0.0402	0.0387	0.0139	0.0062	0.0138	-0.0154
SO	0.4719	0.2842	0.2349	0.4248	-0.1982	0.0608	0.0655
SU	0.2602	0.2158	0.0503	0.2544	0.0880	0.0048	-0.0144
LS	12.5665	8.3775	8.3778	8.3777	0.0001	-0.0001	0.0000

Units are in steradians

showing that the major faults in the region have estimated slip rates which are compatible with rigid-plate kinematics.

With the beginning of the GPS measurements *Le Pichon et al.* [1995] and *Reilinger et al.* [1997] proposed to simplify the model by merging the Aegean Sea and Anatolia plates into one, allowing some internal deformation, but on the contrary *Papazachos* [1998] maintained that the motions of the Aegean Sea and Anatolia are distinct.

After ten years of GPS results, *McClusky et al.* [2000] show that geodesy agrees with

historical seismicity in defining two regions, an Aegean Sea plate, and an Anatolia plate.

According to the model proposed by *Doglioni et al.* [2002], and following results proposed by *Sella et al.* [2002], we decided to merge the two plate into one, the Anatolia plate (AT), considering the difference of velocities as the consequence of the intra–plate deformation. This choice is reinforced by the fact that it is difficult to define the boundaries of the Aegean Sea block, and also *Bird* [2003] considered these regions as extensions of the Alps orogen.

With this set of 20 plates, we modified the digital plate boundaries of *Bird* [2003] (Figure 4.2) and we computed plate geometrical factors, by making use of the equation (1.3) (page 10), closing the Earth's surface with three significant digits. Results are reported in Table 4.1.

4.3 Absolute plate velocities incorporating space geodesy

The plate velocities computed by plate kinematic models based on geological data are sometimes termed "present-day" or "current" because they describe geologically young plate motions, generally for a ≈ 3 Myr time interval (mid–Pliocene) [*Minster and Jordan*, 1978; *DeMets et al.*, 1990, 1994], or for a ≈ 0.8 Myr (mid–Pleistocene) [*DeMets*, 1995; *Conder and Forsyth*, 2000].

Geodetic plate motion models, as REVEL [*Sella et al.*, 2002] are derived from data over a very different time span, roughly the last decade. It is probably representative of plate motions over the Holocene or Recent epoch (last $\approx 10^4$ years). and possibly the late Pleistocene epoch (last few hundred thousand years), even if results show good agreement with geological data [*Robbins et al.*, 1993]. To emphasize the time span over which *Sella et al.* [2002] believed their model to be valid, they have termed it "REVEL" (for Recent velocities).

In this section, we present absolute plate velocities relative to the hotspots incorporating recent relative plate velocities coming from space geodesy, for a ≈ 5.8 Myr time interval.

4.3.1 The Pacific–fixed reference frame

Sella et al. [2002] used GPS sites to estimate plate velocities. They state that the uncertainty in the positions of the GPS satellites is a major error source for the coordinate time series used in their study. By 1993 the global tracking network for GPS satellites became sufficiently robust to produce more accurate satellite ephemerides (satellite positions as

Table 4.2: Variance–covariance matrix (Cartesian Pacific–fixed coordinates).

PLATE	σ^a_{xx}	σ^a_{yy}	σ^a_{xx}	σ^a_{xy}	σ^a_{xz}	σ^a_{yz}
AF	171	37	99	5	7	-4
AM	8666	13495	14440	-10625	-10972	13780
AN	115	72	332	16	-15	-86
AR	1202	1137	776	1084	824	830
AT	1019529	423986	989791	657259	1004307	647598
AU	188	143	149	-83	67	-83
CA	384	1466	256	-609	189	-446
CO[b]	758	8877	653	871	-172	1960
EU	123	28	123	21	36	15
IN	734	13372	942	2905	724	3356
JF[c]	10663	11755	19379	6207	-14034	-11118
NA	94	32	62	10	-4	-9
NZ	246	1426	420	360	149	583
OK	18322	13194	18892	-15369	-18392	15611
PH	3257	3729	1363	-3361	-1925	2081
SA	245	176	106	-125	-39	34
SO	117	43	55	33	-6	-2
SU	1378	17385	217	-4632	199	-758

[a] Units are 10^{-10} radians^2 Myr^{-2}

[b] Data from NUVEL–1 [*DeMets et al.*, 1990]

[c] Data from *Gripp* [1994]

a function of time) compared to earlier periods. Their data span the time period from 1993 to 2000. Hundred thousand of station days of data were analyzed for the REVEL plate kinematic model, most of which lie in stable plate interiors and are used to estimate plate velocities. Site velocity errors are generally the uncertainty of the slope estimate, accounting for uncorrelated and time–correlated noise, total time span of observations, and total number of observations.

Sella et al. [2002] presented a set of angular velocities in the ITRF–97 reference frame [*Boucher et al.*, 1999]. Their results superficially resembles the velocity field predicted by the NUVEL-1 in a no-net-rotation reference system (NNR–NUVEL1) [*Argus and Gordon*, 1991], or its updated version, NNR–NUVEL1A [*Argus and Gordon*, 1991;

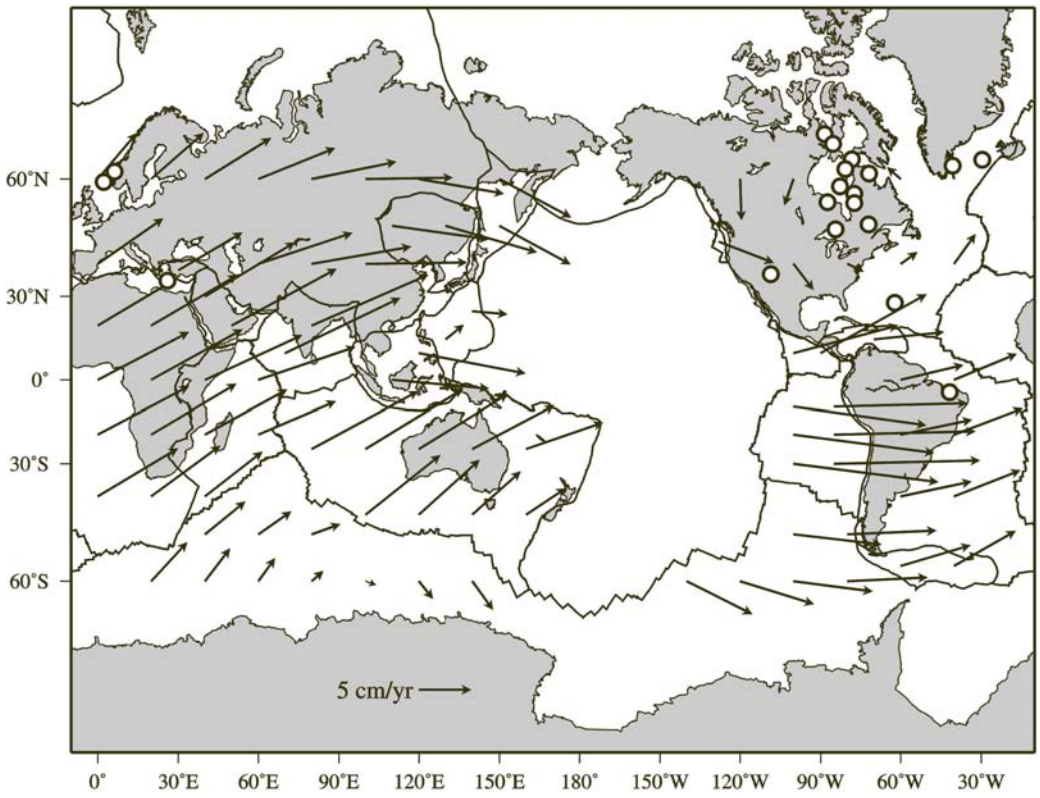

Figure 4.3: Plate velocities in the Pacific–fixed reference frame. Data of the largest 17 plates come frame the REVEL plate kinematic model based on space geodetic data. The velocities of the additional plates (CO, JF, SC) are computed with the Euler vectors of the NUVEL1A [*DeMets et al.*, 1990, 1994]. Open circles represent plate rotation poles.

DeMets et al., 1994], because of the way ITRF is defined, as similar as its most updated version, the ITRF2000 [*Altamimi et al.*, 2002, 2003] (see Chapter 2). They also provided relative plate motions of plates sharing a boundary, and made comparisons with results obtained from geological data [*DeMets et al.*, 1990, 1994].

For the purpose to incorporate space geodetic data into the hotspot reference frame, referring to the methods proposed in the Chapter 3, we had to refer all plate motions with respect to the Pacific plate stated fixed, (Figure 4.3 and Table 4.3). To do this, we used the simple combination properties of the Euler vectors, collected by many textbooks [*Cox and Hart*, 1986; *Fowler*, 1990; *Stein and Wysession*, 2003].

Table 4.3: Plate angular velocities relative to the Pacific–fixed reference frame. Date are from the REVEL plate kinematic model [*Sella et al.*, 2002]

PLATE	Angular Velocity			Standard Error Ellipse			σ_ω
	°N	°E	° Myr^{-1}	σ^a_{max}	σ^a_{min}	ζ^b	° Myr^{-1}
AF	61.027	-71.802	0.9028	0.666	0.352	76	0.0055
AM	67.409	-88.421	0.9564	8.619	0.677	120	0.0380
AN	65.964	-85.384	0.8567	0.587	0.382	92	0.0107
AR	63.404	-29.575	1.1154	1.899	0.445	90	0.0174
AT	59.473	2.096	1.3723	23.150	0.495	58	0.7916
AU	61.390	6.190	1.0800	0.575	0.428	118	0.0082
CA	57.075	-77.388	0.9010	1.536	0.534	107	0.0191
EU	63.487	-78.330	0.9034	0.588	0.346	102	0.0057
IN	62.449	-40.559	1.1040	5.112	0.432	121	0.0054
NA	50.383	-72.114	0.7548	0.604	0.362	79	0.0043
NZ	55.409	-87.290	1.2668	1.532	0.447	73	0.0080
OK	27.763	-62.313	0.7014	13.540	0.924	109	0.0471
PH	-4.630	-41.724	0.8740	1.682	0.584	75	0.0487
SA	58.544	-82.701	0.6372	1.347	0.673	135	0.0057
SO	61.822	-80.621	0.9518	0.551	0.290	99	0.0041
SU	55.152	-77.454	1.0191	4.956	0.526	93	0.0478
Additional Plate Angular Velocity							
CO[c]	36.823	-108.629	1.9975	1.068	0.575	123	0.0498
JF[c]	28.300	29.300	0.5200	16.708	6.768	101	0.0131
SC[c]	49.100	-81.400	0.6600	–	–	–	–

[a] 1–sigma lengths of the semi–major σ_{max} and semi–minor axes σ_{min} of the pole error ellipse. Units of the semi–major and semi–minor axes are in degrees.

[b] ζ is the azimuth of the semi-major ellipse axis in degrees clockwise from north.

[c] Data from the NUVEL1A plate kinematic model [*DeMets et al.*, 1990, 1994]

In Table 4.3, we present 16 plate motions in the Pacific–fixed reference frame, using data from the REVEL plate kinematic model [*Sella et al.*, 2002]. Using the NUVEL1A plate kinematic parameters [*DeMets et al.*, 1990, 1994], three additional plates were included, such as Cocos (CO), Juan de Fuca (JF), and Scotia (SC), that are required to compute net–rotation of the lithosphere. Moreover in Table 4.3, error ellipses of Euler poles and angular velocity rate uncertainties are reported. They were computed following methods proposed in the Appendix B, using covariance matrices presented in Table 4.2.

Covariance matrices come from the REVEL plate kinematic model [*Sella et al.*, 2002], whereas the additional plate matrices are from the NUVEL–1 model [*DeMets et al.*, 1990]. The NUVEL1A model [*DeMets et al.*, 1994] offers some additional plate angular velocities, e.g. the Philippine motion (PH) recalibrated by *Seno et al.* [1993]. Here, the covariance matix of the Philippine plate in substituted with the one presented by *Sella et al.* [2002], whereas we used the NUVEL-1 model for the Cocos plate (CO) and the covariance matrix proposed by *Gripp* [1994] for the Juan de Fuca plate (JF), that represents an updated datum with respect the one used by *Nishimura et al.* [1984].

In contrast, the Scotia plate (SC) was included in the model without any error ellipse evaluation (Table 4.3), because the covariance matrix of the Scotia plate is not reported in the NUVEL–1 kinematic model. Many authors have investigated the motion of the Scotia plate [e.g., *Pelayo and Wiens*, 1989; *Thomas et al.*, 2003; *Eagles et al.*, 2005], but a complete covariance matrix for the kinematics of that plate is not presented. For example, *Eagles et al.* [2005] only studied the west Scotia sea, whereas we defined the Scotia plate as the unification of west and east Scotia seas, and for this reason, we decided to not utilize their covariance matrix. Moreover, *Thomas et al.* [2003] give the error ellipse for Euler poles for the west and east Scotia Sea relative motions, but they did not present matrices of error components. Then, we decide to insert in the Table 4.3 the Euler vector proposed by *Pelayo and Wiens* [1989], also reported in the NUVEL1A plate kinematic model, without any error ellipse or rate uncertainty, following the approach used by *Kreemer et al.* [2006].

In their paper, *Kreemer et al.* [2006] included motions of plates that have insufficient velocities to determine their angular velocity geodetically. They used published geologic rates to determine the no–net–rotation angular velocity, considering the motion of the Capricorn plate [*DeMets et al.*, 2005], the Caroline plate [*Weissel and Anderson*, 1978], the Cocos plate [*DeMets*, 2001], the Juan de Fuca plate [*Wilson*, 1993], the Rivera plate [*DeMets and Wilson*, 1997] and the Scotia plate [*Thomas et al.*, 2003], and presenting the angular velocities of these plates in the NNR framework without uncertainties.

We decided to use a similar approach for the additional plates of the Table 4.3, considering only the Cocos, Juan de Fuca and Scotia plate Euler vectors coming from the NUVEL1A and enclosing the small plates collected by *Kreemer et al.* [2006] in the large plates respectively (see Section 4.2).

Plate motions in the Pacific–fixed reference frame, although have essentially different angular velocity vectors than the ones obtained with geologic data, show anyhow, under a global scale point of view, a similar configuration of rates and azimuths of the Figure 1.9. On a large scale, the rotation poles lie at high latitudes (30°–60°N) in a small range of longitudes (90°–30°W). Error ellipse of Euler poles and rate uncertainties of the Table 4.3 show a similar order of magnitude, except for the error ellipses of the Amuria (AM), Anatolia (AT), Okhotsk (OK) and Juan de Fuca (JF) plate, that exceed two orders, presenting errors of hundreds of kilometers in positioning the rotation poles of those plates respectively.

4.3.2 Space geodesy data and the deep and shallow hotspots

The Pacific–fixed reference frame defined in the previous section represents the first step for propagating relative plate motions in the absolute hotspot system. We basically follow methods presented in the Chapter 3, proposing two different–fed hotspot frameworks, incorporating plate motions coming from recent space geodesy data.

As just mentioned in the Chapter 3, the HS3–NUVEL1A [*Gripp and Gordon*, 2002] absolute plate motion model is based on the deep–fed hotspot hypothesis. *Gripp and Gordon* [2002] computed absolute plate motions, basically estimating propagation rates of Hawaii and Society volcanic tracks, both on the Pacific plate, to position their Pacific Euler vector. Another simple way to reproduce the HS3–NUVEL1A angular velocities consists in adding the Pacific plate angular velocity, estimated by *Gripp and Gordon* [2002], to the relative plate motion model NUVEL-1A [*DeMets et al.*, 1990, 1994].

Here, we follow these methods to refer space geodesy results of the REVEL plate kinematic model in the hotspot reference frame. We tested first the deep–fed hypothesis, adding the Pacific plate angular velocity of *Gripp and Gordon* [2002] to the motions of the Table 4.3, and obtaining absolute plate motions relative to the deep hotspots, incorporating space geodetic data (Table 4.4 and Figure 4.4). We also used the covariance matrix of the model HS3–NUVEL1A [*Gripp and Gordon*, 2002] to obtain uncertainties of the Table 4.4, by making use of properties of the combination of the covariance matrices [*Stock and Molnar*, 1983; *Chang et al.*, 1990] (see Appendix B).

Table 4.4: Plate angular velocities relative to the deep hotspot reference frame, incorporating the REVEL plate kinematic model [*Sella et al.*, 2002]

PLATE	Angular Velocity			Standard Error Ellipse			σ_ω
	°N	°E	° Myr^{-1}	σ^a_{max}	σ^a_{min}	ζ^b	° Myr^{-1}
AF	-41.352	34.388	0.2158	25.703	14.194	48	0.0606
AM	-19.446	87.033	0.1483	48.541	25.926	59	0.0760
AN	-42.951	81.002	0.2201	24.371	16.973	89	0.0582
AR	7.347	31.122	0.5081	10.316	7.413	128	0.0708
AT	15.936	37.507	0.9094	29.773	5.169	99	0.8189
AU	1.186	47.743	0.7604	6.538	4.351	48	0.0717
CA	-58.477	15.586	0.2066	28.002	16.393	121	0.0571
EU	-42.176	54.908	0.1847	28.726	17.439	65	0.0611
IN	6.262	24.428	0.4255	15.939	9.276	111	0.0748
NA	-66.450	18.644	0.3828	15.683	8.471	128	0.0557
NZ	27.333	-81.627	0.2406	21.690	17.565	74	0.0605
OK	-64.517	-8.497	0.6709	11.085	7.035	75	0.1222
PA[c]	-61.467	90.326	1.0613	5.710	3.690	166	0.0498
PH	-56.997	-6.421	1.1959	5.413	3.124	99	0.0681
SA	-64.986	77.470	0.4291	14.001	8.874	91	0.0515
SO	-44.582	42.064	0.1331	37.889	22.637	55	0.0602
SU	-34.829	-26.442	0.1682	39.105	22.364	77	0.0703
	Additional Plate Angular Velocity						
CO	13.171	-116.997	1.1621	4.432	3.064	127	0.0885
JF	-39.516	61.531	1.0780	6.638	3.823	52	0.1223
SC[c]	-76.912	52.228	0.4451	13.560	7.990	19	0.0523

[a] 1–sigma lengths of the semi–major σ_{max} and semi–minor axes σ_{min} of the pole error ellipse. Units of the semi–major and semi–minor axes are in degrees.

[b] ζ is the azimuth of the semi-major ellipse axis in degrees clockwise from north.

[c] Data from the HS3-NUVEL1A plate kinematic model [*Gripp and Gordon*, 2002].

Table 4.5: Variance–covariance matrix incorporating space geodesy (Cartesian hotspot coordinates).

PLATE	σ^a_{xx}	σ^a_{yy}	σ^a_{xx}	σ^a_{xy}	σ^a_{xz}	σ^a_{yz}
AF	7833	15652	8652	3523	-1775	3090
AM	16328	29105	22993	-7102	-12752	16874
AN	7777	15687	8885	3534	-1797	3008
AR	8864	16752	9329	4602	-958	3924
AT	1027662	439615	998353	660818	1002218	650694
AU	7850	15758	8702	3435	-1715	3011
CA	8046	17081	8809	2909	-1593	2648
CO	8420	24492	9206	4389	-1954	1134
EU	7785	15643	8676	3539	-1746	3109
IN	8396	28985	9495	6423	-1058	6450
JF	18325	27370	27932	9725	-15816	-8024
NA	7756	15647	8615	3528	-1786	3085
NZ	7908	17041	8973	3879	-1633	3677
OK	25982	28805	27443	-11852	-20172	18704
PA[b]	7662	15615	8553	3518	-1782	3094
PH	10919	19344	9916	157	-3707	5175
SA	7907	15791	8659	3393	-1821	3128
SO	7779	15658	8608	3551	-1788	3092
SU	9040	32995	8770	-1114	-1583	2336

[a] Units are 10^{-10} radians^2 Myr^{-2}

[b] Data from the HS3–NUVEL1A plate kinematic model [*Gripp and Gordon*, 2002]

Following methods of the Appendix B, we computed error ellipses of Euler pole and rate uncertainties, combining covariance matrices reported in Table 4.2 with the Pacific plate covariance matrix presented by *Gripp and Gordon* [2002], obtaining plate covariance matrices of the Table 4.5. We also recomputed absolute plate motions of the additional plates, especially for the Cocos plate (CO) and the Juan de Fuca plate (JF), and on the contrary we reported in Table 4.4 the Pacific and Scotia plate Euler vectors and uncertainties such as literally presented in the HS3–NUVEL1A [*Gripp and Gordon*, 2002].

Absolute plate motions in the deep–hotspot framework recalibrated with data coming from space geodesy have essentially different rates and rotation poles with respect to the

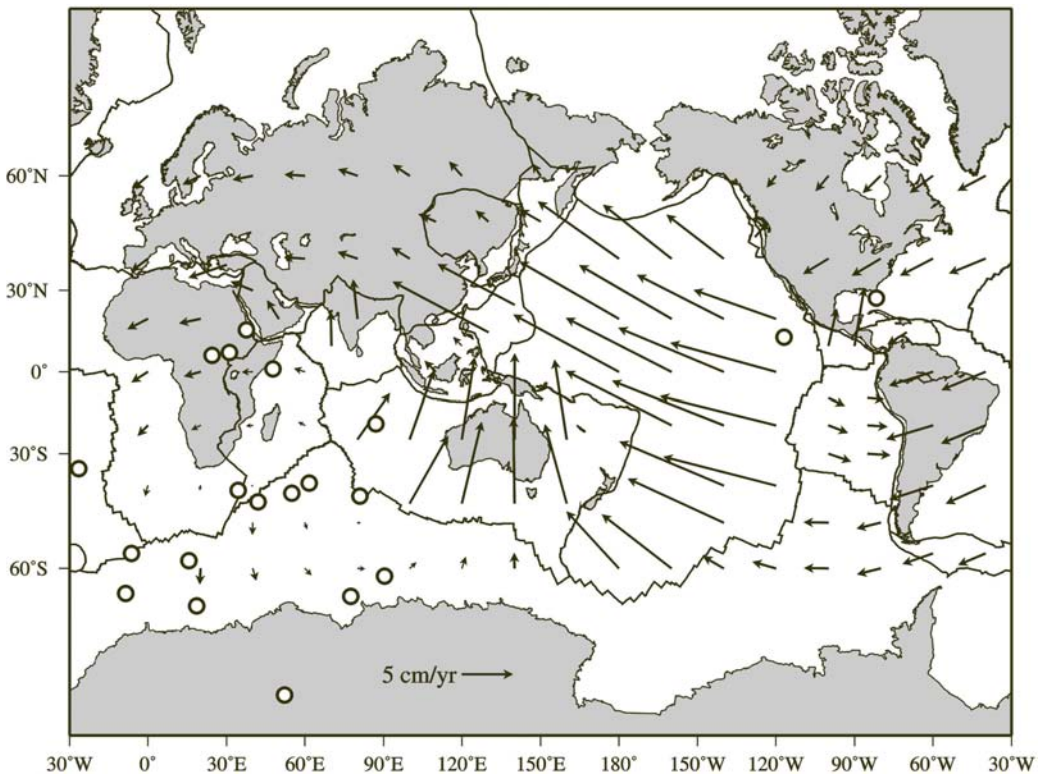

Figure 4.4: Current absolute velocities with respect to the deep hotspot reference frame, incorporating space geodesy data from the REVEL plate kinematic model [*Sella et al.*, 2002]. Open circles represent plate rotation poles.

ones computed with geologic data, especially for Arabia (AR), Caribbean (CA), Eurasia (EU), Philippine (PH), and South America (SA) plates (Table 4.4). Although these discrepancies, the global distribution of plate velocity vectors well describes absolute plate motions obtained with geophysical data (see Figure 3.4). Plates generally move westward with respect to mantle, except for Nazca (NZ) that presents W–E velocity vector directions. Rotation poles generally lie at high latitudes at a mean value of 60 °S, but many of them, e.g. those of the Arabia (AR), the Anatolia (AT), the Australia (AU) and the India (IN) plate are located at low latitudes (Figure 4.4). These positions continue to guarantee that those plates move toward the west. Moreover the addition of the plates defined in the Section 4.2, such as the Amuria (AM), the Anatolia (AT), the Okhotsk (OK), the Somalia (SO) and the Sunda (SU) plate do not change the global scale plate kinematics (e.g., velocity vector azimuths). Plate motions in the hotspot frame have large uncertainties. Though rotation rate errors lies in a range of 0.0498–0.8189 $^\circ\,\mathrm{Myr}^{-1}$, the error ellipses

of the Euler poles reach the highest value (e.g. hundreds of kilometers) especially for the Amuria (AM), the Somalia (SO) and the Sunda (SU) plate. *Jurdy* [1990] calculated an uncertainty of 1.1 degrees for the hotspot reference frame, using errors of 50 km for the location of individual hotspots, and as noticed by *Cuffaro and Jurdy* [2006], large uncertainties would be expected for absolute plate motions, propagating the standard deviations of the HS3–NUVEL1A model.

As also shown in the Chapter 3, after testing absolute plate motions in the deep–hotspot reference frame, we studied absolute kinematics incorporating space geodesy, in the shallow–hotspot framework.

As mentioned in the Chapter 3, the asthenosphere has been shown to be anisotropic, having the main orientation of crystals along the sense of shear [e.g., *Barruol and Granet*, 2002; *Bokelmann*, 2002]. The asthenosphere is present all over the Earth [*Gung et al.*, 2003], and shows an upper low-velocity zone more or less pronounced [*Calcagnile and Panza*, 1978; *Thybo*, 2006]. This layer may have viscosity values far lower [*Scoppola et al.*, 2006] than the estimates assumed for the whole asthenosphere [e.g., *Anderson*, 1989], and it should represent the main decoupling between lithosphere and the underlying mesosphere.

Doglioni et al. [2005] modeled the shear heating between lithosphere and asthenosphere as a possible source for the Hawaii type magmatism. In that model it was assumed the asthenosphere behaving as a Couette flow [*Turcotte and Schubert*, 2001]. In such a channel, the maximum speed and the related shear heating are localized in the middle of the flow. For this reason, we assumed that the source of this type of hotspot could be positioned close to the half thickness of the asthenosphere. As also tested in Chapter 3, making this choice, implies to consider the Pacific plate rotation about a pole located at 61.467 °S, 90.326 °E, but with a rate of 2.1226 °Myr^{-1}, i.e., the double value of the Pacific angular velocity presented by *Gripp and Gordon* [2002].

Adding this Pacific angular velocity to the REVEL plate kinematic model [*Sella et al.*, 2002] (Table 4.3) results in absolute plate motions with respect to the shallow–hotspot reference frame, incorporating space geodesy (Table 4.6 and Figure 4.5).

As in the previous chapter, the shallow hotspots are the framework in which the whole lithosphere move westward. In fact also the Nazca (NZ) plate in this frame have velocity vectors E–W oriented. Moreover all the plates move along trajectories that seem to represent a global lithospheric flow [*Doglioni*, 1990, 1993] (e.g., Figure 1.6).

Table 4.6: Plate angular velocities with respect to the shallow hotspot reference frame, incorporating the REVEL plate kinematic model [*Sella et al.*, 2002]

PLATE	Angular Velocity			Standard Error Ellipse			σ_ω
	°N	°E	° Myr^{-1}	σ^a_{max}	σ^a_{min}	ζ^b	° Myr^{-1}
AF	-60.324	77.670	1.2373	4.888	3.072	91	0.0524
AM	-56.630	89.614	1.1756	8.589	4.136	68	0.0555
AN	-58.379	88.081	1.2711	4.873	3.098	101	0.0518
AR	-44.622	60.820	1.2349	4.975	2.954	76	0.0606
AT	-28.680	56.390	1.4225	40.212	3.303	109	0.2879
AU	-37.740	64.580	1.4976	3.752	2.333	71	0.0626
CA	-63.801	79.311	1.2354	5.015	3.206	90	0.0536
EU	-59.448	83.017	1.2267	4.926	3.148	96	0.0517
IN	-48.580	60.729	1.1815	6.558	2.932	72	0.0658
NA	-65.914	75.664	1.4057	4.346	2.670	90	0.0515
NZ	-70.143	84.542	0.8739	7.339	4.401	100	0.0504
OK	-70.537	58.671	1.6313	6.130	3.189	122	0.0867
PA	-61.467	90.326	2.1226	2.861	1.848	104	0.0498
PH	-68.126	33.965	2.0855	3.231	2.052	127	0.0589
SA	-62.595	86.948	1.4883	4.098	2.658	100	0.0505
SO	-60.753	83.254	1.1757	5.149	3.282	96	0.0513
SU	-65.831	74.837	1.1273	7.229	3.810	70	0.0603
	Additional Plate Angular Velocity						
CO	-42.844	-135.856	0.9818	6.300	4.601	55	0.0695
JF	-51.246	72.366	2.0751	3.296	2.492	62	0.0663
SC	-66.654	84.271	1.4877	–	–	–	–

[a] 1–sigma lengths of the semi–major σ_{max} and semi–minor axes σ_{min} of the pole error ellipse. Units of the semi–major and semi–minor axes are in degrees.

[b] ζ is the azimuth of the semi-major ellipse axis in degrees clockwise from north.

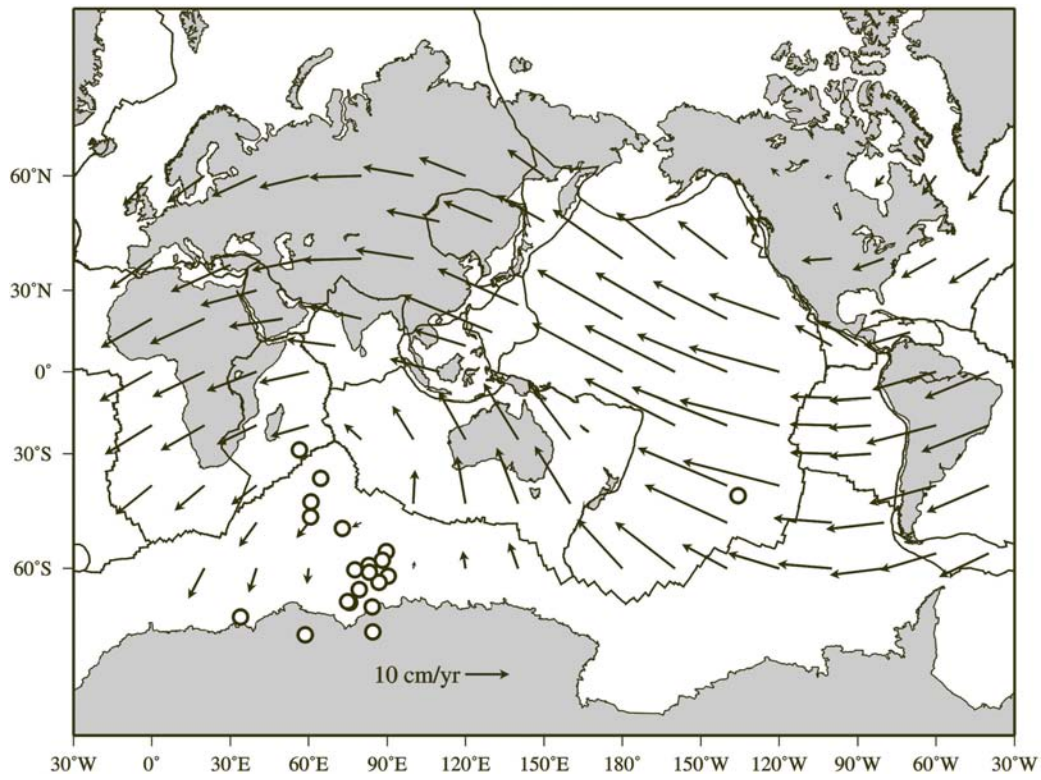

Figure 4.5: Present–day plate absolute velocities relative to the shallow hotspot reference frame, incorporating space geodesy [*Sella et al.*, 2002]. Note that in this frame all plates have a westward component. Open circles are the rotation poles.

Shallow hotspot absolute motions incorporating space geodesy differ from those re-calibrated with geological and geophysical data, but from a global scale point of view show a similar distribution of velocity vectors. The large part of the locations of rotation poles lies at mean latitude of 60 °S, whereas few of them are scattered away, e.g, the Cocos (CO) plate.

With respect the deep-hotspots, the rate uncertainties in the shallow–hotspot frame generally have a similar order of magnitude, whereas the error ellipses result smaller of mostly one order of magnitude, except for the Anatolia (AT) plate (Table 4.6). As mentioned for the Pacific–fixed reference frame, for the Scotia (SC) plate, uncertainties are not reported and the velocity parameters of additional plates, e.g., Cocos (CO) and Scotia (SC), are exactly like the absolute motions relative to the shallow–hotspots recalibrated with geological data.

On a large scale, the addition of the new plates defined in the Section 4.2 does not

Table 4.7: Comparison of computed net–rotation angular velocities after testing two options of the source of the Pacific intraplate hotspots (e.g. deep and shallow source), incorporating the REVEL plate kinematic model [*Sella et al.*, 2002] and NUVEL1A model [*DeMets et al.*, 1990, 1994] respectively. Used geometrical factor come from Table 4.1 and from the NNR–NUVEL1 model [*Argus and Gordon*, 1991] (Table 1.1).

Pacific	Geometrical	Relative	Computed Net–Rotation		
Hotspots	Factors	Plate Motions	$^{\circ}$N	$^{\circ}$E	$^{\circ}$ Myr^{-1}
deep	This Study	REVEL	-52.323	68.840	0.4402
shallow	This study	REVEL	-59.194	82.911	1.4912
deep	NNR–NUVEL1	NUVEL1A	-55.908	69.930	0.4359
shallow	NNR–NUVEL1	NUVEL1A	-60.244	83.662	1.4901

change the global trend of motions in the shallow–hotspot framework, and they also contribute to make evident the global tectonic pattern [*Doglioni*, 1990, 1993].

Finally, we computed the net–rotation angular velocities, testing these two options of depth source for the hotspots (Table 4.7), by making use of geometrical factors of the Table 4.1 and of the methods described in the Chapter 1, and we found that they are similar to the values computed with absolute motions, incorporating geological and geophysical data (Table 4.7).

4.4 Discussion

In this chapter, we have computed absolute plate motions relative to the hotspot framework, incorporating space geodesy data. The accuracy of the GPS acquisitions are here propagated in the hotspot system, producing plate motions with respect to the mantle by making use of data coming from recent space geodetic techniques.

As in the previous chapter, we tested two hypothesis of the depth of the hotspot source, presenting two different absolute reference frames. Results confirm trends and rates of plate motions obtained with geological and geophysical data, both in the deep and shallow hotspot.

Moreover, defining new plate boundaries of the Earth's surface and presenting new plate geometrical factors, two new values of the net–rotation angular velocities are here

proposed, testing again the two options of the hotspots (e.g., deep and shallow).

The use of different relative plate motions, e.g., the REVEL [*Sella et al.*, 2002] and the NUVEL1A [*DeMets et al.*, 1990, 1994], and geometrical factors, e.g., those of *Argus and Gordon* [1991] and those of the Table 4.1, does not globally change results of net–rotation angular velocities. In fact, according to the deep–hotspot condition and using different data (Table 4.7), the computed net–rotation of the lithosphere presents similar rates, and the rotation poles have a deviation of one degree in longitudes and about four degrees of latitudes (Table 4.7). A similar result comes out when we considered the shallow–hotspot hypothesis, because the net–rotation rate equals the deep–hotspot one with two significance digits, whereas the rotation poles differ of one degree both in longitudes and latitudes (see the last three columns of Table 4.7).

As a final remark, the addition of the five new plates (AM, AT, OK, SO, SU), and their absolute plate motions relative to the hotspots, entails a modification of the digital plate boundary files, proposed by *Bird* [2003]. The topology of the new recombined digital files, generally follows the indications proposed by the PB2002 model [*Bird*, 2003]. In fact, plate boundary curves are approximated by sequences of discrete points and since no arc between adjacent points is longer than 111 km (1 degree).

Each point is given as a (latitude, longitude) pair, with coordinates in units of decimal degrees. Latitude is positive in the northern hemisphere and negative in the southern hemisphere. Longitude is generally positive to the east of the Greenwich meridian, and negative to the west, but some points in the western hemisphere are represented with positive longitudes in the range 180–360 °E. All coordinates are given with six significant digits, so that round–off error in positions does not exceed $\pm$60 m.

The most important convention followed to present new plate boundaries concerns the plate boundary points ordered in counter–clockwise style (Figure 4.6), useful to calculate plate geometrical factors and plate areas. In fact, *Jurdy* [1974] integrated the line integrals numerically, to obtain elements of the Equation (1.3), using the following:

$$\int_S \mathbf{M_p} \cdot \mathbf{dS} = \int_l \widetilde{\mathbf{M}}_\mathbf{p} \cdot \mathbf{dl} \tag{4.1}$$

with

$$\widetilde{\mathbf{M}}_\mathbf{p} = \frac{1}{\sin\phi} \int_\phi \mathbf{M_p} \sin\phi \; \mathrm{d}\phi \tag{4.2}$$

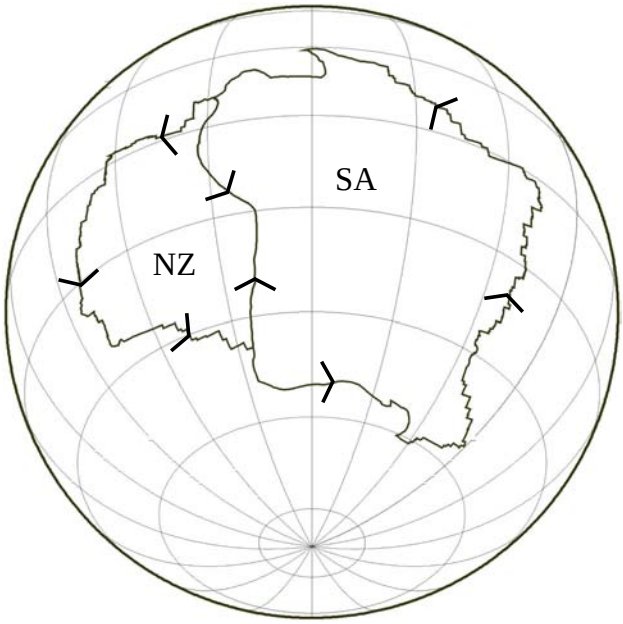

Figure 4.6: Topology of plate boundary data for geometrical factor computation. The example shows the Nazca (NZ) and South America (SA) plates, where boundary points are ordered in a counter–clockwise style useful to apply the Stock theorem and compute plate areas.

where ϕ is the colatitude, S is the surface of the generic plate p and $\mathbf{dS}$ is the area element, l is the contouring line, in a counter–clockwise order, representing the boundary of the plate p and $\mathbf{dl}$ is the line element. Moreover $\mathbf{M_p}$ is a 3×3 matrix defined as following:

$$\mathrm{M_p} = \begin{bmatrix} 1-x^2 & -xy & -xz \\ -xy & 1-y^2 & -yz \\ -xz & -yz & 1-z^2 \end{bmatrix} \tag{4.3}$$

where x,y,z are the Cartesian co–ordinates of the boundary of a generic plate p. The elements of the tensor I_p, i.e., the plate geometrical factors (Equation 1.3, page 10) of a single plate p, computed with the Equation 1.3, correspond to the integrated element of the matrix M_p (Equation 4.3) over the plate area, and they are estimated through plate surface geometry, assuming a uniform density for all plates and neglecting their thickness variations. Considering a unit sphere, it can be shown that the sum of $\mathrm{I}_{i,j}$ elements of the tensor I_p for the total number of plates is defined as it follows:

$$\begin{array}{lll} \sum_p I_{xx,p} = \frac{8\pi}{3} & \sum_p I_{xy,p} = 0 & \sum_p I_{xz,p} = 0 \\ \sum_p I_{yx,p} = 0 & \sum_p I_{yy,p} = \frac{8\pi}{3} & \sum_p I_{yz,p} = 0 \\ \sum_p I_{zx,p} = 0 & \sum_p I_{zy,p} = 0 & \sum_p I_{zz,p} = \frac{8\pi}{3} \end{array} \tag{4.4}$$

For a total of plates $P = 20$, this study provides sums of plate geometrical factors in Steradians, presented as following:

$$\begin{array}{lll} \sum_p I_{xx,p} = 8.3775 & \sum_p I_{xy,p} = 0.0001 & \sum_p I_{xz,p} = -0.0001 \\ \sum_p I_{yx,p} = 0.0001 & \sum_p I_{yy,p} = 8.3778 & \sum_p I_{yz,p} = 0.0000 \\ \sum_p I_{zx,p} = -0.0001 & \sum_p I_{zy,p} = 0.0000 & \sum_p I_{zz,p} = 8.3777 \end{array} \tag{4.5}$$

whereas *Argus and Gordon* [1991], presented results for a total of plates $P = 14$ in this way:

$$\begin{array}{lll} \sum_p I_{xx,p} = 8.3775 & \sum_p I_{xy,p} = -0.0001 & \sum_p I_{xz,p} = 0.0002 \\ \sum_p I_{yx,p} = -0.0001 & \sum_p I_{yy,p} = 8.3777 & \sum_p I_{yz,p} = 0.0002 \\ \sum_p I_{zx,p} = 0.0002 & \sum_p I_{zy,p} = 0.0002 & \sum_p I_{zz,p} = 8.3776 \end{array} \tag{4.6}$$

Plate geometrical factors obtained in this chapter follow the closure condition on the whole lithosphere, as similar as the results proposed by *Argus and Gordon* [1991], because the sum of each element for the tensor I_p is very close to the theoretical values (see Equations 4.4).

The negligible differences have to be brought back at the accuracy of the plate boundary databases used to compute plate geometrical factors. The most updated data proposed by *Bird* [2003], and modified in this study, may represent a more appropriate boundary dataset that guarantees an high precision in computing elements of the tensor I_p.

Chapter 5

Plate sub–rotations

In accordance with the hypothesis of the global tectonic pattern [*Doglioni*, 1990, 1993], and on the basis of geological evidence, the plate sub–rotations are here introduced. Plates can be affected by a contemporaneous sub–rotation while they move on the Earth's surface. We tested this hypothesis in absolute reference frames, applying this model to the North America plate, reconstructing its past motion over most of the Cenozoic Era, and comparing results with those obtained by *Gordon and Jurdy* [1986]. This application shows how the different positions of the North America over most of the Cenozoic can be largely interpreted as a consequence of the two-rotation plate kinematics. Moreover, we applied this model in the NNR framework, showing that the combinations of two contemporaneous rotations generate a third instantaneous rotation pole that does not comprehensively describe the composite motion of the plate.

5.1 Introduction

Each plate is characterized by motion parameters as the Euler pole and the angular velocity. However, during its journey, a plate may be affected by another contemporaneous sub–rotation, while it is rotating about its Euler pole. The kinematic description of this particular plate motion requires a different analytical approach: two angular velocities and two poles are necessary to completely describe the plate displacement. If a sub-rotation occurs, any plate point does not move along circles of the Euler pole, but it follows cycloid trajectories, due to the combination of the two contemporaneous rotations. Regardless the forces that move the lithosphere, every time a plate experiences a sub-rotation, an additional force or resisting force would be applied on the plate, generating the two-rotation

displacement. An analytical method can take into account this sub–rotation with the main plate motion and the instantaneous pole of rotation can be viewed as a third separate pole that changes with time, being the combination of the two basic poles, i.e., the first rotation pole, and the sub–rotation pole.

The sub–rotation pole is the only point of the plate that moves on a circle and does not change distance relative to the primary pole, whereas all the other plate points do not move on circles but on particular trajectories like different epicycloids projected on the terrestrial spherical surface. In both relative and absolute reference frames, every plate displacement is described by a rigid body rotation around an Euler pole, through the application of the Euler theorem for plate kinematics [*Bullard et al.*, 1965; *Heirtzler et al.*, 1968; *Le Pichon*, 1968]. Under this condition, any plate point follows circular trajectories on circles of the Euler pole with a constant angular velocity. However, when a body is moving along a path, but it also revolves, then another pole of rotation is required to describe the kinematics. It is like the revolution of the Earth around the Sun, and its contemporaneous rotation about its axis, or as a car that starts swinging while traveling.

A relative kinematic analysis, made for example by the NUVEL-1 relative plate motion model, [*DeMets et al.*, 1990], is not useful to verify the hypothesis of the sub–rotation, because the motion of one plate is studied relative to one another, stated fixed and only one rotation is necessary for that kinematics. When the relative motion of a plate respect to a second one is computed, the contribution of the sub–rotation (if it occurs) would be equally split between the two plates, even if the real sub–rotation is present only in one.

On the other hand, the passage to absolute reference frames, through the plate motion models relative to the hotspots, as HS2–NUVEL1 or HS3–NUVEL1A [*Gripp and Gordon*, 1990, 2002] or with the no-net-rotation condition, as NNR–NUVEL1 [*Argus and Gordon*, 1991], is not a contribution to recognize the sub–rotation of some plates, because they are an absolute adaptation of the relative plate motion model NUVEL-1, [*DeMets et al.*, 1990], and if the sub–rotation is split between two plates in the relative frame, this splitting is propagated also in absolute frames.

In this chapter, we present how, in absolute frameworks, some plates may be involved in a contemporaneous absolute sub–rotation, while they are rotating around their Euler poles. In this case, two angular velocities and two poles have to be combined in an analytic method (see Appendix A) to completely describe the motion of a plate.

We tested the idea of plate sub–rotations in two different absolute frames, the hotspots and the mean–lithosphere. In the hotspot reference frame, we applied this model to the

North America plate, studying its past motion from 48 Myr up to the present. This application shows how the different positions of the North America over most of the Cenozoic can be largely interpreted as a consequence of the two–rotation plate kinematics.

We also applied this model to the North America plate, which is moving WNW-ward in an absolute NNR reference frame [*Bokelmann*, 2002; *Silver and Holt*, 2002; *Liu and Bird*, 2002] and results would prove that its motion can be interpreted as a first rotation about a main pole located at (-64.30 ± 0.18) °N and (105.52 ± 1.15) °E, and as a contemporaneous counter-clockwise rotation about an internal pole located at (50.78 ± 0.06) °N and (-77.78 ± 0.50) °E. The combination of the two poles generates a third instantaneous pole of rotation, that is located at (-1.55 ± 0.77) °N and (-82.59 ± 0.35) °E, but it does not describe the composite motion of the plate.

5.2 Why a sub-rotation?

The concept of the absolute sub-rotation of a plate is here introduced, because, when plate motions are computed in absolute reference frames, there is evidence that some of them can be interested by a two-rotation kinematics [*Doglioni*, 1990].

Cronin [1987] proposed that, computing relative plate motions, the observed trajectories are generally complex curves, like spherical cycloid, and not small circles of an Euler Pole. During a finite displacement, he principally described systematic variations in velocities directions and trajectories of each plate point, and the wobble of two plates during their relative motion. This particular kinematics requires two angular velocities and two poles, and he also proposed parametric equations describing this two-rotation motion [*Cronin*, 1991].

We resume this concept of two–rotation plate kinematics, extending the application to absolute plate motions.

Considering the motion of all the plates in an absolute framework, geodynamic lines of evidence show how a plate, while it is rotating about an Euler pole, can make a further contemporaneous sub–rotation with respect to another sub–pole.

For example, along with the rifting between Eurasia and North America in the Late Cretaceous and Early Cenozoic, Iberia has rotated counter-clockwise, producing the extension in the Bay of Biscay and most of the shortening in the Pyrenees [*Van der Voo*, 1993]. From an absolute point of view, this implies that the Iberia plate motion was governed by two rotation poles, one over the rifting of the Atlantic, and another sub-rotation pole that was contemporaneously involved in the extension of the Bay of Biscay. These

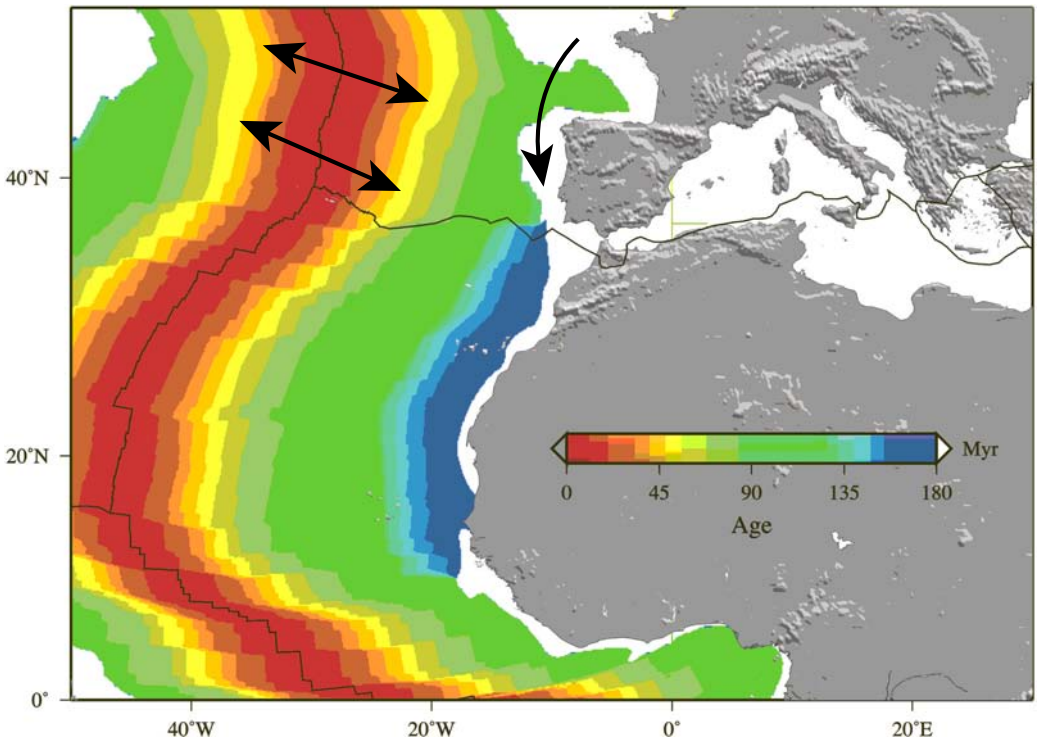

Figure 5.1: The two absolute rotations of the Iberia are contemporaneous because the age of the oceanic lithosphere in the Bay of Biscay corresponds to the Late Cretaceous lithosphere, during the Atlantic rifting.

two rotations of the Iberia are contemporaneous because the age of the oceanic lithosphere in the Bay of Biscay corresponds to the Late Cretaceous lithosphere, during the Atlantic rifting (Figure 5.1).

Another example concerns the larger opening of the Southern Atlantic with respect to the central Atlantic that may be interpreted as a result of the Cretaceous to present clockwise absolute sub-rotation of South America [e.g., *Van der Voo*, 1993].

Data inversions on boundaries and relative plate motions are not useful in showing the sub-rotations, because the motion of a plate is studied relative to one another, and all the plate points are constrained to move on circular trajectories by least square methods.

In finite rotations, it is always possible to describe motion of the Iberia relative to a fixed Eurasia, after the opening of the Atlantic, using the corresponding time intervals; this computation is made considering separately two displacements that are contemporaneous. The introduction of the absolute sub-rotations would be useful to combine these

plate movements. For the case of the Iberia, during the continuum of Late Cretaceous, two poles and two angular velocities are needed to reconstruct the present position.

From an absolute point of view, this two–rotation model would be useful to understand dynamics generating this particular plate motion. Regardless the energy that moves plates, the sub-rotation could require, for example, a couple of forces acting on a single plate. Descriptions of absolute plate kinematics, including every type of displacement should be the base of comparison for plate dynamics results.

5.3 Definitions: first rotation pole and sub-rotation pole, circular and cycloid trajectories

Plate displacements on Earth's surface can be computed by using the Euler's theorem, and plate motions are treated as rigid body rotations, and are uniquely defined by an angular velocity and a rotation pole, called the Euler's pole (see Section 1.2). This pole tends to remain fixed for short period of geological time, and this type of rotation is considered instantaneous. In both absolute and relative frameworks, plates follow traces of small circles centered upon the rotation pole [*McKenzie and Parker*, 1967; *Morgan*, 1968], and, during the continuum of time, at different instants, any generic point of a plate is constrained to move along a piece of circular trajectory (Figures 5.2a and 5.4a).

In this simple configuration, during the continuum of the time, the plate has a main pole of rotation, and any point in the plate maintains the same distance from the pole at two different times t_i ($i = 0 \ldots n$), while the plate moves (Figures 5.2a and 5.4a). The North–South and East–West velocity components, and the magnitude and direction of its instantaneous velocity are obtained from equations of motion of the Appendix A.

Here, we consider that a generic lithospheric plate is moving on a spherical surface in an absolute reference frame, making two contemporaneous rotations, a *first rotation* and a *sub-rotation*. The first rotation is about an external *first rotation pole* with an angular velocity ω_f, whereas the sub–rotation is another about an internal pole (*sub-rotation pole*), inside the plate that moves with the plate itself, with an angular velocity ω_s. This particular displacement is defined as a two-rotation plate motion and instantaneous linear velocities of plate points are obtained by the equations of the composed motion in the Appendix A.

Butler [1992] describes the motion of a single plate as a rotation with respect to an internal rotation axis and with respect to an external Euler pole, but he considers two different and separated cases and both in the two separated situations only one angular

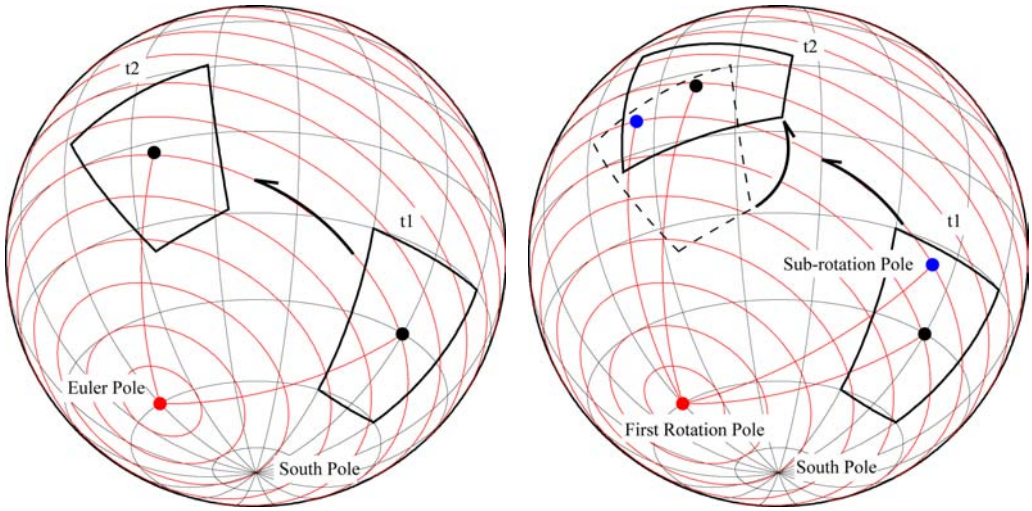

(a) (b)

Figure 5.2: (a) For the simplest case, a plate moves on a sphere about an Euler pole, and, during the continuum of the time, any plate point maintains the same distance from the pole at two different times t_1 and t_2. (b) When plate motion is a two-rotation displacement, a plate is moving about a first rotation pole, and is contemporaneously rotating about a sub–rotation pole. One reference point of the plate changes its distance from the main pole at two different time t_1 and t_2, e.g., increasing or decreasing the length with the main pole. Only one point does not change its distance with the main pole, i.e., the sub-rotation pole, that goes on a parallel of the first pole.

velocity and one Euler pole are required.

If the two-rotation motion occurs, during the continuum of the time, the plate still moves about the first rotation pole, but it contemporaneously revolves around the sub–rotation pole,

One reference plate point changes its distance from the main pole at two different times t_1 and t_2, e.g., increasing and decreasing the length with the main pole (Figure 5.2b) and making a particular trajectory like an epicycloid (Figure 5.4). Only one point does not change its distance with the main pole, i.e., the sub-rotation pole, that goes on a parallel of the first pole and lies on a circular trajectory (Figure 5.4). When the two rotations are mixed during the motion, at every instant, a plate point seems to have an instantaneous pole of rotation and it appears as a third separate pole, (*composed rotation pole*) (Figure 5.3), but it does not completely describe the real motion.

The shape of the cycloid trajectory depends on the ratio of the two angular velocities.

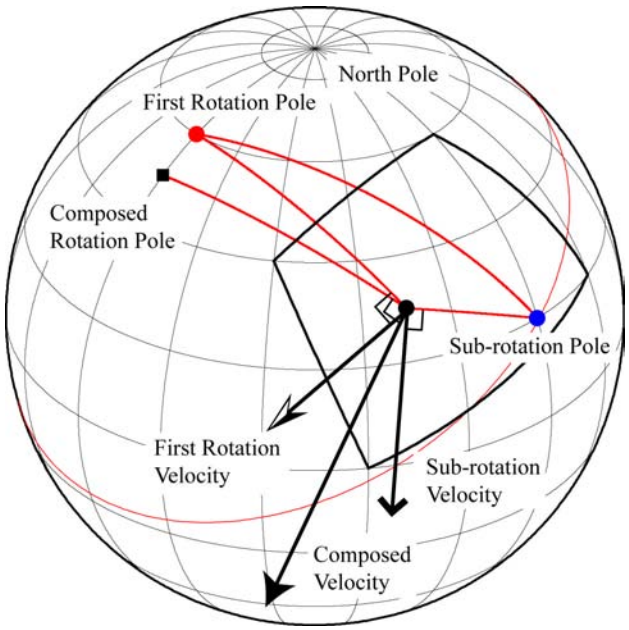

Figure 5.3: When plate motion is composed by a first rotation and a contemporaneously sub-rotation, one reference point is characterized by two linear velocities, one relative to the first rotation pole and the other relative to the sub-rotation pole. The sum of these two velocities is the composed velocity related to a third pole of rotation, (composed rotation pole).

The ideal case (Figure 5.4b) is verified when $\omega_f \ll \omega_s$. Under this condition, the absolute sub-rotation is predominant with respect to the first rotation, and a generic plate point is constrained on the cycloid trajectory with the most common shape (Figure 5.4b), as the trace of the Moon around the Sun, over a year. This case should be ideal, because plates could follow short trails of cycloid trajectories, during geological time intervals. For the case shown in Figure 5.4b, the plate would rotate too fast around its sub–rotation pole, and this phenomenon seems not to be verified in any plate on the Earth's surface over finite intervals of geological time.

More common cases are reported in Figure 5.4c and Figure 5.4d. When $\omega_f \approx \omega_s$ (Figure 5.4d), a plate point follows pieces of a cycloid trajectory very similar to pieces of circular traces. This is probably the reason because is sometime difficult to distinguish differences between the one–rotation model and the two–rotation one.

Moreover, when $\omega_f = \omega_s$ (Figure 5.4c), a plate point moves on a circular trajectory, that is not a small circle of the first rotation pole, but it is the result of the coupling of the two rotations.

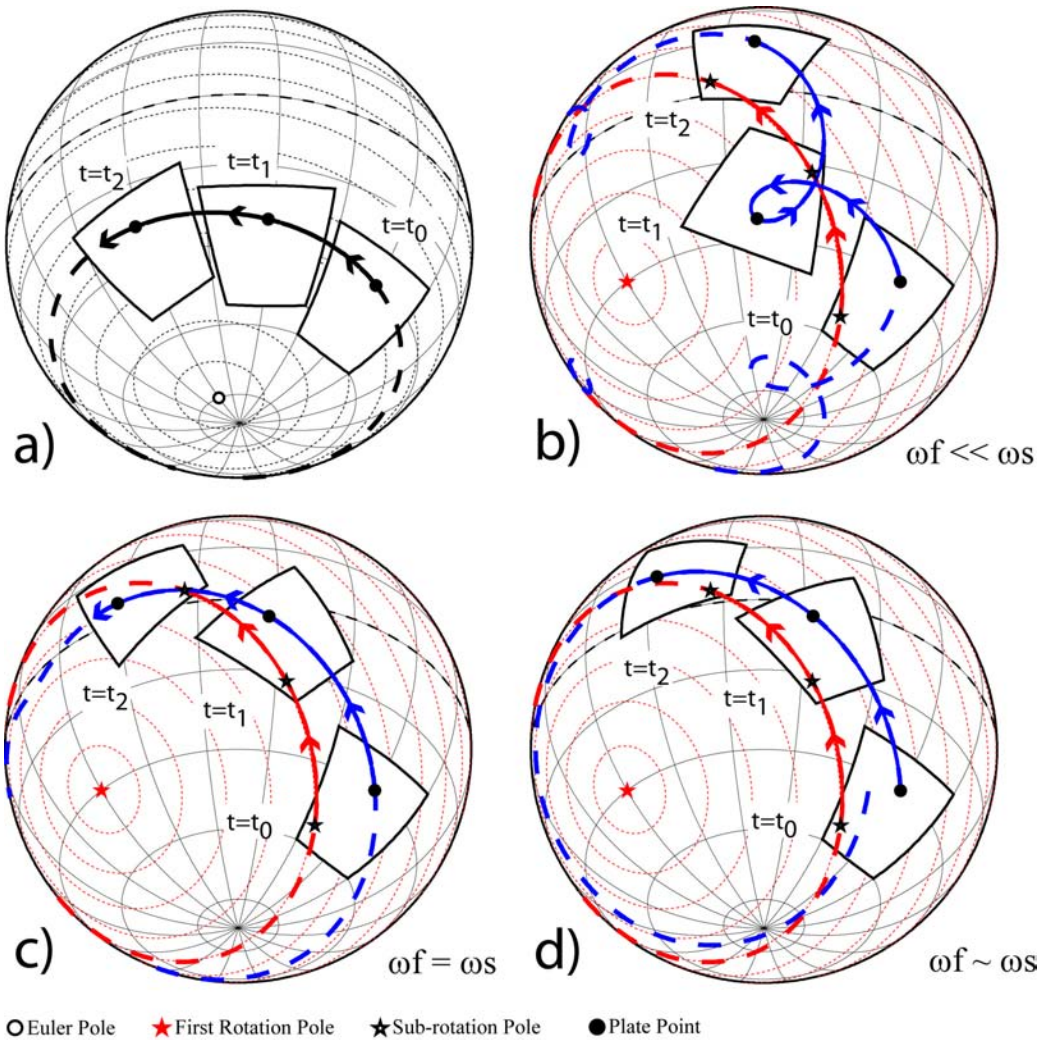

Figure 5.4: (a) One-rotation motion: at three different instants, a plate rotates about an Euler pole and one generic point follows a circular trace on a small circle of the Euler pole. (b) Two-rotation motion with $\omega_f \ll \omega_s$. A generic point is constrained to move on cycloid trajectory similar to the trace of the Moon around the Sun. (c) Two-rotation motion with $\omega_f = \omega_s$. A plate point moves on a circular trajectory, but it is not a small circle of the first rotation pole. (d) When $\omega_f \approx \omega_s$, a point of a plate follows a cycloid trajectory very similar to a circular one. In any case, the sub–rotation pole is the only point on a small circle of the first rotation pole.

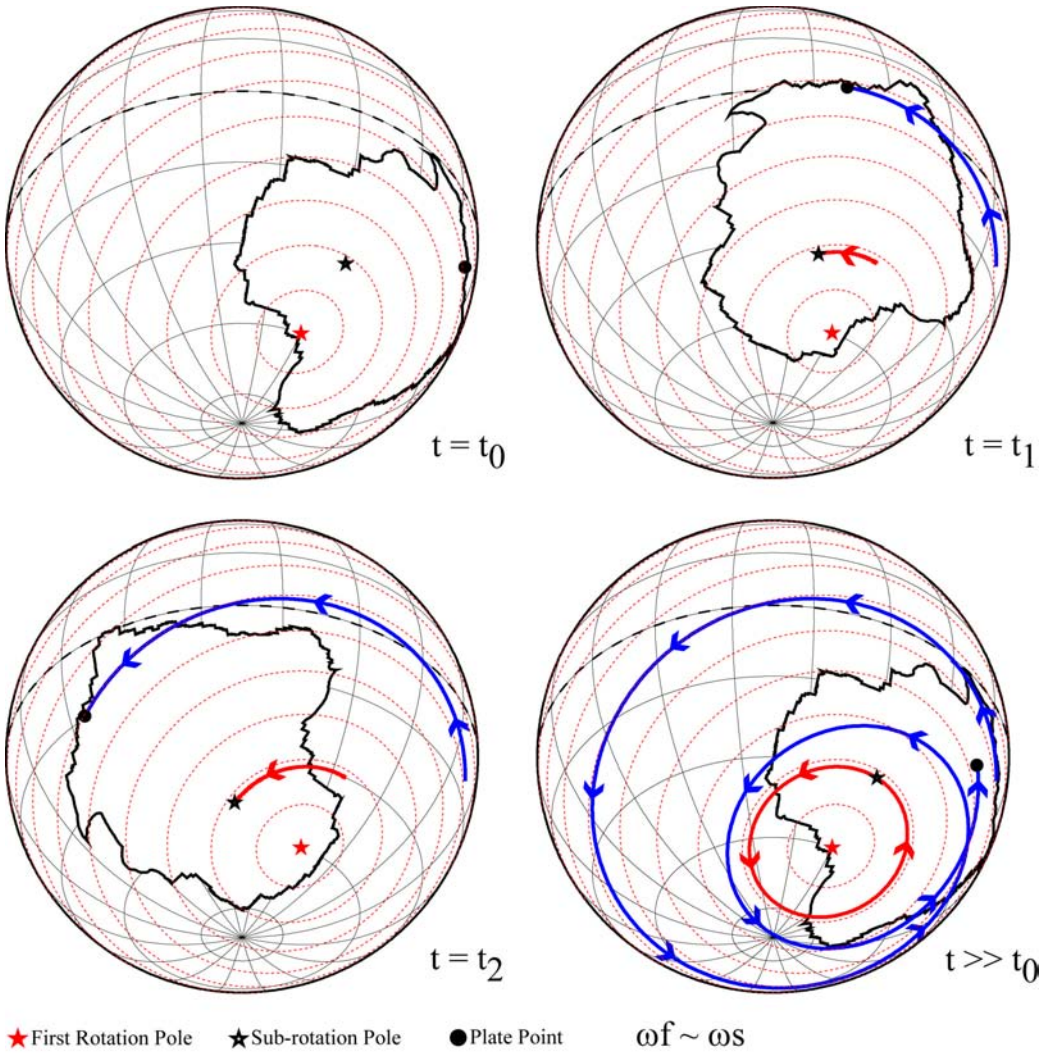

Figure 5.5: Particular two-rotation motion with the first rotation pole and the sub–rotation pole inside the plate, with angular velocities $\omega_f \approx \omega_s$. During the continuum of time, a generic point follows a cycloid trajectory and for $t \gg t_0$ the shape of its trace is a complicated curve. The sub–rotation pole moves along a small circle of the first rotation pole, that stays fixed. The plate itself generally remains in a fixed range of latitudes and longitudes.

A particular case happens when the first rotation pole and the sub–rotation pole are both inside the plate (Figure 5.5). This implies that the trajectories are more complex curves and it is difficult to recognize a two-rotation kinematics. During the continuum of time, the plate remains inside a fixed range of longitudes and latitudes. This could represent the Antarctic plate kinematics.

In each case presented above, it is useful to remember that the sub–rotation pole is the only plate point that follows the circular trace on a small circle of the first rotation pole, as it showed in Figure 5.4 and Figure 5.5.

It is necessary to remark that, from an analytic point of view, the absolute sub–rotation of a plate does not comprehend the linear isometry theorem, that states that, on a plane, every rigid-body rotation can be decoupled in a linear translation and a further body rotation about a fixed axis.

As also *Edelman* [1988] argued, this concept does not work on a spherical geometry, because there are no linear translations on a sphere. For a spherical shell, a translation corresponds to a rotation around an axis passing through the center of Earth.

Cronin [1988] remarked this concept, explaining that the two rotation axes for a cycloid relative motion do not include any linear isometry, but they are necessary to take into account variations of relative velocities, changing direction of relative motions, and the oscillatory nature of cycloid wobble.

In this chapter, we resume the idea of the cycloid motion, and we adapted it in absolute frameworks, introducing the concept of the absolute sub–rotation, that it could be supported by geodynamic evidence (e.g. the Iberia and South America).

5.4 The absolute sub–rotation of the North America over the Cenozoic Era

Instantaneous plate motions are referred to single instants of time or to averaged short periods of geological time. These plate rotations do not give informations about trajectories followed by plates to arrive at positions where instantaneous motions are measured [*Keary and Vine*, 1990].

It is common that an Euler's pole is not necessarily fixed, but it jumps to another location during the continuum of geological time [*Cox and Hart*, 1986]. Many methods are used to reconstruct past plate positions, as for example by making use of paeleomagnetism. Every time a rotation pole changes its position, this corresponds to a change in direction of plate motions.

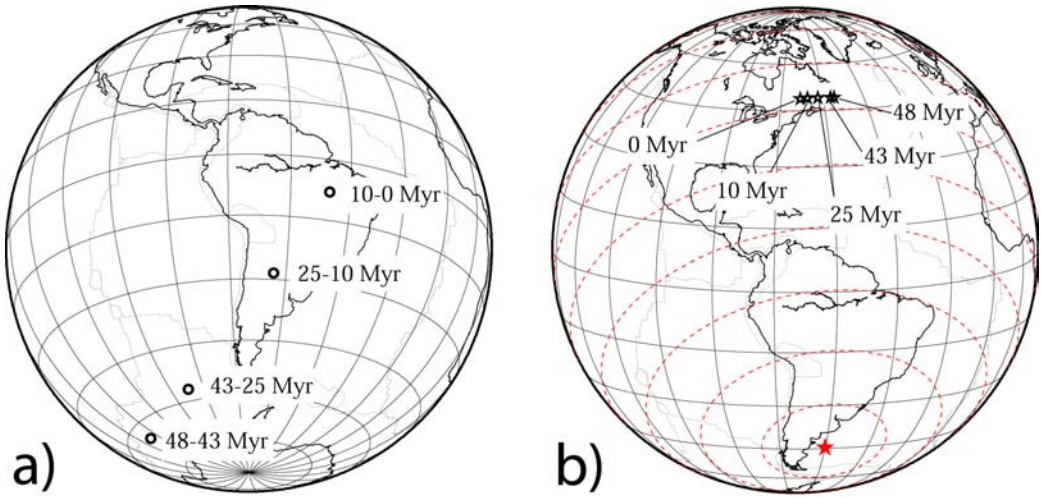

Figure 5.6: Over a time of 48 Myr, at four of the six time intervals selected by *Gordon and Jurdy* [1986] (Table 1), (a) four Euler poles characterize North America one-rotation plate motion. (b) Under the hypothesis of a North America two-rotation kinematics, the first rotation pole is located at $-44.56\,^{\circ}$N and $-60.03\,^{\circ}$E (red star) and remains fixed during 48 Myr; on the contrary the sub–rotation pole (black star) continuously moves on small circle of the first rotation pole (red dash traces) instantaneously changing its position from $48.81\,^{\circ}$N and $-55.97\,^{\circ}$E at 48 Myr to $48.60\,^{\circ}$N and $-68.18\,^{\circ}$E.

Gordon and Jurdy [1986] chose the hotspot reference frame to compute absolute plate motions over the entire Cenozoic Era, using finite rotations for plate reconstructions, found by many authors [e.g., *Srivastava*, 1978; *Morgan*, 1983; *Klitgord and Schouten*, 1986]. They divided the era in six time intervals ($65-56, 56-48, 48-43, 43-25, 25-10, 10-0$ Myr), corresponding with key plate reorganization, and for each of them, they determined global set of absolute angular velocities and rotation poles.

Here, we apply the two–rotation model to the North America plate, reconstructing past plate positions in the hotspot reference frame, over most of the Cenozoic Era, and comparing results with angular parameters reported in the Table 3 of *Gordon and Jurdy* [1986]. We also fixed the comparison for a time interval of 48 Myr up to the present, before the Hawaii-Emperor seamount chain bend. Doing this time interval, we chose the alternative to assume the Pacific basin hotspots fixed with respect to the other hotspots.

The aim of this application is to verify if the motion of the North America, over a large part of the Cenozoic, can be interpreted as a two-rotation displacement.

Over a time of 48 Myr, we selected four of the six time intervals chosen by *Gordon*

and Jurdy [1986]. Over that period, four Euler poles characterize the North America plate motion (Table 5.1 and Figure 5.6a). Over a large part of the Cenozoic, the Euler pole of the North America jumps into four different positions, producing different directions in plate motion. At these four locations, four different angular velocities are associated Table 5.1), with an higher values for the $48 - 43$ Myr time interval with respect to ones at $43 - 25$ Myr, $25 - 10$ Myr and $10 - 0$ Myr.

The one-rotation kinematics of the North America, at four times ($48, 43, 25, 10$ Myr), is here compared with a two-rotation plate motion. The best fit of the two plate kinematic models, minimizing their differences in producing plate positions, indicates the Cenozoic motion of the North America can be interpreted as a two-rotation motion with two constant angular velocities $\omega_f = 0.168\,^\circ\text{Myr}^{-1}$ and $\omega_s = 0.128\,^\circ\text{Myr}^{-1}$. This two combined angular velocities produce a smooth and steady plate motion.

The first rotation pole is located at $-44.56\,^\circ$N and $-60.03\,^\circ$E, a priori chosen as the approximated pole that could represent a flow line of the global tectonic pattern [*Doglioni*, 1990, 1993], during the plate reorganization, remains fixed during 48 Myr; in contrast, the sub–rotation pole continuously moves on small circle of the first rotation pole instantaneously changing its position from $48.81\,^\circ$N and $-55.97\,^\circ$E at 48 Myr to $48.60\,^\circ$N and $-68.18\,^\circ$E at 0 Myr (Table 5.1 and Figure 5.6b). To graphically compare North America positions produced by the two different models over 48 Myr (Figure 5.7 and Figure 5.8), we decide to represent differences on a sphere, i) selecting fixed the present North America plate boundary and ii) only moving the North America continent including the Greenland as a part of the North America. A summarizing global comparison of the two models is reported in Figure 5.9. We left a fifteen-degree geographical net, useful to evidence changes of the continent co–ordinates during plate motion. Comparison between the two models shows good agreement at time $t = 25$ Myr and $t = 10$ Myr, where each model produces similar positions of the North America (Figure 5.8). At the instants $t = 48$ Myr and $t = 43$ Myr, there is an higher misfit: the plate remains in the same range of longitudes, but the one-rotation kinematics makes the North America rotated with an higher angle with respect to the two-rotation one (Figure 5.7). This disagreement can be attributed to the systematic variation in angular velocities during the four time intervals, with respect to the constant values of ω_f and ω_s of the two-rotation model.

These results are tied to the choice of the angular velocity vectors, especially the first rotation, and to the existence of the global tectonic pattern. However the methods presented in this sections open a new possibility to reinterpret plate kinematics and basic concepts of tectonic processes.

Table 5.1: Comparison between one-rotation and two-rotation models in the hotspot reference frame

	One-rotation model[a]			Two-rotation model					
				First Rotation			Sub-rotation		
Time	Latitude	Longitude	ω	Latitude	Longitude	ω_f	Latitude	Longitude	ω_s
Myr	°N	°E	° Myr^{-1}	°N	°E	° Myr^{-1}	°N	°E	° Myr^{-1}
48	-40.00	-69.80	0.407	-44.56	-60.03	0.168	48.81	-55.97	0.128
43	-64.80	-141.70	0.371	-44.56	-60.03	0.168	48.88	-57.24	0.128
25	-56.70	-96.90	0.185	-44.56	-60.03	0.168	48.86	-61.83	0.128
10	-28.50	-63.30	0.145	-44.56	-60.03	0.168	48.75	-65.64	0.128
0	-8.10	-50.30	0.198	-44.56	-60.03	0.168	48.60	-68.18	0.128

[a] Data from *Gordon and Jurdy* [1986]

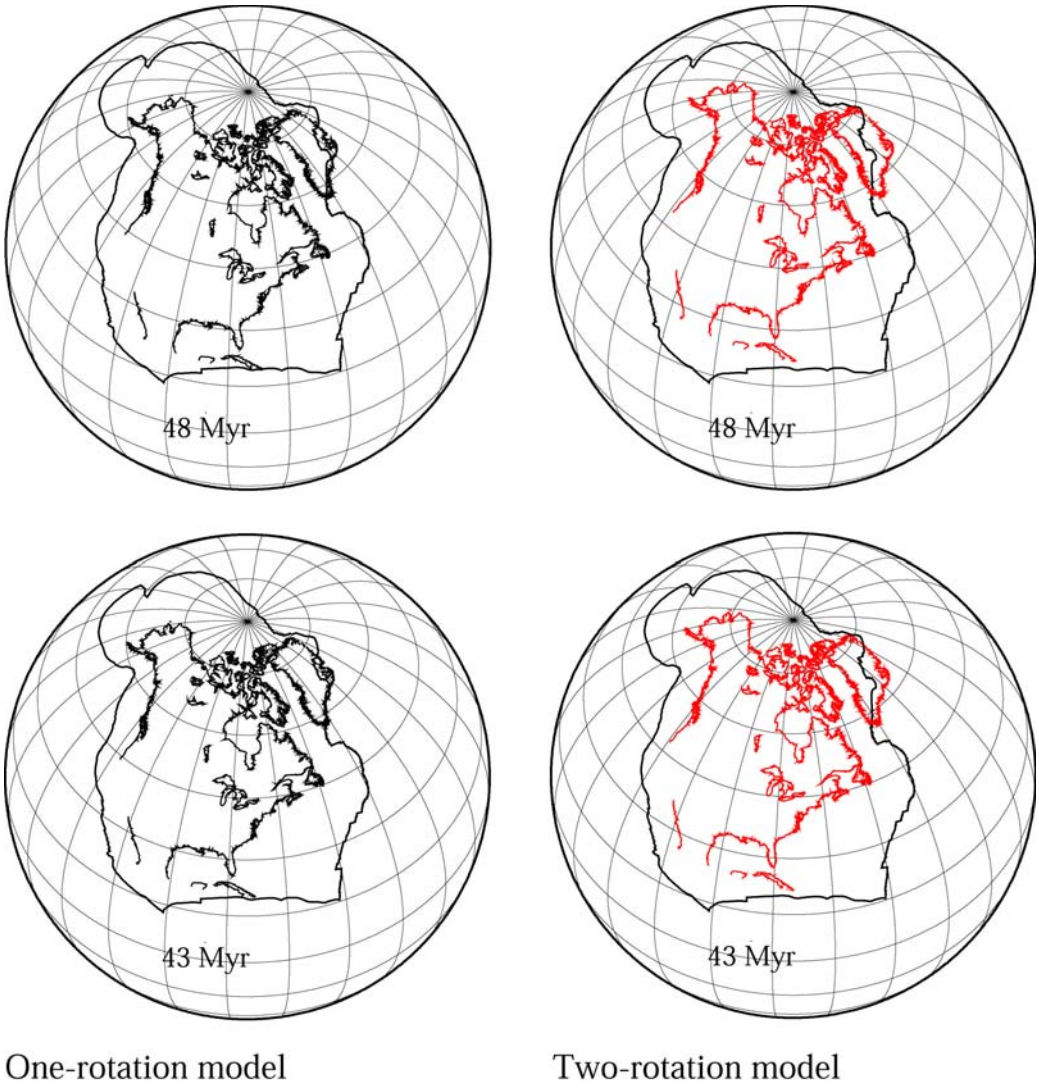

Figure 5.7: At the instants $t = 48\,\text{Myr}$ and $t = 43\,\text{Myr}$, comparisons between the two models shows a higher misfit: the plate remains in the same range of longitudes, but the one-rotation kinematics makes the North America rotated with an higher angle with respect to the two-rotation one. This disagreement can be attributed to the systematic variation in angular velocities of *Gordon and Jurdy* [1986], during the four time intervals (Table 1), with respect to the constant values of ω_f and ω_s of the two-rotation model

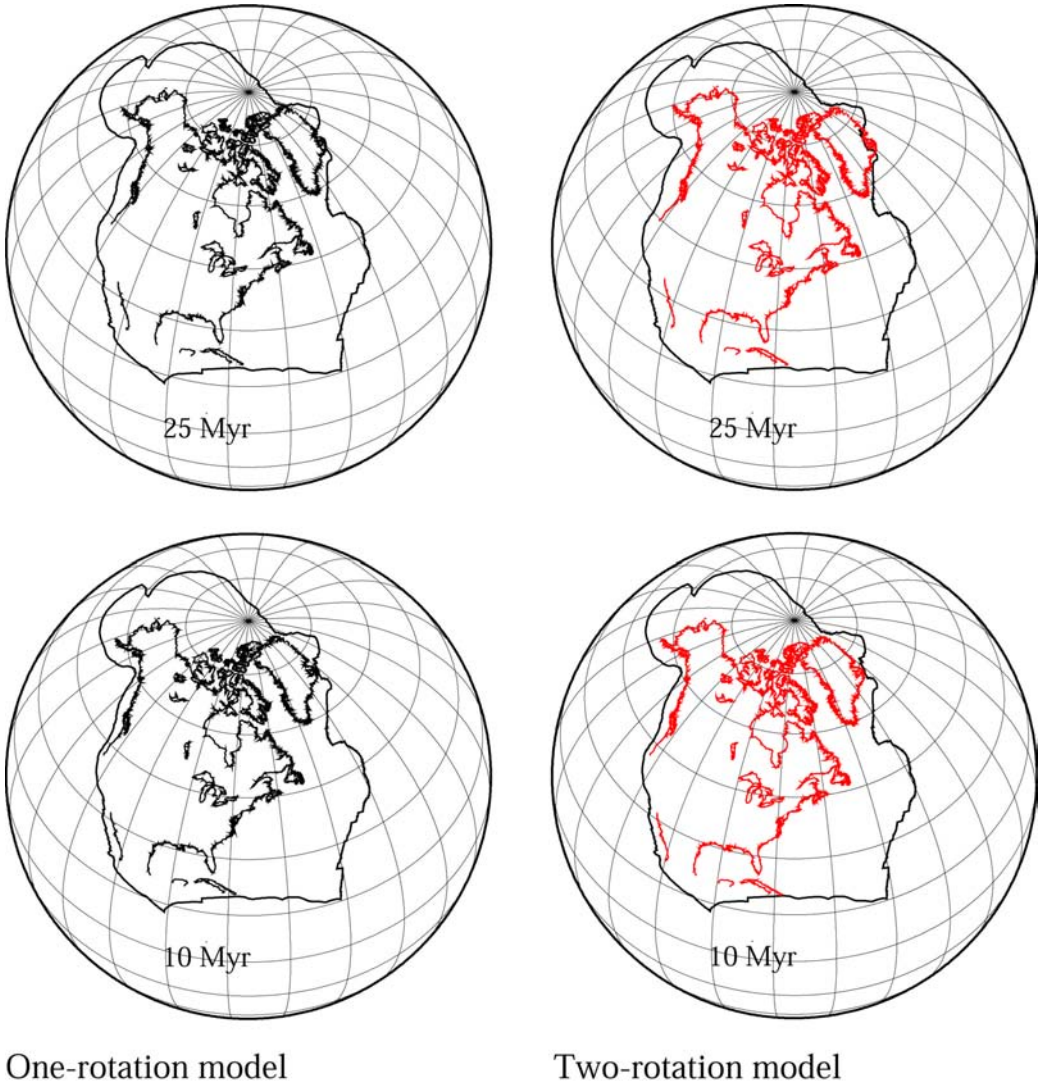

Figure 5.8: Comparison between the two models shows good agreement at time $t = 25$ Myr and $t = 10$ Myr, where each model produces similar positions of the North America

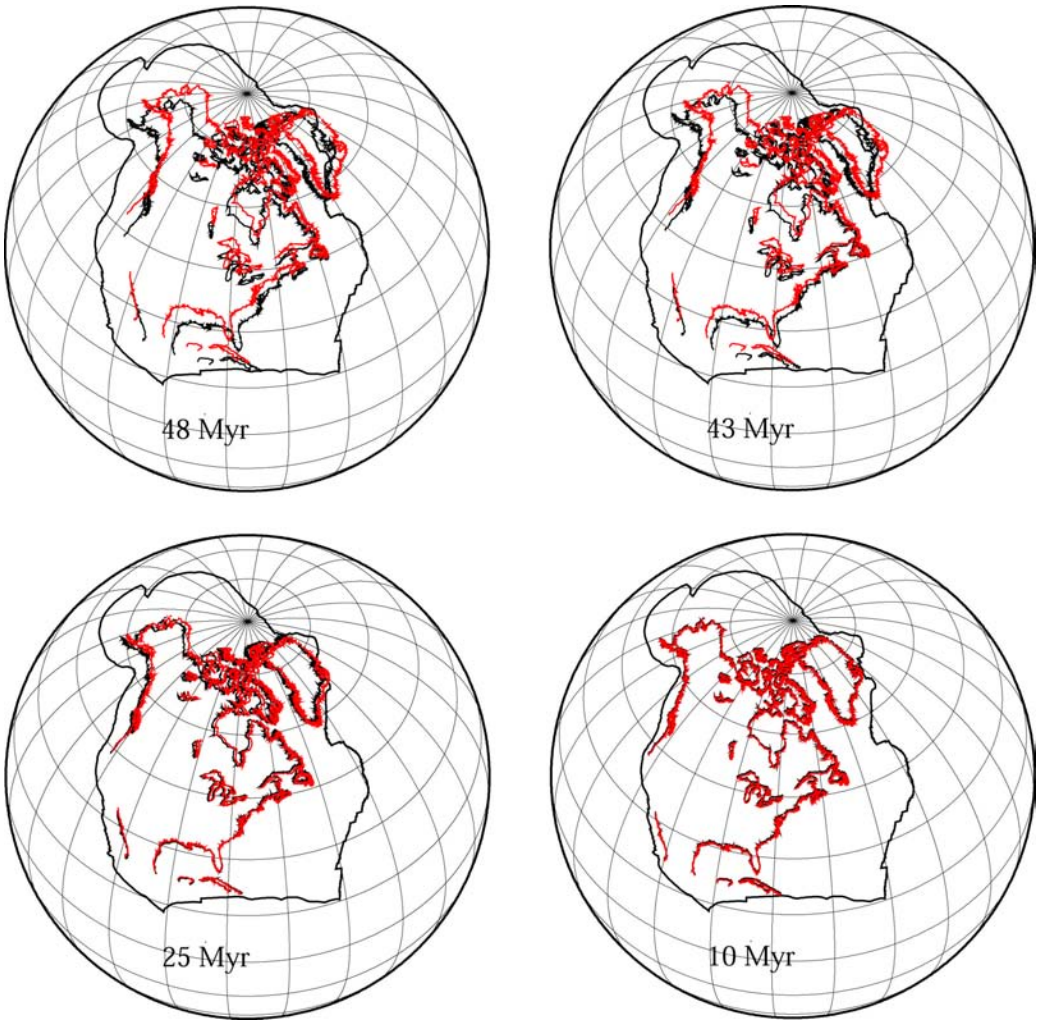

Figure 5.9: Summarizing global comparison between the two models at time $t = 48\,\text{Myr}$, $t = 43\,\text{Myr}$, $t = 25\,\text{Myr}$, and $t = 10\,\text{Myr}$. The black colored North America is the one produced by the one–rotation model, whereas the red North America is the other produced by the two–rotation model. Note that at the two last positions the plates are overlapped.

5.5 The sub-rotation of the North America in the NNR framework

With the previous example, the attention has been focused on plate motions over the geological time, where the use of paleomagnetism for plate reconstructions is required. Instead, if we consider the present–day plate motions in the NNR reference frame, as NNR-NUVEL1 [*Argus and Gordon*, 1991], based on the geological and geophysical data acquired on plate boundaries, or the recent plate motion models, as the REVEL, [*Sella et al.*, 2002], and the APKIM, [*Drewes and Meisel*, 2003], based on the space geodesy techniques, some of instantaneous plate rotations could be also viewed as combined by a first rotation and a sub–rotation (if any). In this interpretation, the instantaneous pole of rotation is a third pole, that changes its position with time, representing the composition of the other two poles, the first rotation pole and the sub–rotation pole.

The North America NNR–kinematics was chosen to test the goodness of the two–rotation model also in the mean–lithosphere and for the fact that it contains the largest number of GPS stations of the global network. GPS velocities are reported in an absolute reference frame, the ITRF2000 [*Altamimi et al.*, 2002], and this is useful for the comparison with model results. Although in this reference frame a no–net–rotation condition (NNR) is conventionally imposed, and this does not allow determination of plate motion relative to the underlying mantle, anyhow it is an absolute reference frame where data are easily accessible. Moreover, our application would be also helpful to demonstrate that, for a lithospheric plate, in an absolute reference frame, a velocity distribution, as the GPS one [*Heflin et al.*, 2004], related to an instantaneous pole or rotation, can be viewed as a resulting motion composed by two contemporaneous rotations.

First of all, using the angular velocities of the present-day plate kinematic and deformation model (APKIM), [*Drewes and Meisel*, 2003], we a priori suppose that the North America first rotation pole is the APKIM Pacific rotation pole located at $(-64.30 \pm 0.18)\,^{o}$N and $(105.52 \pm 1.15)\,^{o}$E with an angular velocity $\omega_r = (0.6588 \pm 0.0039)^{o}$ Myr^{-1}. However, this a priori choice would better fit with a global mainstream for global tectonics [*Doglioni*, 1990], and the Pacific rotation pole and angular velocity from the APKIM plate kinematic model could be representative of the first rotation parameters for the North America plate.

Then, to align the two–rotation plate motion to the GPS velocities distribution [*Heflin et al.*, 2004], it is necessary to introduce a contemporaneous sub–rotation. The result is a sub-rotation pole located at $(50.78 \pm 0.06)\,^{o}$N, and $(-77.78 \pm 0.50)\,^{o}$E, not too far

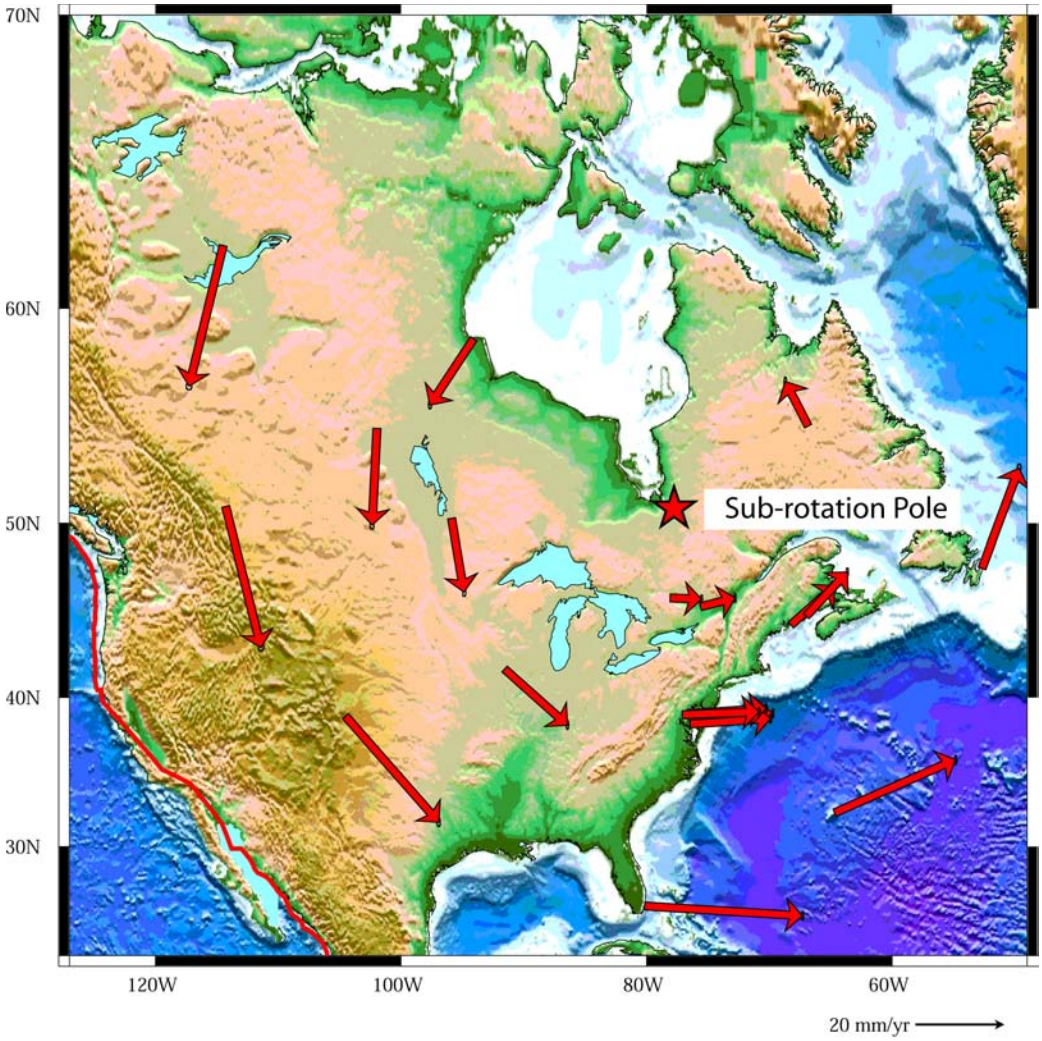

Figure 5.10: Sub–rotation of the selected GPS station of the North America. Small ellipses show the 2-D 95% confidence ellipse of the velocity vectors.

from the rotation pole of *Stein and Sella* [2002], with a sub-rotation angular velocity $\omega_s = (0.7594 \pm 0.0069)\ ^{o}\,\mathrm{Myr}^{-1}$. With these two sets of motion parameters, i.e., first rotation and sub-rotation, we respectively applied equations of the Appendix A for only 20 selected intraplate–located space geodesy stations, far from the diffusely deformed western North America plate margin and the results are shown in Table 5.2.

Figure 5.10 and Figure 5.11 respectively show sub-rotation pole of the GPS stations about the sub–rotation pole and their the first rotation about the first rotation pole. As

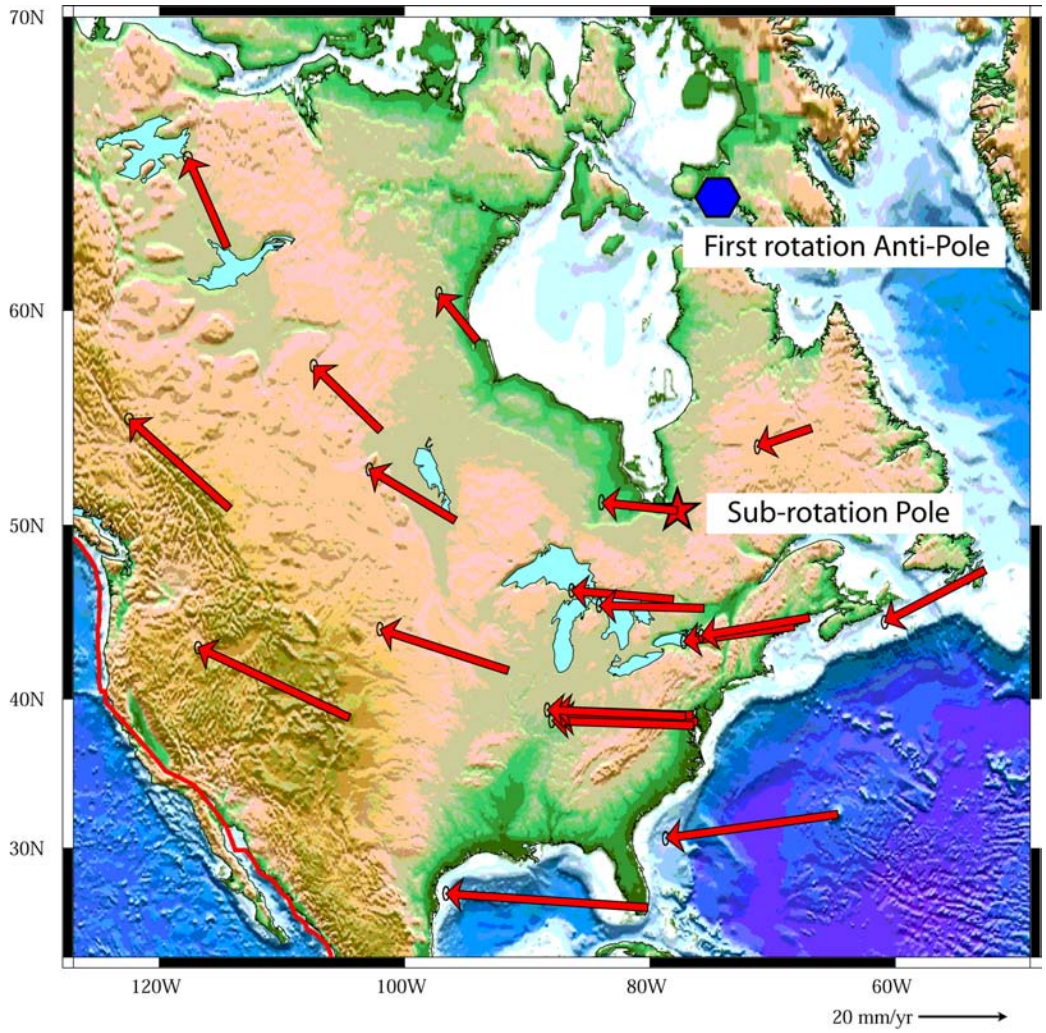

Figure 5.11: First rotation of the North America plate, along the pacific trend (see text), of the selected GPS stations. Small ellipses show the 2-D 95% confidence ellipse of the velocity vectors. Here, we report the Pacific Euler anti-pole located at $64.30\,^{o}$N and $-74.48\,^{o}$E.

shown, when we consider only the sub-rotation, the sub-rotation pole is fixed (Figure 5.10), but if there is also the first rotation, the sub-rotation pole moves along a parallel of the first rotation pole (Figure 5.11).

For the case of North America plate, the sub-rotation pole is moving with a transversal velocity $V_f^{(\theta)} = (1.83 \pm 0.70)\,\mathrm{mm\,yr^{-1}}$ and a longitudinal velocity $V_f^{(\lambda)} = (-17.17 \pm 0.25)\,\mathrm{mm\,yr^{-1}}$, (Figure 5.11).

Table 5.2: First rotation and sub–rotation linear velocities

GPS Station	Position		First rotation		Sub-rotation	
			$V_r^{(\lambda)} \pm 1\sigma$	$V_r^{(\theta)} \pm 1\sigma$	$V_s^{(\lambda)} \pm 1\sigma$	$V_s^{(\theta)} \pm 1\sigma$
	°E	°N	(mm yr^{-1})	(mm yr^{-1})	(mm yr^{-1})	(mm yr^{-1})
ALGO	-78.07	45.96	-23.10 $\pm$ 0.23	1.99 $\pm$ 0.64	7.71 $\pm$ 0.09	-0.28 $\pm$ 0.41
AMC2	-104.52	38.80	-34.21 $\pm$ 0.31	15.91 $\pm$ 0.57	21.09 $\pm$ 0.16	-24.02 $\pm$ 0.38
AOLM	-80.16	25.73	-45.74 $\pm$ 0.27	3.15 $\pm$ 0.64	35.75 $\pm$ 0.09	-2.22 $\pm$ 0.41
BARH	-68.22	44.39	-25.07 $\pm$ 0.24	-3.46 $\pm$ 0.63	9.91 $\pm$ 0.11	8.86 $\pm$ 0.41
BRMU	-64.69	32.37	-38.99 $\pm$ 0.27	-5.40 $\pm$ 0.63	27.40 $\pm$ 0.11	12.08 $\pm$ 0.40
CHUR	-94.08	58.75	-8.65 $\pm$ 0.29	10.66 $\pm$ 0.61	-9.88 $\pm$ 0.15	-14.99 $\pm$ 0.40
DUBO	-95.86	50.25	-19.46 $\pm$ 0.29	11.58 $\pm$ 0.60	2.80 $\pm$ 0.14	-16.57 $\pm$ 0.40
EPRT	-66.99	44.90	-24.51 $\pm$ 0.25	-4.14 $\pm$ 0.63	9.30 $\pm$ 0.11	9.98 $\pm$ 0.40
FLIN	-101.97	54.72	-15.11 $\pm$ 0.31	14.67 $\pm$ 0.58	-1.98 $\pm$ 0.18	-21.88 $\pm$ 0.38
HNPT	-76.13	38.58	-31.79 $\pm$ 0.25	0.92 $\pm$ 0.64	17.84 $\pm$ 0.09	1.53 $\pm$ 0.41
NLIB	-91.57	41.77	-29,00 $\pm$ 0.27	9.34 $\pm$ 0.61	14.24 $\pm$ 0.12	-12.73 $\pm$ 0.40
NRC1	-75.62	45.45	-23.67 $\pm$ 0.24	0.63 $\pm$ 0.64	7.86 $\pm$ 0.09	2.00 $\pm$ 0.41
NRC2	-75.62	45.45	-23.67 $\pm$ 0.24	0.63 $\pm$ 0.64	7.86 $\pm$ 0.09	2.00 $\pm$ 0.41
PRDS	-114.29	50.87	-22.73 $\pm$ 0.38	20.34 $\pm$ 0.52	7.99 $\pm$ 0.23	-31.76 $\pm$ 0.35
SCH2	-66.83	54.83	-12.28 $\pm$ 0.24	-4.23 $\pm$ 0.63	-5.17 $\pm$ 0.12	10.13 $\pm$ 0.40
SOL1	-76.45	38.31	-32.10 $\pm$ 0.25	1.09 $\pm$ 0.64	18.21 $\pm$ 0.09	1.23 $\pm$ 0.41

Table 5.2: (continued)

GPS Station	Position		First rotation		Sub-rotation	
			$V_r^{(\lambda)} \pm 1\sigma$	$V_r^{(\theta)} \pm 1\sigma$	$V_s^{(\lambda)} \pm 1\sigma$	$V_s^{(\theta)} \pm 1\sigma$
	°E	°N	(mm yr^{-1})	(mm yr^{-1})	(mm yr^{-1})	(mm yr^{-1})
STJO	-52.67	47.59	-22.73 $\pm$ 0.29	-11.80 $\pm$ 0.60	8.41 $\pm$ 0.17	22.63 $\pm$ 0.38
USNA	-76.47	38.98	-31.34 $\pm$ 0.25	1.11 $\pm$ 0.64	17.26 $\pm$ 0.09	1.20 $\pm$ 0.41
USNO	-77.06	38.91	-31.42 $\pm$ 0.25	1.43 $\pm$ 0.64	17.35 $\pm$ 0.09	0.66 $\pm$ 0.41
YELL	-114.48	62.48	-8.92 $\pm$ 0.41	20.42 $\pm$ 0.51	-7.73 $\pm$ 0.26	-31.90 $\pm$ 0.35

Table 5.3: Comparison between GPS data and model results.

GPS Station	Positon		GPS data		Composed movement	
			$V_{\mathrm{GPS}}^{(\lambda)} \pm 1\sigma$	$V_{\mathrm{GPS}}^{(\theta)} \pm 1\sigma$	$V_c^{(\lambda)} \pm 1\sigma$	$V_c^{(\theta)} \pm 1\sigma$
	°E	°N	(mm yr^{-1})	(mm yr^{-1})	(mm yr^{-1})	(mm yr^{-1})
ALGO	-78.07	45.96	-16.82 $\pm$ 0.07	1.17 $\pm$ 0.04	-16.00 $\pm$ 0.34	1.71 $\pm$ 0.65

Table 5.3: (continued)

GPS Station	Positon		GPS data		Composed movement	
			$V_{\mathrm{GPS}}^{(\lambda)} \pm 1\sigma$	$V_{\mathrm{GPS}}^{(\theta)} \pm 1\sigma$	$V_c^{(\lambda)} \pm 1\sigma$	$V_c^{(\theta)} \pm 1\sigma$
	°E	°N	(mm yr^{-1})	(mm yr^{-1})	(mm yr^{-1})	(mm yr^{-1})
AMC2	-104.52	38.80	-16.25 $\pm$ 0.15	-7.84 $\pm$ 0.23	-13.12 $\pm$ 0.47	-8.11 $\pm$ 0.69
AOLM	-80.16	25.73	-9.99 $\pm$ 0.08	2.29 $\pm$ 0.16	-9.99 $\pm$ 0.36	0.92 $\pm$ 0.68
BARH	-68.22	44.39	-15.56 $\pm$ 0.17	6.11 $\pm$ 0.27	-15.17 $\pm$ 0.35	5.39 $\pm$ 0.65
BRMU	-64.69	32.37	-11.89 $\pm$ 0.02	7.77 $\pm$ 0.04	-11.60 $\pm$ 0.37	6.68 $\pm$ 0.67
CHUR	-94.08	58.75	-18.79 $\pm$ 0.06	-4.59 $\pm$ 0.10	-18.53 $\pm$ 0.43	-4.33 $\pm$ 0.69
DUBO	-95.86	50.25	-18.91 $\pm$ 0.33	-6.22 $\pm$ 0.20	-16.66 $\pm$ 0.43	-4.99 $\pm$ 0.69
EPRT	-66.99	44.90	-16.22 $\pm$ 0.17	6.61 $\pm$ 0.27	-15.21 $\pm$ 0.36	5.86 $\pm$ 0.65
FLIN	-101.97	54.72	-18.91 $\pm$ 0.16	-7.41 $\pm$ 0.10	-17.10 $\pm$ 0.51	-7.21 $\pm$ 0.71
HNPT	-76.13	38.58	-17.25 $\pm$ 0.32	4.64 $\pm$ 0.22	-13.96 $\pm$ 0.34	2.45 $\pm$ 0.66
NLIB	-91.57	41.77	-14.41 $\pm$ 0.03	-2.96 $\pm$ 0.04	-14.76 $\pm$ 0.40	-3.39 $\pm$ 0.67
NRC1	-75.62	45.45	-15.97 $\pm$ 0.07	2.96 $\pm$ 0.10	-15.80 $\pm$ 0.34	2.64 $\pm$ 0.65
NRC2	-75.62	45.45	-17.27 $\pm$ 0.19	2.81 $\pm$ 0.28	-15.80 $\pm$ 0.34	2.64 $\pm$ 0.65
PRDS	-114.29	50.87	-14.98 $\pm$ 0.08	-11.34 $\pm$ 0.12	-14.73 $\pm$ 0.61	-11.41 $\pm$ 0.74
SCH2	-66.83	54.83	-17.70 $\pm$ 0.09	7.95 $\pm$ 0.12	-17.45 $\pm$ 0.36	5.90 $\pm$ 0.65
SOL1	-76.45	38.31	-14.86 $\pm$ 0.04	2.72 $\pm$ 0.08	-13.88 $\pm$ 0.34	2.33 $\pm$ 0.66
STJO	-52.67	47.59	-14.91 $\pm$ 0.10	11.88 $\pm$ 0.08	-14.32 $\pm$ 0.46	10.84 $\pm$ 0.67
USNA	-76.47	38.98	-14.18 $\pm$ 0.04	0.63 $\pm$ 0.08	-14.07 $\pm$ 0.34	2.36 $\pm$ 0.66

Table 5.3: (continued)

GPS Station	Positon		GPS data		Composed movement	
			$V_{\mathrm{GPS}}^{(\lambda)} \pm 1\sigma$	$V_{\mathrm{GPS}}^{(\theta)} \pm 1\sigma$	$V_c^{(\lambda)} \pm 1\sigma$	$V_c^{(\theta)} \pm 1\sigma$
	°E	°N	(mm yr^{-1})	(mm yr^{-1})	(mm yr^{-1})	(mm yr^{-1})
USNO	-77.06	38.91	-14.40 $\pm$ 0.06	3.00 $\pm$ 0.10	-14.07 $\pm$ 0.34	2.09 $\pm$ 0.66
YELL	-114.48	62.48	-17.82 $\pm$ 0.11	-11.80 $\pm$ 0.08	-16.65 $\pm$ 0.67	-11.48 $\pm$ 0.76

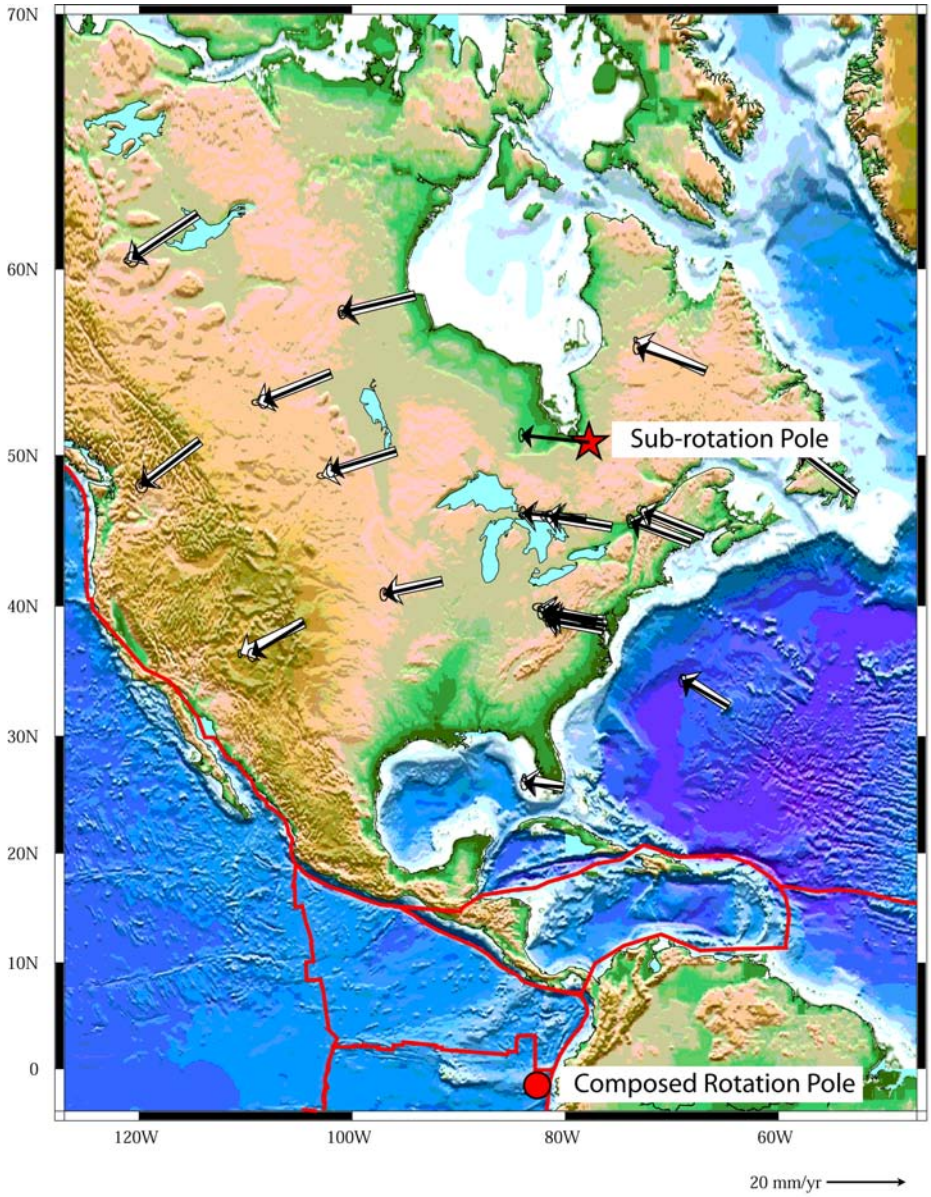

Figure 5.12: Adding the two contemporaneous rotations, comparison between North America GPS selected station velocities (white vectors) and composed motion model results (black vectors) show good agreement. They are both related to a composed rotation pole located at $(-1.55 \pm 0.77)\,^{o}$N and $(-82.59 \pm 0.35)\,^{o}$E that represents their interplay. Ellipses show the 2-D 95% confidence ellipse of the velocity vectors.

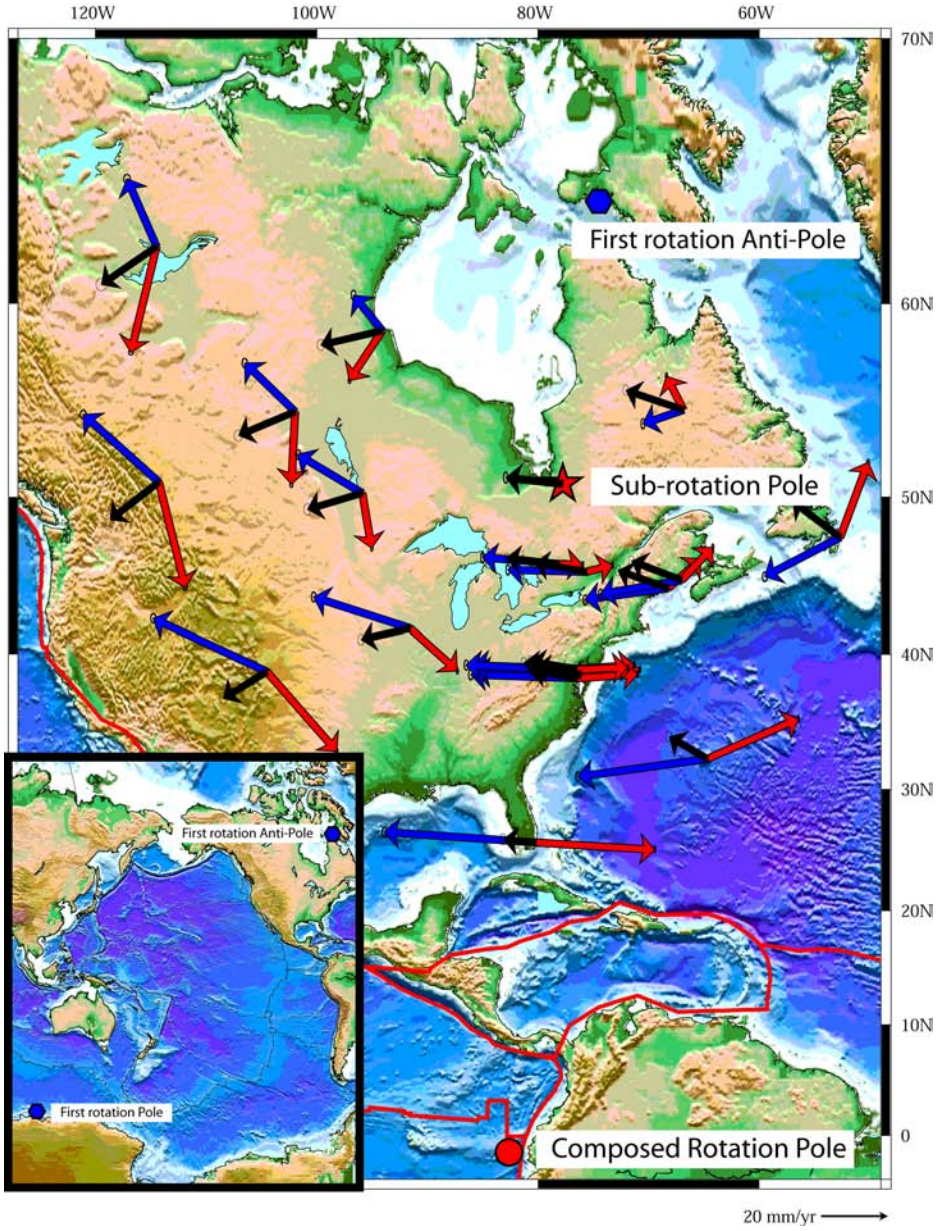

Figure 5.13: Summarizing picture when it is represented the composed motion for North America plate. For the 20 selected GPS station, the first rotation (blue vectors) is about the first rotation pole , the sub-rotation (red vectors) is about the sub-rotation pole. Composition of these two contemporaneous movements (black vectors) are related to a composed rotation pole that is not significant of the composed motion. Ellipses show the 2-D 95% confidence ellipse of the velocity vectors.

Table 5.4: Sub–rotation rotation poles of the North America plate in the NNR reference frame

	Rotation Pole		1σ Standard Deviation	
	$^{\circ}$N	$^{\circ}$E	σ_N	σ_E
First rotation	-64.30	105.52	0.18	1.15
Sub–rotation	50.78	-77.78	0.06	0.50
Composed rotation	-1.55	-82.59	0.77	0.35

Then, we applied equation of the Appendix A and we made a comparison with data proposed by *Heflin et al.* [2004]. Results are shown in Figure 5.12 and in Table 5.3. Velocity uncertainties are obtained by the methods described in the Appendix B.

According to this interpretation, the comparison between GPS data [*Heflin et al.*, 2004] and model results indicate good agreement and their interference generate a third composed rotation pole located at (-1.55 ± 0.77) ºN and (-82.59 ± 0.35) ºE. In Figure 5.13 we report a complete picture where the two instantaneous rotation for the plate, i.e., first rotation and sub-rotation are shown and it is clear how this sum gives an instantaneous velocity distribution related with an instantaneous third composed pole. This pole is very similar to the North America rotation poles presented by plate kinematic model in the NNR framework [*Argus and Gordon*, 1991; *Sella et al.*, 2002]. The summarized rotation poles of the two–rotation model in the NNR frame are reported in Table 5.4.

This pole can be fixed for millions of years describing a well determined plate rotation and well defined geodynamic processes. We instead show that a general rotation pole in the mean–lithosphere can be the third apparent pole of a two-rotation model and can result a different geodynamics. At this stage, could the NNR framework be a good reference system in which to separate the sub-rotations?

To emphasize this concept, we compare the two different results of the two models (i.e. one–rotation and two–rotation) and present in Figure 5.14 the positions of the North America, imaged moving from now to 180 Myr in the future. The two–poles solution maintains North America at higher latitudes with respect to the classic one–pole analysis, suggesting different plate dynamics.

For this reason, this chapter provides an analysis of the movement of plates described by multiple rotations in an absolute reference frame.

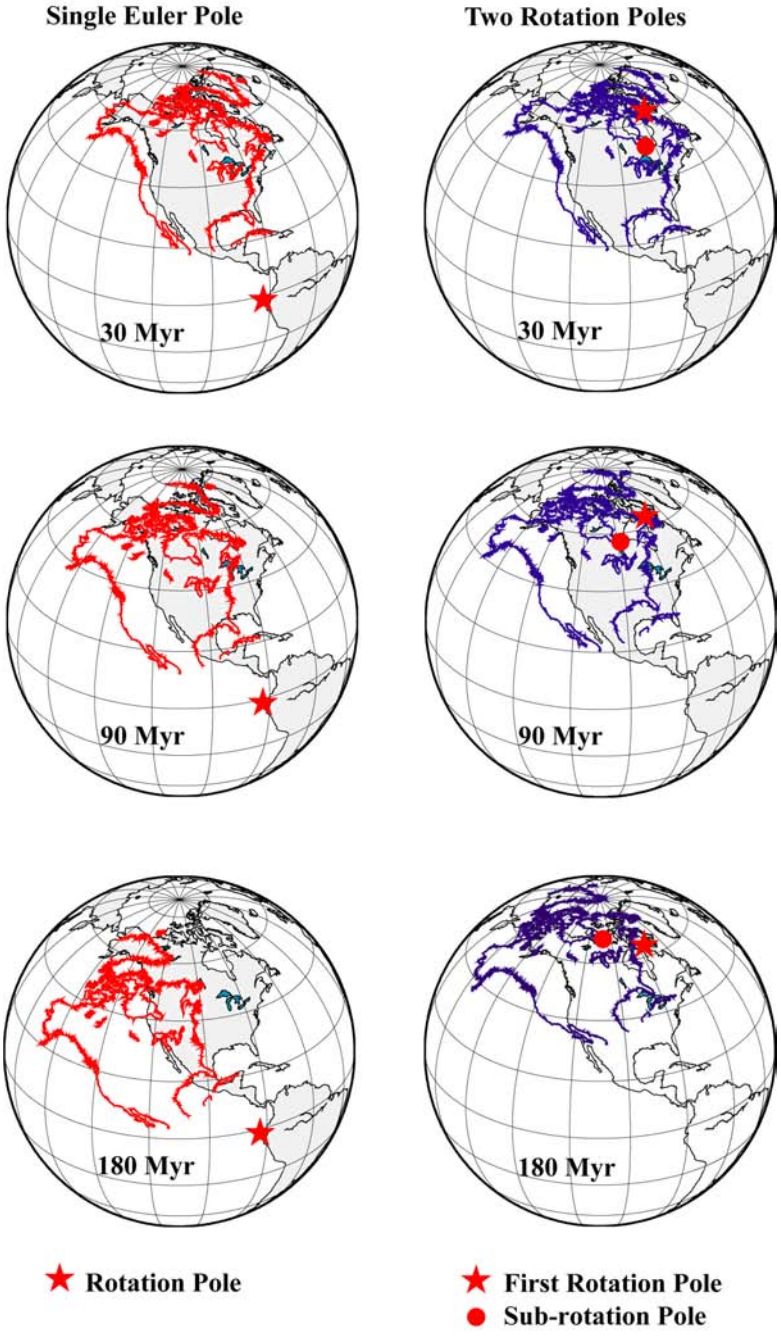

Figure 5.14: Comparison between one-rotation model (left column) and two-rotation model (right column). It is shown how multiple rotations applied to North America generate different kinematics such as in the more northern latitude of the plate.

This model is not a mere mathematical exercise because the analysis of a single Euler pole generates different kinematics with respect to the two–Euler–pole interpretation. Although this kinematic analysis needs more physical data to confirm the result, it is an example suggesting that, if the sub-rotation really occurs, the instantaneous third composed pole would not be representative of the real motion of a plate during the continuum of the time. In fact it would represent, only in one instant, the plate motion on the epycicloid that is the resulting trajectory for a plate motion with two contemporaneous rotations.

5.6 Discussion

This chapter provides an analysis of the movement of plates described by multiple rotations in absolute reference frames. In accordance with this hypothesis, a two–rotation kinematics could produce the North America plate motion during a large part of the Cenozoic. Absolute plate motions governed by two rotations could be useful to justify present plate organization and many characteristic of plate tectonics, e.g. the Iberia and the South America past plate motions.

The introduction of the absolute sub–rotation could be also useful to investigate principal features of plate tectonics, as for the example the fracture zones [*Cronin*, 1991; *Friedrich and Leduc*, 2004], their meaning, and their role in computing plate kinematics.

About past plate reconstructions, the applications of the absolute sub–rotation to the North America could explain jumps of the Euler poles in different locations. From a dynamic point of view, jumps of the Euler poles and changes in plate direction of plate motions have been interpreted as related to variations in the mechanical strength [*Le Pichon et al.*, 1973]. On the contrary, the jumps of the poles and the changes in plate direction may be explained assuming a two-rotation kinematics. In this case, a pole may apparently jump into other locations, while instead the plate motion would be governed by two rotations. Past plate positions can be also reconstructed with the two-rotation plate motion, e.g. the North America.

We have also shown how in the NNR reference frame, the introduction of the sub–rotation could change the view of plate tectonic processes.

Dynamic implication of the absolute sub–rotation have to be investigated. Apart the forces that move the lithosphere, every time a plate experiences a sub-rotation, there would act an additional force, as for example a couple of forces possibly due to an anisotropic mantle response, generating the two-rotation motion. Regardless the kinematic implications, the absolute sub-rotations could indicate a differential mantle drag

at the base of the lithosphere, and support a passive behavior of the lithospheric motion [*Cruciani et al.*, 2005; *Doglioni et al.*, 2006a,b].

The concept of the absolute sub–rotation implies that to a better understanding of the Earth's dynamics, it would be useful to verify all the hypotheses for plate kinematics, principally studying the motion of the all plates in absolute reference frames and not only in relative analysis where sub-rotations might be hidden.

There is still a lot of difficult work to be done to cross and test the idea of plate sub–rotations with all the other geological and geophysical data. This chapter provides the basics of the sub–rotation theoretical concepts, and offers two applications, which show how what we know about geodynamics could change, introducing alternative plate kinematic models.

Chapter 6

Microplate motions in the hotspot reference frame

This chapter provides motions of the major plates and 38 microplates relative to the hotspot reference frame, and present velocities of these 52 plates. Moreover, using updated plate boundaries for the present, we have computed new geometrical factors for plates and microplates, useful for kinematic calculations and to obtain the net-rotation of the lithosphere and plate velocities in the mean–lithosphere reference frame. Instead of a continuum or gradational distribution of the plates by size, the plates clearly partition into three groups each having their own characteristics. For the seven large plates, rotation poles generally lie in high latitudes; the seven medium–sized plates have rotation poles in a restricted equatorial area; the 38 small plates show the greatest scatter. Moreover subsets of the 52 plates reveal differing fractal behavior: the large, middle and small groupings each have a characteristic fractal dimension, suggestive of microplate clustering. The highest angular velocities occur for some of the smallest plates, with the location of their rotation poles closely.

6.1 Introduction

In this chapter we compute absolute motions that describe the motion of plates and microplates with respect to the mesosphere. We generally used methods described in the previous chapters, and again the choice of the absolute reference frame that better represents plate motions with respect to the mesosphere may be the hotspots.

The addition of the microplates proposed by *Bird* [2003] produces a different value

of the the net–rotation of the lithosphere, but it does not largely change its value. Moreover, we investigate the fractal nature of plates and microplates, finding that plates and microplates have a characteristic fractal dimension depending of their size,

In this Chapter, we propose plate and microplate angular velocities testing only the deep–fed hotspot reference frame, with methods used by *Gripp and Gordon* [2002] to describe 52 plate and microplate motions. In addition, we compute plate and microplate velocities in the corresponding NNR frame, founding the net–rotation Euler vector.

6.2 Methods and Results

As just remarked in the Chapter 3, *Gripp and Gordon* [2002] defined a hotspot reference frame using segment trends and volcanic propagation rates, obtaining absolute plate motions for a ≈ 5.8 Myr time interval. First, they estimated segment trends and volcanic propagation rates by least–square methods and then, in this frame, computed a set of angular velocities consistent with the relative plate motions model NUVEL-1A [*DeMets et al.*, 1990, 1994].

We used the addition of their Pacific Euler vector to the PB2002 model [*Bird*, 2003], to compute plate and microplate motions in the hotspot frame for 52 plates (Table 6.1 and Figure 6.1). The PB2002 model also gives 52 new plate boundaries in digital form, and relative plate and microplate motions are referred to an arbitrary Pacific plate fixed, some coming from the literature, others newly interpreted. In that model, the velocities of the ten largest plates, Africa (AF), Antarctica (AN), Arabia (AR), Australia (AU), Cocos (CO), Eurasia (EU), India (IN), Nazca (NZ), North America (NA) and South America (SA) come from the NUVEL–1A [*DeMets et al.*, 1990, 1994], therefore for these plates we exactly reproduced the HS3-NUVEL1A results [*Gripp and Gordon*, 2002] (Table 6.1). Using the other relative motions collected and proposed by *Bird*, 2003, (his Table 1), we obtain new Euler vectors relative to the hotspots for the remaining 42 plates and microplates (see Table 6.1).

Though the covariance matrix of the Pacific plate is computed by *Gripp and Gordon* [2002], the uncertainties of the angular velocities for plates and microplates in the hotspots are not presented in this chapter, because the errors of relative plate motions of the PB2002 model [*Bird*, 2003] are not reported.

Table 6.1: Microplate and plate Euler vectors relative to the hotspots.

PLATE		Area	Angular Velocity		
		Steradians	°N	°E	°Myr^{-1}
PA	Pacific	2.5768	-61.467	90.326	1.0613
AF	Africa	1.4407	-43.386	21.136	0.1987
AN	Antarctica	1.4326	-47.339	74.514	0.2024
NA	North America	1.3657	-74.705	13.4	0.3835
EU	Eurasia	1.1963	-61.901	73.474	0.2047
AU	Australia	1.1329	-0.091	44.482	0.7467
SA	South America	1.0305	-70.583	80.401	0.4358
SO	Somalia	0.4719	-53.406	4.344	0.1192
NZ	Nazca	0.3967	35.879	-90.913	0.3231
IN	India	0.3064	26.467	3.069	0.5211
SU	Sunda	0.2197	-6.772	-26.816	0.2037
PS	Philippine Sea	0.1341	-52.742	-16.819	1.1978
AM	Amur	0.1306	-70.123	12.836	0.1553
AR	Arabia	0.1208	2.951	23.175	0.5083
OK	Okhotsk	0.0748	-74.713	28.719	0.2454
CA	Caribbean	0.0731	-64.494	-6.969	0.2196
CO	Cocos	0.0722	13.171	-116.997	1.1621
YA	Yangtze	0.0543	0.005	108.306	0.1617
SC	Scotia	0.0419	-77.268	51.747	0.4512
CL	Caroline	0.0377	-67.826	54.057	0.9482
ND	North Andes	0.0239	-66.874	88.61	0.3629
AP	Altiplano	0.0205	-57.402	-65.177	0.5044
BS	Banda Sea	0.0171	-7.931	116.22	2.5106
NH	New Hebrides	0.0158	-7.206	-0.892	2.5912
AT	Anatolia	0.0142	21.319	35.874	1.1875
BH	Birds Head	0.0130	-47.199	89.453	1.181
BU	Burna	0.0127	-13.616	-72.199	2.2091
KE	Kermadec	0.0124	30.673	11.939	2.2652
WL	Woodlark	0.0112	-10.765	121.708	1.8733
MA	Mariana	0.0104	-2.188	129.087	1.2627

Table 6.1: (continued)

PLATE		Area	Angular Velocity		
		Steradians	°N	°E	°Myr^{-1}
MS	Molucca Sea	0.0103	-2.378	-52.33	3.582
NB	North Bismarck	0.0096	-51.303	109.171	1.2242
TI	Timor	0.0087	-12.605	106.497	1.9539
ON	Okinawa	0.0080	28.131	132.145	2.5439
AS	Aegean Sea	0.0080	-42.838	89.03	0.4515
SB	South Bismarck	0.0077	4.427	-29.965	8.0525
PM	Panama	0.0068	-82.553	-101.535	0.1998
JF	Juan De Fuca	0.0064	-39.368	61.745	1.0117
TO	Tonga	0.0063	23.449	5.813	8.9185
BR	Balmoral Reef	0.0049	-64.237	97.967	0.8758
SW	Sandwich	0.0046	-46.255	-24.275	2.1207
EA	Easter	0.0042	23.065	67.522	11.4154
CR	Caonway Reef	0.0036	-25.548	167.064	3.9894
SS	Solomon Sea	0.0032	-13.765	123.523	1.8422
NI	Niuafo'ou	0.0031	-9.705	182.111	3.222
MO	Maoke	0.0029	-9.667	84.933	0.9678
RI	Riviera	0.0025	17.605	-107.298	3.8881
JZ	Juan Fernandez	0.0024	33.26	70.701	22.3832
SL	Sherland	0.0018	-51.811	112.365	0.2151
FT	Futuna	0.0008	-20.476	175.617	5.1096
GP	Galapagos	0.0003	-0.713	77.892	5.6985
MN	Manus	0.0002	-4.056	149.967	51.6116
LS	Lithosphere	12.5666	55.319	69.384	0.4296

Using errors of 50 km for the location of individual hotspots, *Jurdy* [1990] calculated an uncertainty of 1.1 degrees for the hotspot reference frame. Thus, in view of that study and also the standard deviations of the HS3-NUVEL1A model [*Gripp and Gordon*, 2002] for plate Euler vectors, we would obtain rather large uncertainties for microplate angular velocities.

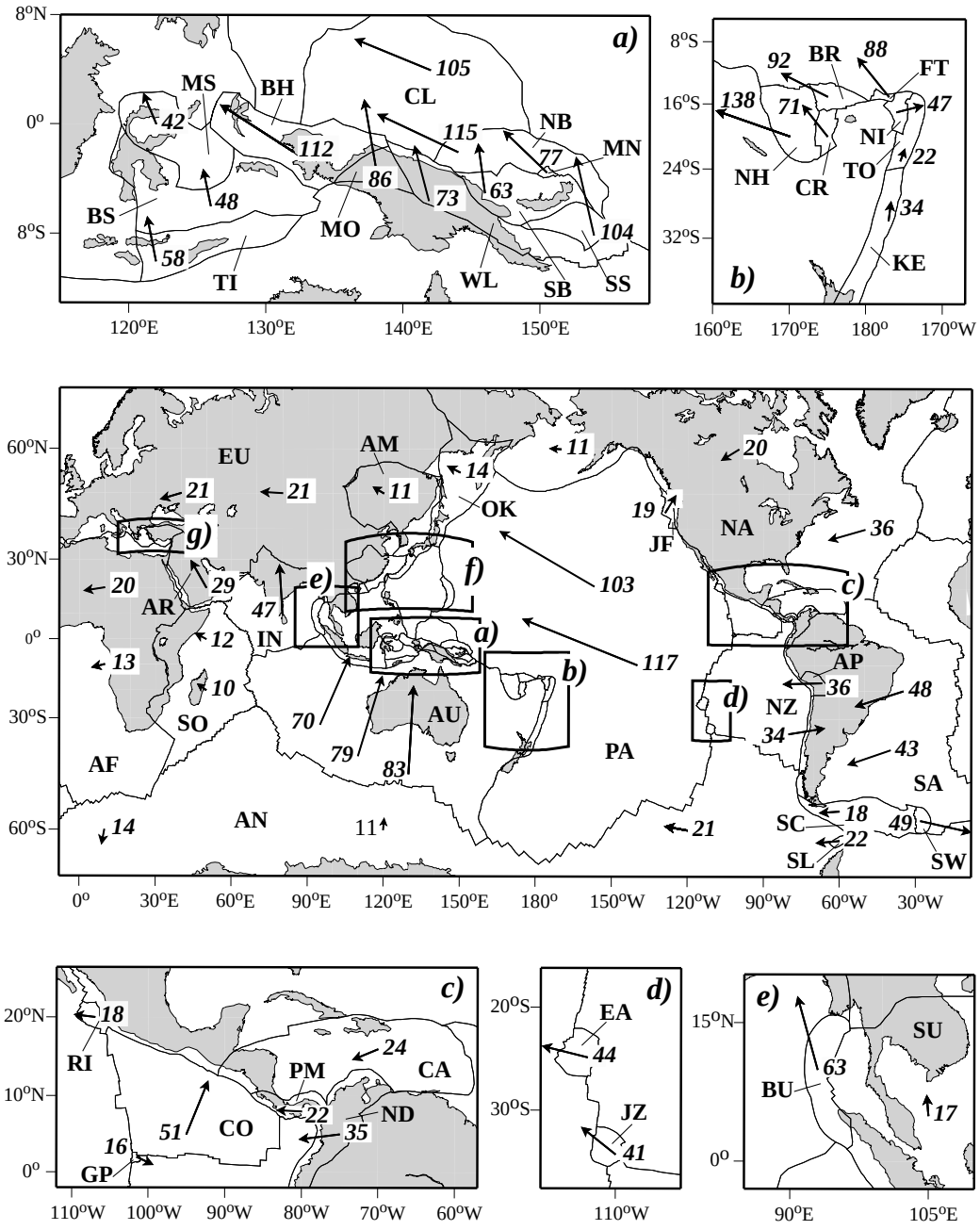

Figure 6.1: Microplate and plate motions with respect to the hotspot reference frame. Units are in mm yr $^{-1}$

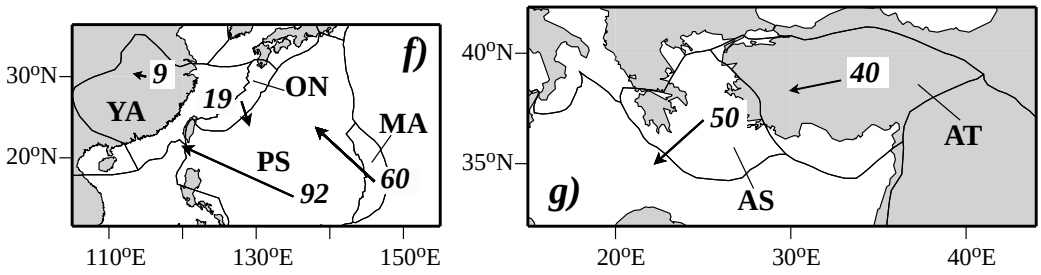

Figure 6.1: (continued)

Figure 6.1 shows current plate and microplate linear velocities relative to the hotspots. Most of the microplates are on the Pacific-Australia boundary (Figure 6.1a and 6.1b). Their motions are principally W-NW-ward directed with different velocities, except for the Niuafo'ou (NI), Kermadec (KE) and Tonga (TO) microplates (E-NE-ward directed) (Figure 6.1b). The other small plate velocities are generally W-NW-ward oriented except for the Sandwich (SW) and Galapagos (GP) microplate (Figure 6.1c) (SW-ward oriented). Easter Island (EA) and Juan Fernandez (JZ) show a NW-ward direction (Figure 6.1d), whereas Burna (BU) (Figure 6.1e) is mostly N-ward directed and Okinawa (ON) (Figure 6.1f) is SE-ward directed. Egean Sea (AS) and Anatolia (AT) (Figure 6.1g) have instead SW-ward oriented linear velocities.

Starting with these data, we compute plate and microplate geometrical factors, useful to compute net–rotation of the lithosphere. We define the symmetric tensor I_p [*Gordon and Jurdy*, 1986; *Jurdy*, 1990] describing plate geometry for a single plate p on a unit sphere using the Equation 1.3 (page 10), and we computed the net–rotation of the lithosphere using the Equation 1.4 (page 10), where, for this special case, $P = 52$ is the the total number of plates and microplates, I_p are the geometrical factors for a plate p (Table 6.2), and ω_p is the angular velocity for that plate (Table 6.1).

The resulting present net–rotation of the lithosphere relative to the mesosphere is described by a right–handed rotation about an Euler pole at 55.319 °S, 69.384 °E, 0.4296 °Myr^{-1}.

To obtain the angular velocity of a single plate p in the mean–lithosphere frame, the net–rotation angular velocity ω_{nr} is subtracted from the angular velocity ω_p. The mean–lithosphere framework is a reference frame based on the global plate geometry and velocities of every plate. Thus, any change in the assumed relative plate velocities and geometry results in a different net–rotation of the lithosphere.

Table 6.2: Microplate and plate geometrical factors

PLATE	I_{xx}	I_{yy}	I_{zz}	I_{xy}	I_{xz}	I_{yz}
AF	0.3726	1.3012	1.2075	-0.0513	-0.0054	0.0442
AM	0.1082	0.0895	0.0636	0.0287	0.0363	-0.0513
AN	1.3267	1.1747	0.3638	-0.0510	0.0525	0.0813
AP	0.0182	0.0042	0.0187	0.0061	0.0021	-0.0054
AR	0.0742	0.0668	0.1006	-0.0488	-0.0296	-0.0310
AS	0.0038	0.0070	0.0051	-0.0019	-0.0034	-0.0016
AT	0.0080	0.0116	0.0088	-0.0040	-0.0058	-0.0037
AU	0.8003	0.5884	0.8772	0.2032	-0.2132	0.2881
BH	0.0072	0.0058	0.0129	0.0064	-0.0002	0.0002
BR	0.0004	0.0048	0.0045	0.0003	-0.0012	0.0001
BS	0.0113	0.0060	0.0170	0.0080	-0.0009	0.0012
BU	0.0126	0.0004	0.0123	0.0009	0.0001	-0.0019
CA	0.0660	0.0120	0.0681	0.0180	-0.0052	0.0171
CL	0.0153	0.0225	0.0375	0.0182	0.0016	-0.0013
CO	0.0711	0.0030	0.0704	-0.0055	0.0011	0.0101
CR	0.0004	0.0035	0.0032	0.0003	-0.0011	0.0001
EA	0.0036	0.0013	0.0034	-0.0013	-0.0006	-0.0014
EU	1.0059	0.8948	0.4919	-0.0356	-0.2132	-0.3103
FT	0.0001	0.0008	0.0007	0.0000	-0.0002	0.0000
GP	0.0003	0.0000	0.0004	-0.0001	0.0000	0.0000
IN	0.2863	0.0423	0.2841	-0.0570	-0.0131	-0.0605
JF	0.0052	0.0044	0.0031	-0.0015	0.0019	0.0025
JZ	0.0022	0.0009	0.0017	-0.0006	-0.0004	-0.0010
KE	0.0038	0.0124	0.0087	-0.0001	-0.0056	0.0000
MA	0.0040	0.0074	0.0094	0.0044	0.0025	-0.0017
MN	0.0000	0.0002	0.0002	0.0001	0.0000	0.0000
MO	0.0013	0.0016	0.0028	0.0014	-0.0001	0.0001
MS	0.0072	0.0031	0.0103	0.0047	-0.0001	0.0002
NA	1.2286	0.9416	0.5612	0.0662	-0.0036	0.3963
NB	0.0026	0.0070	0.0095	0.0042	-0.0004	0.0002
ND	0.0224	0.0020	0.0235	0.0058	-0.0007	0.0025
NH	0.0019	0.0154	0.0143	0.0023	-0.0045	0.0008

Table 6.2: (continued)

PLATE	I_{xx}	I_{yy}	I_{zz}	I_{xy}	I_{xz}	I_{yz}
NI	0.0003	0.0030	0.0028	-0.0002	-0.0008	-0.0001
NZ	0.3854	0.0684	0.3396	-0.0126	-0.0030	-0.1134
OK	0.0534	0.0664	0.0298	0.0130	0.0303	-0.0179
ON	0.0056	0.0041	0.0063	0.0030	0.0020	-0.0026
PA	1.1757	1.9612	2.0168	-0.4295	0.0774	-0.0574
PM	0.0066	0.0003	0.0066	0.0010	-0.0002	0.0010
PS	0.0777	0.0713	0.1192	0.0583	0.0266	-0.0276
RI	0.0023	0.0005	0.0022	-0.0006	0.0002	0.0008
SA	0.6255	0.6092	0.8262	0.3403	0.1914	-0.1716
SB	0.0021	0.0056	0.0076	0.0033	-0.0006	0.0003
SC	0.0367	0.0345	0.0126	0.0057	0.0120	-0.0145
SL	0.0017	0.0015	0.0004	0.0002	0.0004	-0.0006
SO	0.2842	0.2349	0.4248	-0.1982	0.0608	0.0655
SS	0.0007	0.0025	0.0031	0.0013	-0.0004	0.0002
SU	0.1888	0.0363	0.2142	0.0691	0.0065	-0.0168
SW	0.0035	0.0043	0.0013	0.0005	0.0018	-0.0009
TI	0.0058	0.0031	0.0085	0.0040	-0.0008	0.0011
TO	0.0008	0.0062	0.0055	-0.0005	-0.0019	-0.0002
WL	0.0035	0.0078	0.0110	0.0050	-0.0011	0.0007
YA	0.0457	0.0200	0.0429	0.0166	0.0096	-0.0195
LS	8.3777	8.3777	8.3778	0.0002	-0.0002	0.0004

Units are in steradians

Indeed, using various plate motion models, hotspot locations or geometrical factors, yields different values of net–rotation angular velocity: 0.251 $^{\circ}$Myr^{-1} about a pole located at 51.50 $^{\circ}$S, 65.60 $^{\circ}$E [*Harper*, 1986]; 0.150 $^{\circ}$Myr^{-1} about a pole located at 56.00 $^{\circ}$S, 84.00 $^{\circ}$E [*Ricard et al.*, 1991]; 0.33 $^{\circ}$Myr^{-1} about a pole located at 49.20 $^{\circ}$S, 64.90 $^{\circ}$E [*Argus and Gordon*, 1991]; 0.436 $^{\circ}$Myr^{-1} about a pole located at 55.91 $^{\circ}$S, 69.93 $^{\circ}$E [*Gripp and Gordon*, 2002]. Although unresolved questions about hotspots remain, nonetheless the hotspot reference frame remains a geodynamic framework in which to study plate kinematics and dynamics.

6.3 Discussion

We have estimated current velocities for the lithospheric plates including 38 new microplates in the hotspot reference frame, incorporating the PB2002 model [*Bird*, 2003]. We also present a new net–rotation angular velocity including microplate contributions and necessary rotation to obtain plate angular velocities in the mean–lithosphere framework. The addition of the 38 microplates, results in a net–rotation of 0.4296 $^{\circ}\mathrm{Myr}^{-1}$ around a pole located at 55.319 °S, 69.384 °E, that it is not more different than the one computed by *Gripp and Gordon* [2002] (0.436 $^{\circ}\mathrm{Myr}^{-1}$ about a pole located at 55.91 °S, 69.93 °E) or the one obtained in the Chapter 4, with the deep–fed hotspots hypothesis, incorporating the REVEL [*Sella et al.*, 2002] plate kinematic model (0.4402 $^{\circ}\mathrm{Myr}^{-1}$ about a pole located at 52.324 °S, 68.840 °E).

Our results (Table 6.1, Figures 6.2, 6.3, 6.4, 6.5) show some kinematic and geometric patterns related to plate size. No continuum or gradational distribution of plate size exists, but they clearly partition into three groups: large, middle and small. The seven large plates (PA, AF, AN, NA, EU, AU, SA) all exceed 1.03 Steradians; together these comprise 81.0% of the Earth's surface and dominate with 85.3% of the net–rotation velocity computation. Next, the seven middle plates (SO, NZ, IN, SU, PS, AM, AR), in the range of 0.47 to 0.12 Steradians, cover 14.0% of the surface area and contribute 9.8% of the velocity computation. The remaining 38 plates span three orders of magnitude in size and lie in the range 0.0748 to 0.0002 Steradians, accounting for 4.9% of the total area and 5.2% of the total net–rotation.

The distribution of the plates over the Earth's surface shows a relation to the size–grouping of plates. The large–sized lithospheric plates cover most of the Earth's surface. Middle–sized plates are positioned in equatorial regions (except AM, Figure 2), whereas most of the small plates lie on the interfaces of the large plates, i.e. the Australia–Pacific, the Eurasia–Pacific and the Nazca-South America boundary (Figure 6.2), suggesting that some might be interpreted as parts of the diffuse margin of the two large plates. In addition, the plate angular velocities show a pattern with plate size: these generally increase with decreasing plate area (Figure 6.3) reaching the highest values for some of the smallest plates (e.g. JZ and MN).

Fractals relate geometry at different scales, as *Feder* [1988] argues, and can give insight into our understanding of naturally occurring objects. The plates, which range in areas over four orders of magnitude (Table 6.1), provide a compelling opportunity for fractal analysis.

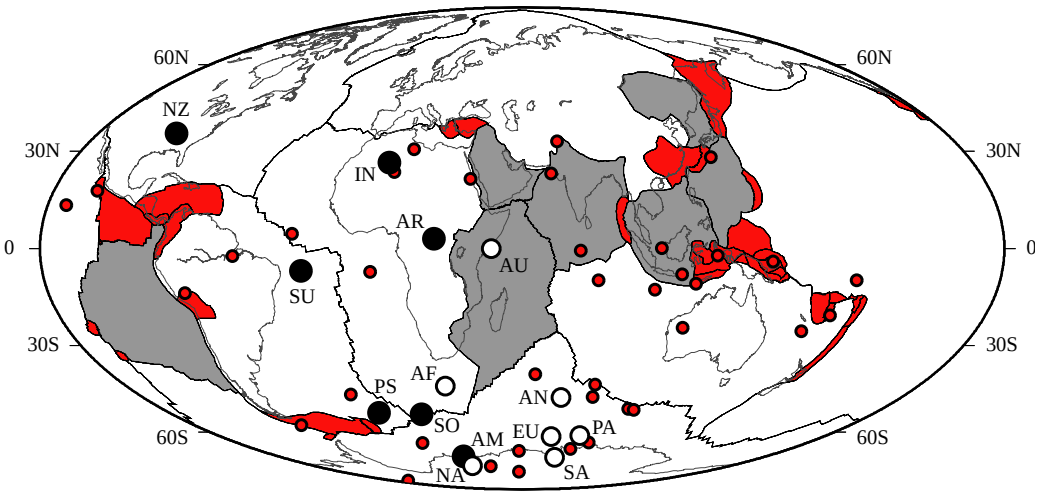

Figure 6.2: Large (white), middle (gray) and small (red) plates and respective rotation poles, open, black and red circles.

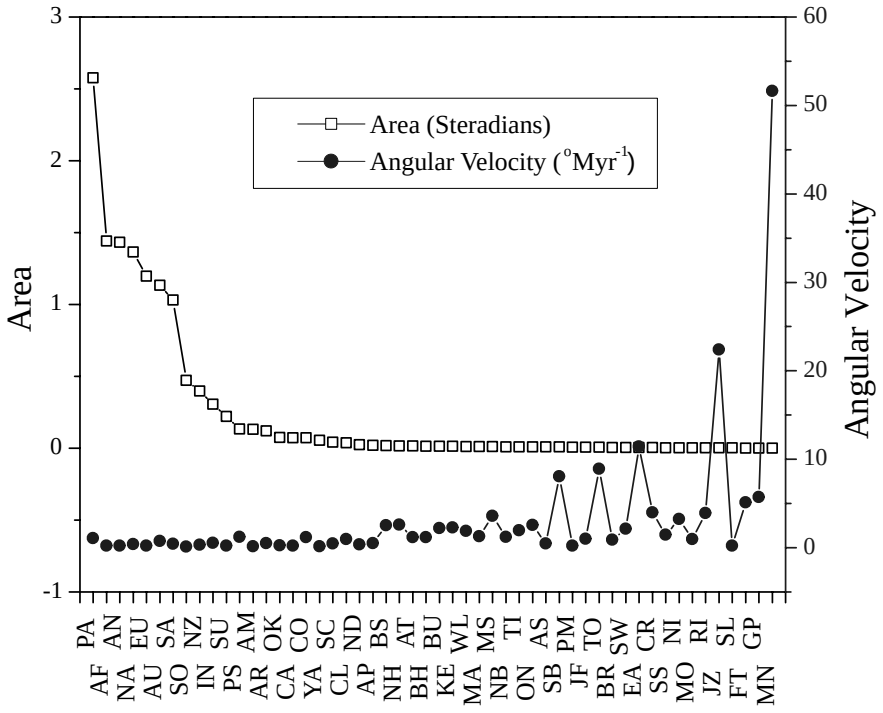

Figure 6.3: Microplates and plates (sorted by area) vs plate area (left axis) and angular velocities relative to the hotspots (right axis)

We examine the fractal behavior of the plates by plotting the log of the plate area in Steradians versus the log of plate count, shown in Figure 6.4. Peter Bird has considered the fractal properties of the plates (*Bird*, 2003, his Figure 19) and finds that the plates having areas between 0.002 and 1.000 Steradians (JZ to SA for his 38 plates) can be approximately described by a power law:

$$Cc \simeq 7A^{-\frac{1}{3}} \tag{6.1}$$

where Cc is the cumulative count of plates and A is the plate area in Steradians.

Here, we note that the fractal behavior of the plates also depends on the size range. In Figure 6.4, we show that the largest seven plates define one slope, or fractal behavior, and the middle seven another slope, whereas remaining 38 plates have a different fractal behavior. The largest seven (omitting the Pacific as an exception, as Bird has done) have a slope less than -2 (Figure 6.4a). The middle-sized plates (Figure 6.4b) have a slope of about -2 (the reference line), and the small plates – particularly # 22–48 match the reference line slope of -2 (Figure 6.4c). The change in slope from -2 may be a consequence of a clustering behavior for the smaller plates.

This clustering ceases once the plate's size increases from about 4% to more than 12% of the surface of the Earth. *Feder* [1988] shows a similar fractal behavior for the clustering of silica particles (e.g. *Feder*, 1988, chap 3). The curve flattens for the smallest plates. Bird's explanation for this flattening of the curve lies in the current incompleteness of the dataset for plates smaller than SL, 0.0002 Steradians.

Additional patterns emerge concerning the absolute motions of the plates based on their groupings by size. The Euler poles for large plates concentrate over less than 10% of a hemisphere near a mean latitude of 60°S, except for AU, a consequence of its northwest motion (Figure 5a). However, the Euler poles for middle–sized plates are generally more equatorial in distribution, but scatter more, spread over about 20% of a hemisphere (Figure 6.5a). The rotation poles of the small plates generally show considerable scatter, though poles avoid the regions populated by the poles for the large and middle-sized plates (Figure 6.5b).

This is a consequence of microplate behavior, as noted by *Engeln et al.* [1998]: the rotation poles describing microplate motions lie close by, thus have large rotations. This may explain the difference in location of rotation poles and size of the rotation for small microplates, as compared with the seven larger plates.

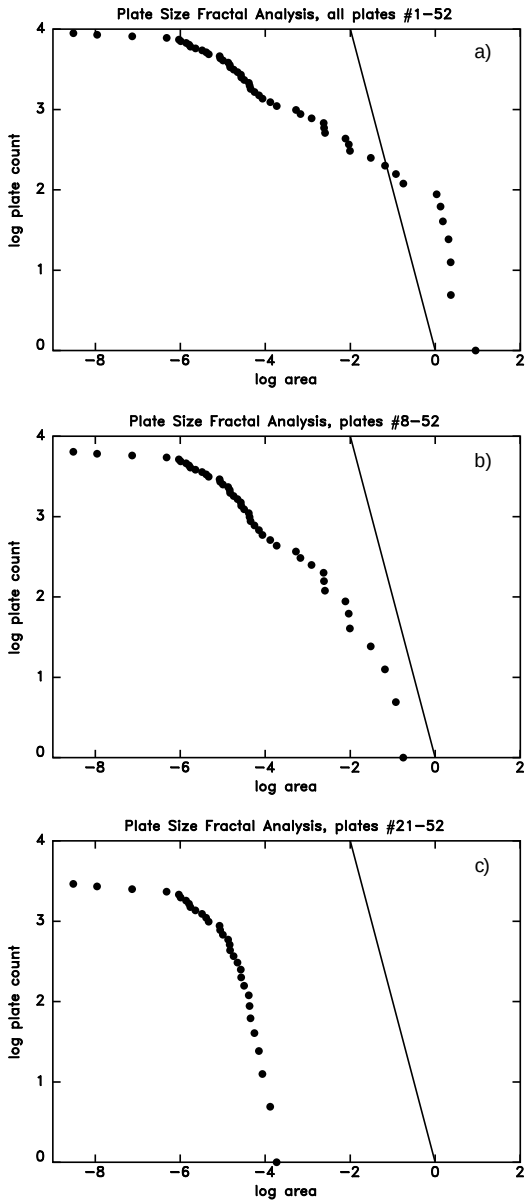

Figure 6.4: Log of plate count versus the log of the plate area in Steradians. The 52 plates microplates have non-fractal behavior. The largest seven plates show one slope (a), whereas the remaining plates show another, (b) for middle plates, (c) for the remaining microplates. Reference line has a slope of -2

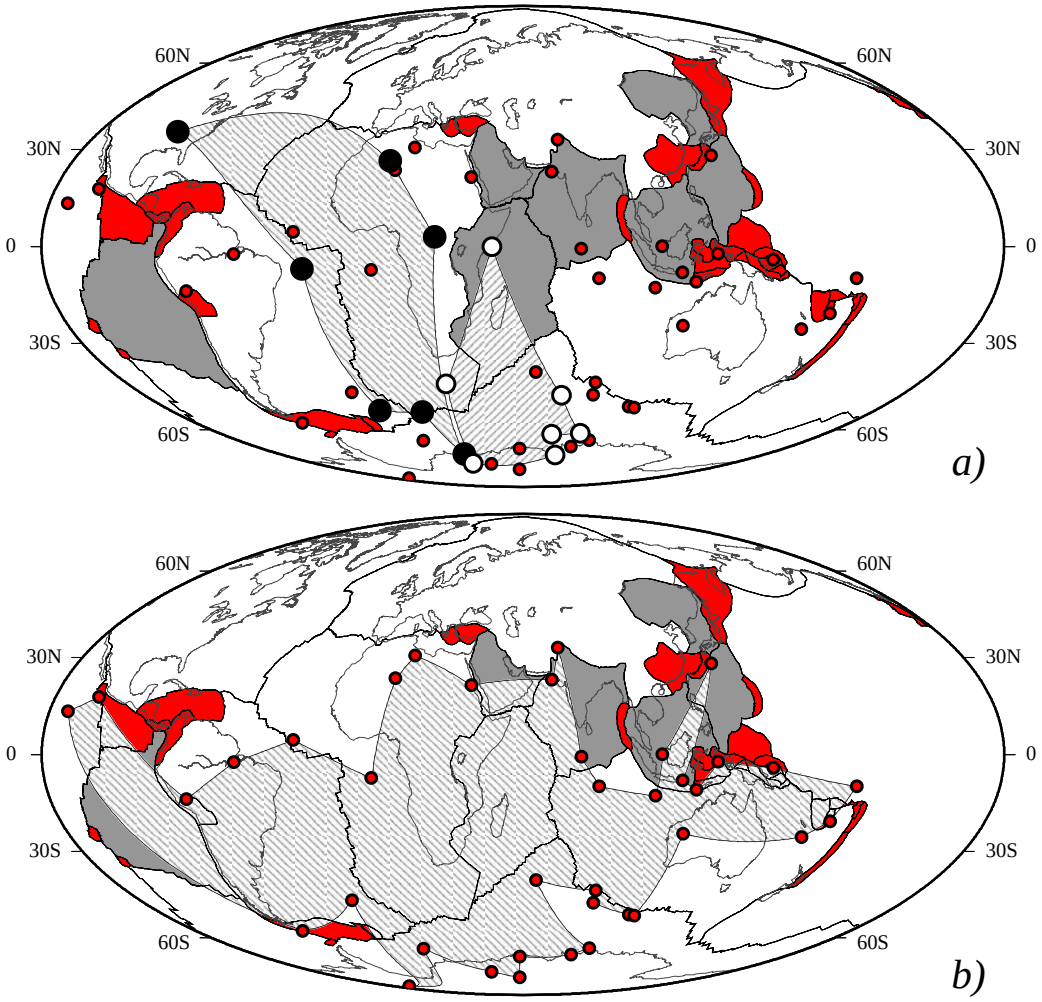

Figure 6.5: (a) The Euler poles for large plates concentrate over less than 10% of a hemisphere near a mean latitude of 60°S, except for AU. However, the Euler poles for middle-sized plates are generally more equatorial in distribution, and these scatter more, about 20% of a hemisphere. (b) The rotation poles of the small plates generally show considerable scatter, though poles avoid the regions populated by the poles for the large and most of middle-sized plates.

These high velocities and the locations of rotation poles fairly close to the corresponding plates may offer a criterion to distinguish independent microplates from diffuse margins.

We have shown in this chapter that there appears to be a natural partitioning of plates into three groups based on their size. Each subset of plates share some common characteristics. These similarities within groups include the nature of plate distribution over the Earth, location of rotation poles, size of the corresponding rotations, as well as the observed fractal behavior. This breakdown by plate size may be a natural consequence of plate tectonics: large plates and most of the middle being moved predominantly by driving forces, and small ones clustering at the interfaces.

Chapter 7

Horizontal versus vertical plate motions

In this chapter, we review both present and past motions at major plate boundaries, finding that the horizontal components are in average 10 to 100 times faster (10-100 mm/yr) than the vertical components (0.01-1 mm/yr) in all the geodynamic settings. This could indicate a passive role of plate boundaries with respect to far field forces determining the velocity of plates. The faster horizontal velocity of the lithosphere with respect to the upward or downward velocities at plate boundaries could support dominating tangential forces acting on plates. These forces acting on the lithosphere can be subdivided in coupled and uncoupled, as a function of the shear at the lithosphere base. Higher the asthenosphere viscosity, more important should be the coupled forces, i.e., the mantle drag and the trench suction. Lower the asthenosphere viscosity, more the effects of uncoupled forces might result determinant, i.e., the ridge push, the slab pull and the tidal drag. Although a combination of all forces acting on the lithosphere is likely, the decoupling between lithosphere and mantle suggests that a torque acts on the lithosphere independently from the mantle drag. Slab pull and tidal drag are the best candidates for generating this torque, but the Earth's rotation might have the primary role if the viscosity of the upper asthenosphere is sufficiently low.

7.1 Introduction

It is expected from the $\vec{v} = \vec{\omega} \times \vec{R}$ relation that all plate motions ideally are horizontal, and that vertical effects should be second order and hence smaller, being $\vec{v}$ the horizontal

plate velocity, $\vec{\omega}$, the angular velocity and $\vec{R}$ the Earth's radius. We test this idea compiling present and past horizontal and vertical rates of plate motions. The advent of space geodesy makes it possible to measure present day plate movements [*Heflin et al.*, 2004] and to test the velocities estimated from NUVEL - 1 plate velocity model [*DeMets et al.*, 1990]. Until recently, the relative contribution of past horizontal and vertical motions had to be inferred indirectly. Past horizontal movements are recorded by ocean magnetic anomalies, by hotspot notion, and shortening in the orogens. Along plate boundaries, vertical movements (subsidence or uplift) always accompany horizontal movements. Past subsidence rates in oceanic realms are inferred from bathymetry, which is controlled primarily by the cooling of the lithosphere. Subsidence rates in passive continental margins and in foredeep basins, bordering subduction zones, are inferred from backstripping of basin stratigraphy. Uplift of past marine terraces, apatite fission track analyses and metamorphic PTt paths constrain the past uplift and denudation rates in orogenic areas.

Present rates of horizontal and vertical motion give a reliable idea of plate movements in the geological past because, as already noted, present-day velocities roughly match the past rates computed studying the magnetic anomalies of the sea-floor spreading [*Gordon and Stein*, 1992].

In this chapter we have made a worldwide comparison of the horizontal and vertical component of plate motions along plate boundaries, using both present and past rates. We quantify the faster horizontal vs slower vertical motions, and briefly discuss the implications of on this observation.

7.2 Movement rates

7.2.1 Present plate motions

For the present plate motions, our analysis is based on the NASA data set [*Heflin et al.*, 2004], where both horizontal and vertical rates determined from the motion of GPS sites are given in the ITRF2000 reference frame [*Altamimi et al.*, 2002]. In that framework, the epoch is January 1, 2004 and the reference ellipsoid for latitude, longitude and height is WGS84. Both horizontal and vertical motions are obtained from least squares methods, using GPS time series over time periods of the order of years (Figure 7.1).

Here, we are interested in evaluating differences between horizontal and vertical plate motions using an official data set, as the NASA one [*Heflin et al.*, 2004]. Regardless the goodness of the solutions of plate motions from GPS data, we chose data proposed by

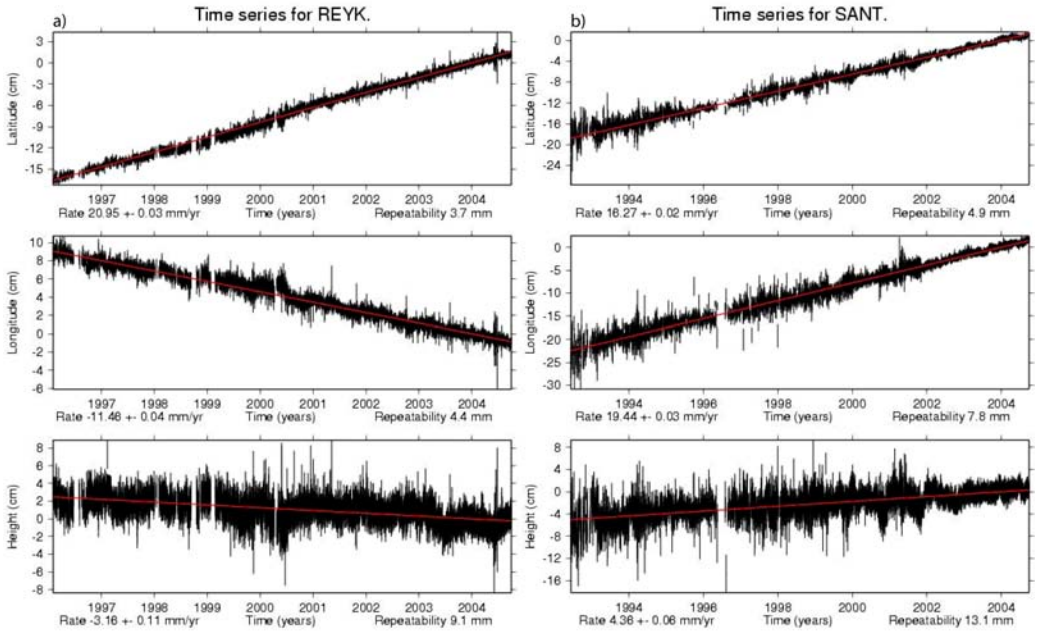

Figure 7.1: Examples of time series, for the station of REYK (a) and SANT (b). Horizontal and vertical velocities are given by the slope of the least squares fit (red line). Note that vertical rate shows subsidence of the site for the case (a), and viceversa uplift in the case (b)

Heflin et al. [2004] to have the most updated information about vertical plate motions. For this reason, data utilized here are referred to April 2006.

Plate boundaries accommodate plate motions, and can be even several hundreds km wide [e.g. *Gordon*, 2000]. Therefore horizontal plate motion between two plates is best evaluated using sites located intraplate, far from plate boundaries. Conversely, motions from the sites located along the plate boundaries better indicate entities of vertical components.

For the purpose to make a comparison between horizontal and vertical rates along different plate margins, we selected GPS stations located on boundaries, or as close as possible, and we considered the vertical rate [*Heflin et al.*, 2004] with a negative sign for subsidence and positive for uplift (Table 7.1).

Every GPS station was also chosen for computing horizontal relative plate motions. In each point, we obtained the horizontal velocity by making use of the relative angular velocities and Euler poles of pairs of plates sharing a boundary, using the kinematic parameters of the model REVEL [*Sella et al.*, 2002].

Table 7.1: Present horizontal vs vertical plate motions from GPS data.

	Position			Rate $\pm 1\sigma$ (mm yr^{-1})	
GPS Station[a]	°N	°E	Plate Pair[b]	Horizontal Motion	Vertical Motion
Western Pacific and South Asia					
GUAM	13.58	144.86	PA – PH	-18.787 $\pm$ 3.204	3.810 $\pm$ 0.150
TSKB	36.10	140.08	OK – PA	-72.018 $\pm$ 14.862	0.270 $\pm$ 0.080
PETP	-31.80	115.88	OK – PA	-78.027 $\pm$ 14.399	-1.990 $\pm$ 0.190
PIMO	14.63	121.07	PH – SU	-102.291 $\pm$ 7.840	0.920 $\pm$ 0.350
BAKO	-6.49	106.84	AU – SU	-64.061 $\pm$ 1.579	5.700 $\pm$ 0.400
South Western Pacific					
NOUM	-22.26	166.41	AU – PA	-79.479 $\pm$ 1.087	5.030 $\pm$ 0.160
AUCK	-36.60	174.83	AU – PA	-52.268 $\pm$ 1.072	2.010 $\pm$ 0.090
MAC1	-54.49	158.93	AU – PA	-32.096 $\pm$ 1.081	0.910 $\pm$ 0.080
North Eastern Pacific					
KODK	57.73	-152.50	NA –PA	-59.274 $\pm$ 0.814	7.820 $\pm$ 0.290
UCLU	48.92	-125.54	NA – PA	-46.786 $\pm$ 0.847	3.840 $\pm$ 0.230
COSO	35.98	-117.80	NA – PA	-48.885 $\pm$ 0.849	-3.670 $\pm$ 0.190
Peru-Chile Trench					
RIOP	-1.65	-78.65	NZ – SA	-57.524 $\pm$ 2.606	4.240 $\pm$ 1.150
AREQ	-16.46	-71.49	NZ – SA	-66.430 $\pm$ 2.387	3.180 $\pm$ 0.920
UNSA	-24.72	-65.40	NZ – SA	-69.339 $\pm$ 2.387	1.660 $\pm$ 0.380
SANT	-33.15	-70.66	NZ – SA	-70.299 $\pm$ 2.246	4.360 $\pm$ 0.060
Himalayan Collision Zone					
KIT3	39.13	66.88	EU – IN	-28.736 $\pm$ 8.568	-1.830 $\pm$ 0.090
LHAS	29.65	91.10	EU – IN	-36.789 $\pm$ 8.029	1.230 $\pm$ 0.110
Atlantic Ridge					
REYK	64.13	-21.95	EU – NA	19.897 $\pm$ 0.498	-3.160 $\pm$ 0.110
ASC1	-7.95	-14.41	NU – SA	29.567 $\pm$ 1.069	0.170 $\pm$ 0.140
GOUG	-40.34	-9.88	NU – SA	29.580 $\pm$ 1,043	-10.670 $\pm$ 0.240
East Pacific Rise					
GALA	-0.74	-90.30	NZ – PA	117.082 $\pm$ 2.444	-1.780 $\pm$ 0.200
EISL	-27.14	-109.38	NZ – PA	140.281 $\pm$ 2.211	0.250 $\pm$ 0.110

Table 7.1: (continued)

	Position			Rate $\pm$ 1σ (mm yr^{-1})	
GPS Station[a]	°N	°E	Plate Pair[b]	Horizontal Motion	Vertical Motion
Indian Ridge					
DGAR	-7.26	72.37	AU – SO	36.331 $\pm$ 8.596	1.720 $\pm$ 0.180

[a]AREQ Arequipa – Peru, ASC1 Ascension Island, AUCK Whangaparaoa Peninsula – New Zealand, BAKO Cibinong – Indonesia, COSO Coso Junction – USA, DGAR Diego Garcia Island – U.K. Territory, EISL, Easter Island – Chile, GALA Galapagos – Ecuador, GOUG Gough Island – dependent territory of the U.K., GUAM Dededo – Guam, KIT3 Kitab – Uzbekistan, KOKD Kodiak – USA, LHAS Lhasa – China, MAC1 MacQuarie Island, Sub-Antarctic – Southern Ocean, NOUM Noumea – France, PETP Petropavlovsk-Kamchatka – Russian Federation, PIMO Quezon City – Phillipines, REYK Reykjavik – Iceland, RIOP Riobamba – Ecuador, SANT Santiago – Chile, TSKB Tsukuba – Japan, UCLU Ucluelet – Canada, UNSA Salta – Argentina.

[b]The first plate rotates counterclockwise relative to the second and vicecersa. AU – Australia, EU – Eurasia, IN – India, NA – North America, NU – Nubia, NZ – Nazca, OK – Okhotsk, PA – Pacific, PH – Philippine, SA – South America, SO – Somalia, SU – Sunda.

Because we are interested in investigating horizontal relative plate motions along boundaries, we preferred to use a plate motion model (e.g. REVEL), estimated with GPS data, instead of the use of the single time series (Figure 7.1). Beacuse *Sella et al.* [2002] used a much more extensive space geodetic dataset to construct their model for recent plate velocities and a robust statistical approach to estimate the uncertainties of the motion rates, this choice guarantees an accurate evaluations of the horizontal relative motion. Moreover, the use of REVEL model guarantees that the calculated relative horizontal motion is not affected by stress along plate margins, because plate motions are evaluated choosing sites located far from significant plate boundaries.

The use, here, of the REVEL plate kinematic model do not imply a comparison between GPS solutions. The NASA database and the REVEL model have probably different results (e.g. vertical motion estimations or order of magnitude of uncertainties), but we utilized both their results, using the updated vertical data of the first, and the accurate evaluation of the horizontal relative motion of the second.

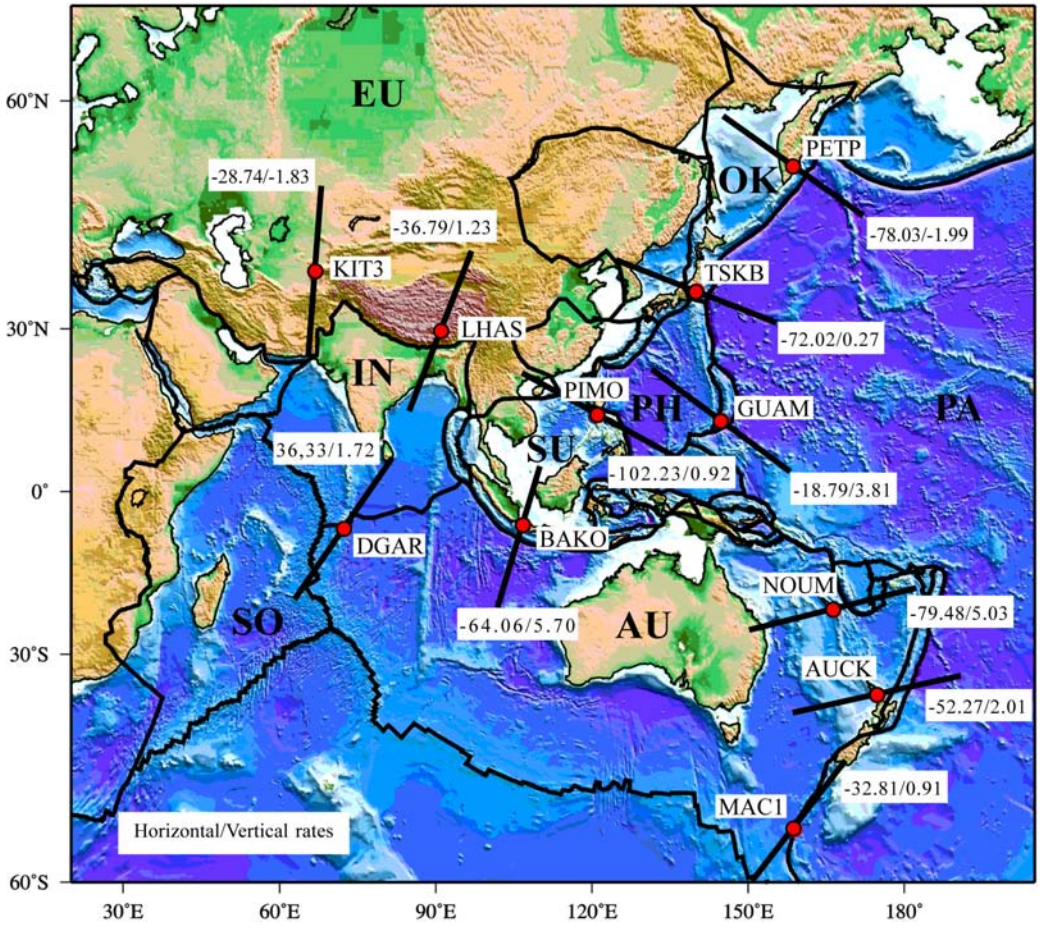

Figure 7.2: Comparisons between relative horizontal and vertical motions of selected GPS stations for paths in the Western Pacific and South Asia, South Eastern Pacific, Himalaya and Indian Ridge. About horizontal velocities, negative signs show contraction and positive signs show extension. About vertical velocities, negative signs show subsidence and positive signs show uplift. Oriented segments show relative motion directions. Units are in mm yr^{-1}

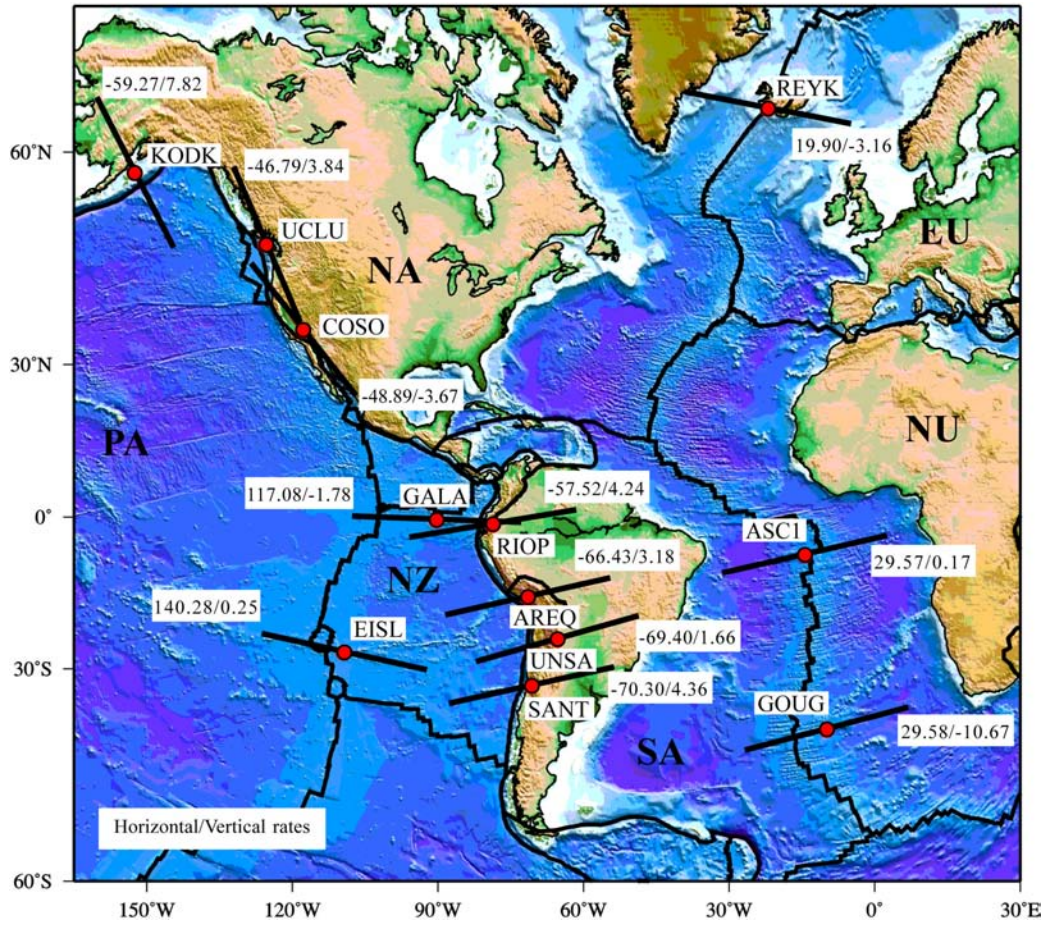

Figure 7.3: Comparisons between relative horizontal and vertical motions of selected GPS stations for paths in the North Eastern Pacific, East Pacific Rise, Peru – Chile Trench and the Atlantic Ridge. About horizontal velocities, negative signs show contraction and positive signs show extension. About vertical velocities, negative signs show subsidence and positive signs show uplift. Oriented segments show relative motion directions. Units are in mm yr^{-1}

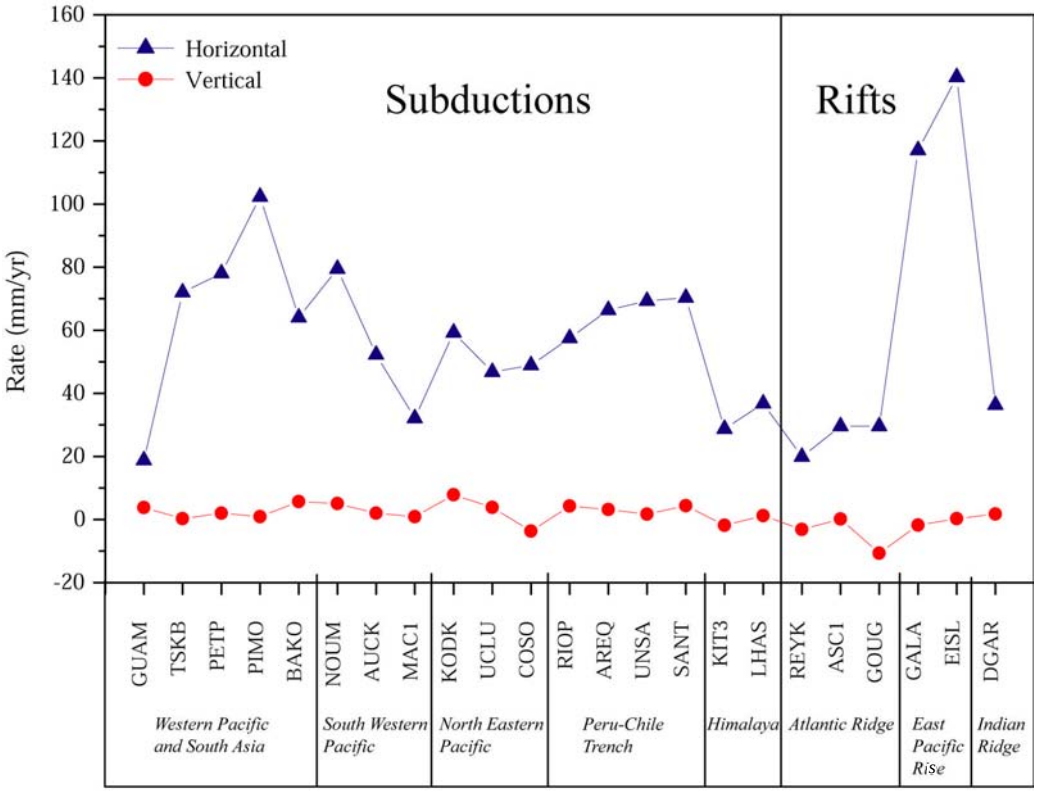

Figure 7.4: Comparison of the present horizontal and vertical plate motions rates along subudction and rift zones for selected GPS stations. The horizontal rates of subduction and rift settings are plotted as absolute values, and are respectively the negative and the positive values of Figures 7.2 and Figure 7.3. Negative and positive vertical rates respectively indicate subsidence and uplift.

The uncertainties of the horizontal plate motions (Table 7.1) are computed with the methods proposed in the Appendix B, whereas the errors of the vertical motions (Table 7.1) are those of the NASA database [*Heflin et al.*, 2004].

Using this method, we tried to cover most of the plate boundaries for a global analysis. About subduction zones, we selected stations along the Western Pacific and South Asia boundaries, using for the horizontal velocity analysis several relative motion parameters, Pacific plate motion (PA) with respect Philippine (PH), Okhotsk (OK) with respect to Pacific (PA), Philippine (PH) relative to Pacific (PA) and to Sunda (SU), and Australia (AU) with respect to Sunda (SU). Then we studied other convergent margins, and we chose stations along the South Western Pacific boundary, North Eastern Pacific, Peru – Chile trench and Himalayan Collision zone, respectively using motion of Australia (AU)

relative to Pacific (PA), North America (NA) relative to the Pacific (PA), Nazca (NZ) relative to South America (SA) and Eurasia (EU) with respect to India (IN) (Table 7.1, Figure 7.2 and Figure 7.3).

About rift zones, we studied motion of GPS stations close to the Atlantic Ridge, computing the relative horizontal motion with the angular vectors of Eurasia (EU) relative to North America (NA) and Nubia (NU) relative to South America (SA). Then we considered also the East Pacific Rise and the Indian Ridge, respectively using motion parameters of Nazca (NZ) relative to Pacific (PA) and Australia (AU) with respect to Somalia (SO) (Figure 7.2 and Figure 7.3).

The negative and positive signs indicate relative horizontal contraction and extension respectively (Table 7.1). Though vertical rates from GPS data have greater error values than horizontal rates, sometimes comparable with the rate value (e.g. ASC1, Ascension Island), the comparison results (Table 7.1 and Figure 7.4) show that relative horizontal motions are steadily 10 or 100 times faster than vertical motions. Relative horizontal motions have rates of 18.787 – 140.281 mm yr^{-1}, whereas vertical motions have on large-scale rates of 0.170 – 10.670 mm yr^{-1}.

7.2.2 Past plate motions

For past movements, magnetic anomaly record, spreading rates along oceanic rifts and the stratigraphic record help to unravel with sufficient accuracy the rates of vertical movements, computed with subsidence curves in basinal settings, or apatite fission tracks of uplifting areas, and other techniques.

Plate motions are a consequence of the lithosphere-mantle interaction, and the relative plate motion might not have the same velocity occurring between lithosphere and mantle. For example the ”absolute” motions computed in the hotspot reference frame [*Gripp and Gordon*, 2002] give faster velocities of plates relative to the mantle than relative to each other, albeit of the same order of magnitude. In case the hotspot source is shallow, say in the asthenosphere, these ”absolute” velocities can be even faster [*Doglioni et al.*, 2005].

Vertical movements along subduction zones such as uplift in the overriding plate and subsidence in the subducting plate generate respectively the growth of an orogen and the deepening of a foredeep basin. *Bernet et al.* [2001], use apatite fission-track grain-age distributions for detrital zircons to infer a steady-state exhumation in the Alps at rates of 0.4 – 0.7 mm yr^{-1} since at least 15 Myr. Subsidence rates in the alpine foredeep are in the order of 0.1 – 0.3 mm yr^{-1} [*Doglioni*, 1994]. Rates along the Andean subduction zone are of the order of 1 – 4 mm yr^{-1} for uplift and less than 0.5 mm yr^{-1} for subsidence.

Fission-track analysis in the Peruvian Andes suggests 1.1 mm yr^{-1} uplift [*Montario*, 2001]. Convergence rates along the same subduction zone are in the order of 30 – 100 mm yr^{-1}.

In Alaska, exhumation rates of about 3 mm yr^{-1} have been suggested [*Spotila et al.*, 2004]. Faster (5 – 10 mm yr^{-1}) uplift rates have been computed in Taiwan and Papua New Guinea [*Liu*, 1982; *Dadson et al.*, 2003; *Baldwin et al.*, 2004].

Worldwide, foredeeps and trenches during the last 100 Ma worldwide have subsidence rates spanning on average from 0.1 to 1.6 mm yr^{-1} [*Doglioni*, 1994], with the fastest rates located along the west-directed subduction zones. Along the Marianas subduction zone, where the slab pull is theoretically the highest on Earth, the Pacific plate moves WNW-ward faster than 100 mm yr^{-1}, whereas the subsidence in the trench is in the order of few mm yr^{-1}.

In extensional settings, subsidence rates determined by lithosphere stretching and thermal cooling are in the order of 0.02 – 0.5 mm yr^{-1} in passive continental margins, backarc settings and oceanic embayments [*McKenzie*, 1978; *Doglioni*, 1995]. Flexural isostatic response to lithosphere stretching produces episodic rift flank uplift [*Braun and Beaumont*, 1989]. In the Northern Ethiopian plateau the maximum flank uplift rates are around 0.5 – 1 mm yr^{-1} [*Faure*, 1975]. In oceanic basins, a progressive deepening of the sea floor away from the ridges is observed. This subsidence, controlled by cooling and contraction of the lithosphere emplaced at ridges, is proportional to the square root of floor age and occurs with rates around 0.04 – 0.1 mm yr^{-1} [*Parsons and Sclater*, 1977].

Horizontal velocities are more variable. The break-up, i.e., the transition from continental rifting to oceanic rifting and drifting, marks a strong acceleration of the horizontal velocity, suddenly shifting from about 0.1 mm yr^{-1} for the continental rift, to 10 – 100 mm yr^{-1} for the oceanic spreading as computed with the magnetic anomalies (e.g., *Nürnberg and Müller*, 1991; *Cande and Kent*, 1995). This anomalous increase in speed needs to be explained. One possibility is the decrease in coupling between lithosphere and mantle, once the continental lithosphere is broken apart. The spreading rates were also used for the computation of the relative plate kinematic models for a period of 3 – 10 Myr [*Minster and Jordan*, 1978; *DeMets et al.*, 1990, 1994]. During rifting, the uplift of the mantle beneath oceanic ridges compensating the volume of stretched lithosphere may have comparable velocity in order of magnitude to spreading rates [*Bonatti et al.*, 2003].

In strike-slip settings, either subsidence or uplift can occur. Along tranform boundaries, oceanic crust slices of different ages (and hence different depths) are juxtaposed, producing fault scarps. Hence vertical motion along transform faults results from dif-

ferences in thermal subsidence and has therefore rates comparable to those for oceanic floor thermal subsidence. However, compressional or tensional stresses resulting from small changes in the direction of spreading [*Bonatti*, 1978], can lead to uplift or additional subsidence. Episodic compression and extension can also occur, such as in the St Peter-Paul island [*Bonatti and Crane*, 1984]. Uplift of transverse ranges along the Romanche fracture zone was followed by subsidence with rates of 0.2 mm yr^{-1} [*Bonatti*, 1978]. In contrast, most horizontal velocities along transform boundaries range between 10 and 100 mm yr^{-1}.

Transcurrent margins can be characterised by uplift and subsidence, depending on the orientation of the fault with respect to the plate motion or on the departure of the fault from a simple linear trend. In pull apart basins of California, subsidence can initially occur with rates up to 2 mm yr^{-1} due to local extension [*Link and Osborne*, 1978] and continue with far lower rates due to cooling [*Pitman and Andrews*, 1985]. In the Californian coastal ranges, bedrock and surface uplift from fission track studies are respectively of the order of 0.85 and 0.2 mm yr^{-1} [*Ducea et al.*, 2003]. Horizontal rates along the San Andreas fault are constrained by geodetic studies to about 40 mm yr^{-1} [*Freymueller et al.*, 1999]. In transpressional subduction margins, such as the New Zealand Southern Alps, uplift occurs with rates of $1 - 3$ mm yr^{-1}, as determined from the position of marine terraces [*Berryman*, 1993], whereas the horizontal velocity is 45 mm yr^{-1}.

Dynamic topography (either subsidence or uplift) is also characterized by slow rates in cratonic or intraplate areas (e.g. *Wheeler and White*, 2000). Exceptions to the general rule can be post glacial rebound that can be faster than 10 mm/yr [*Larsen et al.*, 2004], or postseismic uplift of even 80 mm/yr after gigantic earthquakes [*Freymueller et al.*, 2000].

7.3 Discussion

The faster horizontal motion of plates (Figure 7.5) could suggest that tangential forces are more efficient than vertical forces in plate deformation. It is obvious that horizontal motion does not compete with gravity as vertical motion does. Moreover, it could be argued that the horizontal movement of plates is accommodated in by a diffuse strain. However this discrepancy is intriguing, particularly along subduction zones and extensional margins.

The aforementioned kinematic observations allow us to make a few dynamic considerations (see also Chapter 8). All types of tectonic–geodynamic settings at plate boundaries show a much faster horizontal velocity with respect to the vertical motion (Figure

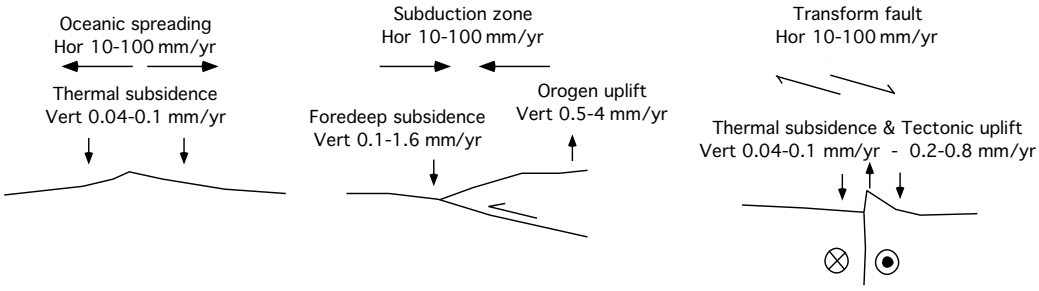

Figure 7.5: Present and past horizontal relative plate motions are about 10 – 100 times faster with respect to the vertical movements in all geodynamic settings.

7.5). Is this a trivial observation, or is it rather telling us something fundamental on the dynamics of plate tectonics? Does the slower vertical motion imply strain partitioning and passive role of plate boundaries?

Plate motions are driven either by coupled or uncoupled forces. A comparison between horizontal and vertical motions does not allow to state which plate tectonics driving mechanism prevails. However, the steady one or two order of magnitude faster horizontal over vertical motion could point for a stronger tangential component in plate tectonics than previously inferred.

Regardless the Rayleigh number that can be computed for the upper mantle convection, the ridges and the subduction zones alone activate some convection, because the asthenosphere uplifts along rifts, and the lithospheric mantle sinks with slabs. However, if ridges and subduction zones trigger convection, but are nevertheless still passive features, what moves plates? Whatever the mantle convection works, it cannot explain the lithosphere decoupling alone. Therefore the uncoupled forces, such as the tidal drag [*Scoppola et al.*, 2006], appear to dominate, but we cannot exclude that possibly more than one force, both coupled and uncoupled, energize plate motions.

Comparison between horizontal and vertical plate motions can be the starting point for plate dynamic discussions: which forces drive plate tectonics? In the next chapter a brief speculation about the possible mechanisms of tectonic processes is presented.

Chapter 8

Dynamic speculations

This brief chapter does not have the role to give answers, or numerical models of plate dynamics, but, on the basis of results previously presented, many questions arise concerning the connection between plate kinematics and related plate dynamic models. We tried to make the basic hypotheses of an alternative dynamics that would be useful to reproduce plate kinematics obtained in the reference frames proposed in this study.

8.1 Plate driving forces: how many?

The main forces acting on the lithosphere can be subdivided into coupled and uncoupled forces [*Carlson et al.*, 1983a,b; *Jurdy and Stefanick*, 1988]. Mantle drag and trench suction [e.g., *Bercovici*, 1998; *Conrad and Lithgow-Bertelloni*, 2003] need high coupling (higher viscosity) between the lithosphere and the asthenosphere to be more effective. The ridge push, the slab pull and the tidal drag should rather need low coupling (lower viscosity) to be efficient.

The kinematic observations give directions for preliminary dynamic considerations. All types of tectonic–geodynamic settings at plate boundaries show a much faster horizontal velocity with respect to the vertical motion. Is this onlt an observation, or is it rather showing something fundamental on the dynamics of plate tectonics? Does the slower vertical motion imply strain partitioning and passive role of plate boundaries?

The mechanisms driving plate motions, e.g., plates driven by “the boundary forces”, slab pull and ridge push [*Forsyth and Uyeda*, 1975], versus plates actively dragged by the asthenospheric flow [e.g., *Bokelmann*, 2002] seem not relevant to the preceding discussion of horizontal versus vertical motion rates, because the rates themselves do not

provide evidence for or against any particular mechanism. Either “active plates and passive asthenosphere” or “an active asthenospheric flow dragging passive plates” may be consistent with faster horizontal motions.

It can be argued that the horizontal movement of plates is accommodated by a diffuse strain. However, this discrepancy is intriguing, particularly along subduction zones and extensional margins. Along rift zones, subsidence is accommodated either by normal faulting or thermal cooling. The underlying mantle contemporaneously compensates the space that is liberated by the overlying lithosphere, contributing to rift flank uplift. Lateral pressure gradients caused by uplift have been proposed as effective tectonic forces in extensional settings both in rift (active rifting) and oceanic realms (ridge push) [*Forsyth and Uyeda*, 1975; *Bott and Kusznir*, 1979]. However, it has been noticed that no dramatic differences in vertical rates occur between rifting and drifting stages, whereas a dramatic increase in horizontal motion is observed. This observation suggests that, in extensional settings, vertical deformation is more a consequence of the horizontal movement of the plates (passive rifting) rather than its primary cause.

For subduction zones, comparing vertical and horizontal rates, less clear inferences can derived on plate dynamics. Slab pull is widely considered the engine of plate motions [e.g., *Anderson*, 2001; *Conrad and Lithgow-Bertelloni*, 2003; *Sabadini and Vermeersen*, 2004]. Most numerical models for vertical motions in subduction zones use this assumption, although the excess mass of subducted slabs predicted by slab pull models is greater than that predicted by geoid models [*Chase*, 1979].

Such models might be able to reproduce surface topography and subsidence rates of trenches [e.g., *Zhong and Gurnis*, 1992; *Giunchi et al.*, 1996; *Sabadini and Vermeersen*, 2004] and suggest that topography could be a dynamic feature depending on the balance between tectonic and buoyancy forces [*Melosh and Raefsky*, 1980; *Wdowinski*, 1992]. However, a sensitivity analysis of the effects of slab buoyancy showed that typical trench bathymetries are obtained with both positive and negative density anomalies of the slab [*Hassani et al.*, 1997].

According to this modeling, slab buoyancy controls overriding plate topography, but overriding plate topography is dramatically influenced by parameters not included in calculations, such as the accretional [*Karig and SharmanIII*, 1975] or erosional [*von Huene and Lallemand*, 1990] nature of the subduction, the amount of shortening and the depth of the decollement [*Woodward et al.*, 1989], the deformation partitioning between brittle and ductile levels and erosion [*Willett and Brandon*, 2002]. The negative buoyancy of slabs should determine the pull of plates, but it has been shown that the dip of the subduc-

tion zones is not correlated with the age and the thermal state of the down going plates [*Cruciani et al.*, 2005]. Moreover relative convergence rates at subduction zones do not correlate with age of oceanic lithosphere at the trench.

The slab pull has a number of further counterarguments, such as it is inferred on the assumption that the slab is heavier than the country mantle, but several uncertainties remain on the composition of both bodies at variable depth; The supposed pull of the slab is bigger than the strength of the lithosphere under extension, so how can it be transferred to the whole plate? Down–dip compression affects most of the slabs, all below 300 km [*Isacks and Molnar*, 1971], some of them even at shallower depth [e.g., *Frepoli et al.*, 1996]. The 700 km long W–Pacific slab, where only the upper 300 km show some potential down–dip extension seismicity should pull and carry the 10,000 km wide Pacific plate, 33 times bigger, winning the strong shear resistance at the plate base, and the opposing basal drag induced by the relative eastward mantle flow inferred from the hotspots migration; there are plates moving without any slab actively subducting in the direction of their absolute motion (e.g., Africa and Somalia plates).

Among the uncoupled forces, the ridge push is at least one order of magnitude lower than the slab pull [e.g., *Ranalli*, 1995]. However, the dissipation of energy by tidal friction is even larger (1.6×10^{19} J/yr) than the energy released by tectonic activity [1.3×10^{19} J/yr, *Denis et al.*, 2002]. The tidal drag can effectively move plates, only if very low viscosity intra-asthenospheric layers occur [*Scoppola et al.*, 2006]. In this case, tidal forces [*Bostrom*, 1971, 2000], combined with mantle convection, could trigger plate tectonics. Therefore, the viscosity of the upper layers of the asthenosphere plays a crucial role in controlling plate tectonics. Moving from the highest viscosity (10^{19-20} Pa s) to the lowest (10^{12-14} Pa s), the most likely mechanisms able to move plates are in order: the mantle drag, the trench suction, the slab pull, the ridge push and the tidal drag.

Relatively small forces can move a floating plate fast horizontally, because no work has to be done against gravity, whereas non-isostatic vertical motions require work to be done against gravity. However this can be true when at the base of the lithosphere there is a very low viscosity in the decoupling layer, i.e., the weaker low velocity zone in the upper asthenosphere. Increasing the asthenosphere viscosity, larger forces are required to decouple the lithosphere. On the other hand, if the lithosphere is not moved by lateral forces such as the slab pull, but rather passively dragged by the mantle, the higher viscosity will enable a better coupling, but then what is generating the decoupling of the lithosphere? Are there external tangential forces acting on the lithosphere?

There are lines of evidence that the lithosphere is partly decoupled from the mantle as

suggested for example by the hotspot tracks [*Gripp and Gordon*, 2002], the asthenosphere anisotropy [*Silver and Holt*, 2002] and sheared mantle xenoliths [*Kennedy et al.*, 2002]. Moreover, plate boundaries move relative to the mantle [e.g., *Garfunkel et al.*, 1986]. If so, where does the energy providing this torque come from? What is moving plates relative to the mantle? The lithosphere has a net rotation relative to the sub–asthenospheric mantle of 0.44 $^{\circ}\mathrm{Myr}^{-1}$ [*Gripp and Gordon*, 2002] or faster (e.g., this study, Chapter 3 and Chapter 4). "This westward" lithospheric motion with respect to the mantle has been attributed to either lateral variations in asthenosphere viscosity [*Ricard et al.*, 1991], or to the Earth's rotation [*Scoppola et al.*, 2006]. The westward drift [*Le Pichon*, 1968] is consistent with the asymmetry of subduction and rift zones worldwide along an undulated plate motion flow [*Doglioni et al.*, 2006a,b]. A number of authors [e.g., *Dickinson*, 1978; *Uyeda and Kanamori*, 1979; *Doglioni*, 1990] proposed a shear at the lithosphere base driven by mantle drag or relative mantle flow. The E–ward mantle flow (or the W–ward drift of the lithosphere) could be attributed to a rotational component and the consequent tidal drag [*Bostrom*, 1971; *Moore*, 1973; *Scoppola et al.*, 2006].

8.2 Astronomical forces and global polarity of plate motions

Could plates rather be driven by Earth's rotation and tidal drag [*Scoppola et al.*, 2006]? Are plates moved by a combination of the aforementioned mechanisms? Although a combination of all forces acting on the lithosphere is likely, the decoupling between lithosphere and mantle suggests that a torque acts on the lithosphere independently of the mantle drag. Slab pull and ridge push are candidates for generating this torque, but, unlike these boundary forces, the advantage of the Earth's rotation and related tidal drag is to be a volume force, acting simultaneously and tangentially on the whole plates.

Tidal drag maintains the lithosphere under a permanent high frequency vibration, polarized and sheared toward the "west". Earth's rotation and the resisting force exerted by the lag of the tidal bulge [*Bostrom*, 1971] can be efficient only if very low viscosity occurs at the lithosphere–asthenosphere transition [*Jordan*, 1974]. Growing evidence is emerging on the presence of an ultra-low viscosity layer at the very top of the asthenosphere [e.g., *Rychert et al.*, 2005], possibly related also to higher fluids concentration in the mantle. Lateral variations in the low–velocity layer could control the different velocity of plates. An advantage of an astronomical contributing force acting on the lithosphere could explain the homogeneous velocity of each plate, the decoupling at the lithosphere base, and the westerly polarized migration of plate boundaries, consistent with the geo-

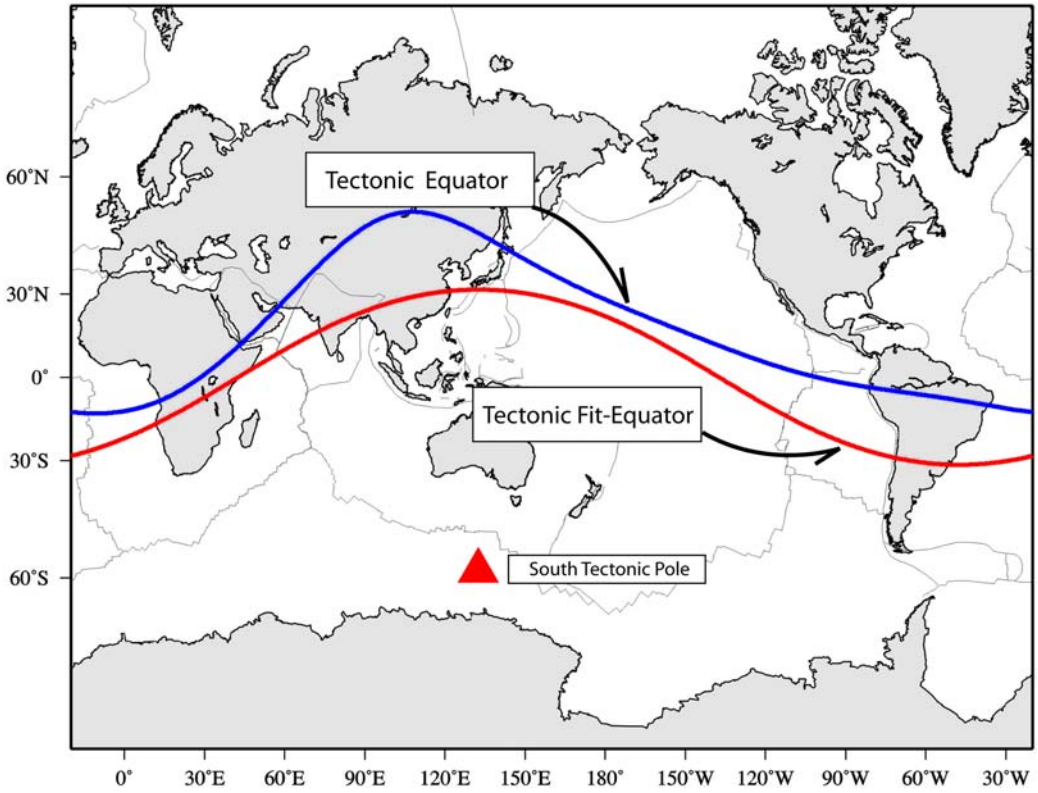

Figure 8.1: Great circle (tectonic–fit equator), that minimalises the distance from the tectonic equator, has a main tectonic pole located at -58.655 °N and 132.512 °E (red triangle).

logical asymmetries of subduction and rift zones as a function of the geographic polarity. Therefore a plausible model of plate dynamics could be a combination of convection triggered by the negative slab buoyancy, the shear induced by the tidal drag, and a transient bottom up uplift of the mantle along migrating ridges.

The tectonic equator, studied and defined in analytic way in the Chapter 2, is not a great circle. However, as a preliminary test, we generated the great circle that minimalises the distance from the tectonic equator, showing that the discrepancy is not so exaggerated (Figure 8.1). We named this approximate great circle the *tectonic fit–equator*, and we obtained this particular curve with the Generic Mapping Tools of *Wessel and Smith* [1995], by making use of the "fitcircle" function.

"fitcircle" reads longitude and latitude values from a standard input and these are converted to Cartesian three–vectors on the unit sphere. Then, the mean of the input positions, and the poles to the great circle which best fits the input positions are found. We

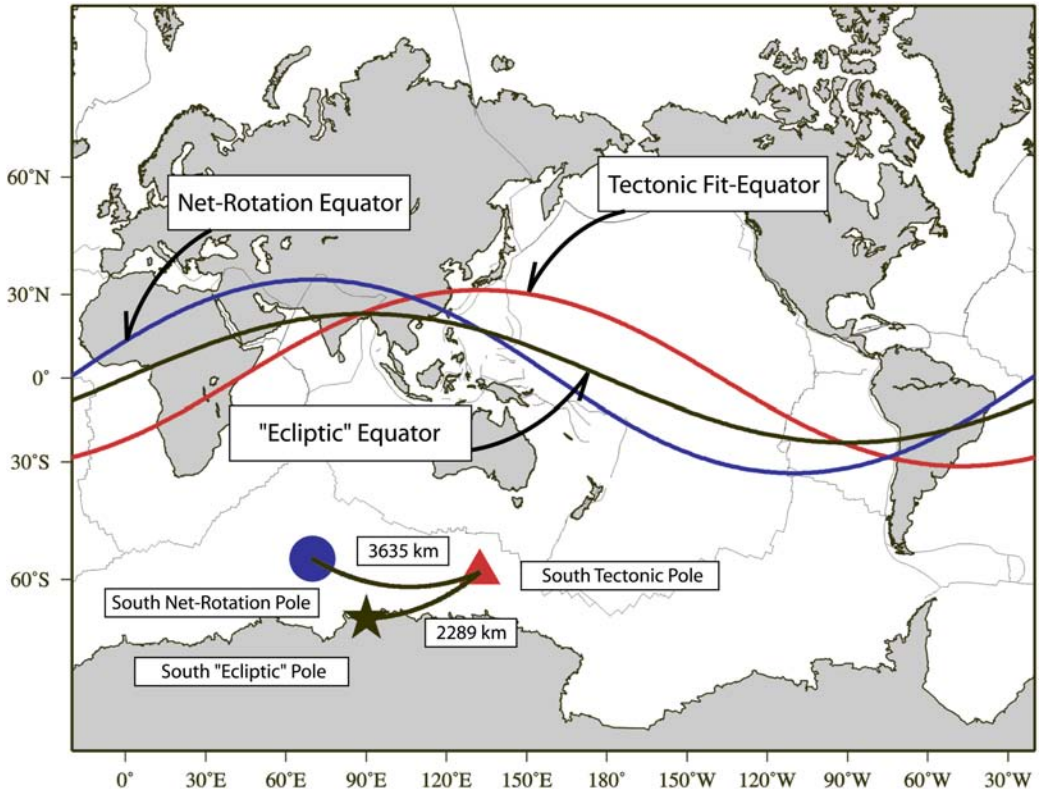

Figure 8.2: The inclination of the tectonic fit–equator (red line) is very close (31 degrees) to the net "westward" rotation great circle computed by *Gripp and Gordon* [2002] (blue line). Their main poles, respectively the red triangle and the blue circle, lie at distance of 3625 km. Adding the projection of the ecliptic plane on the Earth's surface (black line) shows a similar inclination (23 degrees) and the main pole (black star) of the ecliptic great circle lies 2289 km far form the main pole of the tectonic fit–equator.

defined an input file for the co–ordinates of the tectonic equator, using the equation 2.1, and we applied the "fitcircle" function using the solution that approximates the minimization of the sum of squares of cosines of angular distances, and creates a 3 by 3 matrix of sums of squares of components of the data vectors. The eigenvectors of this matrix give the mean and pole locations.

With these methods, we found that the great circle that minimizes the tectonic equator has a pole, here called the "south tectonic pole", located at -58.655 °N and 132.512 °E and the angle that the tectonic equator, and the related approximated great circle, is inclined about 31 degrees with respect to the geographic equator.

Comparing this result with the most qualified net-rotation great circle [*Gripp and*

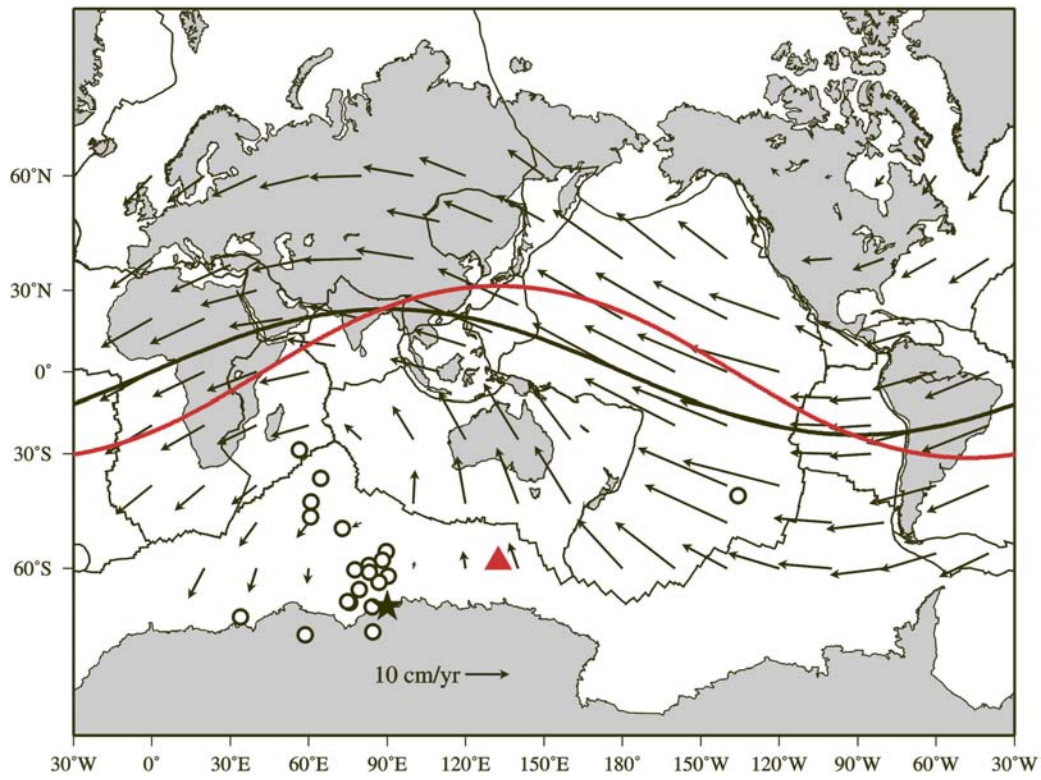

Figure 8.3: Current plate velocities relative to the shallow hotspot reference frame show that there is good agreement between the directions of global velocity vectors and the shape of the "ecliptic equator" (black great circle) and the fit–equator (red line). Moreover the rotation poles of plates lie at a mean latitude very close to the position of the south ecliptic pole (black star) not to far from the south tectonic pole (red triangle).

Gordon, 2002], that has the main pole located at -55.908 °N and 69.930 °E, we found that the distance between the two poles is 3635 km and the two great circles have, on large scale, a similar inclination (31 degrees) with respect to the geographical equator (Figure 8.2), but they differ on about 60 degrees of longitudes. Moreover, plotting the section of the ecliptic plane of the Earth's surface (Figure 8.2) results in that it has a similar shape with respect to the other great circles before mentioned. The main pole of the equator representing the ecliptic plane lies at -66.558 °N and 90.000 °E, far for the pole of the fit–equator about 2289 km. Moreover, the ecliptic plane could be interpreted as the main trajectory that global plate motions accomplish in the shallow hotspot reference frame (Figure 8.3). Most of the poles of rotation of plates, in the shallow hotspots lie close to the main pole of the ecliptic and tectonic fit–equator great circle (Figure 8.3).

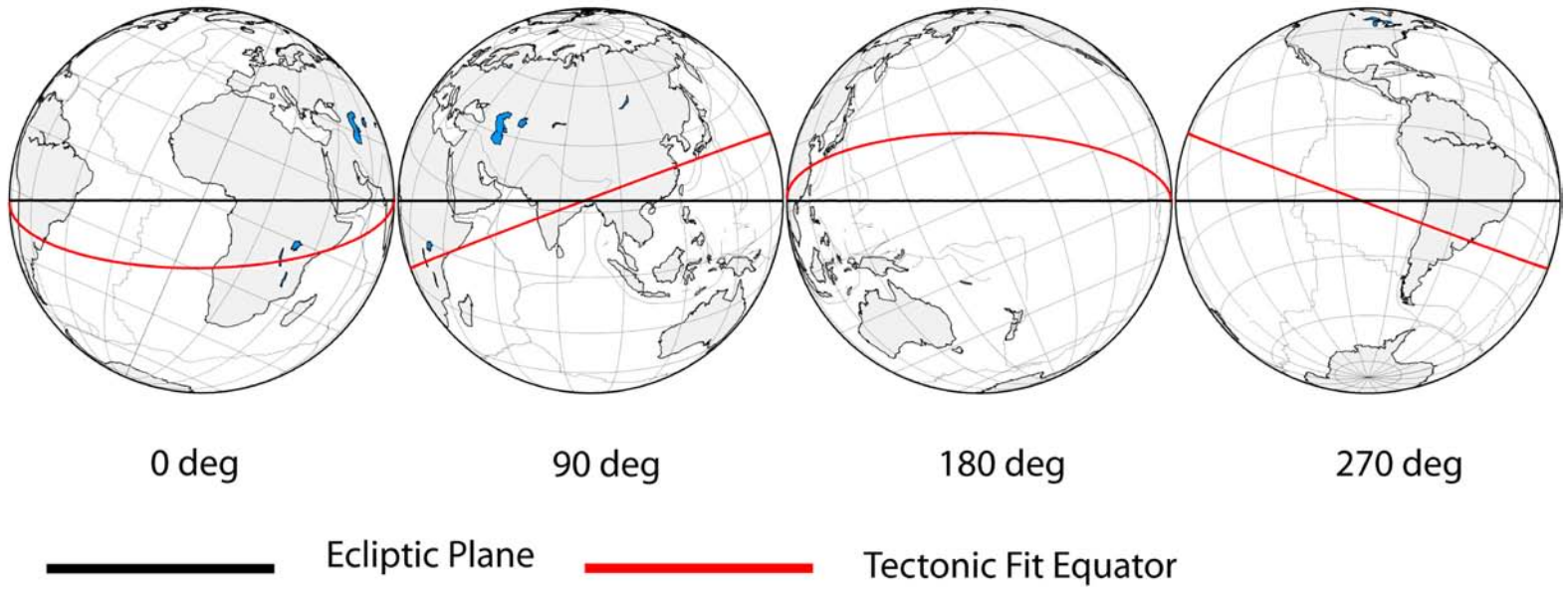

Figure 8.4: Comparison between the shape of the tectonic fit–equator (red great circle) and the revolution plane of the Earth, i.e. the ecliptic (black line), in a spherical projection, at four views, 0, 90, 180, 270 degrees. Comparing current plate velocities in the shallow hotspot reference frame, the angle formed by the great circles suggests a strong correlation between astronomical parameters and the global polarity of plate motions. In this Figure, the Earth rotation axis is tilted by 23 degrees, as a useful configuration to represent the ecliptic plane as a straight line.

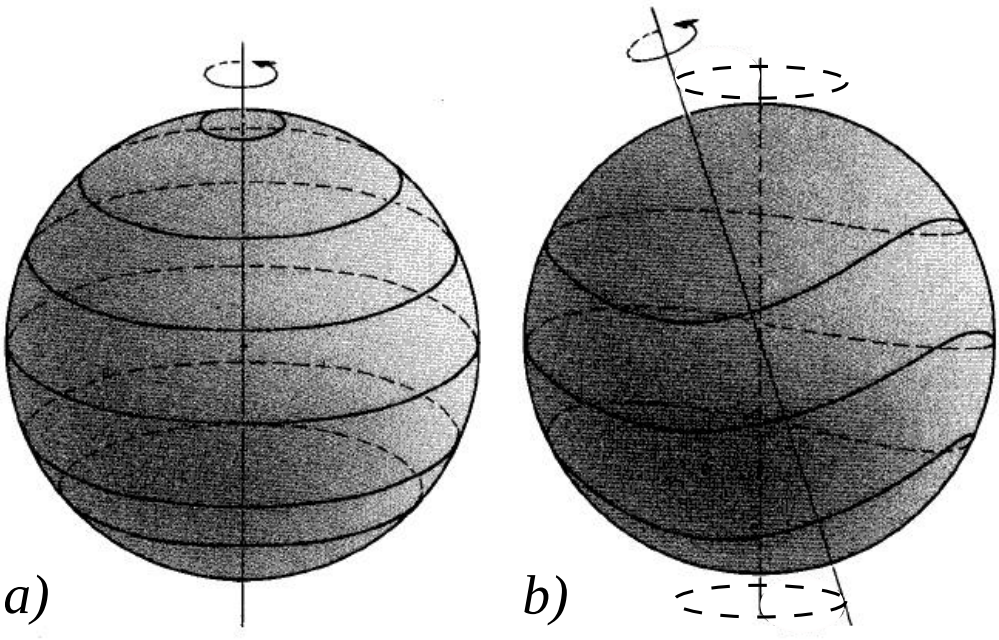

Figure 8.5: The Earth is not a perfect sphere rotating about its rotating axis (a), but is rather close to an ellipsoid of revolution characterized by wobble of the rotation axis (b). This could result in the undulations in rotational flow of the upper mantle. Figure from *Doglioni* [1990]

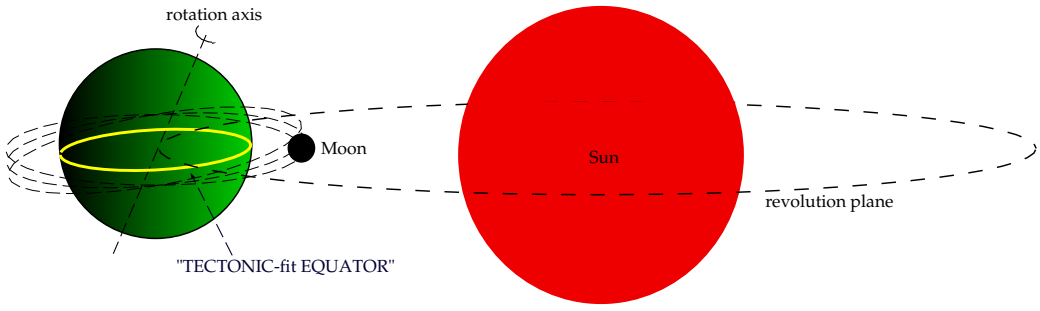

Figure 8.6: Cartoon, not to scale, showing how the main tectonic sinusoid (see Section 1.5) falls close to the ecliptic plane, and within the band of oscillation of the Moon's revolution, suggesting a rotational origin of the tectonic flow pattern.

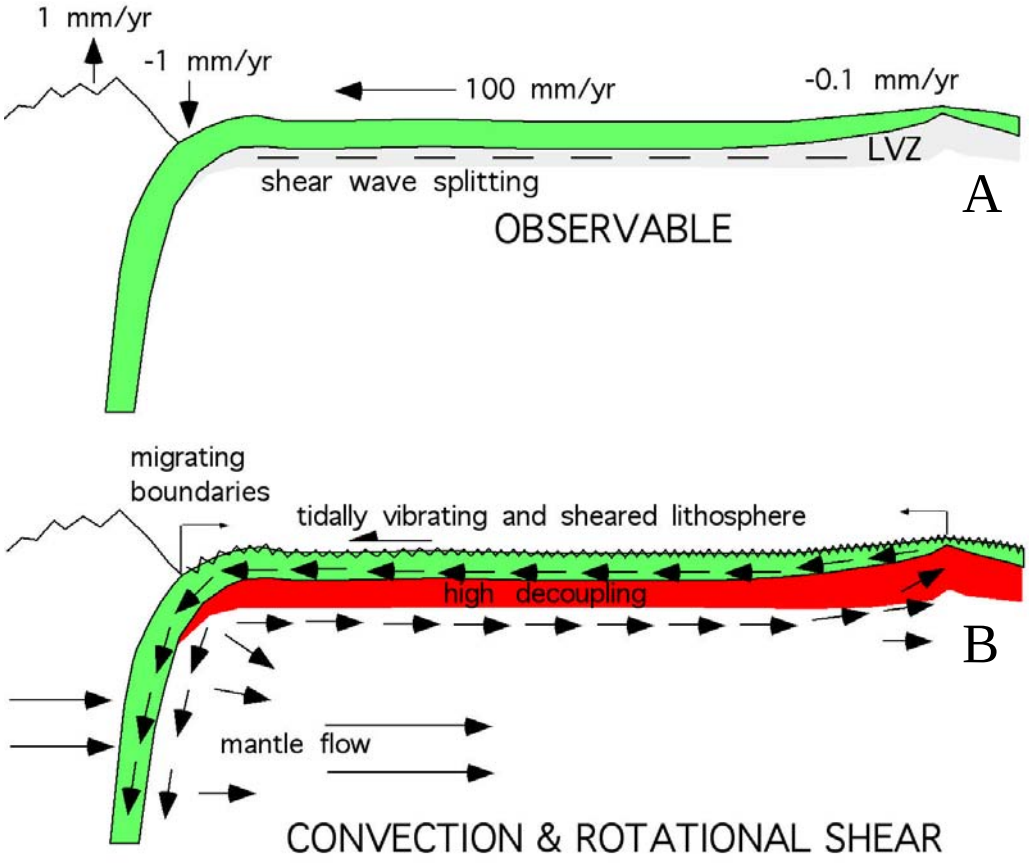

Figure 8.7: The surface observables (A) is compared with an alternative model of plate dynamics (B), where plate motion is induced basically by Earth rotational and tidal drag mechanisms and by a combination of classic mantle convection and boundary forces. LVZ means the Low Velocity Zone. See text for further explanations.

A comparison between the shapes of tectonic fit–equator and ecliptic equator is shown in Figure 8.4, suggesting a possible correlation between the astronomical parameters (as the wobble of the rotation axis) and the global polarity of plate motions. In fact, *Doglioni* [1990] related the motion of the Earth with the origin of plate tectonics and argued that, being the planet an imperfect spheroid characterized by wobble of the rotation axis, this could result in the undulations in rotational flow of the upper mantle (Figure 8.5). Moreover, the angle of the inclination of the tectonic fit–equator and the net–rotation great circle are close to the ecliptic plane (23 degrees) plus the band of oscillation of revolution orbit of the Moon (5 degrees), which is around 28 degrees (Figure 8.6). This would

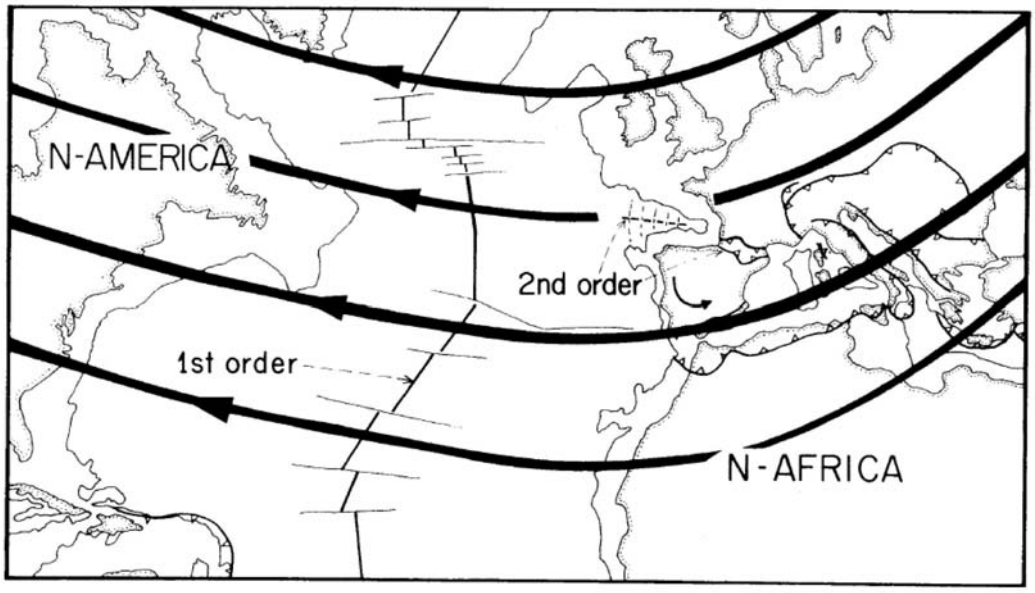

Figure 8.8: First–order and second–order tectonic structures. The Atlantic ridge, the Apennines and the Dinarides are first–order structures because they are developed perpendicularly with respect to the global flow lines. The rotation of the Iberia is a second–order local rotation (i.e. a sub–rotation), producing extension in the Bay of Biscay and shortening in the Pyrenees. This features are defined as second–order structures, because do not remain perpendicular to the lines of the global tectonic pattern. This could be related to the response of the anisotropic mantle to the astronomical control of plate tectonics. Figure modified after *Doglioni* [1990].

suggest an astronomical control on the tectonic equator and the global tectonic pattern [*Doglioni*, 1990], due to the Earth's rotation, the wobble of the rotation axis and tidal resisting force (Figure 8.7).

On top on these basic forces, the response of an anisotropic mantle, regarding the degree of coupling between lithospheric plates and the mantle itself, could reproduce the classic features of plate tectonics, as the rifting and subduction zones, and the sub–rotations of plates (Figure 8.8).

What drives the plates? The most direct evidence to answer this question is kinematics: the plate motions themselves. According to the absolute plate motions inferred in the no-net-rotation reference frame and the hotspot framework, two different dynamic hypotheses are still under discussion: i) plates actively drive themselves by subsidence and subduction of cooling lithosphere, and ii) they are passively carried by mantle convection.

On the contrary, plate kinematic models proposed in the shallow hotspot reference

frame, incorporating both geophysical and geodetic data, open a third possibility, plates are generally driven by an astronomical control, that could reproduce features of plate tectonic processes.

8.3 Concluding remarks

This chapter does not answer to the questions regarding causes of plate tectonics, but, on the base of results of plate kinematic models, could be the first step to discuss plate dynamic models and, most important, could give the first conditions to an alternative dynamics, controlling plate motions.

In accordance with the previous kinematic results, many processes could be involved in plate dynamics:

- the Earth's rotation, representing one of the possible engines of plate tectonics;
- the wobble of the Earth's axis, resulting in the undulations of trajectories of plates;
- the tidal drag, engendering the westward drift of the lithosphere;
- the mantle response, generating features of plate tectonics and the sub–rotations;
- plate boundary forces and mantle drag, supporting the aforementioned basic dynamic forces.

Could these processes reproduce observed plate kinematics? Are plates dragged horizontally by mantle convection [e.g. *Bercovici*, 1998]? Are they dragged and sheared at the base by a faster moving mantle [*Bokelmann*, 2002]? Are they rather pulled by slab pull forces [*Forsyth and Uyeda*, 1975; *Anderson*, 2001]? Could they be driven by Earth's rotation and tidal drag [*Scoppola et al.*, 2006]? We have not a final word, but plate kinematic models in the shallow hotspots could be the basic standard of comparison with results of different plate dynamics. Moreover, further studies on the composition, water content and viscosity of the asthenosphere might significantly contribute to these basic questions.

Conclusions and future directions

The research described in this dissertation provides a new point of view about plate kinematics and plate tectonic processes. We evaluated absolute plate motions with respect to different reference frames, in order to provide constraints for the understanding of lithospheric plate dynamics. The main purpose of this study concerned the application of consolidate plate kinematic techniques, and compelling geodynamic ties (e.g., the number of the reliable hotspots and the depth of their source), to verify an alternative hypothesis of plate tectonics: the westward drift of the lithosphere, preferentially occurring on well–defined trajectories. Indeed, a quantified plate kinematic model reaching this result has never been proposed, since this idea, supported by geological evidence, was presented in the early years of the last decade (see Chapter 1). This research could represent a first step to determine the basic rules for an alternative mechanism of plate tectonics. This entails that what we know about the physics of the Earth's surface could change, introducing alternative plate kinematic models.

We basically started from the assumption that geological and geophysical aspects of plate tectonics imply the existence of a global tectonic pattern, defining firstly its shape in an analytical form, as a comparison tool, and testing then previous plate kinematic models, constructed both by geophysical and space geodesy data. Results show that in these tied reference frames, absolute plate motions can effectively be directed toward the west, at different velocities, following an undulate mainstream (e.g., Chapter 2).

Moreover, due to the high number of constrains, we decided to cross these results, with others, obtained with different computations without any assumption about the global tectonic polarity, and we investigated absolute plate motions relative to the hotspots (Chapter 3). Growing lines of evidence suggest a shallow nature of the hotspots, located in the asthenosphere, and we found that changing the depth of the their source, it is possible to find a new framework in which the westward drift of the lithosphere become a real and well–quantified phenomenon. The unexpected result concerns the fact that

all the plates move toward the west following undulate trajectories, as predicted by the geological signature of rift and subduction zones. These important results, mostly representing the core of the dissertation, are validated incorporating relative plate motions both coming from geology and space geodesy. The recalibration in a hotspot framework of data acquired from geodetic techniques provides a better computation of absolute plate motions, due to the high level of accuracy, evaluating relative plate kinematics, and to the estimation of plate motion uncertainties. Furthermore, the inclusion in the model of additional plates results in a new database of plate boundaries in digital form, for a total of 20 plates, closing the Earth's surface with high precision (e.g., Chapter 4).

The introduction of the absolute sub–rotations contributes to refer plate kinematics to other possibilities (Chapter 5). Many of the processes, studied starting form kinematic observations, could be reinterpreted in different ways, taking into account further and contemporaneous displacements of plates. We have proposed the concepts and theoretical methods to separate plate sub–rotations from the main plate motions, and the two applications presented in absolute reference frames show that it is possible to reproduce the observables with an alternative kinematics. The sub–rotations could represent the second–order plate displacement, in the most general global polarity of plate motions, and could be useful to demonstrate further implications of mantle and lithosphere dynamics.

Global plate kinematics is reinforced by the study of the role of microplate motions in absolute reference frames (Chapter 6). We have investigated motions of plates and microplates relative to the hotspots, proposing a set of angular velocities for a total of 52 plates. Results show some kinematic and geometric patterns related to plate size. No continuum or gradational distribution of plate size exists, but they clearly partition into three groups: large, middle and small. Each subset of plates share some common characteristics. These similarities within groups include the nature of plate distribution over the Earth, location of rotation poles, size of the corresponding rotations, as well as the supposed fractal behavior. This breakdown by plate size may be a natural consequence of plate tectonics: large plates and most of the middle being moved predominantly by driving forces, and small ones clustering and involved at the interfaces.

Finally, comparisons between horizontal and vertical plate motions (Chapter 7), open a brief discussion about causes of plate tectonics (Chapter 8). In all geodynamic settings, present and past motions at major plate boundaries, have the horizontal component in average 10 to 100 times faster than the vertical one. This could indicate a passive role of plate boundaries with respect to far field forces determining the velocity of plates. The

decoupling between lithosphere and mantle suggests that a torque acts on the lithosphere independently from the mantle drag. Slab pull and tidal drag are the best candidates for generating this torque, but the Earth's rotation might have the primary role if the viscosity of the upper asthenosphere is sufficiently low.

The most direct evidence to investigate which forces drive plates is kinematics: the plate motions themselves. Since the first absolute plate motion models were formulated, geoscientists believe that plates actively drive themselves, or they are passively carried by mantle convection.

This study provides plate kinematic models which open a different dynamic possibility: plates are generally driven by an astronomical control, that, combined with mantle response and boundary forces, could reproduce features of plate tectonic processes.

Is this model true? We cannot answer to this questions now, but there are some pieces of geodynamic evidence suggesting that it could be possible. Future directions concern plate dynamic research, trying to quantify in an analytic way these concepts, combining results with plate kinematics. The plate kinematic models described in this dissertation could represent an alternative standard for comparisons with results of plate dynamic models. Every possible dynamics must be investigated to understand plate tectonics and the evolution of the Earth itself. A global point of view about kinematics and dynamics of the planet and its surface processes could be also useful to other branches of geophysics, to comprehend related phenomena occurring at plate boundaries, such as earthquakes and volcanism.

Appendix A

The equations of motion

Both in relative and absolute frameworks, equations of motion of a single plate point can be derived from cartesian components of the angular velocity [*Zhong*, 2001; *Stein and Wysession*, 2003]. Here, an alternative method to derive equations is presented, starting from basic principles of spherical trigonometry [*Ayres*, 1954; *Fowler*, 1990; *Butler*, 1992; *Turcotte and Schubert*, 2001].

A.1 Spherical trigonometry

Under the approximation of the Earth as a sphere, the spherical trigonometry can be often useful for geophysical applications to the geodynamics.

A sphere with a unit radius and center located in the origin of a three-axis reference frame is called a *trigonometric sphere*. A *great circle* is a generic circle, that is obtained by the intersection of a generic plane, passing through the center of the framework, with the trigonometric sphere. In particular, the three great circles that lie on the xy, xz, and yz planes are the *fundamental great circles*. Thus, a *small circle* is a generic circle obtained with the intersection between the trigonometric sphere and a generic plane not passing through the center of the reference frame.

On the spherical surface, the *spherical distance* between two points represents the length of the arc of a great circle, smaller than the half of the circumference. Moreover, the spherical surface obtained by the intersection of three great circles is called *spherical triangle* (Figure A.1). The points representing the intersection of the three arcs are called the *vertices* of the spherical triangle, whereas the *sides* of the spherical triangle, a, b and c are respectively the lengths of th arcs CB, AB and AC, and the *angles* α, β and γ are

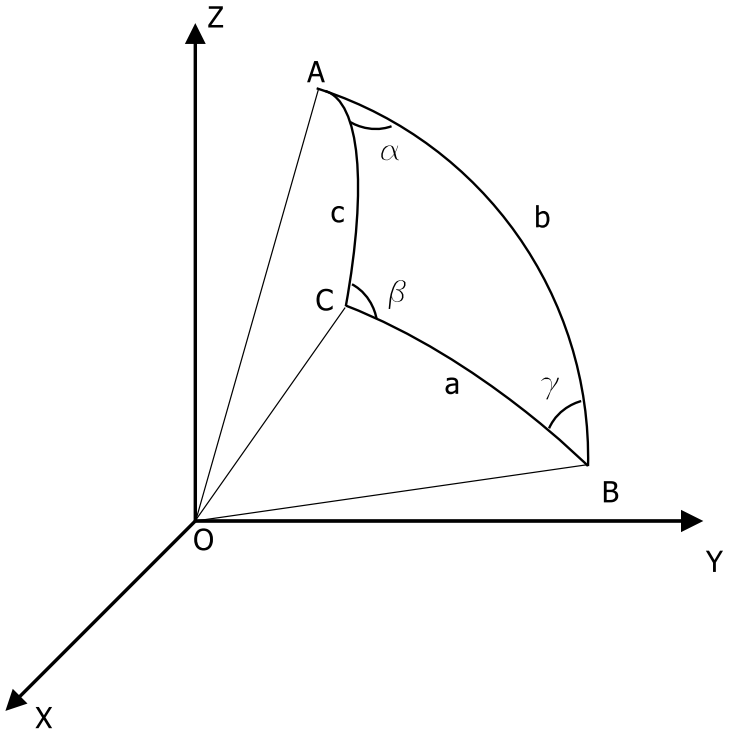

Figure A.1: The intersection of three great circles built a spherical triangle, with vertices A, B, C, sides a, b, c ed angles α, β, γ.

the angles among the arcs of the three great circles.

In a spherical triangle, three basic trigonometric rules are defined and they are reported as it follows:

$$\begin{cases} \cos a = \cos b \cos c + \sin b \sin c \cos \alpha \\ \cos b = \cos a \cos c + \sin a \sin c \cos \beta \\ \cos c = \cos a \cos b + \sin a \sin b \cos \gamma \end{cases} \tag{A.1}$$

that is defined as the *cosine theorem*;

$$\frac{\sin a}{\sin \alpha} = \frac{\sin b}{\sin \beta} = \frac{\sin c}{\sin \gamma} \tag{A.2}$$

that is called the *sine theorem*, and

$$\begin{cases} \cot a \sin b = \cos b \cos \gamma + \sin \gamma \cot \alpha \\ \cot b \sin c = \cos c \cos \alpha + \sin \alpha \cot \beta \\ \cot c \sin a = \cos a \cos \beta + \sin \beta \cot \gamma \\ \cot a \sin c = \cos c \cos \beta + \sin \beta \cot \alpha \\ \cot b \sin a = \cos a \cos \gamma + \sin \gamma \cot \beta \\ \cot c \sin b = \cos b \cos \alpha + \sin \alpha \cot \gamma \end{cases} \tag{A.3}$$

that represents the *cotangent theorem*.

Starting from these simple relations, it is possible to derive equations of motion for a single plate. Because a plate is considered rigid, its kinematics can be studied without any dynamical treatment [*Gordon*, 1995]. On a spherical Earth, two equations, respectively representing the South–North (transversal), and the East–West (longitudinal) components of the linear velocity of a plate point, characterize the one–rotation model.

A.2 Linear velocities of the one–rotation displacements

During plate motion, a plate rotates about an Euler pole (E), and a single plate point (Q) follows a circular trajectory, corresponding to a circle of the Euler pole (Figure A.2). The co–ordinates of E($\Theta^{(E)}, \Lambda^{(E)}$), respectively the latitude and the longitude of the Euler pole, are time–independent, because the pole is stated fixed, whereas the co–ordinates of the generic plate point Q($\theta(t), \lambda(t)$) are time–dependent, because the point changes its position instant by instant. Also the angle $\beta(t)$ is time–dependent, and changes its value at every instant (Figure A.2).

Choosing the North Pole (O) as the origin of the coordinates, in the spherical triangle OEQ, the length of the arc a = EQ, is an invariant relative to the time. To obtain linear velocity expressions of the equations of motion for a single plate point, the basic rules of spherical trigonometry has to be used with the colatitudes ϕ and longitudes λ of points involved in the computation. To avoid this constrain and for a direct use of the point co–ordinates, there will be utilized the latitudes θ instead of the colatitudes ϕ (Figure A.3), by making use of the following:

$$\phi = \frac{\pi}{2} - \theta \tag{A.4}$$

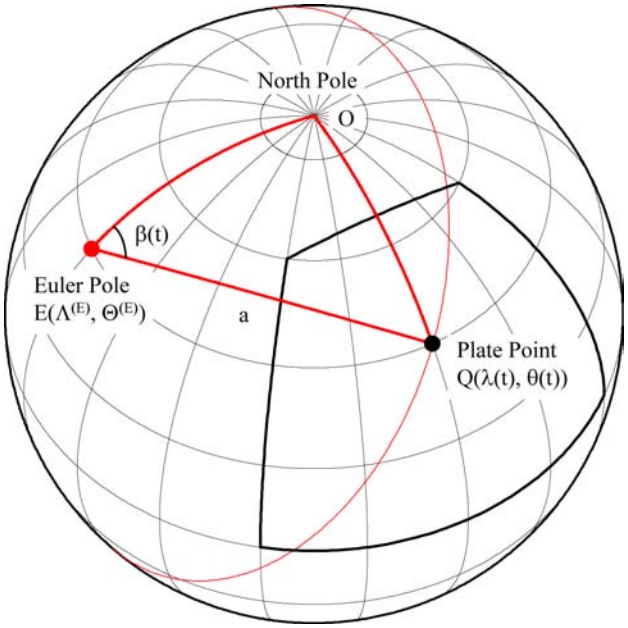

Figure A.2: For the simple plate motion, in the spherical triangle OEQ, Q is the generic plate point, E is the Euler pole, and the length $a = EQ$ is an invariant during plate motion. The thin line is the circular trajectory of the point Q an corresponds to a circle of the point E.

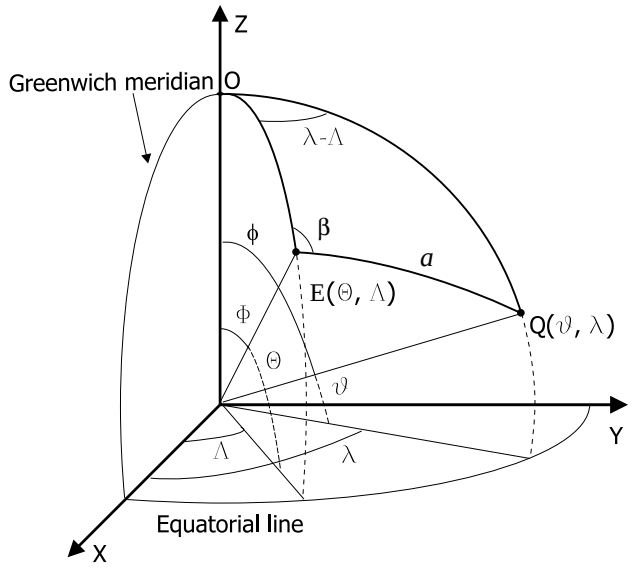

Figure A.3: Co–ordinates of the vertices of a spherical triangle: the points E and Q have respectively Θ e θ latitudes, but also Φ e ϕ colatitudes, and Λ e λ longitudes.

On a unit trigonometric sphere, and in the spherical triangle OEQ, using the Equation A.1, it can be written as it follows:

$$\cos\left(\frac{\pi}{2}-\theta(t)\right)=\cos a\cos\left(\frac{\pi}{2}-\Theta^{(E)}\right)+\sin a\sin\left(\frac{\pi}{2}-\Theta^{(E)}\right)\cos\beta(t) \tag{A.5}$$

whereas, referring to the Equation A.2, it is verified that:

$$\sin a=\frac{\sin\left(\lambda(t)-\Lambda^{(E)}\right)\sin\left(\frac{\pi}{2}-\theta(t)\right)}{\sin\beta(t)} \tag{A.6}$$

Differentiating the (A.5) relative to the time, substituting the (A.6) into the derivate of the (A.5), and simplifying, it becomes:

$$\frac{\mathrm{d}}{\mathrm{d}t}\theta(t)=\sin\left(\lambda(t)-\Lambda^{(E)}\right)\cos\Theta^{(E)}\frac{\mathrm{d}}{\mathrm{d}t}\beta(t) \tag{A.7}$$

Thus, considering the Earth as a sphere with a radius R=6371 km, being $V^{(\theta)}=\mathrm{R}\dfrac{\mathrm{d}}{\mathrm{d}t}\theta(t)$ and the angular velocity $\omega=\dfrac{\mathrm{d}}{\mathrm{d}t}\beta(t)$, the linear velocity of the transversal displacement of a single plate point is obtained in this form:

$$V^{(\theta)}=\mathrm{R}\omega\left[\sin\left(\lambda(t)-\Lambda^{(E)}\right)\cos\Theta^{(E)}\right] \tag{A.8}$$

To calculate, instead, the velocity of the longitudinal displacement, the following is considered:

$$\begin{aligned}\cos a=&\cos\left(\frac{\pi}{2}-\theta(t)\right)\cos\left(\frac{\pi}{2}-\Theta^{(E)}\right)+\\&+\sin\left(\frac{\pi}{2}-\theta(t)\right)\sin\left(\frac{\pi}{2}-\Theta^{(E)}\right)\cos\left(\lambda(t)-\Lambda^{(E)}\right)\end{aligned} \tag{A.9}$$

and differentiating the (A.9) relative to the time, substituting the (A.8) into the derivative of the (A.9) and simplifying, it becomes:

$$\frac{\mathrm{d}}{\mathrm{d}t}\lambda(t)=\left[\sin\Theta^{(E)}-\tan\theta(t)\cos\Theta^{(E)}\cos\left(\lambda(t)-\Lambda^{(E)}\right)\right]\frac{\mathrm{d}}{\mathrm{d}t}\beta(t) \tag{A.10}$$

Then, considering the Earth as a sphere with a radius R=6371 km, being $V^{(\lambda)} = \mathrm{R}\cos\theta(t)\dfrac{\mathrm{d}}{\mathrm{d}t}\lambda(t)$ and the angular velocity $\omega = \dfrac{\mathrm{d}}{\mathrm{d}t}\beta(t)$, the linear velocity of the longitudinal displacement of a single plate point is obtained in this form:

$$V^{(\lambda)} = \mathrm{R}\omega\ \cos\theta(t)\Big[\sin\Theta^{(E)} - \tan\theta(t)\cos\Theta^{(E)}\cos\Big(\lambda(t) - \Lambda^{(E)}\Big)\Big] \qquad \text{(A.11)}$$

Summarizing, two equations describe respectively the velocity of the transversal and of the longitudinal displacement of a single plate point about an Euler pole, in the form:

$$\begin{cases} V^{(\theta)} = \mathrm{R}\omega\ \Big[\ \sin\Big(\lambda(t) - \Lambda^{(E)}\Big)\cos\Theta^{(E)}\Big] \\ \\ V^{(\lambda)} = \mathrm{R}\omega\ \cos\theta(t)\Big[\sin\Theta^{(E)} - \tan\theta(t)\cos\Theta^{(E)}\cos\Big(\lambda(t) - \Lambda^{(E)}\Big)\Big] \end{cases} \qquad \text{(A.12)}$$

where $V^{(\theta)}$ and $V^{(\lambda)}$ depend only by the point co-ordinates, by the length of the angular velocity ω, and by the co–ordinates of the Euler pole. Because the motion of a plate is smooth and steady, $V^{(\theta)}$, $V^{(\lambda)}$ and ω are constant. Thus, the expressions to obtain the magnitude and the azimuth of the velocity of a geographical plate point are the following:

$$\begin{cases} V = \sqrt{\Big(V^{(\lambda)}\Big)^2 + \Big(V^{(\theta)}\Big)^2} \\ \\ \text{azimuth} = \Big(\dfrac{\pi}{2}\Big) - \tan^{-1}\Big(\dfrac{V^{(\theta)}}{V^{(\lambda)}}\Big) \end{cases} \qquad \text{(A.13)}$$

The second of the Equation A.13 ensures that zero is aligned with the true north to correspond to the geological convention of measuring direction of strike, [*Henderson*, 2001].

A.3 Linear velocities of the two-rotation displacements

Under the hypothesis of the sub-rotation (see Chapter 5), the motion of a plate is composed, i.e. a two–rotation motion. Two rotations are contemporaneously acting, and two angular velocities are needed to describe this composed motion,, one (ω_f) related to the first rotation and the other (ω_s) related to the sub-rotation. The two–rotation model here presented, represents an advance with respect to the one proposed by *Cuffaro* [2003], that

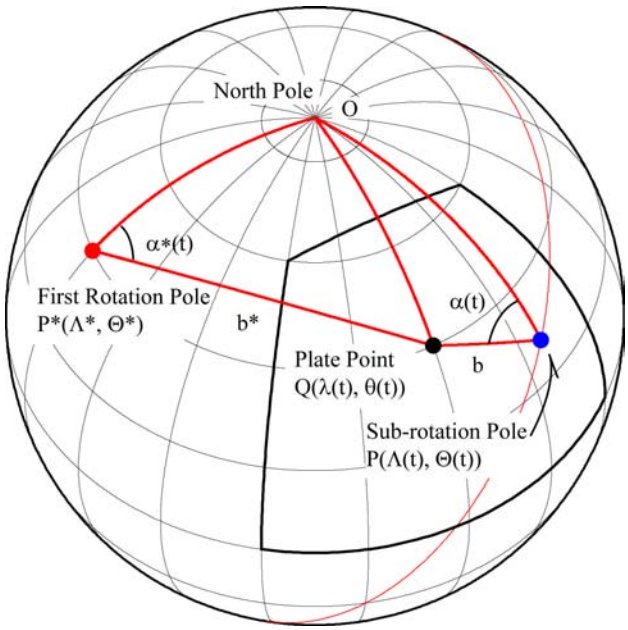

Figure A.4: When the motion is composed by a first rotation and the sub-rotation, there are two spherical triangles, $\mathrm{OP^*Q}$ and OPQ, and the lengths $\mathrm{b^*} = \mathrm{P^*Q}$ and $\mathrm{b} = \mathrm{PQ}$ are separately invariant. The length $\mathrm{b^*} = \mathrm{P^*Q}$ is not invariant during the motion. The only point that moves along the parallel of the first rotation pole is the sub-rotation pole.

was useful only in a particular case. When the two components of the two–rotation motion, e.g., the first rotation and the sub-rotation are separately studied, there are two spherical triangles, ($\mathrm{OP^*Q}$ and OPQ), (Figure A.4), and, as the simple motion, the lengths $\mathrm{b^*} = \mathrm{P^*Q}$ and $\mathrm{b} = \mathrm{PQ}$ are invariant at one instant of plate motion.

Considering first of all the first rotation, with the same procedure of the simple case, the equations of motion are the following:

$$\begin{cases} V_f^{(\theta)} = \mathrm{R}\omega_f \left[\sin\left(\lambda(t) - \Lambda^*\right) \cos\Theta^* \right] \\ \\ V_f^{(\lambda)} = \mathrm{R}\omega_f \cos\theta(t) \left[\sin\Theta^* - \tan\theta(t) \cos\Theta^* \cos\left(\lambda(t) - \Lambda^*\right) \right] \end{cases} \tag{A.14}$$

where (Θ^*, Λ^*) are respectively the latitude and the longitude of the first rotation pole, that are time-independent, $(\theta(t), \lambda(t))$ are the coordinates of the generic plate point, that are time-dependent and $\omega_f = \dfrac{\mathrm{d}}{\mathrm{d}t}\alpha^*(t)$ is the first rotation angular velocity.

Also considering the contemporaneous sub-rotation, it can be written as it follows:

$$\begin{cases} V_s^{(\theta)} = \mathrm{R}\omega_s \left[\sin\Big(\lambda(t) - \Lambda(t)\Big) \cos\Theta(t) \right] \\ \\ V_s^{(\lambda)} = \mathrm{R}\omega_s \cos\theta(t) \Big[\sin\Theta(t) - \tan\theta(t) \cos\Theta(t) \cos\Big(\lambda(t) - \Lambda(t)\Big) \Big] \end{cases} \tag{A.15}$$

where $(\Theta(t), \Lambda(t))$ are respectively the latitude and the longitude of the sub-rotation pole (time-dependent), $(\theta(t), \lambda(t))$ are the coordinates of the generic plate point, that are time-dependent and $\omega_s = \dfrac{\mathrm{d}}{\mathrm{d}t}\alpha(t)$ is the sub-rotation angular velocity.

Adding the two contemporaneous rotations, e.g. first rotation and sub–rotation, the expression of the coupled movements is ontained as it follows:

$$\begin{cases} V_c^{(\theta)} = V_f^{(\theta)} + V_s^{(\theta)} \\ \\ V_c^{(\lambda)} = V_f^{(\lambda)} + V_s^{(\lambda)} \end{cases} \tag{A.16}$$

where $V_c^{(\theta)}$ and $V_c^{(\lambda)}$ are respectively the instantaneous velocities of the transversal and longitudinal coupled displacement of a single plate point.

In this case, the expressions to obtain the magnitude and the azimuth of the velocity of a geographical plate point are the following:

$$\begin{cases} V = \sqrt{\Big(V_f^{(\lambda)} + V_s^{(\lambda)}\Big)^2 + \Big(V_f^{(\theta)} + V_s^{(\theta)}\Big)^2} \\ \\ \text{azimuth} = \Big(\frac{\pi}{2}\Big) - \tan^{-1}\left(\dfrac{V_f^{(\theta)} + V_s^{(\theta)}}{V_f^{(\lambda)} + V_s^{(\lambda)}}\right) \end{cases} \tag{A.17}$$

During the continuum of the time, every instantaneous composed linear velocity, defined by the equation (A.17), and related to a plate point, implies that the plate is moving on a cycloid trajectory, showing a different absolute kinematics with respect the one-rotation model.

Appendix B

Uncertainties and plate motions

The uncertainties of plate motions can be calculated both for present and past plate kinematics. Different methods are used in plate reconstructions [*Hellinger*, 1981; *Jurdy and Stefanick*, 1987; *Petronotis and Jurdy*, 1990; *Kirkwood et al.*, 1999; *Andrews et al.*, 2006] where simple additions of covariance matrices cannot be used. We basically focused the attention about errors of present–day plate angular velocities, and we used two computational methods, one concerning the error propagation function and the second regarding the error ellipse theory. The first was applied to compute uncertainties of linear velocities (see Chapter 5) of single plate points, whereas the second was used to estimate error ellipse of Euler vectors (see Chapter 4).

B.1 The error propagation function

Statistical errors of undirectly computed quantities can be obtained with the error propagation function [*Cametti and Biasio*, 1994; *Brandt*, 1999; *D'Agostini*, 2003]. If we have a dependent function Y, defined as:

$$Y = f(X_1, X_2, X_3, \ldots, X_n) \tag{B.1}$$

where the $X_1, \ldots, X_n$ are the independent variables, its statistical error σ_Y is obtained as following:

$$\sigma_Y = \sqrt{\sum_{k=1}^{n} \left(\frac{\partial Y}{\partial X_k} \right)^2 \sigma_k^2} \tag{B.2}$$

where σ_k is the standard deviation of the variable X_k. As an example of the application of the error propagation function, here we present methods to calculate the statistical errors of the Cartesian components of the generic plate angular velocity.

A generic plate, rotating with an angular velocity $\vec{\omega}$ about an Euler pole P(Θ, Λ), where Θ and Λ are the latitude and the longitude respectively, has Cartesian components of the rotation rate, defined as it follows:

$$\begin{aligned} \omega_x &= \omega \cos\Theta \cos\Lambda \\ \omega_y &= \omega \cos\Theta \sin\Lambda \\ \omega_z &= \omega \sin\Theta \end{aligned} \tag{B.3}$$

where the x-, y-, and z-directions are defined from the center of the Earth to (0°N, 0°E), (0°N, 90°E), and (90°N, 0°E) respectively. If variables Θ, Λ and ω have associated standard deviations σ_Θ, σ_Λ and σ_ω, the equation Equation B.2 can be used to compute uncertainties of the Cartesian components of the Equation B.3.

Considering for sake of simplicity the third of the (B.3), its standard deviation σ_{ω_z} corresponds to:

$$\sigma_{\omega_z} = \sqrt{\left(\frac{\partial \omega_z}{\partial \omega}\right)^2 \sigma_\omega^2 + \left(\frac{\partial \omega_z}{\partial \Theta}\right)^2 \sigma_\Theta^2} \tag{B.4}$$

and making the complete computation for this specific component of the rotation rate, we have:

$$\sigma_{\omega_z} = \sqrt{(\sin\Theta)^2 \sigma_\omega^2 + (\omega \cos\Theta)^2 \sigma_\Theta^2} \tag{B.5}$$

B.2 Estimating rotation rate uncertainties

Many authors have applied statistical error analysis to plate motions [*Stock and Molnar*, 1983; *Nishimura et al.*, 1984; *Chang*, 1987, 1988; *Chang et al.*, 1990] obtaining refined estimations of uncertainties of angular velocities. Here, to compute errors of the rotation rate and error ellipse, we basically followed multivariate error analisys [*Clifford*, 1973] and basic methods described in *Gripp* [1994]

Most of the plate kinematic models, both relative or absolute, generally give variance–covariance (or simply covariance) matrix of Cartesian components of plate angular velocities [*DeMets et al.*, 1990; *Sella et al.*, 2002; *Kreemer and Holt*, 2003].

Any change of reference frame, modifies elements of the variance–covariance matrix. As the rotation vectors can be added when there is a change of framework, since the two vectors have associated covariance matrices, also these matrices can be added and combined. Following methods proposed by *Chang et al.* [1990], we notice that, if we add two independent vectors $\vec{\omega}_1$ and $\vec{\omega}_2$, the covariance matrix describing the uncertainty of the resulting vector $\vec{\omega}_3 = \vec{\omega}_1 + \vec{\omega}_2$ is simply given by the sum of the covariance matrices:

$$\text{cov}(\vec{\omega}_1 + \vec{\omega}_2) = \text{cov}(\vec{\omega}_1) + \text{cov}(\vec{\omega}_2) \tag{B.6}$$

The covariance matrix in Cartesian components is defined as 3×3 symmetric matrix as following:

$$\text{C}_{\text{cart}} = \begin{pmatrix} \sigma_{xx} & \sigma_{xy} & \sigma_{xz} \\ \sigma_{xy} & \sigma_{yy} & \sigma_{yx} \\ \sigma_{xz} & \sigma_{yz} & \sigma_{zz} \end{pmatrix} \tag{B.7}$$

To obtain the error of the rotation rate, the matrix C_{cart} has to be transformed from Cartesian co–ordinates (x, y, z) into local co-ordinates (n, e, d), where the rotation rate vector is applied [*Gripp*, 1994]. The local down direction $\hat{\mathbf{d}}$ is anti–parallel to the angular velocity $\vec{\omega}$. The local north $\hat{\mathbf{n}}$ and the local east $\hat{\mathbf{e}}$ define a plane tangent to the Earth's surface at the pole of rotation.

To transform the covariance matrix C_{cart} into the local co–ordinates, we use the matrix P of the passage of co–ordinates proposed by *Cox and Hart* [1986], defined as it follows:

$$\text{P} = \begin{pmatrix} P_{nx} & P_{ny} & P_{nz} \\ P_{ex} & P_{ey} & P_{ez} \\ P_{dx} & P_{dy} & P_{dz} \end{pmatrix} \tag{B.8}$$

where, being Θ and Λ the latitude and the longitude of the rotation pole respectively, the

elements of P are defined as following:

$$\begin{array}{lll} P_{nx} = -\sin\Theta\cos\Lambda & P_{ny} = -\sin\Theta\sin\Lambda & P_{nz} = \cos\Theta \\ P_{ex} = -\sin\Lambda & P_{ey} = \cos\Lambda & P_{ez} = 0 \\ P_{dx} = -\cos\Theta\cos\Lambda & P_{dy} = -\cos\Theta\sin\Lambda & P_{dz} = -\sin\Theta \end{array} \tag{B.9}$$

After making the passage of co-ordinates with:

$$\mathrm{C_{loc}} = \mathrm{P}\,\mathrm{C_{cart}}\,\mathrm{P}^{-1} \tag{B.10}$$

the covariance matrix of the angular velocity ω in local co-ordinates (n, e, d), has the following form:

$$\mathrm{C_{loc}} = \begin{pmatrix} \sigma_{nn} & \sigma_{ne} & \sigma_{nd} \\ \sigma_{en} & \sigma_{ee} & \sigma_{ed} \\ \sigma_{dn} & \sigma_{de} & \sigma_{dd} \end{pmatrix} \tag{B.11}$$

Finally, the uncertainty σ_ω (1–D standard error at 68% confident limit) of the lenght ω of the rotation vector corresponds to:

$$\sigma_\omega = \sqrt{\sigma_{dd}} \tag{B.12}$$

B.3 Error ellipse of Euler poles

The first step to obtain the error ellipse of the rotation poles regards the 2×2 submatrix of the north and east components of the covariance matrix $\mathrm{C_{loc}}$ (B.11), defined as:

$$\mathrm{C_{sub}} = \begin{pmatrix} \sigma_{nn} & \sigma_{ne} \\ \sigma_{en} & \sigma_{ee} \end{pmatrix} \tag{B.13}$$

After finding the eigenvalues λ_1 and λ_2 ($\lambda_1 > \lambda_2$) and the eigenvectors $\hat{\mathbf{u}}_\mathbf{1}$ and $\hat{\mathbf{u}}_\mathbf{2}$ of the matrix C_{sub}, the convenient geometry to measure the angle σ_{max} and σ_{min}, corresponding to the semi–major and semi–minor axes of the error ellipse of the rotation pole is:

$$\begin{aligned} \sigma_{max} &= \tan^{-1}\left(\frac{2\lambda_1}{\omega^2}\right)^{\frac{1}{2}} \\ \sigma_{min} &= \tan^{-1}\left(\frac{2\lambda_2}{\omega^2}\right)^{\frac{1}{2}} \end{aligned} \tag{B.14}$$

where ω is the length of the angular velocity vector. The semi–major (σ_{max}) and the semi–minor (σ_{min}) axes calculated with the equation (B.14) characterize an error ellipse of the rotation pole at the 62.5% confidence level. An important consequence of the tangent function is that for estimating the 95% confidence ellipse, the standard errors must be multiplied by 1.73 before the tangent operation is performed, otherwise the 95% error ellipse will be overstimed [*Gripp*, 1994].

Finally, the azimuth ζ (clockwise of north) of the semi–major axis of the error ellipse can be calculated with:

$$\zeta = \tan^{-1}\left(\frac{u_{1_e}}{u_{1_n}}\right) \tag{B.15}$$

where u_{1_e} and u_{1_n} are the east and north component respectively of the semi–major axis.

All these methods were first tested to reproduce results of many plate kinematic models, as the NUVEL–1 [*DeMets et al.*, 1990], the HS3-NUVEL1A [*Gripp and Gordon*, 2002] and the REVEL [*Sella et al.*, 2002], then were applied to the results of the Chapter 4.

List of Figures

List of Tables

References

Altamimi, Z., P. Sillard, and C. Boucher (2002), ITRF2000: a new release of the international terrestrial reference frame for Earth Sciences applications, *J. Geophys. Res.*, *107*, doi:10.1029/2001JB000561.

Altamimi, Z., P. Sillard, and C. Boucher (2003), The impact of the no-net-rotation condition on ITRF2000, *Geophys. Res. Lett.*, *30*, doi:10.1029/2002GL016279.

Anderson, D. L. (1989), *Theory of the Earth*, Blackwell Scientific Publications.

Anderson, D. L. (2000), Thermal state of the upper mantle; no role for mantle plumes, *Geophys. Res. Lett.*, *22*, 3623–3626.

Anderson, D. L. (2001), Topside tectonics, *Science*, *293*, 2016–2018.

Anderson, D. L., and K. A. Schramm (2005), Global hotspot maps, in *Plates, Plumes and Paradigms*, edited by G. R. Foulger, J. H. Natland, D. C. Presnall, and D. L. Anderson, Geol. Soc. Am. Spec. Publ.

Andrews, D. L., R. G. Gordon, and B. C. Horner-Johnson (2006), Uncertainties in plate reconstructions relative to the hotspots; Pacific–hotspot rotations and uncertainties for the past 68 million years, *Geophys. J. Int.*, *166*, 939–951.

Argus, D. F., and R. G. Gordon (1990), Pacific-North American plate motion from very long baseline interferometry compared with motion inferred from magnetic anomalies, transform faults, and earthquake slip vectors, *J. Geophys. Res.*, *95*, 315–324.

Argus, D. F., and R. G. Gordon (1991), No-net-rotation model of current plate velocities incorporating plate motion model NUVEL-1, *Geophys. Res. Lett.*, *18*, 2039–2042.

Argus, D. F., and R. S. Gross (2004), An estimate of motion between the spin axis and the hotspots over the past century, *Geophys. Res. Lett.*, *31*, doi:10.1029/2004GL019657.

Argus, D. F., and M. B. Heflin (1995), Pate motion and crustal deformation estimated with geodetic data from Global Positionig System, *Geophys. Res. Lett.*, *22*, 1973–1976.

Ayres, F. (1954), *Trigonometry*, Schaum Publications Company, New York.

Baldwin, S. L., B. D. Monteleone, L. E. Webb, P. G. Fitzgerald, M. Grove, and E. J. Hill (2004), Pliocene eclogite exhumation at plate tectonic rates in eastern Papua New Guinea, *Nature*, *431*, 263–267.

Barker, P. F., and L. A. Lawver (1988), South American–Antarctic plate motion over the past 50 myr, and the evolution of the South American–Antarctic ridge, *Geophy. J.*, *94*, 377–386.

Barruol, G., and M. Granet (2002), A Tertiary asthenospheric flow beneath the southern French Massif Central indicated by upper mantle seismic anisotropy and related to the west Mediterranean extension, *Earth Planet. Sci. Lett.*, *2002*, 31–47.

Bercovici, D. (1998), Generation of plate tectonics from lithosphere-mantle flow and void-volatile self-lubrication, *Earth Planet. Sci. Lett.*, *154*, 139–151.

Bergh, H. W., and I. O. Norton (1976), Prince Edward fracture zone and the evolution of the Mozambique basin, *J. Geophys. Res.*, *81*, 5221–5239.

Bernet, M., M. Zattin, J. I. Garver, M. T. Brandon, and J. A. Vance (2001), Steady-state exhumation of the European Alps, *Geology*, *29*, 35–38.

Berryman, K. R. (1993), Distribution, age, and deformation of Late Pleistocene marine terraces at Mahia Peninsula, Hikurangi Subduction margin, New Zealand, *Tectonics*, *12*, 1365–1379.

Bird, P. (2003), An updated digital model of plate boundaries, *Geochem. Geophys. Geosyst.*, *4*, doi:10.1029/2001GC000252.

Bokelmann, G. H. R. (2002), Which forces drive North America?, *Geology*, *30*, 1027–1030.

Bokelmann, G. H. R., and P. G. Silver (2000), Mantle variation within the Canadian Shield: Travel times from the portable broadband Archean–Proterozoic Transect 1989, *J. Geophys. Res*, *105*, doi:10.1029/1999JB900387.

Bonatti, E. (1978), Vertical tectonism in oceanic fracture zones, *Earth Planet. Sci. Lett.*, *37*, 369–379.

Bonatti, E. (1990), Not so hot “hot spots”in the oceanic mantle, *Science*, *250*, 107–110.

Bonatti, E., and K. Crane (1984), Oceanic fracture zones, *Sci. Am.*, *250*, 36–47.

Bonatti, E., M. Ligi, D. Brunelli, A. Cipriani, P. Fabretti, V. Ferrante, L. Gasperini, and L. Ottolini (2003), Mantle thermal pulses below the mid-atlantic ridge and temporal variations in the formation of oceanic lithosphere, *Nature*, *423*, 499–505.

Bostrom, R. C. (1971), Westward displacement of the lithosphere, *Nature*, *234*, 536–538.

Bostrom, R. C. (2000), *Tectonic Consequences of the Earth’s Rotation*, Oxford University Press.

Bott, M. H. P., and N. J. Kusznir (1979), Stress distribution associated with compensated plateau uplift structures with application to the continental splitting mechanism, *Geophys. J. R. astr. Soc.*, *56*, 451–459.

Boucher, C., Z. Altamimi, and P. Sillard (1999), The 1997 International Terrestrial Reference Frame (ITRF–97), *IERS Tech. Note*, *27*, Obs. de Paris, Paris.

Brandt, S. (1999), *Data Analysis: Statistical and Computational Methods for Scientists and Engineers*, 273 pp., Springer-Verlag, New York.

Braun, J., and C. Beaumont (1989), A physical explanation of the relation between flank upliftsand the breakup unconformity at rifted continental margins, *Geology*, *17*, 760–764.

Bullard, E. C., J. E. Everett, and A. G. Smith (1965), Fit of continents around the Atlantic, in *A Symposium on Continental Drift*, edited by P. M. S. Blackett, E. C. Bullard, and S. K. Runcorn, Phil. Trans, Roy. Soc. London, Ser. A, v. 258.

Butler, R. F. (1992), *Paleomagnetism: Magnetic Domains to Geologic Terranes*, 319 pp., Blackwell Scientific Publications.

Calcagnile, G., and G. Panza (1978), Crust and upper mantle structure under the Baltic shield and Barents sea from the dispersion of Rayleigh waves, *Tectonophysics*, *47*, 59–71.

Cametti, C., and A. D. Biasio (1994), *Introduzione all'elaborazione dei dati sperimentali*, CISU, Centro d' Informazione e Stampa Universitaria.

Cande, S. C., and D. V. Kent (1995), Revised calibration of the geomagnetic time scale for the Late Cretaceous and Cenozoic, *J. Geophys. Res.*, *100*, 6093–6095.

Carlson, R. L., T. W. C. Hilde, and S. Uyeda (1983a), The driving mechanism of plate tectonics; relation to age of the lithosphere at trenches, *Geophys. Res. Lett.*, *10*, 297–300.

Carlson, R. L., T. W. C. Hilde, and S. Uyeda (1983b), Correction to the "The driving mechanism of plate tectonics; relation to age of the lithosphere at trenches", *Geophys. Res. Lett.*, *10*, 987.

Cazenave, A., J. J. Valette, and C. Boucher (1992), Positioning results with DORIS on SPOT-2 after first year of mission, *J. Geophys. Res.*, *97*, 7109–7119.

Cazenave, A., P. Gegout, L. Soudarin, K. Dominh, F. Barlier, P. Exertier, and Y. Boudon (1993), Geodetic results from Lageos 1 and DORIS satellite data, in *Contributions of Space Geodesy and Geodynamics, Crustal Dynamics*, edited by D. E. Smith and D. L. Turcotte, Geodyn. Series, AGU, Washington, D. C.

Chamot-Rooke, N., and X. Le Pichon (1999), GPS determined eastward Sundaland motion with respect to Eurasia confirmed by earthquakes slip vectors at Sunda and Philippine trenches, *Earth Planet. Sci. Lett.*, *173*, 439–455.

Chang, T. (1987), On the statistical properties of estimated rotations, *J. Geophys. Res.*, *92*, 6319–6329.

Chang, T. (1988), Estimating the relative rotation of two tectonic plates from boundary crossing, *J. Amer. Statistical Ass.*, *83*, 1178–1183.

Chang, T., J. Stock, and P. Molnar (1990), The rotation group in plate tectonics and the representation of uncertainties of plate reconstructions, *Geophys. J. Int.*, *101*, 649–661.

Chapman, M. E., and S. C. Solomon (1976), North American–Eurasian plate boundary in northeast Asia, *J. Geophys. Res.*, *81*, 921–930.

Chase, C. G. (1972), The n-plate problem of plate tectonics, *Geophys. J. R. astr. Soc.*, *29*, 117–122.

Chase, C. G. (1978), Plate kinematic: the America, East Africa and the rest of the world, *Earth Planet. Sci. Lett.*, *37*, 355–368.

Chase, C. G. (1979), Subduction, the geoid, and lower mantle convection, *Nature*, *282*, 464–468.

Choy, G. L., and J. W. Dewey (1988), Rupture process of an extended earthquake sequence: Teleseismic analysis of the Chilean earthquake of March 3, 1985, *J. Geophys. Res.*, *93*, 1103–1118.

Chu, D., and R. G. Gordon (1999), Evidence for motion between Nubia and Somalia along the Southwest Indian ridge, *Nature*, *398*, 64–67.

Clark, T. A., D. Gordon, W. E. Himwich, C. Ma, A. Mallama, and J. W. Ryan (1987), Determination of relative site motions in the western United States using Mark III very long baseline radio interferometry, *J. Geophys. Res.*, *92*, 12,741–12,750.

Clifford, A. A. (1973), *Multivariate error analysis: a handbook of error propagation and calculation in many-parameter system*, 112 pp., Wiley, New York.

Conder, J. A., and W. Forsyth (2000), Do the 1998 Antarctic plate earthquake and its aftershocks delineate a plate boundary?, *Geophys. Res. Lett.*, *27*, 2309–2312.

Conrad, C. P., and C. Lithgow-Bertelloni (2003), How mantle slabs drive plate tectonics, *Science*, *298*, 207–209.

Cook, D. B., K. Fujita, and C. A. McMullen (1986), Present–day plate interactions in northeast Asia, North America, Eurasian, and Okhotsk plates, *J. Geodyn.*, *6*, 33–51.

Cox, A., and R. B. Hart (1986), *Plate tectonics. How it works*, Blackwell Scientific Publications.

Crespi, M., M. Cuffaro, C. Doglioni, F. Giannone, and F. Riguzzi (2007), Space geodesy validation of the global lithospheric flow, *Geophys. J. Int.*, *168*, 491–506.

Cretaux, J. F., L. Soudarin, A. Cazenave, and F. Bouille (1998), Present–day tectonic plate motions and crustal deformations from the DORIS space system, *J. Geophys. Res.*, *103*, 30,167–30,181.

Cronin, V. S. (1987), Cycloid kinematics of relative plate motion, *Geology*, *15*, 1006–1009.

Cronin, V. S. (1988), Reply to comment on “Cycloid kinematics of relative plate motion”, *Geology*, *16*, 473–474.

Cronin, V. S. (1991), The cycloid relative motion and the kinematics of transform faulting, *Tectonophysics*, *187*, 215–249.

Cruciani, C., E. Carminati, and C. Doglioni (2005), Slab dip vs. lithosphere age: No direct function, *Earth Planet. Sci. Lett.*, *238*, 298–310.

Cuffaro, M. (2003), Plate kinematics and application to the North America, *Undergraduate Thesis*, Department of Physics, University of Rome La Sapienza, Rome, Italy, in italian.

Cuffaro, M., and C. Doglioni (2007), Global kinematics in the deep vs shallow hotspot reference frames, in *The Origins of Melting Anomalies: Plumes, Plates, and Planetary Processes*, edited by G. R. Foulger and D. M. Jurdy, Geol. Soc. Am. Sp. Paper, in press.

Cuffaro, M., and D. M. Jurdy (2006), Microplate motions in the hotspot reference frame, *Terra Nova*, *18*, 276–281.

Cuffaro, M., M. Caputo, and C. Doglioni (2004), On the sub–rotation of a plate, *J. Virtual Explorer*, *14*, 1–15, Electronic Edition, ISSN 1441-8142.

Cuffaro, M., E. Carminati, and C. Doglioni (2006), Horizontal versus vertical plate motions, *eEarth Discussion*, *1*, 63–80.

Dadson et al. (2003), Links between erosion, runoff variability and seismicity in the taiwan orogen, *Nature*, *426*, 648–651.

D’Agostini, G. (2003), Probabilità e incertezza di misura, Department of Physics, University of Rome La Sapienza, Rome, Italy, in italian.

Dalrymple, G. B., M. A. Lanphere, and D. A. Clauge (1980), Conventional and $^{40}\mathrm{Ar}$–$^{39}\mathrm{Ar}$ and K–Ar ages of volcanic rocks from Ojin (site 430), Nintoku (site 432), and Suiko (site 423) seamounts and the chronology of volcanic propagation along the Hawaiian–Empeor chain, *Init. Rep. Deep Sea Drill Proj.*, *55*, 659–676.

Davis, D. M., and S. C. Solomon (1981), Variations of the velocities of the major plates since Late Cretaceous, *Tectonophysics*, *74*, 180–208.

DeMets, C. (1995), A reappraisal of seafloor spreading lineations in the Gulf of California: Implications for the transfer of Baja California to the Pacific plate and estimates of Pacific–North American motion, *Geophys. Res. Lett.*, *22*, 3545–3548.

DeMets, C. (2001), A new estimate for present–day Cocos–Caribbean plate motion: Implications for slip along the Central American volcanic arc, *Geophys. Res. Lett.*, *28*, 4043–4046.

DeMets, C., and D. Wilson (1997), Relative motions of the Pacific, Rivera, North American, and Cocos plates since 0.78 Ma, *J. Geophys. Res.*, *102*, 2789–2806.

DeMets, C., R. G. Gordon, D. F. Argus, and S. Stein (1990), Current plate motions, *Geophys. J. Int.*, *101*, 425–478.

DeMets, C., R. G. Gordon, D. F. Argus, and S. Stein (1994), Effect of recent revisions to the geomagnetic reversal time scale on estimates of current plate motions, *Geophys. Res. Lett.*, *21*, 2121–2194.

DeMets, C., R. G. Gordon, and J. Royer (2005), Motion between the Indian, Capricorn and Somalian plates since 20 Ma: Implications for the timing and magnitude of distributed lithospheric deformation in the equatorial Indian ocean, *Geophys. J. Int.*, *161*, 445–468.

Denis, C., A. A. Schreider, P. Varga, and J. Zavoti (2002), Despinning of the Earth rotation in the geological past and geomagnetic paleointensities, *J. Geodyn.*, *34*, 667–685.

Dermanis, A. (2001), Global reference frames: Connecting observation to theory and geodesy to geophysics, IAG Scientific Assembly.

Dermanis, A. (2002), The rank deficiency in estimation theory and the definition of reference frames, proceedings of V Hotine-Marussi Symposium on Mathematical Geodesy, F. Sanso‘ Editor, IAG Symposia, vol. 127, 145-156, Springer.

Dickinson, W. R. (1978), Plate tectonic evolution of North Pacific rim, *J. Phys. Earth*, *26: Suppl*, S1–S19.

Dixon, T. H. (1993), GPS measurement of strain accumulation across the middle America trench and relative motion of the Cocos and Caribbean plates, *Geophys. Res. Lett.*, *20*, 2167–2179.

Dixon, T. H., and A. Mao (1997), A GPS estimate of relative motion between North and South America, *Geophys. Res. Lett.*, *24*, 535–538.

Dixon, T. H., G. Gonzalez, S. M. Lichten, D. M. Tralli, G. Ness, and P. Dauphin (1991), A preliminary determination of Pacific–North America relative motion in the southern Gulf of California using the Global Positioning System, *Geophys. Res. Lett.*, *18*, 861–864.

Dixon, T. H., M. Miller, F. Farina, H. Wang, and D. Johnson (2000), Present–day motion of the Sierra Nevada block, and some tectonic implications for the Basin and Range province, North American Cordillera, *Tectonics*, *19*, 1–24.

Doglioni, C. (1990), The global tectonic pattern, *J. Geodyn.*, *12*, 21–38.

Doglioni, C. (1991), Una interpretazione della tettonica globale, *Le Scienze*, *270*, 32–42.

Doglioni, C. (1993), Geological evidence for a global tectonic polarity, *J. Geol. Soc., London*, *150*, 991–1002.

Doglioni, C. (1994), Foredeeps versus subduction zones, *Geology*, *22*, 271–274.

Doglioni, C. (1995), Geological remarks on the relationships between extension and convergent geodynamic settings, *Tectonophysics.*, *252*, 253–267.

Doglioni, C., P. Harabaglia, S. Merlini, F. Mongelli, A. Peccerillo, and C. Piromallo (1999), Orogens and slabs vs their direction of subduction, *Earth Sciences Reviews*, *45*, 167–208.

Doglioni, C., S. Agostini, M. Crespi, F. Innocenti, P. Manetti, F. Riguzzi, and Y. Savasçin (2002), On the extension in western Anatolia and the Aegean Sea, *J. Virt. Expl.*, *7*, 167–181.

Doglioni, C., E. Carminati, and E. Bonatti (2003), Rift asymmetry and continental uplift, *Tectonics*, *22*, doi:10.1029/2002TC001459.

Doglioni, C., D. Green, and F. Mongelli (2005), On the shallow origin of hotspots and the westward drift of the lithosphere, in *Plates, Plumes and Paradigms*, edited by G. R. Foulger, J. H. Natland, D. C. Presnall, and D. L. Anderson, Geol. Soc. Am. Spec. Publ.

Doglioni, C., E. Carminati, and M. Cuffaro (2006a), Simple kinematics of subduction zones, *Int. Geol. Rev.*, *48*, 479–493.

Doglioni, C., M. Cuffaro, and E. Carminati (2006b), What moves plates?, *Boll. Geof. Teor. App.*, *47*, 227–247.

Drewes, H., and B. Meisel (2003), An actual plate motion and deformation model as a kinematic terrestrial reference system, *Geotechnologien Science Report*, *3*, 40–43.

Du Troit, A. (1937), *Our wondering continents*, Oliver and Boyd, Edinburgh.

Ducea, M., M. A. House, and S. Kidder (2003), Late cenozoic denudation and uplift rates in the santa lucia mountains, california, *Geology*, *31*, 139–142.

Eagles, G., R. A. Livermore, J. D. Fairhead, and P. Morris (2005), Tectonic evolution of the west Scotia Sea, *J. Geophys. Res.*, *110*, doi:10.1029/2004JB003154.

Edelman, S. H. (1988), Comment on "Cycloid kinematics of relative plate motion", *Geology*, *16*, 472.

Engeln, J. F., S. Stein, S. Werner, and R. G. Gordon (1998), Microplate and shear zone models for oceanic spreading center reorganizations, *J. Geophys. Res.*, *93*, 2839–2856.

Faure, H. (1975), Recent crustal movements along the Red Sea Gulf of Aden coasts in Afar (Ethiopia and TFAI), *Tectonophysics*, *29*, 479–486.

Feder, J. (1988), *Fractals*, 300 pp., Plenum Press, New York.

Forsyth, D. W., and S. Uyeda (1975), On the relative importance of the driving forces of plate motion, *Geophys. J. R. astr. Soc.*, *43*, 163–200.

Foulger, G. R. (2002), Plumes or plate tectonic processes?, *Astronomy and Geophysics*, *43*, 19–23.

Foulger, G. R., J. H. Natland, D. C. Presnall, and D. L. Anderson (2005), Plates, Plumes, and Paradigms, *GSA Sp. Paper*, *388*.

Fowler, C. M. R. (1990), *The Solid Earth, an introduction to Global Geophysics*, Cambridge Univ. Press.

Frepoli, A., G. Selvaggi, C. Chiarabba, and A. Amato (1996), State of stress in the Southern Tyrrhenian subduction zone from fault–plane solutions, *Geophys. J. Int.*, *125*, 879–891.

Freymueller, J. T., M. H. Murray, P. Segall, and D. Castillo (1999), Kinematics of the Pacific-North America plate boundary zone, northern California, *J. Geophys. Res.*, *104*, 7419–7442.

Freymueller, J. T., S. C. Cohen, and H. Fletcher (2000), Variations in present-day deformation, Kenai Peninsula, Alaska, and their implications, *J. Geophys. Res.*, *105*, 8079–0101.

Friedrich, J., and G. G. Leduc (2004), Curvilinear patterns of oceanic fracture zones, *J. Geodyn.*, *37*, 169–179.

Gallo, D. G., P. J. Fox, and K. C. MacDonald (1986), A sea beam investigation of the Clipperton transform fault: The morphotectonic expression of a fast slipping transform boundary, *J. Geophys. Res.*, *91*, 3455–3468.

Garfunkel, Z., C. A. Anderson, and G. Schubert (1986), Mantle circulation and the lateral migration of subducted slabs, *J. Geophys. Res.*, *91*, 7205–7223.

Genrich, J. F., Y. Bock, R. McCaffrey, E. Calais, C. W. Stevens, and C. Subarya (1996), Accretion of the southern Banda arc to the Australia plate margin determined by Global Positioning System measurements, *Tectonics*, *15*, 288–295.

Giardini, D., G. Grunthal, K. Shedlock, and P. Zhang (1999), *Global Seismic Hazard Map*, 1:35,000,000, Global Seismic Hazard Assessment Program, UN/International Decade of Natural Disaster Reduction, International Lithosphere Program. (Available at http://seismo.ethz.ch/GSHAP).

Giunchi, C., R. Sabadini, E. Boschi, and P. Gasperini (1996), Dynamic models of subduction: geophysical and geological evidence in the Tyrrhenian Sea, *Geophys. J. Int.*, *126*, 555–578.

Gordon, R. G. (1995), Present plate motions and plate boundaries, in *Global Earth Physics: A Handbook of Physical Constants*, edited by T. J. Ahrens, AGU Reference Shelf 1, Am. Geophys. Union.

Gordon, R. G. (2000), Diffuse oceanic plate boundaries: strain rates, vertically averaged rheology, and comparison with narrow plate boundaries and stable plate interiors, *AGU, Geophys. Monogr.*, *121*, 143–159.

Gordon, R. G., and D. M. Jurdy (1986), Cenozoic global plate motions, *J. Geophys. Res.*, *91*, 12,384–12,406.

Gordon, R. G., and S. Stein (1992), Global tectonics and space geodesy, *Science*, *256*, 333–342.

Green, D. H., and T. J. Falloon (1998), Pyrolite: A ringwood concept and its current expression, in *The Earth's Mantle; Composition, Structure, and Evolution*, edited by I. N. S. Jackson, Cambridge University Press.

Green, D. H., T. J. Falloon, S. M. Eggins, and G. M. Yaxley (2001), Primary magmas and mantle temperatures, *European J. Min.*, *13*, 437–451.

Gripp, A. E. (1994), Current plate motions; reference frames and uncertainties, *PhD Thesis*, Northwestern University, Evanston, Illinois.

Gripp, A. E., and R. G. Gordon (1990), Current plate velocities relative to the hotspots incorporating NUVEL-1 global plate motion, *Geophys. Res. Lett.*, *17*, 1109–1112.

Gripp, A. E., and R. G. Gordon (2002), Young tracks of hotspots and current plate velocities, *Geophys. J. Int.*, *150*, 321–364.

Gung, Y., M. Panning, and B. Romanowicz (2003), Global anisotropy and the thickness of continents, *Nature*, *422*, 707–711.

Harper, J. F. (1986), Mantle flow and plate motions, *Geophys. J. R. astr. Soc.*, *87*, 155–171.

Hassani, R., D. Jongmans, and J. Chery (1997), Study of plate deformation and stress in subduction processes using two-dymensional numerical models, *J. Geophys. Res.*, *102*, 17,951–17,965.

Heflin et al. (2004), GPS Time Series, Jet Propulsion Laboratory, California Institute of Technology, http://sideshow.jpl.nasa.gov/mbh/series.html.

Heirtzler, J. R., G. O. Dickson, H. M. Herron, W. C. Pitmanand, and X. Le Pichon (1968), Marine magnetic anomalies, geomagnetic field reversals, and motion of the ocean floor and continents, *J. Geophys. Res.*, *73*, 2119–2136.

Heki, K., S. Miyazaki, H. Takahashi, M. Kasahara, F. Kimata, S. Miura, N. F. Vasilenko, A. Ivaschenko, and K. D. An (1999), The Amurian plate motion and current plate kinematics int the eastern Asia, *J. Geophys. Res.*, *104*, 29,147–29,155.

Hellinger, S. J. (1981), The uncertainties of finite rotations in plate tectonics, *J. Geophys. Res.*, *86*, 9312–9318.

Henderson, D. M. (2001), New visualization of global tectonic plate motions and plate boundary interactions, *Terra Nova*, *13*, 70–78.

Hess, H. H. (1962), History of ocean basins, in *Petrologic studies: a volume in honor of A. F. Buddington*, edited by A. E. J. Engel, H. L. James, and B. F. Leonard, Geol. Soc. Am.

Isacks, B., and P. Molnar (1971), Distribution of stresses in the descending lithosphere from a global survey of focal–mechanism solutions of mantle earthquakes, *Rev. Geophys.*, *9*, 103–174.

Jackson, J. (1992), Partitioning of strike–slip and convergent motion between Eurasia and Arabia in eastern Turkey and the Caucusus, *J. Geophys. Res.*, *97*, 12,471–12,479.

Janney, P. E., J. D. Macdougall, J. H. Natland, and M. A. Lynch (2000), Geochemical evidence fom he Pukapuka volcanic ridge system for a shallow enriched mantle domain beneath the South Pacific Superswell, *Earth Planet. Sci. Lett.*, *181*, 47–60.

Jeffreys, H. (1975), *The Earth*, 420 pp., Cambridge University Press.

Jin, S., and W. Zhu (2004), A revision of the parameters of the NNR–NUVEL1A plate velocity model, *J. Geodyn.*, *38*, 85–92.

Jordan, T. H. (1974), Some comments on tidal drag as a mechanism for driving plate motions, *J. Geophys. Res.*, *79*, 2141–2142.

Jurdy, D. M. (1974), A determination of the polar wander since the Early Cretaceous, *PhD Thesis*, University of Michigan, Ann Arbor, MI, United States (USA).

Jurdy, D. M. (1978), An alternative model for the Early Tertiary absolute plate motion, *Geology*, *6*, 469–472.

Jurdy, D. M. (1990), Reference frames for plate tectonics and uncertainties, *Tectonophysics.*, *182*, 373–382.

Jurdy, D. M., and R. G. Gordon (1984), Global plate motions relative to the hot spots 64 to 56 Ma, *J. Geophys. Res.*, *89*, 9927–9936.

Jurdy, D. M., and M. Stefanick (1987), Errors in plate rotations as described by covariance matrices and their combination in reconstructions, *J. Geophys. Res.*, *92*, 6310–6318.

Jurdy, D. M., and M. Stefanick (1988), Plate-driving forces over the Cenozoic Era, *J. Geophys. Res.*, *93*, 11,833–11,844.

Karig, D. E., and G. F. SharmanIII (1975), Subduction and accretion in trenches, *Geol. Soc. Am. Bull.*, *86*, 377–389.

Keary, P., and F. Vine (1990), *Global Tectonics*, Blackwell Scientific Publications.

Kennedy, L. A., J. K. Russell, and M. G. Kopylova (2002), Mantle shear zones revisited: The connection between the cratons and mantle dynamics, *Geology*, *30*, 419–422.

Kirkwood, B. H., J. Royer, T. C. Chang, and R. G. Gordon (1999), Statistical tools for estimating and combining finite rotations and their uncertainties, *Geophys. J. Int.*, *137*, 408–428.

Klitgord, K. D., and H. Schouten (1986), Plate kinematics of the central Atlantic, in *The Geology of North America, The Western Atlantic Region*, edited by B. E. Tucholke and P. R. Vogt, Geol. Soc. Am. Spec. Publ.

Knopoff, L., and A. Leeds (1972), Lithospheric momenta and the deceleration of the Earth, *Nature*, *237*, 93–95.

Kreemer, C., and W. E. Holt (2001), A no-net-rotation model of present-day surface motions, *Geophys. Res. Lett.*, *28*, 4407–4410.

Kreemer, C., and W. E. Holt (2003), An integrated global model of present-day plate motions and plate boundary deformation, *Geophys. J. Int.*, *154*, 8–34.

Kreemer, C., D. A. Lavallée, G. Blewitt, and W. E. Holt (2006), On the stability of a geodetic no–net–rotation frame and its implication for the International Terrestrial Reference Frame, *Geophys. Res. Lett.*, *33*, doi:10.1029/2006GL027058.

Larsen, C. F., R. J. Motyka, J. T. Freymueller, K. A. Echelmeyer, and E. R. Ivins (2004), Rapid uplift of southern Alaska caused by recent ice loss, *Geophys. J. Int.*, doi:10.1111/j.1365-246X.2004.02356.x.

Larson, K. M., J. T. Freymuller, and S. Philipsen (1997), Global plate velocities from Global Positionig System, *J. Geophys. Res.*, *102*, 9961–9981.

Lawver, L. A., and H. J. B. Dick (1983), The American–Antarctic ridge, *J. Geophys. Res.*, *88*, 8193–8202.

Le Pichon, X. (1968), Sea-floor spreading and continental drift, *J. Geophys. Res.*, *73*, 3661–3697.

Le Pichon, X., J. Francheteau, and J. Bonnin (1973), *Plate Tectonics*, 300 pp., Elsevier, New York.

Le Pichon, X., N. Chamot-Rooke, and S. Lallemant (1995), Geodetic determinations of the kinematics of central Greece with respect to Europe: Implications for eastern Mediterranean tectonics, *J. Geophys. Res.*, *100*, 12,675–12,690.

Link, M. H., and R. H. Osborne (1978), Lacustrine facies in the Pliocene ridge basin group: Ridge Basin, California, *Spec. Publ. Int. Assoc. Sedimentol.*, *2*, 169–178.

Liu, T. K. (1982), Tectonic implications of fission-track ages from the central range, taiwan, *Proc. Geol. Soc. China*, *25*, 22–37.

Liu, Z., and P. Bird (2002), North America plate is driven westward by lower mantle flow, *Geophys. Res. Lett.*, *29*, doi:10.1029/2002GL016002.

Lliboutry, L. (1974), Plate movement relative to a rigid lower mantle, *Nature*, *250*, 298–300.

Lynch, M. A. (1999), Linear ridge groups: Evidence for tensional cracking in the Pacific plate, *J. Geophys. Res.*, *104*, doi:10.1029/1999JB900241.

McClusky et al. (2000), Global Positioning System constraints on plate kinematics and dynamics in the eastern Mediterranean and Caucasus, *J. Geophys. Res.*, *105*, 5695–5719.

McKenzie, D. P. (1972), Active tectonics of the Mediterranean region, *Geophys. J. R. Astron. Soc.*, *30*, 109–185.

McKenzie, D. P. (1978), Some remarks on the development of sedimentary basins, *Earth Planet. Sci. Lett.*, *40*, 25–32.

McKenzie, D. P., and R. L. Parker (1967), The North Pacific: an example of tectonics on a sphere, *Nature*, *216*, 1276–1280.

McKenzie, D. P., D. Davies, and P. Molnar (1970), Plate tectonics of the Red Sea and East Africa, *Nature*, *226*, 243–248.

Melosh, H., and A. Raefsky (1980), The dynamic origin of subduction zone topography, *Geophys. J. R. astr. Soc.*, *60*, 333–354.

Minster, J. B., and T. H. Jordan (1978), Present-day plate motions, *J. Geophys. Res.*, *83*, 5331–5354.

Minster, J. B., T. H. Jordan, P. Molnar, and E. Haines (1974), Numerical modeling of istantaneous plate tectonics, *Geophys. J. R. astr. Soc.*, *36*, 541–576.

Miyazaki, S., K. Heki, Y. Hatanaka, T. Sagiya, and H. Tsuji (1996), Determination of the Euler vector between the Amurian and the Eurasian plates with GPS data, paper presented at 86th Meeting of the Geodetic Society of Japan, Geod. Soc. of Jpn., Kochi.

Montario, M. J. (2001), *Exhumation of the Cordillera Blanca, Northern Peru, based on apatite fission track analysis*, 55 pp., Department of Geology, Union College, Schenectady, New York, unpublished Thesis.

Moore, G. W. (1973), Westward tidal lag as the driving force of plate tectonics, *Geology*, *1*, 99–100.

Morgan, W. J. (1968), Rises, trenches, great faults and crustal blocks, *J. Geophys. Res.*, *73*, 1959–1982.

Morgan, W. J. (1971), Convection plumes in the lower mantle, *Nature*, *230*, 42–43.

Morgan, W. J. (1972), Plate motions and deep mantle convection, *Studies in Earth and Space Sciences, Geol. Soc. Am. Mem.*, *132*, 7–22.

Morgan, W. J. (1983), Hotspot tracks and the early rifting of the Atlantic, *Tectonophysics*, *94*, 123–139.

Natland, J. H., and E. L. Winterer (2003), What really happened in the Pacific?, in *Beyond the plume hypothesis, abstracts volume*, Hveragerdi, Iceland.

Nishimura, C., D. S. Wilson, and H. B, N (1984), Pole of rotation analysis of present–day Juan de Fuca, *J. Geophys. Res.*, *89*, 10,283–10,290.

Norton, I. O. (1976), The present relative motion between Africa and Antarctica, *Earth Planet. Sci. Lett.*, *33*, 219–230.

Norton, I. O. (2000), Global hotspot reference frames and plate motion, in *The history and dynamics of global plate motions*, edited by M. A. Richards, R. G. Gordon, and R. D. V. der Hilst, Geophys. Monograph.

Nürnberg, D., and R. D. Müller (1991), The tectonic evolution of the South Atlantic from Late Jurassic to Present, *Tectonophysics.*, *191*, 27–53.

O'Connell, R. G., G. G. Gable, and B. H. Hager (1991), Toroidal-poloidal partitioning of lithospheric plate motion, in *Glacial Isostaty, Sea-Level and Mantle Rheology*, edited by K. L. R. Sabadini and E.Boschi, Kluwer Acad. Publ.

Papazachos, C. B. (1998), Seismological and GPS evidence for the Aegean–Anatolia interaction, *Geophys. Res. Lett.*, *26*, 2653–2656.

Parsons, B., and J. Sclater (1977), An analysis of the variation of ocean floor bathymetry and heat flow with age, *J. of Geophys. Res.*, *82*, 803–827.

Pelayo, A. M., and D. A. Wiens (1989), Seismotectonics and relative plate motions of the Scotia Sea region, *J. Geophys. Res.*, *94*, 7293–7320.

Perez, O. J., and K. H. Jacob (1980), Tectonic model and seismic potential of the eastern Gulf of Alaska and Yakataga seismic gap, *J. Geophys. Res.*, *85*, 7132–7150.

Petronotis, K. E., and D. M. Jurdy (1990), Pacific plate reconstructions and uncertainties, *Tectonophysics.*, *182*, 383–391.

Pitman, W. C., and J. A. Andrews (1985), Subsidence and thermal history of small pull apart basins, *Spec. Publ. Soc. econ. Paleont. Mineral.*, *37*, 45–49.

Pitman, W. C., and J. R. Heirtzler (1966), Magnetic anomalies over the Pacific–Atlantic ridge, *Science*, *154*, 1164–1171.

Pollitz, F. F., R. Brgmann, and B. Romanowicz (1998), Viscosity of oceanic asthenosphere inferred from remote triggering of earthquakes, *Science*, *280*, 1245–1249.

Prawirodirdjo, L., and Y. Bock (2004), Instantaneous global plate motion from 12 years of continuous GPS observation, *J. Geophys. Res.*, *109*, doi:10.1029/2003JB002944.

Raff, A. D. (1968), Sea–floor spreading–another rift, *J. Geophys. Res.*, *73*, 3699–3705.

Ranalli, G. (1995), *Rheology of the Earth*, Chapman and Hall, London.

Rangin, C., X. Le Pichon, S. Mazzotti, M. Pubellier, N. Chamot-Rooke, M. Aurelio, A. Walpersdorf, and R. Quebral (1999), Plate convergence measured by GPS across the Sundaland/Philippine Sea plate deformed boundary: The Philippines and eastern Indonesia, *Geophys. J. Int.*, *139*, 296–316.

Reilinger, R., S. C. McClusky, M. B. Oral, R. W. King, M. N. Toksoz, A. A. Barka, I. Kinik, O. Lenk, and I. Sanli (1997), Global Positioning System measurements of present–day crustal movements in the Arabia–Africa–Eurasia plate collision zone, *J. Geophys. Res.*, *102*, 9983–10,000.

Ricard, Y., C. Doglioni, and C. Sabadini (1991), Differential rotation between lithosphere and mantle: a consequence of lateral viscosity variations, *J. Geophys. Res.*, *96*, 8407–8415.

Riguzzi, F., M. Crespi, M. Cuffaro, C. Doglioni, and F. Giannone (2006), A model of plate motions, in *Geodetic Deformation Monitoring: From Geophysical to Engineering Roles, International Association of Geodesy Symposia*, vol. 131, edited by F. Sansò and J. Gil, pp. 200–208, Springer.

Robaudo, S., and C. G. A. Harrison (1993), Plate tectonics from SLR and VLBI data, in *Contributions of Space Geodesy and Geodynamics, Crustal Dynamics*, edited by D. E. Smith and D. L. Turcotte, Geodyn. Series, AGU, Washington, D. C.

Robbins, J. W., D. E. Smith, and C. Ma (1993), Horizontal crustal deformation and large scale plate motions inferred from space geodetic techniques, in *Contributions of Space Geodesy to Geodynamics: Crustal Dinamics*, Amer. Geophys. Un., Geodynamics.

Russo, R. M., and P. G. Silver (1994), Trench-parallel flow beneath the Nazca plate from seismic anisotropy, *Science*, *263*, 1105–1111.

Russo, R. M., and P. G. Silver (1996), Cordillera formation, mantle dynamics, and the Wilson cycle, *Geology*, *24*, 511–514.

Ryan, J. W., T. A. Clark, C. Ma, D. Gordon, D. S. Caprette, and W. E. Himwich (1993), Global scale tectonic plate motions measured with CDP VLBI data, in *Contributions of Space Geodesy and Geodynamics, Crustal Dynamics*, edited by D. E. Smith and D. L. Turcotte, Geodyn. Series, AGU, Washington, D. C.

Rychert, C. A., K. M. Fischer, and S. Rondenay (2005), A sharp lithosphere–asthenosphere boundary imaged beneath eastern North America, *Nature*, *436*, 542–545.

Sabadini, R., and L. L. A. Vermeersen (2004), Global dynamics of the Earth: Applications of normal mode relaxation theory to solid-earth geophysics, Chapters 5 and 6, *Kluwer Modern Approaches in Geophysics Series*, *20*, pp. 328.

Sandwell, D. T., E. L. Winterer, J. Mammerickx, R. A. Duncan, M. A. Lynch, D. A. Levitt, and C. L. Johnson (1995), Evidence for diffuse extension of the Pacific plate from Pukapuka ridges and cross-grain gravity anomalies, *J. Geophys. Res.*, *100*, 15,087–15,099.

Sato, K. (1993), Tectonic plate motion and deformation inferred from very long baseline interferometry, *Tectonophysics*, *220*, 69–87.

Savostin, L. A., A. I. Verzhbitskaya, and B. V. Baranov (1982), Holocene plate tectonics of the Sea of Okhotsk region, *Dokl. Acad. Sci. USSR, Earth Sci. Ser., Engl. Trans.*, *266*, 62–65.

Savostin, L. A., L. Zonenshain, and B. V. Baranov (1983), Geology and plate tectonics of the Sea of Okhotsk, in *Geodynamics of the Western Pacific–Indonesian Region*, edited by T. W. C. Hilde and S. Uyeda, Geodyn. Ser. AGU, Washington, D. C.

Schettino, A. (1999a), Polygon intersections in spherical topology: application to plate tectonics, *Computers & Geosciences*, *25*, 61–69.

Schettino, A. (1999b), Computational methods for calculating geometric parameters of tectonic plates, *Computers & Geosciences*, *25*, 897–907.

Schubert, G., D. L. Turcotte, and P. Olson (2001), *Mantle convection in the Earth and Planets*, 940 pp., Cambridge University Press.

Scoppola, B., D. Boccaletti, M. Bevis, E. Carminati, and C. Doglioni (2006), The westward drift of the lithosphere: a rotational drag?, *Geol. Soc. Amer. Bull.*, *118*, doi: 10.1130/B25734.1.

Searle, R. C. (1986), GLORIA investigations of oceanic fracture zones: comparative study of the trasform fault zone, *J. Geol. Soc., London*, *143*, 743–756.

Sella, G. F., T. H. Dixon, and A. Mao (2002), REVEL: A model for recent plate velocity from space geodesy, *J. Geophys. Res.*, *107*, doi:10.1029/2000JB000033.

Sengoku, A. (1998), A plate motion study using Ajisai SLR data, *Earth Planets Space*, *50*, 611–627.

Seno, T., S. Stein, and A. E. Gripp (1993), A model for the motion of the Philippine Sea plate consistent with NUVEL–1A and geological data, *J. Geophys. Res.*, *98*, 17,941–17,948.

Seno, T., T. Sakurai, and S. Stein (1996), Can the Okhotsk plate be discriminated from the North American plate?, *J. Geophys. Res.*, *101*, 11,305–11,316.

Shaw, H. R. (1973), Mantle convection and volcanic periodicity in the Pacific: evidence from Hawaii, *Geol. Soc. Amer. Bull.*, *84*, 1505–1526.

Silver, P. G., and W. E. Holt (2002), The mantle flow field beneath western North America, *Science*, *295*, 1054–1057.

Smith, A. D., and C. Lewis (1999), The planet beyond the plume hypothesis, *Earth Sci. Rev.*, *48*, 135–182.

Smith, D. E., R. Kolenkiewicz, P. Dunn, J. W. Robbins, M. H. Torrence, S. M. Klosko, R. G. Williamson, E. C. Pavlis, N. B. Douglas, and S. K. Fricke (1990), Tectonic motion and deformation from satellite laser ranging to LAGEOS, *J. Geophys. Res.*, *95*, 23,013–22,041.

Solomon, S. C., and N. H. Sleep (1974), Some simple physical models for absolute plate motions, *J. Geophys. Res.*, *79*, 2557–2567.

Solomon, S. C., N. H. Sleep, and D. M. Jurdy (1977), Mechanical models for absolute plate motion in the Early Tertiary, *J. Geophys. Res.*, *82*, 203–212.

Soudarin, L., and A. Cazenave (1993), Global geodesy using DORIS data on SPOT-2, *Geophys. Res. Lett.*, *20*, 289–292.

Soudarin, L., and A. Cazenave (1995), Large–scale tectonics plate motions measured with the DORIS space geodesy system, *Geophys. Res. Lett*, *22*, 469–472.

Spotila, J. A., J. T. Buscher, A. J. Meigs, and P. W. Reiners (2004), Long-term glacial erosion of active mountain belts: Example of the chugach-st. elias range, alaska, *Geology*, *32*, 501–504.

Srivastava, S. P. (1978), Evolution of the Labrador Sea and its bearing of the early evolution of the North America, *Geophys. J. R. astr. Soc.*, *52*, 313–357.

Stein, S. (1993), Space geodesy and plate motions, *Amer. Geophys. Union, Geodynamics Series*, *25*, 5–20.

Stein, S., and G. F. Sella (2002), Plate boundary zones: Concept and approaches, *AGU Geodyn. Series*, *30*, doi:10.1029/030GD01.

Stein, S., and M. Wysession (2003), *An introduction to seismology, earthquakes, and Earth structure*, 498 pp., Blackwell Publishing.

Steinberger, B. (2000), Plumes in a convecting mantle: Models and observations for individual hotspots, *J. Geophys. Res.*, *105*, 11,127–11,152.

Steinberger, B., and R. J. O'Connell (1998), Advection of plumes in mantle flow; implications on hotspot motion, mantle viscosity and plume distribution, *Geophys. J. Int.*, *132*, 412–434.

Stock, J. M., and P. Molnar (1983), Some geometrical aspect of uncertainties in combined plate reconstructions, *Geology*, *11*, 697–701.

Takahashi et al. (1999), Velocity field of around the Sea of Okhotsk and Sea of Japan regions determined from a new continuous GPS network data, *Geophys. Res. Lett.*, *26*, 2533–2536.

Thomas, C., L. Livermore, and F. Pollitz (2003), Motion of the Scotia Sea plates, *Geophys. J. Int.*, *155*, 789–804.

Thybo, H. (2006), The heterogeneous upper mantle low velocity zone, *Tectonophysics*, *416*, 53–79.

Turcotte, D. L., and G. Schubert (2001), *Geodynamics, Application of Continuum Physics to Geological Problems*, 2nd ed., 528 pp., John Wiley & Sons, New York.

Uyeda, S., and H. Kanamori (1979), Back-arc opening and the mode of subduction, *J. Geophys. Res.*, *84*, 1049–1061.

Van der Voo, R. (1993), *Paleomagnetism of the Atlantic, Tethys and Iapetus Oceans*, Cambridge Univ. Press.

Vine, F. J. (1966), Spreading of the ocean floor: new evidence, *Science*, *154*, 1405–1415.

Vine, F. J., and D. H. Matthews (1963), Magnetic anomalies over oceanic ridges, *Nature*, *199*, 947–949.

von Huene, R., and S. Lallemand (1990), Tectonic erosion along the japan and peru convergent margins, *Geol. Soc. Am. Bull.*, *102*, 704–720.

Wang, S., and M. Liu (2006), Moving hotspots or reorganized plates, *Geology*, *34*, 465–468.

Wang, S., and R. Wang (2001), Current plate velocities relative to hotspots: implications for hotspot motion, mantle viscosity and global reference frame, *Earth Planet. Sci. Lett.*, *189*, 133–140.

Wdowinski, S. (1992), Dynamically supported trench topography, *J. Geophys. Res.*, *97*, 17,651–17,656.

Wegener, A. (1915), *Die Entstehung der Kontinente und der Ozeae*, 94 pp., Samml. Vieweg.

Wegener, A. (1924), *The origin of continents and oceans*, Dutton, New York.

Wei, D., and T. Seno (1998), Determination of the Amurian plate motion, in *Mantle Dynamics and Plate Interactions in East Asia*, edited by M. F. J. Flower et al., Geodyn. Series, AGU, Washington, D. C.

Weissel, J. K., and R. N. Anderson (1978), Is there a Caroline plate?, *Earth Planet. Sci. Lett.*, *41*, 142–158.

Wessel, P., and L. Kroenke (1997), A geometric technique for relocating hotspots and refinig absolute plate motion, *Nature*, *387*, 365–369.

Wessel, P., and W. H. F. Smith (1995), New version of Generic Mapping Tools (gmt) version 3.0 released, *Eos Trans. AGU*, *76*, 329.

Westaway, R. (1994), Present–day kinematics of the Middle East and eastern Mediterranean, *J. Geophys. Res.*, *99*, 12,071–12,090.

Wheeler, P., and N. White (2000), Quest for dynamic topography: Observations from southeast asia, *Geology*, *28*, 963–966.

Willett, S. D., and M. T. Brandon (2002), On steady states in mountain belts, *Geology*, *30*, 175–178.

Wilson, D. S. (1993), Confidence intervals for motion and deformation of the Juan de Fuca plate, *J. Geophys. Res.*, *98*, 16,053–16,071.

Wilson, J. T. (1973), Mantle plumes and plate motions., *Tectonophysics*, *19*, 149–164.

Winterer, E. L., and D. T. Sandwell (1987), Evidence from en–echelon cross–grain ridges for tensional cracks in the Pacific plate, *Nature*, *329*, 534–537.

Woodward, N. B., S. E. Boyer, and J. Suppe (1989), Balanced geological cross-sections: an essentialm technique in geological research and exploration, *Amer. Geophys. Union, Short Course Geology*, *6*, 132.

Zhong, S. (2001), Role of ocean-continent contrast and continental keels on plate motion, net–rotation of the lithosphere and the geoid, *J. Geophys. Res.*, *106*, 703–712.

Zhong, S., and M. Gurnis (1992), Viscous flow model of subduction zone with a faulted lithosphere: long and short wavelength topography, gravity and geoid, *Geophys. Res. Lett.*, *19*, 1891–1894.